

IMPACT RESISTANCE OF CONCRETE

by

NEMKUMAR P. BANTHIA

B.E., Nagpur University, 1980

M.Tech., Indian Institute of Technology, 1982

A THESIS SUBMITTED IN PARTIAL FULFILMENT OF

THE REQUIREMENTS FOR THE DEGREE OF

DOCTOR OF PHILOSOPHY

in

THE FACULTY OF GRADUATE STUDIES

Department of Civil Engineering

We accept this thesis as conforming

to the required standard

THE UNIVERSITY OF BRITISH COLUMBIA

March 1987

© Nemkumar P. Banthia, 1987

In presenting this thesis in partial fulfilment of the requirements for an advanced degree at the University of British Columbia, I agree that the Library shall make it freely available for reference and study. I further agree that permission for extensive copying of this thesis for scholarly purposes may be granted by the head of my department or by his or her representatives. It is understood that copying or publication of this thesis for financial gain shall not be allowed without my written permission.

Department of Civil Engineering

The University of British Columbia  
1956 Main Mall  
Vancouver, Canada  
V6T 1Y3

Date March 23, 1987

## ABSTRACT

During its service life, a structure may be subjected to various environmental and loading conditions. However, in general, the properties determined under one set of conditions may not be used to determine the behaviour of the material under a different set of conditions. For example, it is well known that concrete is a strain rate sensitive material; therefore, its properties determined under conventional static loading cannot be used to predict the performance of concrete subjected to high strain rates. The problem is serious because these high strain rate loadings are associated with large amounts of energy imparted to the structure in a very short period of time, and concrete is a brittle material. Since the strain rate sensitivity of concrete prohibits the use of its statically determined properties in assessing its behaviour under dynamic conditions, high strain rate tests are required.

Impact tests were carried out on about 500 concrete beams. An instrumented drop weight impact machine was used. The instrumentation included strain gauges mounted in the striking end of the hammer (called 'the tup'), and also in one of the support anvils. In addition, three accelerometers were mounted along the length of the beam in order to obtain the beam response, and also to enable the inertial correction to the observed tup load to be made.

Two different concrete mixes, normal strength with a compressive strength of 42 MPa, and high strength with a compressive strength of 82 MPa, were tested. The effect of two types of fibres, high modulus steel, and low modulus fibrillated polypropylene, in enhancing concrete properties was investigated. In addition, tests were also conducted on beams with conventional reinforcement. Hammer drop heights ranging from 0.15m to 2.30m were used. Static tests were conducted on companion specimens for a direct comparison with the dynamic results.

In general, it was found that concrete is a very strain rate sensitive material. Both the peak bending loads and the fracture energies were higher under dynamic conditions than under static conditions. Fibres, particularly the steel fibres, were found to significantly increase the ductility and the impact resistance of the composite. High strength concrete made with microsilica, in certain circumstances, was found to behave in a far more brittle manner than normal strength concrete.

High speed photography (at 10,000 frames per second) was used to study the propagation of cracks under impact loading. In general, the crack velocities were found to be far lower than the theoretical crack velocities. The presence of reinforcement, either in the form of fibres, or of continuous bars was found to reduce the crack velocity.

A model was proposed based on a time step integration technique to evaluate the response of a beam subjected to an external impact pulse. The model was capable of predicting not only the experimentally observed non-linear behaviour of concrete under impact loading, but also the more pronounced brittle behaviour of high strength concrete.

## Table of Contents

1.	INTRODUCTION .....	1
2.	OBJECTIVE AND SCOPE .....	5
3.	LITERATURE SURVEY .....	13
4.	EXPERIMENTAL PROCEDURES .....	40
4.1	Introduction .....	40
4.2	Specimen Preparation .....	45
4.2.1	Normal Strength Plain Concrete Beams ....	45
4.2.2	High Strength Plain Concrete Beams .....	49
4.2.3	Fibre Reinforced Concrete Beams .....	50
4.2.4	Conventionally Reinforced Concrete Beams .....	51
4.2.5	Notched Beams .....	51
4.3	Testing Program .....	53
4.3.1	Static Testing .....	53
4.3.1.1	Flexural Tests on Beams .....	53
4.3.1.2	Tension Tests on Reinforcing Bars .....	54
4.3.1.3	Stiffness Test on the Rubber Pad .....	54
4.3.1.4	Compressive Strength Determination from the Broken Halves of the Beams .....	55
4.3.2	Impact Testing .....	56
4.3.2.1	The Impact Testing Machine .....	56
4.3.2.2	Calibration .....	70
4.3.2.3	Analysis of the Test Results ....	75
4.3.2.4	The Support Reactions .....	94
5.	INERTIAL LOADING IN INSTRUMENTED IMPACT TESTS .....	98
5.1	Introduction .....	98

5.2	Nature of the Inertial Load .....	99
5.3	Experimental Observations .....	102
5.4	The Use of a Rubber Pad .....	105
5.5	Instrumenting the Support Anvils .....	110
6.	PLAIN CONCRETE UNDER IMPACT .....	112
6.1	Introduction .....	112
6.2	Comparison between the Impact Behaviour of Paste and Concrete Beams .....	114
6.3	Effect of Stress Rate on Plain Normal Strength Concrete Beams .....	119
6.4	Effect of Stress Rate on Plain High Strength Concrete Beams .....	129
6.5	Comparison between Normal Strength and High Strength Concrete .....	134
6.6	Effect of Moment of Inertia .....	141
6.7	Crack Development in Paste under Impact .....	143
7.	MODEL ANALYSIS .....	149
7.1	Introduction .....	149
7.2	Model A - Evaluation of Beam Response to an External Impact Pulse : Energy Balance Principle .....	153
7.2.1	Assumptions .....	153
7.2.2	Notation .....	154
7.2.3	Evaluation of the Kinetic Energy .....	155
7.2.4	Evaluation of the Bending Energy .....	156
7.2.5	The Total Energy .....	156
7.2.6	Finite Difference Technique .....	157
7.2.7	Results .....	158
7.3	Model B - Evaluation of Beam Response to an External Impact Pulse : Solution to the Equation of Dynamic Equilibrium using Time Steps .....	162

7.3.1	The Constitutive Law for Concrete .....	163
7.3.2	Time Step Analysis and the Results .....	165
	Appendix - 7.1 Evaluation of Beam Response : Beam Modelled as a Single Degree of Freedom System .....	169
	Appendix - 7.2 Evaluation of Beam Response : Beam Modelled as a Multi Degree of Freedom System .....	174
	Appendix - 7.3 Time Step Analysis .....	179
8.	ENERGY BALANCE IN INSTRUMENTED IMPACT TESTS .....	184
8.1	Introduction .....	184
8.2	Energy Balance at the Peak Load .....	186
8.3	Energy Balance just after Failure .....	194
8.4	The Machine Losses .....	195
9.	NOTCHED BEAMS UNDER IMPACT .....	201
9.1	Introduction .....	201
9.2	Plain and Fibre Reinforced Notched Beams under Impact .....	202
10.	FIBRE REINFORCED CONCRETE UNDER IMPACT .....	212
10.1	Introduction .....	212
10.2	Steel Fibre Reinforced Normal Strength Concrete under Variable Stress Rate .....	215
10.3	Polypropylene Fibre Reinforced Normal Strength Concrete under Variable Stress Rate .....	220
10.4	Comparison between Steel and Polypropylene Fibre Reinforced Normal Strength Concrete .....	224
10.5	Effect of Varying the Stress Rate in the Dynamic Range on the Performance of Steel Fibre Reinforced Normal Strength Concrete .....	227
10.6	Steel Fibre Reinforced High Strength Concrete under Variable Stress Rate .....	232
10.7	Polypropylene Fibre Reinforced High Strength Concrete under Variable Stress Rate .....	236

10.8	Comparison Between Fibre Reinforced Normal Strength Concrete and Fibre Reinforced High Strength Concrete .....	237
10.9	Crack Development in Steel Fibre Reinforced Normal Strength Concrete Under Impact .....	242
11.	CONVENTIONALLY REINFORCED CONCRETE UNDER IMPACT ...	244
11.1	Introduction .....	244
11.2	Conventionally Reinforced Normal Strength Concrete with Deformed Reinforcing Bars under Variable Stress Rate .....	245
11.3	The Use of Smooth Reinforcing Bars .....	258
11.4	The Use of Shear Reinforcement .....	266
11.5	Conventionally Reinforced High Strength Concrete with Deformed Reinforcing Bars under Variable Stress Rate, and its Comparison with Normal Strength Concrete .....	269
11.6	Crack Development in Conventionally Reinforced High Strength Concrete under Impact .....	279
12.	CONVENTIONALLY REINFORCED CONCRETE CONTAINING FIBRES UNDER IMPACT .....	281
12.1	Introduction .....	281
12.2	Conventionally Reinforced Normal Strength Concrete with Polypropylene Fibres under Variable Stress Rate .....	282
12.3	Conventionally Reinforced High Strength Concrete with Polypropylene Fibres under Variable Stress Rates .....	285
12.4	Comparison between Conventionally Reinforced Normal Strength Concrete with Polypropylene Fibres and Conventionally Reinforced High Strength Concrete with Polypropylene Fibres ..	287
12.5	Pre-damaged Beams .....	290
	CONCLUSIONS .....	295
	SCOPE FOR FUTURE WORK .....	306
	BIBLIOGRAPHY .....	308

## LIST OF FIGURES

1.	INTRODUCTION	
2.	OBJECTIVE AND SCOPE	
3.	LITERATURE SURVEY	
3.1	Three different ways of determining the constant "n" .....	29
4.	EXPERIMENTAL PROCEDURES	
4.1	The Drop Weight Impact Testing Machine .....	57
4.2	The dimensions of the machine and the tup ....	58
4.3	Layout of the Impact Testing Apparatus .....	60
4.4	Triggering of the data acquisition system ....	62
4.5	The striking end of the hammer or the "Tup" ..	63
4.6	The circuit of the tup .....	64
4.7	The support anvil .....	65
4.8	The support reactions .....	66
4.9	The circuit of the support anvil .....	67
4.10	The accelerometers .....	68
4.11	The calibration of the support and the striking tup .....	71
4.12	The Calibration of the Hammer Acceleration ...	72
4.13	Typical output from the five channels of instrumentation .....	76
4.14	(a) Positions of the accelerometers, (b) Acceleration distribution, and (c) Generalized inertial load .....	80
4.15	Acceleration distribution for plain concrete beams .....	84
4.16	Acceleration distribution for conventionally reinforced concrete beams .....	85
4.17	(a) Linear acceleration distribution, (b) Sinusoidal acceleration distribution .....	86
4.18	(a) Dynamic loading on the beam, (b) Equivalent static loading .....	88

4.19	The flow chart of analysis .....	93
4.20	Comparison between the evaluated and the observed support reaction .....	94
4.21	A rough check on the validity of the technique used to account for Inertia .....	96
4.22	The horizontal support reaction .....	97
5.	INERTIAL LOADING IN INSTRUMENTED IMPACT TESTS	
5.1	The period of inertial oscillations .....	99
5.2	Observed tup and inertial loads for plain concrete .....	103
5.3	Observed tup and inertial loads for (a) plain and (b) conventionally reinforced concrete .....	104
5.4	Effect of hammer drop height on (a) Tup and (b) Inertial loads .....	105
5.5	Effect of rubber pad on plain concrete beams	108
5.6	Effect of rubber pad on conventionally reinforced concrete beams .....	110
6.	PLAIN CONCRETE UNDER IMPACT	
6.1	Impact behaviour of paste and concrete .....	116
6.2	Impact behaviour of paste and concrete upto the peak load .....	116
6.3	Static and dynamic load vs. deflection plots for normal strength concrete .....	122
6.4	Determination of parameter "n" .....	125
6.5	Determination of the parameter "n" for normal strength concrete .....	126
6.6	Mix with and without microsilica .....	129
6.7	Determination of the parameter "n" for high strength concrete .....	133
6.8	Comparison between normal strength and high strength concrete .....	136
6.9	Photograph showing the fracture surfaces for high strength and normal strength concrete ..	137

6.10	The finite width zone of microcracking surrounding a crack .....	138
6.11	Stress rate sensitivity of high strength concrete .....	140
6.12	Crack development in paste under impact .....	145
6.13	(a) Energy absorbed and (b) Crack velocity as the crack propagates in paste .....	147
7.	MODEL ANALYSIS	
7.1	Assumed beam displacements .....	154
7.2	Finite difference technique .....	157
7.3	Energy predictions using Model A .....	160
7.4	Model predictions vs. the experimental findings (Model A) .....	161
7.5	Model B predictions for normal strength concrete .....	166
7.6	Model B predictions for high strength concrete .....	167
7.7	Bending energy at the peak load (Model B) ...	168
	A7.1-1 : Single degree of freedom model .....	169
	A7.1-2 : Determination of the generalized mass .....	171
	A7.2-1 : Multi-degree of freedom model .....	171
	A7.3-1 : Single degree of freedom model to evaluate the beam response using the Time Step Analysis .....	180
8.	ENERGY BALANCE IN INSTRUMENTED IMPACT TESTS	
8.1	Typical tup load vs. time plot .....	185
8.2	Components of bending energy .....	188
8.3	Energy balance at the peak load .....	190
8.4	Components of bending energy .....	191
8.5	Energy balance just after the failure .....	196
8.6	The machine losses .....	199

9.	NOTCHED BEAMS UNDER IMPACT	
9.1	Effect of hammer drop height on peak bending load .....	204
9.2	Effect of hammer drop height on energies ....	209
9.3	Effect of hammer drop height on fracture toughness .....	210
10.	FIBRE REINFORCED CONCRETE UNDER IMPACT	
10.1	Static behaviour of plain and steel fibre reinforced normal strength concrete .....	216
10.2	Dynamic behaviour of plain and steel fibre reinforced normal strength concrete .....	217
10.3	Static and dynamic behaviour of steel fibre reinforced normal strength concrete .....	219
10.4	Static behaviour of plain and polypropylene fibre reinforced normal Strength Concrete ...	221
10.5	Dynamic behaviour of plain and polypropylene fibre reinforced normal strength concrete ...	222
10.6	Static and dynamic behaviour of polypropylene fibre reinforced normal strength concrete .....	223
10.7	Behaviour of steel fibre reinforced concrete at variable stress rates .....	228
10.8	Static behaviour of plain and steel fibre reinforced high strength concrete .....	233
10.9	Dynamic behaviour of plain and steel fibre reinforced high strength concrete .....	234
10.10	Static and dynamic behaviour of steel fibre reinforced high strength concrete .....	235
10.11	Static behaviour of plain and polypropylene fibre reinforced high strength concrete .....	237
10.12	Dynamic behaviour of plain and polypropylene fibre reinforced high strength concrete .....	238
10.13	Static and dynamic behaviour of polypropylene fibre reinforced high strength concrete .....	240
10.14	Crack development in steel fibre reinforced concrete under impact .....	243

11.	CONVENTIONALLY REINFORCED CONCRETE UNDER IMPACT	
11.1	Effect of stress rate on conventionally reinforced normal strength concrete .....	249
11.2	Effect of hammer drop height on (a) peak bending load and (b) fracture energy of conventionally reinforced normal strength concrete .....	250
11.3	Energy at various midspan deflections absorbed by conventionally reinforced normal strength concrete beam with deformed bars ...	252
11.4	Beam section .....	253
11.5	Theoretically limiting and the experimentally observed moment of resistance	256
11.6	Effect of hammer drop height on (a) peak bending load and (b) fracture energy for normal strength concrete with smooth reinforcing bars .....	262
11.7	Energy at various midspan deflections for beams with smooth bars .....	263
11.8	Comparison between beams with deformed reinforcing bars and those with smooth reinforcing bars .....	265
11.9	Comparison between beams with stirrups and those without stirrups .....	268
11.10	Load vs. deflection plots for conventionally reinforced high strength concrete .....	271
11.11	Comparisons between normal strength and high strength beams .....	273
11.12	Tup load vs. time plot and velocity vs. time plot for high strength concrete under 0.5m drop .....	274
11.13	Tup load vs. time plot and velocity vs. time plot for high strength concrete under 1.5m drop .....	274
11.14	Tup load vs. time plot and velocity vs. time plot for normal strength concrete under 0.5m drop .....	275
11.15	Tup load vs. time plot and velocity vs. time plot for normal strength concrete under 1.5m drop .....	275

11.16	Comparison between normal strength and high strength concrete .....	276
11.17	Photographs showing conventionally reinforced beams after impact .....	278
11.18	crack development in a high strength conventionally reinforced concrete beam .....	280
12.	<b>CONVENTIONALLY REINFORCED CONCRETE CONTAINING FIBRES UNDER IMPACT</b>	
12.1	Effect of adding polypropylene fibres to conventionally reinforced normal strength concrete .....	283
12.2	Effect of adding polypropylene fibres to conventionally reinforced high strength concrete .....	286
12.3	Comparison between the effect of polypropylene fibres on conventionally reinforced normal and high strength concrete beams .....	289
12.4	Photographs showing conventionally reinforced normal strength concrete with fibres under impact .....	293
12.5	Photographs showing conventionally reinforced high strength concrete with fibres under impact .....	294

## List of Tables

1.	INTRODUCTION	
2.	OBJECTIVE AND SCOPE	
3.	LITERATURE SURVEY	
4.	EXPERIMENTAL PROCEDURES	
4.1	Types of specimens .....	46
5.	INERTIAL LOADING IN INSTRUMENTED IMPACT TESTS	
5.1	Effect of rubber pad on plain concrete beams under impact .....	107
5.2	Effect of rubber pad on conventionally reinforced concrete beams under impact .....	107
6.	PLAIN CONCRETE UNDER IMPACT	
6.1	Comparison between the dynamic properties of paste and concrete .....	115
6.2a	Static behaviour of normal strength plain concrete beams .....	120
6.2b	Dynamic behaviour of normal strength plain concrete beams .....	121
6.3a	Static behaviour of high strength plain concrete beams .....	131
6.3b	Dynamic behaviour of high strength plain concrete beams .....	132
6.4a	Effect of moment of inertia on the dynamic behaviour of normal strength concrete beams	.142
6.4b	Effect of moment of inertia on the dynamic behaviour of high strength concrete beams	...142
7.	MODEL ANALYSIS	
7.1	Beam properties for the attempted application of Model A .....	159
7.2	The constants in the constitutive law proposed for concrete .....	164
8.	ENERGY BALANCE IN INSTRUMENTED IMPACT TESTS	
8.1	Energy balance at the peak load (normal strength concrete .....	192

8.2	Energy balance at the peak load (high strength concrete .....	193
8.3	Energy balance just after failure (normal strength concrete .....	197
8.4	Energy balance just after failure (high strength concrete .....	198
9.	NOTCHED BEAMS UNDER IMPACT	
9.1	Behaviour of notched normal strength concrete beams .....	205
9.2	Behaviour of notched high strength concrete beams .....	206
9.3	Behaviour of notched normal strength concrete beams with polypropylene fibres ....	207
10.	FIBRE REINFORCED CONCRETE UNDER IMPACT	
10.1	Static behaviour of plain and steel fibre reinforced normal strength concrete .....	216
10.2	Dynamic behaviour of plain and steel fibre reinforced normal strength concrete .....	217
10.3	effect of moment of inertia on steel fibre reinforced normal strength concrete .....	219
10.4	Static behaviour of plain and polypropylene fibre reinforced normal strength concrete ...	221
10.5	Dynamic behaviour of plain and polypropylene fibre reinforced normal strength concrete ...	222
10.6	Effect of moment of inertia on polypropylene fibre reinforced normal strength concrete ...	223
10.7	Dynamic behaviour of steel fibre reinforced normal strength concrete .....	229
10.8	Static behaviour of plain and steel fibre reinforced high strength concrete .....	233
10.9	Dynamic behaviour of plain and steel fibre reinforced high strength concrete .....	234
10.10	Effect of moment of inertia on steel fibre reinforced high strength concrete .....	235
10.11	Static behaviour of plain and polypropylene fibre reinforced high strength concrete .....	237

10.12	Dynamic behaviour of plain and polypropylene fibre reinforced high strength concrete .....	238
10.13	Effect of moment of inertia on polypropylene fibre reinforced high strength concrete .....	240
11.	CONVENTIONALLY REINFORCED CONCRETE UNDER IMPACT	
11.1a	Static behaviour of conventionally reinforced normal strength concrete .....	246
11.1b	Dynamic behaviour of conventionally reinforced normal strength concrete, w/c ratio = 0.4 .....	247
11.1c	Dynamic behaviour of conventionally reinforced normal strength concrete, w/c ratio = 0.33 .....	248
11.2a	Static behaviour of conventionally reinforced normal strength concrete with smooth reinforcing bars .....	259
11.2b	Dynamic behaviour of conventionally reinforced normal strength concrete with smooth reinforcing bars, w/c ratio = 0.4 .....	260
11.2c	Dynamic behaviour of conventionally reinforced normal strength concrete with smooth reinforcing bars, w/c ratio = 0.5 .....	261
11.3	Static and dynamic behaviour of conventionally reinforced normal strength concrete with stirrups .....	267
11.4	Static and dynamic behaviour of conventionally reinforced high strength concrete .....	270
12.	CONVENTIONALLY REINFORCED CONCRETE WITH FIBRES UNDER IMPACT	
12.1	Static and dynamic behaviour of conventionally reinforced normal strength concrete with polpropylene fibres .....	284
12.2	Static and dynamic behaviour of conventionally reinforced high strength concrete with polypropylene fibres .....	287
12.3	Dynamic behaviour of conventionally reinforced pre-damaged concrete beams with and without polypropylene fibres .....	291

## LIST OF SYMBOLS

B: Breadth of the beam  
D: Depth of the beam  
l: Supported span of the beam  
h: Length of the overhanging portion of the beam  
A: The cross-sectional area of the beam  
 $D_1, D_2, D_3$ : The distances between the accelerometers  
 $V_h$ : Hammer velocity  
 $m_h$ : Hammer mass  
 $a_h$ : Hammer acceleration  
g: Earth's gravitational acceleration  
h: Height of hammer drop  
 $P_t$ : The tup load  
 $P_i$ : The generalized inertial load  
 $P_b$ : The generalized bending load  
 $\ddot{u}_0$ : Acceleration at the centre of the beam  
 $\dot{u}_0$ : Velocity at the centre of the beam  
 $u_0$ : Deflection at the centre of the beam  
 $\sigma_f$ : Failure stress  
 $\dot{\sigma}$ : Stress rate  
 $\epsilon_f$ : Failure strain  
 $\dot{\epsilon}$ : Strain rate  
 $K_{IC}$ : Critical Stress Intensity Factor  
a: Crack length  
 $f_{US}$ : Ultimate tensile strength of steel under static load

$f_{ud}$ : Ultimate tensile strength of steel under dynamic load

$A_s$ : Area of steel in the section

NS: Normal strength concrete

HS: High strength Concrete

$\Delta E$ : Energy lost by the hammer

$E_s$ : Energy gained by the specimen

$E_{ker}$ : Rotational kinetic energy in the specimen

$E_b$ : Bending energy in the beam

$E_{wof}$ : Work of fracture energy

$E_m$ : Energy lost to the machine

## ACKNOWLEDGEMENTS

First and foremost, I wish to thank Prof. Sidney Mindess, a dedicated researcher, for his friendly support, talent for organization, and invaluable guidance. His constant encouragement as my supervisor was much appreciated. My next acknowledgement must go to Prof. N.D. Nathan for his unstinting help. I am also very grateful to Dr. Arnon Bentur of the Technion, Israel for his invaluable support and guidance. My special thanks are also due to Dr. R.J. Gray, Dr. L.J. Gibson, and the late Prof. J.S. Nadeau.

The efforts of Mr. C. Town in preparing the specimens are greatly appreciated. I also wish to thank Mr.M. Nazar for maintaining the impact machine, and Mr. G.D. Jolly and Mr. R.B. Nussbaumer for designing and constructing the data acquisition system.

Finally, I take this opportunity to show my appreciation to my wife, Kavita, for her patience and support.

to my parents

## 1. INTRODUCTION

A structural engineer is required to predict the nature, duration and magnitude of the loading on a structure. On the other hand, he is also required to know the properties of the materials he is working with.

There are a number of types of loadings to which a structure can be subjected. Loadings can be divided broadly into two categories: dead loads or quasistatic loads, and suddenly applied loads. These are generally referred to as static loading and dynamic loading, respectively. Load prediction for static conditions is fairly straightforward and does not pose any particular problem. But in the case of dynamic loading, the precise prediction of load and its variation with time can be fairly involved.

Dynamic loading itself can be subdivided into two categories: single cycle and multicycle. An example of single cycle dynamic loading is a mass impacting against a structural element. However, a structure undergoing an earthquake would have its elements subjected to multicycle dynamic loading. Single cycle dynamic loading is called impact loading for brevity.

There are, further, two basic types of impact loadings: single point impact loading and distributed impact loading. A structure hit by a missile-like object would undergo a single point impact, whereas blasts or explosions would result in a distributed impact load. The present work is concerned primarily with single point impact loading.

One basic problem with single point impacts is the difficulty in assessing the exact load versus time history of the impact. As a result, energy values are generally chosen as the basic variable. The impact resistance of a material or a structure may be defined in terms of the energy the system is capable of absorbing before failure. While momentum or impulse could also have been chosen as the basic variable, they can easily be related to the energy; the calculation of one from the other is not difficult.

The size and the mass of the impacting body are very important in a typical impact event. Three distinct situations can arise:

1. A very large object struck by a small impacting mass.
2. An impact involving comparable masses.
3. A small object struck by a large impacting mass.

While the third case is comparatively rare, the first and second cases are often encountered. In the first case, because of the massiveness of the impacted object, damage is limited mainly to the contact zone. In the case of comparable masses, however, the response of the impacted mass is governed by shear and bending, and a relatively large portion of the impacted mass reacts to the impact. While the case of a small object hitting a massive target has been considered by many investigators, and solutions have been suggested in the form of empirical formulae, the case of impact between comparable masses, to date, remains

unsolved.

On the materials side, most materials have been found to be strain rate sensitive, thus further complicating the whole problem. The degree of strain rate sensitivity depends upon the loading system, support characteristics, environmental factors, and so on. Since the energy that a structure is capable of absorbing before failure depends upon its material properties, which, in the case of impact, depend upon the rate of stressing, the problem is one which cannot be solved without a thorough knowledge of the material properties.

Of all of the major materials of construction used today, the behaviour of concrete under high rates of strain is the least understood. The inherently brittle nature of plain concrete, its extreme weakness in tension, and its heterogeneous structure are some of the reasons for its markedly low impact strength. Its lack of toughness and tensile strength have meant that it is almost always used in conjunction with conventional steel reinforcement. But the discovery of fibre reinforced concrete (frc), and frc's greatly improved impact resistance over plain concrete, have triggered an interest in understanding the impact performance of both frc and plain concrete, since a proper understanding of the composite behaviour of frc calls for an understanding of its individual components.

With present design trends, there are two reasons for the incorporation of fibres in cementitious matrices: First,

since the impact resistance of these components is higher, they can withstand occasional shocks or overloadings without extensive damage. Secondly, the behaviour of frc under load, which is characterized by large postelastic deformations, means that failure, if it occurs at all, generally does so only after sufficient warning.

Experimental work, especially with instrumented impact machines, is being carried out by several investigators, but these instrumented impact tests have inherent problems, and the results can be grossly misleading if caution is not exercised in their interpretation. Inertial loading effects, energy loss predictions and so on are some of the problems which need consideration. The basic aim of the present work, therefore, was to develop a valid testing technique for testing concrete under impact, and to use such a technique to evaluate the impact behaviour of concrete. The various factors that affect the impact resistance of concrete, and the various reinforcing techniques that can be made use of in order to enhance its impact resistance were also investigated.

## 2. OBJECTIVE AND SCOPE

Concrete, with its heterogeneous composition and inelastic behaviour, behaves quite differently from other materials such as metals. The random distribution of fine and coarse aggregate particles throughout the hardened cement matrix and the nonlinear behaviour under loading, separate concrete from the much more homogeneous metals. It is the very structure and composition of concrete which impart its strain rate sensitive characteristics.

The present knowledge of the behaviour of concrete under high rates of loading is inadequate to explain its performance as a structural material when subjected to impact loadings. The strain rate sensitivity of concrete makes it improper to use its statically determined properties under high strain rate or impact loading. Moreover, the results obtained at low or intermediate strain rates may not be used to predict the behaviour under impact loading because, (a) no universally accepted rule exists for such an extrapolation, and (b) impact may not be regarded simply as a case of extreme strain rate application. Not only don't we understand plain concrete, we can't even begin to predict the behaviour of fibre reinforced concrete, and of conventionally reinforced concrete at high stress rates.

High stress rate testing of concrete necessitates a testing machine capable of generating high stress rates, a method of acquiring the data, and finally, a valid technique for analysing the test results. An instrumented drop weight

impact machine was designed and constructed for this purpose as described in Chapter 4. Load measurements were made at the point of the hammer-beam contact, and also at one of the supports. Three accelerometers mounted along the length of the beam were used to make the inertial load correction. An analysis was developed to evaluate the generalized inertial load from the accelerometer readings. Subsequent evaluation of the "true" or the generalized bending load and the fracture energy could be made using the observed tup load vs. time data and the integrated acceleration record. The support load measurements were compared with the evaluated generalized bending load as a check of the validity of the technique used in this study for inertial load correction (Chapter 4).

Considerable simplification is possible in the treatment of the impact data if some assumptions about the acceleration distribution along the length of the beam specimen can be made. In the present work, acceleration distributions were studied for plain, fibre reinforced, and conventionally reinforced concrete beams undergoing impact, and it is shown that simple mathematical functions may be used to define the acceleration distribution along the length of the beam (Chapter 4).

Rubber pads between the striking tup and the beam are sometimes used in order to reduce the inertial load oscillations. It has even been suggested that, with the proper pads, the inertial loading may be entirely

eliminated. The validity of these arguments has been examined in Chapter 5.

The testing program involved the testing of approximately 350 concrete beams under widely different stress rates. The lowest stressing rate chosen was that of quasi-static testing, using a conventional mechanical testing machine; the highest stressing rate was achieved using the highest possible hammer drop height in the impact machine, 2.30m. This gave a range of cross-head velocities from  $4.2 \times 10^{-7}$  m/sec to about 6.71m/sec.

Concrete is a conglomerate of randomly distributed aggregate particles bound together by hydrated portland cement. The overall properties of concrete depend upon the properties of the paste and on its bond with the aggregates. Thus, as a first step in the study of the strain rate sensitivity of concrete the behaviour of paste itself under impact loading was studied (Chapter 6). The effect of stress rate on the behaviour of plain concrete was also studied by subjecting plain concrete beams to stress rates associated with static loading and those associated with impact. The most important properties studied were the strength and the fracture energy (Chapter 6).

The role of microsilica (finally divided silica fume) in improving the static strength of concrete is well known. However, high strength concrete is also known to be more brittle than normal strength concrete. The effect of high strength (achieved by the use of microsilica) on the

properties of concrete subjected to varying stress rates was investigated. Of particular interest was the behaviour of high strength concrete beams under the very high stress rates associated with impact, and its comparison with normal strength concrete (Chapter 6).

Analytical prediction of concrete behaviour under high stress rates requires a model and some assumptions regarding its behaviour. A constitutive law for concrete with the applied stress rate as an independent variable was proposed. With the proposed constitutive law, the behaviour of a beam under an external load pulse was determined using a single degree of freedom model and the time step integration technique (Chapter 7).

The concept of energy balance, which has its basis in the law of conservation of energy, was examined in the case of plain concrete beams undergoing impact. The energies lost by the hammer up to the peak external load, and just after the completion of the impact event, were compared to the energy gained by the beam in various forms. The machine losses, if any, were computed (Chapter 8).

Concrete is a brittle material, and as such the strength of a concrete element under tension or flexure is determined by the size of the largest flaw present. Stresses in the vicinity of the tip of a flaw can be expressed in terms of basic fracture mechanics parameters. However, the critical value of the fracture toughness ( $K_{IC}$ ) depends, amongst other things, upon the rate at which the load is

applied. This stress rate dependence of  $K_{IC}$  was investigated for normal strength, high strength, and fibre reinforced concrete using notched beams subjected to both static and impact loading. The common belief that the fibres retard crack propagation by acting as crack arresters was also examined (Chapter 9).

The use of fibres has proven to be of importance in improving the "ductility" of concrete. This desirable contribution of fibres is particularly welcome in impact loading situations, where a large amount of energy is suddenly imparted to the structure, demanding a high energy absorption capacity from its elements. Steel and polypropylene fibre reinforced beams were subjected to impact and the strength and fracture energy values thus obtained were compared with those obtained under static loading. Comparison was also made with beams without fibres (Chapter 10).

The low strength of concrete under tension has led to its use almost always in conjunction with reinforcing steel. In spite of the advantages of adding fibres, they cannot replace conventional reinforcing bars. Strategically placed reinforcing bars have performed better than randomly distributed fibres in terms of both strength and ductility in static situations. However, very little is known about the performance of conventionally reinforced concrete under impact. To examine this, conventionally reinforced beams were subjected to impact with varying hammer drop heights,

and their impact performance was compared with their static performance. Both deformed and smooth reinforcing bars were tested. Conventionally reinforced concrete beams made with high strength concrete were also tested (Chapter 11).

Confinement has been found to increase the ductility of concrete under static loading. The effect of confinement under impact loading was examined by confining conventionally reinforced concrete using rectangular stirrups, and subjecting the resulting specimens to both static and impact loading (Chapter 11).

The effects of a combination of conventional reinforcement and fibre reinforcement were also studied, using both normal and high strength concretes. Such combinations are known to be very effective in static loading, and an attempt was made to evaluate this combination under impact loading (Chapter 12).

A structural element is required to carry dead and live static loads on a continuous basis. Thus, in practice, at the time of impact the elements will already have been subjected to static loading. Since the appearance of tension cracks in concrete is allowed by most design codes, the element may be pre-damaged before it is subjected to impact. To check the performance of beams pre-damaged by static loading, such pre-damaged beams were subjected to impact and their performance was compared to that of undamaged beams. The effect of fibre reinforcement on preserving the integrity of the predamaged beams undergoing impact was also

studied (Chapter 12).

The failure of concrete is caused by the propagation of cracks. Under load, micro-cracks in the concrete grow and coalesce into macro-cracks that propagate to cause separation. Once unstable propagation of cracks begins, the behaviour of the element depends upon the mode in which the crack propagates, the velocity of the crack, crack branching, and so on. In the case of impact, since the entire event takes place in a fraction of a second, the propagation of the crack cannot be observed with the naked eye. One has therefore to resort to high speed photography to observe the crack propagation. High speed photography was carried out using a motion picture camera running at 10,000 frames per second on hydrated cement paste, steel fibre reinforced concrete, and conventionally reinforced concrete beams. The films were then viewed frame by frame in a small hand viewer to study the crack propagation, crack velocities, crack branching, and the crack arrest due to the presence of the fibres. (Chapters 6, 10, and 11).

The present study, thus, was directed towards: (a) The development of a valid testing method to test concrete beams under impact loading, and (b) The assessment of the impact resistance of plain, fibre reinforced, and conventionally reinforced concrete beams using such a testing method. The output from the testing program is more in the form of trends, and less in the form of basic material properties, although an attempt has been made to evaluate the basic

material properties wherever possible.

### 3. LITERATURE SURVEY

#### 3.1 INTRODUCTION

The possibility of a structure being subjected to impact, accidental or otherwise, has long been recognized. A structure as a whole, or a particular structural component, could be called upon to sustain the large amount of energy imparted to it by a sudden application of load. In order to design a structure for dynamic loading, we should be able to assess the energy absorbing capacity both of the individual components of the structure, and of the entire structure itself. For example, to assess correctly the energy absorption of a structure when subjected to earthquake loading, we should know the basic material properties at the strain rate in question. In addition to the material properties, we also need to know the failure mechanisms and the various energy dissipating mechanisms.

Unfortunately, our knowledge of the behaviour of cementitious materials is still largely qualitative. Although some work at high strain rates has been carried out, the quantitative side is far from clear. This may be due to the wide variations observed between different experimental investigations, which often result in contradictory conclusions. Our present knowledge, and consequently our design practice as such, are still at least partly empirical in nature. In the absence of a better understanding of the reaction of the impacted structure to the external impact load, nothing can be said with certainty. The stress

distribution in an impacted mass of plain concrete or fibre reinforced concrete is far from simple, due mainly to the heterogeneous internal structure, the variable distribution of strains, the steep strain gradients, and the poorly characterized interface between the cement and the aggregates. It is also worth noting that in many instances a correct estimation of the external load and its variation with time is also not possible. The input load function, which among other things depends upon the precise manner in which the impacted body absorbs the incident energy and on the relative masses of the bodies colliding, forms an important area of study. The input in the form of the external load function and the output, in the form of the structural response, are thus highly interdependent. Mainstone and Kavyrchine (1), Struck and Voggenteiler (2), and Kavyrchine and Struck (3) have cited examples of impact and impulsive loading that may possibly occur in practice and the consequences that may follow. They have also described the problems associated with the evaluation of the impact response of structures. In the case of impact loading, the response of the structure can be divided into two types: local response and overall response (3). Depending on the relative masses of the impacted and the impacting bodies, the overall structural response may or may not be significant. The case of a very small object hitting a very large mass, which is particularly interesting from the military point of view, is a case in which the local

response is critical.

The National Defence Research Committee (NDRC) has proposed various empirical formulae to estimate the penetration depths ( $x$ ) for the case of nondeformable cylindrical missiles impacting concrete masses. The general form of the formulae is

$$x=f(k,W,d,V) \quad (3.1)$$

where

$k$  is a constant,

$W$  is the missile weight,

$d$  is the diameter of the missile,

and  $V$  is the velocity of the missile.

Sliter(4) found the NDRC formulae to work satisfactorily for high velocity impacts; for low velocity impacts the observed penetrations were much smaller than the predicted ones. Also, these formulae do not apply to deformable missiles (4). NDRC formulae do not consider any reinforcement present in the impacted body, thus making the differentiation between a reinforced target and an unreinforced target an impossibility. Various other investigators have also presented independent empirical formulae based on their experimental findings, but a universally accepted formula does not exist.

### 3.2 IMPACT TESTING

So far, no results of full scale impact tests on buildings or other structures are available, but various investigators have subjected structural elements made of cementitious materials (e.g., flexural members, compression members, tension members, and slabs) to dynamic loadings. Attempts were made to ascertain the energy absorbing capacities of the cementitious materials under variable strain rate loadings. The various methods employed by these investigators (5,6) include: free fall drop weight tests, explosive tests, Charpy or Izod tests, Hopkinson split bar tests, and the use of fracture mechanics as an analytical tool. Unfortunately, the earlier tests of this type were not fully instrumented; investigators now realize that much important information can be lost in the absence of proper instrumentation. Most of these tests were directed at finding 'work of fracture' values, or 'toughness'. Attempts were also made to obtain the basic material properties, such as the constitutive laws in compression or tension, critical stress intensity factors, and the critical strain energy release rates.

The extent to which useful information can be derived from these variable strain rate tests depends upon our general understanding of the process of loading at high stress rates and of the energy transformations and dissipations occurring during a test. The data obtained from an instrumented impact test may be very misleading if proper

caution in not exercised in their interpretation. The most basic form of instrumentation provided in any of these instrumented impact tests is the instrumentation of the striking head or 'tup'. This form of instrumentation is often supplemented by instrumented anvils (specimen supports) or by instrumented specimens. The strain gauges provided in the striking head generate a time-base signal which, with proper calibration, can generate the load vs. time record of the impact. This load vs. time record of the impact can then be used to obtain the impulse acting against the moving tup, which in turn can be used to obtain the energy lost by the tup (7). Other information obtainable from the load vs. time trace includes the maximum load occurring in an impact, which is useful from the strength calculation point of view.

Many investigators have realized that these tests are not free from parasitic effects such as inertial loading effects. A major part of the tup load, at the beginning of the impact event, is used up in accelerating the specimen from rest. Thus, not all of the tup load acts upon the specimen as the bending load. This is termed the "inertial loading effect". Cotterell(8), and later others (9-12), noticed an initial discontinuity in the load vs. time traces obtained from impact tests on metallic specimens. This discontinuity was explained by Cotterell (8) using elastic wave theory. He argued that the compression wave in the striking head is reflected as a tension wave from the free

boundaries of the striker. Radon and Turner (10) later found that the nature of the discontinuity observed in the load vs. time curves was the same even for tups with different configurations.

A clear picture of inertial loading is presented by Saxton, Ireland and Server (13) and by Server (14). The inertial loading in the instrumented impact tests is characterized by oscillations about the actual beam deformation load in the load vs. time curve. The magnitude of this deviation of the apparent tup load signal from the actual beam deformation load depends on the masses involved, the velocity of impact, the stiffness of the contact zone, and so on. Server (14) recommended that reliable measurements should be made only after three oscillations of this type. However, in the case of brittle materials such as concrete, it may not be possible to avoid failure during the first inertial oscillation. Thus, the guidelines suggested by Server (14) can not be met. As a result, the entire mechanical response of the beam may be overshadowed by its inertial response. The interpretation of the test results in the case of concrete, thus, may be very different from that of metallic materials where the time to fracture is normally very long.

Remedies to the problem of inertial loading have been presented by various investigators. These remedies may be broadly classified into two categories: analytical and experimental. It is worth noting here that each method has

its own underlying and simplifying assumptions, and thus no universally applicable method yet exists.

Saxton et al (13) conducted instrumented impact tests on different materials. They reported a linear dependence of the maximum inertial load upon the initial velocity, and a systematic increase in the maximum inertial load with an increase in the acoustic impedance of the material tested. Thus they concluded that the initial impact load is governed by elementary elastic wave mechanics. They extended the argument further, by proposing a series of tests on steel specimens with known properties, thus evaluating the test machine parameters in order to estimate the inertial load for any other material to be tested. The equations proposed by them are therefore restricted to their particular machines and instrumentation.

Venzi, Priest and May (12) modelled the beam as having pure rotatory motion and zero transverse stiffness. They also assumed that the inertial load per unit length was proportional to the displacement from the mean position. They thus determined the reaction of the tup and the anvils to this inertial load from a knowledge of their respective spring constants. Knowing these reactions, the actual bending load was calculated using statics.

Radon and Turner (10) also suggested an approximate correction for inertial load in instrumented impact tests. They assumed that the acceleration of each particle in the beam was a constant with time, as a function only of its

position along the beam. They obtained the inertial force acting on an infinitesimal element as a function of the displacement at the instant of failure. Then, considering the problem as one of a beam on elastic foundation, with the inertial loading as the foundation reaction, they solved for the deflected shape as a function of the tup load and the other physical parameters. Once the deflected shape was known, it could be used to find the bending moment in the centre. This was finally equated to the bending moment of a simply supported beam and the value of the actual bending load was obtained.

On the experimental side, evaluation and subsequent elimination of the parasitic effects involved resorting to more sophisticated instrumentation. An estimation of the actual bending load on the beam undergoing impact was attempted by Gopalaratnam, Shah, and John (15), by instrumenting the anvils. The difference between the recorded tup load and the recorded anvil load yielded the inertial load on the beam.

Hibbert (7) tried to eliminate the effect of inertial loading from the energy computations by measuring the kinetic energy acquired by the broken halves of the beam. The Charpy specimens in Hibbert's tests were secured at the two ends by means of specimen holders and these specimen holders were allowed to rotate after fracture against a spring and ratchet system.

Suaris and Shah (16) introduced a rubber pad between the tup and the beam and subsequently showed that the difference between the bending load and the tup load was reduced because of this modification to the test system. The procedure adopted by Suaris and Shah has two points worth noting. First, the introduction of the rubber pad significantly reduced the applied strain rate. Secondly, a large amount of energy was absorbed in the elastic deflection of the rubber pad, which should have been considered while calculating the bending energy of the beam.

Another major problem that occurs in interpreting results of instrumented impact tests is the problem of the energy balance. In an instrumented impact test the energy as obtained by integrating the load vs. time plot is a measure of the total energy expended by the hammer. Obviously, not all of this energy is spent in creating new fracture surfaces. Most of the energy is consumed in secondary effects. An exact evaluation of this energy loss is impossible, which means that the energy balance equation can never be fully satisfied. The generally accepted energy balance equation(17,18) is,

$$\Delta E_0 = E_s + E_m + E_{vib} + E_{kpf} + E_{wof} + E_{raf} \quad (3.2)$$

where,

$\Delta E_0$  is the total energy obtained from the

load vs. time record,

$E_s$ ,  $E_m$  are the strain energies imparted to the specimen and the machine, respectively,

$E_{vib}$  is the vibrational energy of the specimen,

$E_{kpf}$  is the kinetic energy prior to fracture of the specimen,

$E_{wof}$  is the work of fracture,

and  $E_{raf}$  is the rotational kinetic energy after fracture.

Abe, Chandan and Bradt (17) attempted an evaluation of the total energy loss. The load point deflection, obtained as the product of the average velocity and the total time to fracture, was used to evaluate the total deflection at fracture. Knowing the compliance of the specimen and the maximum load, the compliance of the hammer could be calculated. This could conveniently be used, then, to evaluate the strain energy in the machine. Lueth (18) and Iyer and Miclot (19) have also described the method of applying the compliance correction to the measured gross energy values.

When the energy balance concept is applied to concrete, additional problems arise. First of all, a compliance correction requires a knowledge of the properties of the material being tested at a high strain rate. For concrete our understanding of these properties is only qualitative, so the compliance of the specimen can not be calculated

accurately. A second problem in the case of concrete, which was not considered by the above investigators, is the complicated nature of the contact zone. With crushing occurring in the contact zone, the energy balance equation has to incorporate an additional term,  $E_{\text{cru}}$ , which may be substantial but unfortunately is very difficult to evaluate. This crushing also renders the entire compliance correction procedure doubtful.

One major problem with applying the energy balance concept to concrete is the interchangeability of the various energies involved. Obviously, the strain energy of the specimen appears, at least in part, as the work of fracture. Quite possibly some of the strain energy too is used to reach the post-fracture velocity, and some of the kinetic energy to form the fracture surfaces. With this hazy picture on the energy front, only approximate evaluations are possible with our present understanding of the problem.

### 3.3 VARIABLE STRAIN RATE TESTS ON PLAIN CONCRETE

Basic studies of cement paste, of mortar, and of concrete have revealed the inherently brittle nature of these materials. To exacerbate the situation, these cement-based construction materials have very low tensile strengths. The weakness of concrete under tensile stress, and its low failure strain, have meant that concrete has a very low toughness; the toughness of some metals may be almost three orders of magnitude higher than that of

concrete. Moreover, concrete is strain rate sensitive. Its properties were found to vary with stress application rates. Variation was found not only between different stress application rates, but also between various stress application systems at the same stress rate. This has made the problem all the more complicated.

A number of attempts have been made to assess the behaviour of cement-based materials under varying strain rates. Concrete, in the form of compression, tension, or flexural specimens has been subjected to increasingly high strain rates, and the various strength and energy values determined.

Possibly the first experimental study was that of Abrams (20) in 1917, who subjected concrete cylinders to impact compression loading and observed an increase in the impact strength over the static strength. Abrams also observed that the rate at which the first 88% of the ultimate load was applied did not have any effect on the compressive strength. Many other investigators have also concluded that at least the first 50% of the load can be applied at any rate without affecting the ultimate strength.

Watstein(21), by performing compression tests on concrete at variable strain rates ( $10^{-6}$  to 10/sec) found that the ratio of the dynamic to the static strength was substantially greater than unity. He also observed that this ratio for strong concrete did not differ much from that for weak concrete. The failure strains at high rates of loading

were higher than their static counterparts. Similarly, the secant modulus and maximum load were considerably higher in the case of higher strain rates.

Green(22) used the type of cement, the type of coarse aggregate, shape of the coarse aggregate, curing conditions, sand grading, mix proportion and the age of the specimens as the independent variables in evaluating the performance of concrete at variable strain rates. Contrary to Watstein's (21) findings, he found that the ratio of the impact to static strength increased with the static strength of concrete. Concrete with angular aggregates showed a higher impact strength than the concrete with rounded and smooth aggregates. The water-cured specimens showed higher impact strengths than the ones that were air cured.

McNeely and Lash(23) determined the effect of the loading rate on the tensile strength of concrete. They found a linear relationship between the modulus of rupture ( $f_t$ ) and the rate of loading (R), given by

$$f_t = A + B \log_{10} R \quad (3.3)$$

where A and B are constants.

Atchly and Furr (24) performed compression tests under both static and dynamic conditions at 0.05 to  $12 \times 10^4$  MPa per sec. They also found that the compressive strength, energy absorption, secant modulus and the strain at failure increased with an increase in the strain rate. Contrary to Watstein's (21) findings, they found the compressive

strength and the energy absorption to reach a constant value at higher rates of loading.

Goldsmith, Kenner and Ricketts (25) used ballistically suspended Hopkinson split bars to test concrete with different aggregates. Grain cleavage in the aggregate particles of diorite was found to be responsible for the high energy absorption capacity of concrete made using this aggregate. Strains, when measured for exposed aggregates, and for the matrix, (at the same longitudinal positions along the bar) seemed to have lower values at the aggregate location than at the matrix location. This suggested that the aggregates were the deciding factor in the stiffness of concrete.

Birkimer and Lindemann (26) have shown that the critical fracture strain energy theory provides a meaningful fracture criterion. They also found that the critical fracture strain is directly proportional to the strain rate raised to the one-third power.

Hughes and Gregory (27) used "low friction" pads to reduce the platen friction in the case of dynamic compression tests on concrete prisms. The load column method was used to develop high strain rates of up to 30/sec, and a value of 1.9 was found as the ratio of dynamic to static strength. This ratio was found to be largely independent of the water-cement ratio, age, and cement content, but dependent upon the type of coarse aggregate.

Sparks and Menzies (28) tested concrete prisms in uniaxial compression under both static and fatigue loading. The sensitivity of the static strength to the rate of loading was found to be related to the stiffness of the aggregate used. Lytag, the least stiff of all the aggregates, was found to be the most rate sensitive; limestone, the stiffest aggregate, was found to be the least rate sensitive. They also found that this strain rate dependence could be expressed as

$$\sigma_f = C + n \log \dot{\sigma} \quad (3.4)$$

where

$\sigma_f$  is the failure stress

$\dot{\sigma}$  is the stress rate.

and C and n are constants.

Hughes and Watson (29) tested concrete cubes with varying mix proportions and two different types of coarse aggregates under compressive impact loading (strain rates up to 17/sec). They found that the ultimate strains decreased with an increase in the stress rates, opposite to the findings reported in (24) and (26). This was attributed to the absence of creep strains for high strain rate loadings. Also, the crack propagation path in the high strain rate tests was much straighter than that in the low strain rate tests. Aggregate failures were observed more in the impact tests than in the static tests. In the static tests the crack was found to propagate around the aggregate but never

through it. They considered this as the reason for the large energy requirement in the impact tests.

The fracture mechanics approach to rate of loading effects involves a combination of the classical Griffith theory with an empirical relationship describing the sub-critical crack growth (30). According to the concept of sub-critical crack growth, under a sustained load, a crack of sub-critical size will eventually grow to the critical size, and failure will then occur. The velocity of such a growing crack is given by

$$V = AK_I^n \quad (3.5)$$

where

$V$  is the crack velocity.

$K_I$  is the stress intensity factor.

$A, n$  are constants.

In the case of rapid loading, a sub-critical crack simply does not have enough time to grow to the critical size, and hence the specimen can support a higher load. The three different ways of determining the constant  $n$  in Equation 3.5 are given in Figure 3.1. Figure 3.1(a) represents a constant load test, with  $\sigma_c$  the applied load causing failure and  $\tau$  the time to failure. Figure 3.1(b) corresponds to the direct observation of the growing crack and Figure 3.1(c) is the outcome of a constant rate of loading test.

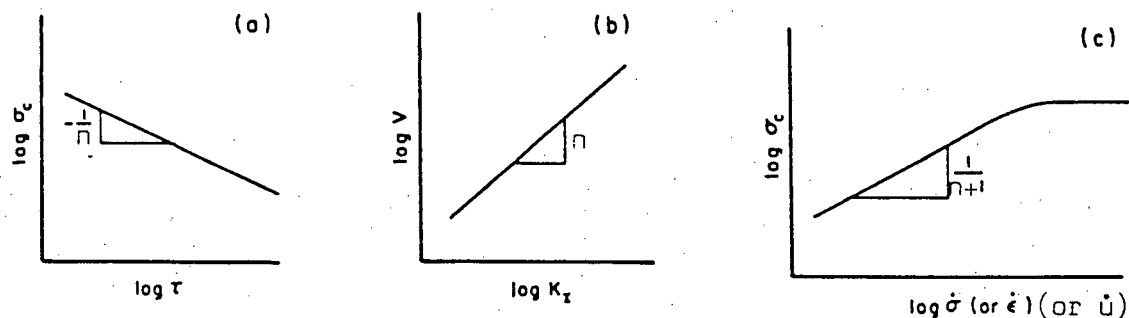


FIGURE 3.1—Three different ways of determining the constant "n"

Mindess and Nadeau (31) tried to compare the slope ( $n$ ) of the  $\log V$ - $\log K_I$  plot, obtained from controlled crack growth in double torsion tests, with the slope of the  $\log \text{MOR}$ - $\log \dot{u}$  plot (Figure 3.1(c)), where  $\dot{u}$  is the displacement rate. They found that  $n$  was almost the same in the case of mortar, but that there was a discrepancy of a factor of two for the cement paste. They also analyzed the data obtained by the other investigators in order to find the value of  $n$  in each case. It was found that  $n$  was larger for compression tests than for tension and flexural tests.

Zech and Wittmann (32) attempted to find the distribution function of the flexural strength of mortars at varying strain rates. A missile falling on the flexural mortar specimens was employed to generate strain rates of

about 2/sec. The theoretical approach developed by Mihashi and Izumi(33), which relates the ratio of the dynamic to static strengths to the rates at which these strengths were measured was found to describe the results satisfactorily:

$$(f_d/f_s) = (\dot{\sigma}_d/\dot{\sigma}_s)^{1/(1+\beta)} \quad (3.6)$$

where

$f_d$  and  $f_s$  are the dynamic and the static strengths, respectively,  
 $\dot{\sigma}_d$  and  $\dot{\sigma}_s$  are the dynamic and the static stress rates, respectively, and  
 $\beta$  is a material parameter.

The parameter  $\beta$  was found to increase with an increase in the strength of concrete. Thus stronger concretes were predicted to be less strain rate sensitive than weaker ones. Zech and Wittmann (32) also found that the variability was not influenced by the rate of loading.

Suaris and Shah(34) performed instrumented variable strain rate tests (strain rates from  $0.67 \times 10^{-6}$  to 0.27) on mortar using a flexural testing system. They noted that, in general, the higher the static flexural strength, the lower was the relative increase in the flexural strength with increasing strain rate. They deduced that on a comparative basis, the tensile response was the most strain rate

sensitive, the compressive response the least strain rate sensitive, with the flexural response lying somewhere in between. They tried to find the value of the parameter  $n$  in Equation 3.5. However, on the basis of the observed data, they found that  $n$  did not seem to be a constant; rather, it decreased with increasing strain rate.

Zielinski and Reinhardt (35) and Zielinski (36) used the split Hopkinson bar technique in order to investigate the tensile stress-strain behaviour of mortar and concrete at high stress rates (5000-30000 MPa/sec). They concluded that the remarkable increase in the tensile strength of concrete and mortar at high stress rates was due to the extensive microcracking in the whole volume of the stressed specimen. To support this argument they observed that the ultimate strains at higher stress rates were also higher. Moreover, the specimens subjected to high rates of stress fractured at more than one place along their lengths. The difference between the impact strength of concrete and mortars was explained on the basis of the direct crack arresting action of the aggregates. It was also postulated that in the case of very rapid loading, since much energy was introduced into the system in a short time, cracks are forced to develop along the shorter paths of higher resistance, through stronger matrix zones and also through some aggregates.

Alford (37) studied the behaviour of a crack, i.e., its velocity and its path, as the crack approaches a disturbance

(e.g. an aggregate or a void). An 'around the aggregate mode' and a 'through the aggregate mode' were recognized for crack propagation. The main factors determining the mode were found to be the angularity and the toughness of the aggregates. High speed photography results showed that the observed crack velocity was much less than the theoretical Rayleigh wave velocity. As a result, the dynamic value of the critical strain energy release rate ( $G_d$ ) was found to be approximately the same as the static value ( $G_s$ ).

#### 3.4 VARIABLE STRAIN RATE TESTS ON FIBRE REINFORCED CONCRETE

The poor impact resistance of plain concrete has led to the incorporation of fibrous substances into the basic brittle cementitious matrix to enhance its impact performance. Initially, these fibres were thought to increase the strength of the composite, but it was soon realized that the major advantage in adding these fibres was not in the enhanced strength, but in enhanced ductility. This enhanced ductility of the composite may be particularly useful in situations where accidental impacts can occur and the energy absorption capacity of the structure must be considered in design. Thus, various investigators started studying the composite behaviour of fibrous concrete at variable strain rates.

Shah and Rangan (38) conducted static tests on fibre reinforced concrete specimens in tension, flexure, and compression and concluded that the basic advantage derived

from the fibres occurred only after the matrix cracked. Bond strength of fibres was found to be a very important factor.

Naaman and Shah (39) carried out pull-out tests on steel fibre reinforced concrete in order to study the effect of fibre orientation and fibre grouping on the peak pull-out load, the ultimate load and the pull-out work. They found that the mechanism of fibre pull-out in the case of straight fibres is very different from the mechanism in the case of inclined fibres. The performance of a group of fibres pulling out of a matrix could not always be estimated by knowing the performance of a single fibre. This was because of the increased spalling and disruption of the matrix with an increase in the number of fibres. Thus the efficiency of a group of fibres was less than that of a single fibre. They finally concluded that this effect should be more pronounced in the case of inclined fibres because more matrix crushing is involved in this case.

Kobayashi and Cho (40) considered the flexural behaviour of polyethylene fibre reinforced concrete and found the fibres to be useful in improving the toughness of the composite. The strain rate sensitivity of the composite was also measured by the authors.

Bhargava and Rehnstrom (41) tested plain concrete, polymer cement concrete and polypropylene fibre reinforced concrete under high rates of compressive loading. They made use of the principle that for viscoelastic materials there is an optimum stress transmission limit. If the material is

subjected to stress above this limit, the excess energy is dissipated in fracture and failure, and results in no increase in the transmitted stress. They found that polymer cement concrete had 30-35% higher dynamic strengths than plain concrete. For fibre reinforced concrete the increase was about 15%.

Ramakrishnan et al (42) presented a comparative evaluation of two types of fibres. The performance of straight 25mm long steel fibres was compared to 50mm long steel fibres with deformed ends. The fibres, held together by a water soluble glue before mixing, were found to be free from tangling or balling. Hooked fibres were also found to produce higher flexural strength, higher load carrying capacity, higher ductility and higher impact strength.

Jamrozy and Swamy(43) described their experience with the application of steel fibre reinforced concrete in building machine foundations that were subjected to impact loading. They designed a free fall drop weight impact tester capable of repeatedly dropping a mass on a standard specimen until a predetermined failure criterion was reached. Fibres in general were helpful in increasing the impact performance of concrete. The fibre volume, fibre geometry and fibre size were all found to influence the impact strength. They also found that for a given fibre geometry and size, there existed an optimum fibre volume, which gave the maximum efficiency. Some actual foundations were instrumented, and it was found that the use of fibre reinforced concrete was

really useful. They also concluded, however, that fibres cannot replace conventional reinforcement.

Radomsky (44) discussed the construction and the use of a rotating impact machine to investigate the impact properties of concrete reinforced with straight round steel fibres. He concluded that the impact resistance of these composites increased with increasing velocity of impact, and also with the angle of impact with respect to the fibre direction. One-dimensional orientation of fibres was found to give about twice the impact strength of two-dimensional fibre orientation. A comparison of rotating impact machine data with Charpy impact data revealed that these data cannot be compared. This clearly demonstrates the influence of the type of machine on the results obtained.

Hibbert (7) and Hibbert and Hannant (45) used an instrumented Charpy impact machine to study the behaviour of fibre reinforced concrete under impact loading. They calculated the total energy lost by the pendulum from the load vs. time plot and also independently from the residual pendulum swing. These two values were found to be in agreement. They also attempted to calculate the energy losses during impact. The kinetic energy of the broken halves of the specimen was determined by allowing the specimen holders to rotate after fracture against a spring and ratchet system. On the basis of their results, they concluded that for fibre reinforced materials, the energy absorbed after the matrix had cracked was not substantially

different under slow flexure than that obtained under impact conditions. Thus strain rate, they concluded, had no effect on fibre-matrix bond properties. The matrix failure strain was also found not to be sensitive to strain rate. These findings, when put together, indicated that the energy absorbing properties of fibre reinforced concrete under impact conditions could also be reasonably estimated by performing conventional static tests and by measuring the area under the load vs. deflection curves. The authors used a variety of steel and polypropylene fibres. Amongst the steel fibres, the crimped fibres and the hooked end fibres were found to be the best. Polypropylene was not found to be as effective as the steel fibres.

Gokoz and Naaman (46) carried out pull-out tests on steel, glass and polypropylene fibres at various rates of loading from a portland cement mortar matrix. The entire process of pulling out in the case of steel fibres was modelled as comprising a first peak denoting a combination of bond failure and friction, a second peak which was only friction dependent, and a final peak corresponding to final tilting of the specimen due to the uneven pull out resistance of different fibres. Steel fibres at all strain rates were found to pull-out, while the glass fibres were found to break. With an increase in the strain rate, the polypropylene fibres had an increasing percentage of fibres being pulled out. For all of the fibres tested, no substantial increase in the first peak load with increasing

strain rate was observed. The same was true for the second peak. On the energy side, steel and glass fibres did not show any change in the pull-out energy with changing strain rate. On the other hand polypropylene fibres showed a dramatic increase in the pull-out energy with an increase in strain rate.

Knab and Clifton (47) studied the cumulative damage of steel fibre reinforced slabs subjected to repeated impact. The crater depth measured right under the point of impact was found to be a good indicator of the cumulative damage. The addition of steel fibres was found to increase the total number of blows to failure considerably.

Suaris and Shah(34) compared the performance of plain concrete and plain mortar with their steel, glass and polypropylene fibre reinforced counterparts. They found that the flexural strength (MOR) of both steel and glass fibre reinforced mortars was more strain rate sensitive than that of the mortar matrix itself. Polypropylene fibre reinforced mortar, on the contrary, was apparently not strain rate sensitive. The energy absorption values of fibre reinforced mortar with various fibres, subjected to impact, were found to be 7 to 100 times larger than those of the unreinforced matrix.

Naaman and Gopalaratnam (48) also studied the strain rate sensitivity of steel fibre reinforced mortar. They concluded that an increase in the aspect ratio and fibre volume, in general, increased the strain rate sensitivity.

The increase in the composite flexural strength and energy absorbed with increased loading rate was attributed primarily to the strain rate sensitivity of the matrix and the pull-out resistance of the fibres.

Gopalaratnam et al(15) used a modified instrumented Charpy machine for testing cement based composites at higher rates of loading. They observed an increase of about 60% in the MOR when the strain rate was increased from  $10^{-6}$ /sec to 0.3/sec. The peak strains recorded showed an increase at higher rates of loading. The secant modulus was also found to increase at higher rates of loading, which was attributed to a decrease in the amount of microcracking at higher rates of loading.

Harris et al (49) tested cement/sand mortar beams reinforced with short randomly distributed fibres of glass, high carbon steel, and mild steel in bending, and determined the value of the work of fracture ( $\gamma_f$ ), and the critical stress intensity factor ( $K_c$ ). The critical stress intensity factor, which depends upon the peak load obtained and the specimen geometry was found to increase by a factor of two. The work of fracture, on the other hand, which considers the entire load vs. deflection plot, was found to increase by as much as an order of magnitude, when plain concrete was compared with fibre reinforced concrete.

Thus, on the basis of the literature survey, the following conclusions may be made:

(a) Results obtained by the various investigators are often contradictory. For example, Hibbert (7) has found that the strain rate has no effect on the properties of fibre reinforced concrete; most others find that this is not so.

(b) No general agreement over the phenomena responsible for strain rate effects exists.

(c) No general agreement over the magnitudes of the observed effects exists.

(d) The effects seem to depend on the type of test and the type of interpretation.

Thus, the nature of the impact behaviour of even a cementitious matrix is not well understood, let alone the impact behaviour of frc.

## 4. EXPERIMENTAL PROCEDURES

### 4.1 INTRODUCTION

Destructive tests on concrete have been in use for many years. However, strength is not a fundamental material property; it depends upon how it is measured. The mechanical properties of concrete have been found to depend upon, amongst other things, the geometry of the specimen, the stiffness and type of testing machine, loading configuration, moisture content, temperature, and the rate of loading. The effect of the rate of loading, which was probably first pointed out by Abrams(20) in 1917, has recently become a major area of investigation. Many investigations have recently been carried out to study the rate of loading, or the stress rate effect on the properties of concrete. Unfortunately, while for the static properties there are a number of standard test methods, no such standard test method exists for concrete under high rates of loading, or under dynamic conditions.

High stress rate testing on any material is based on suddenly imparting a large amount of energy to the test specimen. In most impact machines potential energy is stored in a spring, a pendulum, a hammer, or a simple ball, and this stored energy is transferred to the specimen over an extremely short interval of time. The specimen deforms in response to this energy transfer, leading to the development of high stresses in the specimen over a very short length of

time. But, there is a limit to the amount of energy any material can absorb as strain energy before failing. If the externally available energy exceeds this limit, failure will result. Various techniques have been used to test concrete at high stress rates. The most common are:

- (a) Free fall drop weight tests;
- (b) Work of fracture tests;
- (c) Explosive tests;
- (d) Hopkinson's Split Bar test;
- (e) Charpy/Izod tests; and
- (f) Fracture mechanics tests.

In all of the above test methods, there is an attempt to quantify the energy required to achieve failure. However, because both the failure criteria and the physical processes by which failure occurs vary from test to test, comparisons between any of these tests is very difficult.

In the Charpy tests, a pendulum bob is used to store potential energy, which is suddenly transferred to the specimen when the pendulum is released. Historically, the Charpy machine was developed primarily for testing metals. Thus, when this test method is used for concrete, modifications have to be made. First, the specimen holders have to be modified in order to hold the much bigger concrete specimens. Another modification is in the form of strain gauges mounted in the striking end of the pendulum (7), in the specimen supports, and possibly on the specimen

itself. The monitoring of the load developed in the instrumented pendulum bob permits an approach towards the quantification of energies. The load vs. time curve thus obtained also allows a calculation of the stress rate achieved in a test.

ACI Committee 544 (50) has recommended an impact test in which a 4.5kg steel ball is dropped repeatedly through a standard height of 457mm (18 inches) on a 152.4mm diameter by 63.5mm thick concrete test specimen. The number of blows to a predetermined failure criterion is noted. The number of blows can also be converted to an energy value by multiplying the energy given to the specimen with each blow (20.2 N-m, in this case) by the total number of blows to failure. There are several major problems with this type of testing. The selection of the failure criterion is completely arbitrary, and not all of the energy goes in to the specimen, being dissipated in the test device itself.

The Hopkinson's split bar technique is often used as a means of generating high stress rate loading. Basically, it consists of two elastic bars between which the specimen is sandwiched. An incident stress pulse is generated in the first elastic bar and the pulse transmitted through the specimen is measured at the second elastic bar. Thus, the force that acted on the specimen can be evaluated. This technique can be used for uniaxial compressive loading (51,52) or uniaxial tensile loading (36); stress rates up to about 60 MPa/ms can be achieved.

The work of fracture tests conducted using a conventional static machine involve stressing a flexural specimen at conventional rates of loading and monitoring the load and the load point deflection. The energy expended in creating two new fracture surfaces ( $E_f$ ), which is equal to the area under the load vs. deflection plot, can then be used to determine the work of fracture  $\gamma_f$ ,

$$\gamma_f = \frac{E_f}{2A} \quad (4.1)$$

where  $A$  is the area of cross section of the specimen. The results obtained from such work of fracture tests may be used to predict the energy absorption capabilities in dynamic conditions only if the strain rate sensitivity of concrete can be ignored, a very doubtful assumption. Nevertheless, such tests may, at best, predict the lower limit on energy absorption values.

Explosive tests are sometimes used to generate uniformly distributed dynamic loading. The problems often encountered in such tests include the uncertainty in the quantification of energy, loads, and the specimen response.

Fracture mechanics has been used as an analytical tool to predict the behaviour of concrete under high rates of loading. However, the success of such a tool is limited since there is no universal agreement over the basic fracture mechanics material constants, and the constants

themselves are stress rate dependent.

In this study, an instrumented drop weight impact machine was used in order to test concrete beams at high stress rates. This type of machine was considered to be a suitable means of testing large specimens of concrete under flexural impact loading. The mass of the hammer was chosen to be about eight times the mass of the impacted beam, in order to induce specimen failure in a single blow of the hammer. Conventionally reinforced concrete beams, which due to the steel are much tougher than plain concrete beams could also be tested with the same hammer without having to carry out any modifications to the machine.

## 4.2 SPECIMEN PREPARATION

For the experimental work, plain, fibre reinforced, and conventionally reinforced concrete beams were cast. Three different sizes were chosen; (length x width x depth) 1525mmx150mmx150mm, 1400mmx100mmx125mm, and 1200mmx100mmx125mm. The 1500mmx150mmx150mm beams were found to be too heavy and awkward to handle. The 1400mmx100mmx125mm beams were found to have a large segment of the beam overhanging the supports, which were only 960mm apart. Finally, most of the beams were made 1200mm x 100mm x 125mm in size; a size not difficult to handle and not too long. The cement used was CSA Type 10 normal portland cement (equivalent to ASTM type 1). The maximum size of the pea gravel aggregate was 10mm. A summary of the specimens prepared has been presented in Table 4.1.

### 4.2.1 NORMAL STRENGTH PLAIN CONCRETE BEAMS

For the production of normal strength plain concrete beams the following mix proportions, by weight, were used: water:cement:fine aggregate:coarse aggregate = 0.5:1.0:2.0:3.5.

In addition, 9.45ml of superplasticizer (Mighty 150) per kg of cement were added to the mix.

A pan type mixer (0.170m<sup>3</sup> capacity) was used for mixing the concrete. All of the aggregates were placed in the mixer and it was turned on for about one minute. Next the cement, the water, and the additives were added. These were then

**Table 4.1**  
**Types of Specimens**

BEAM TYPE	Quantity Cast	Mix Proportions <sup>1</sup>	S.plasticizer <sup>2</sup>	Fibre (%)	Strength <sup>3</sup> (MPa)	Designation
Paste	10	0.35:1.0	-	-	-	P
Normal Strength Plain Concrete	35	0.50:1.0:0.0:2.0:3.5	9.45ml	-	42	NS
High Strength Plain Concrete	35	0.33:0.86:0.14:1.57:1.04	14.2ml	-	82	HS
Normal Strength Steel Fibre Reinforced Concrete	20	0.50:1.0:0.0:2.0:3.5	14.2ml	1.5	50	NSSFRC
High Strength Steel Fibre Reinforced Concrete	20	0.33:0.86:0.14:1.57:1.04	14.2ml	1.5	82	HSSFRC
Normal Strength Polypropylene Fibre Reinforced Concrete	20	0.50:1.0:0.0:2.0:3.5	14.2ml	0.5	49	NSPFRC
High Strength Polypropylene Fibre Reinforced Concrete	20	0.33:0.86:0.14:1.57:1.04	14.2ml	0.5	82	HSPFRC
Conventionally Reinforced Normal Strength Concrete with Deformed Reinforcing Bars	35	0.40:1.0:0.0:2.0:3.5 0.33:1.0:0.0:2.0:3.5	9.45ml	-	49	CRNSC

Conventionally Reinforced High Strength Concrete with Deformed Reinforcing Bars	35	0.33:0.86:0.14:1.57:1.04	14.2ml	-	82	CRHSC
Conventionally Reinforced Normal Strength Concrete with Smooth Reinforcing Bars	20	0.5:1.0:0.0:2.0:3.5 0.4:1.0:0.0:2.0:3.5	9.45ml	-	42	CRNSC-S
Conventionally Reinforced Normal Strength Concrete with Deformed Rebars and Stirrups	20	0.4:1.0:0.0:2.0:3.5	9.45ml	-	49	CRNSC-ST
Conventionally Reinforced Normal Strength Concrete with Polypropylene Fibres	20	0.40:1.0:0.0:2.0:3.5	14.2ml	0.5	49	CRNSC-P
Conventionally Reinforced High Strength Concrete with Polypropylene Fibres	20	0.33:0.86:0.14:1.57:1.04	14.2ml	0.5	49	CRHSC-P
Normal Strength Plain with Notch	20	0.5:1.0:0.0:2.0:3.5	9.45ml	-	42	NS-NT
High Strength Plain with Notch	20	0.33:0.86:0.14:1.57:1.04	14.2ml	-	82	HS-NT

Normal Strength	20	0.5:1.0:0.0:2.0:3.5	14.2ml	0.5	49	NS-P-NT
-----------------	----	---------------------	--------	-----	----	---------

Plain Concrete with  
Polypropylene Fibres,  
Notched

---

- <sup>1</sup> Water:Cement:Microsilica:Fine Aggregate:Coarse Aggregate (by weight).
- <sup>2</sup> Per kilogram of cement.
- <sup>3</sup> Equivalent Cube Strength obtained by using 125mmx125mm plates.

mixed for about 10 minutes. Once the mixing was completed, the concrete was shovelled into oiled wooden forms in a single layer, and was roughly compacted with a shovel. Proper compaction was then achieved using an electric immersion vibrator. Each beam was vibrated for about fifteen seconds at six different locations along its length. The forms were then covered with polyethylene sheets. The beams remained in the forms for about 24 hours. At the end of this period, the beams were demoulded and transferred to a moist room until tested. The test ages ranged from about one month to about one year.

On the day of the testing, the beams were removed from the moist room and the accelerometer locations were marked. Those marked spots were surface dried with a blow drier and cleaned with a wire brush. The mounting bases of the accelerometers were then carefully fastened to the beam using an epoxy adhesive. The epoxy was allowed to dry for a minimum period of about 15 minutes, at the end of which the beams were ready for testing.

#### 4.2.2 HIGH STRENGTH PLAIN CONCRETE BEAMS

High strength plain concrete beams were made in very much the same way as were the normal strength plain concrete beams. For the production of high strength concrete, 16% microsilica<sup>1</sup> by weight of the cement was also added, the

-----  
<sup>1</sup> Produced by Elkem Chemicals, Inc., Pittsburgh, Pennsylvania.

water/(cement+microsilica) ratio was reduced to 0.33, and a triple dose of the superplasticizer was used. The mix proportions were then:

water:cement:microsilica:fine aggregate:coarse aggregate =  
0.33:0.86:0.14:1.57:1.04

The casting and storage of the high strength beams was carried out in the same way as for the normal strength beams.

#### 4.2.3 FIBRE REINFORCED CONCRETE BEAMS

Fibre reinforced concrete beams were made by incorporating steel or polypropylene fibres into both the normal strength and high strength concrete mixes. To produce steel fibre reinforced concrete, 1.5% by volume of steel fibres were added. These fibres were 50mm long and had their ends hooked<sup>2</sup>. The fibres were originally held together by a water soluble sizing, and special care was exercised in adding the fibres to the mix, to minimize balling and nonuniform distribution of the fibres through out the body of the beam.

Polypropylene fibre reinforced concrete contained 0.5% by weight of 37mm long fibrillated polypropylene fibres<sup>3</sup>. The fibres had a very high water demand and it proved impossible, with the technique described above, to add a higher volume of fibrillated polypropylene fibres to the

<sup>2</sup> Produced by Bekaert N.V., Belgium.

<sup>3</sup> Produced by Forta Fibres, Inc., Grove City, Pennsylvania.

mix.

#### 4.2.4 CONVENTIONALLY REINFORCED CONCRETE BEAMS

The conventionally reinforced concrete beams were cast with either deformed steel reinforcing bars or smooth reinforcing bars.

In the case of the deformed reinforcing bars, two 9.52mm (cross-sectional area =  $2 \times 71 \text{mm}^2$ ) nominal diameter deformed steel bars were placed in the forms so as to provide a clear cover of 25mm from the bottom and the sides of the forms to the bars.

The smooth reinforcing bars used were also 9.52mm in diameter and were placed in the forms in the same way as the deformed bars.

Some of the reinforced concrete beams were provided with 5mm diameter stirrups spaced 100mm apart.

For the reinforced concrete beams, both normal strength and high strength beams, and beams containing fibres, were produced, as shown in Table 4.1.

#### 4.2.5 NOTCHED BEAMS

To study the effect of notches on the dynamic performance of concrete, several of the beams made with both normal strength and high strength mixes were notched. The notches were cut at midspan using a circular diamond cutting saw; they were 65 to 70mm deep. The actual notch depths in the individual beams were measured just before the test and

were used in the analysis.

### 4.3 TESTING PROGRAM

The basic aim of the testing program was to develop a valid testing technique to test concrete under impact, and to investigate the effect of stress rate on the performance of plain, fibre reinforced, and conventionally reinforced concrete beams. The tests carried out may be broadly classified into two categories: static and dynamic. All of the tests, static or dynamic, were conducted on beams in a three point bending configuration using a 960mm span.

#### 4.3.1 STATIC TESTING

##### 4.3.1.1 Flexural tests on beams

The static flexural tests were carried out on a universal testing machine.<sup>4</sup> The beams were simply supported on rollers on a span of 960mm, and the load was applied at midspan. The machine was equipped with a load cell capable of measuring loads up to 90 kN. The machine was also equipped with an x-y plotter, with the y channel of the plotter connected to the load cell and the x channel connected to a linear variable differential transducer (LVDT) reading deflections under the load point.

The cross head speed chosen for the static testing was  $4.2 \times 10^{-7}$  m/sec. At this rate, in a typical test, it took about 1 hour to reach the peak load. Once the load vs. deflection plots were obtained, a planimeter was used to

-----  
<sup>4</sup>Baldwin Model GBN, manufactured by Satec Systems, Inc., USA.

measure the area under the load vs. deflection plot. This area represented the energy absorbed by the beam.

In general, three specimens of each type were tested in this way.

#### **4.3.1.2 Tension tests on reinforcing bars**

The same universal testing machine was also used to carry out tension tests on both the deformed and smooth reinforcing bars used for the conventionally reinforced concrete. A clip gauge with an LVDT fitted to it was used to read the strain over a 50mm gauge length. A load vs. displacement plot was obtained. The speed of the crosshead was maintained at about 1mm/minute. The area under the load vs. displacement plot to failure was measured with a planimeter. As before, this represented the energy required to fail the bars in tension. The yield strength of the bars was found to be 425 MPa, while their ultimate strength was found to be 720 MPa. With the ultimate strain of 0.12, the energy required upto failure was found to be 70 MNm/m<sup>3</sup>

#### **4.3.1.3 Stiffness test on the rubber pad**

Some of the dynamic tests were carried out with a rubber pad in between the tup and the beam. This technique had originally been devised as a way of eliminating the inertial loading effects (16). The Baldwin universal testing machine was used for this purpose. The load vs. deflection

plot for the rubber pad in compression was obtained, using a pad with the dimensions of 150mm (width), 150mm (breadth), and 50mm (depth). The deflections were measured by measuring the movement of the cross head itself. For such a soft material, this was considered to be a valid technique for displacement measurement. The stiffness of the rubber pad was obtained by measuring the slope of the load vs. displacement plot thus obtained.

#### **4.3.1.3 Compressive strength determination from broken halves of the beams**

Equivalent cube tests were performed on the halves of beams broken in static flexure. Two 125mm x 125mm steel plates were used on the top and the bottom of the beam lying on its 125mm side. Load was applied in a hydraulically controlled testing machine until the concrete failed by crushing.

### 4.3.2 IMPACT TESTING

The impact testing was carried out using a drop weight impact machine. The following sections provide a description of the machine, the instrumentation, calibration, data acquisition, and the analysis of the test results.

#### 4.3.2.1 The impact testing machine

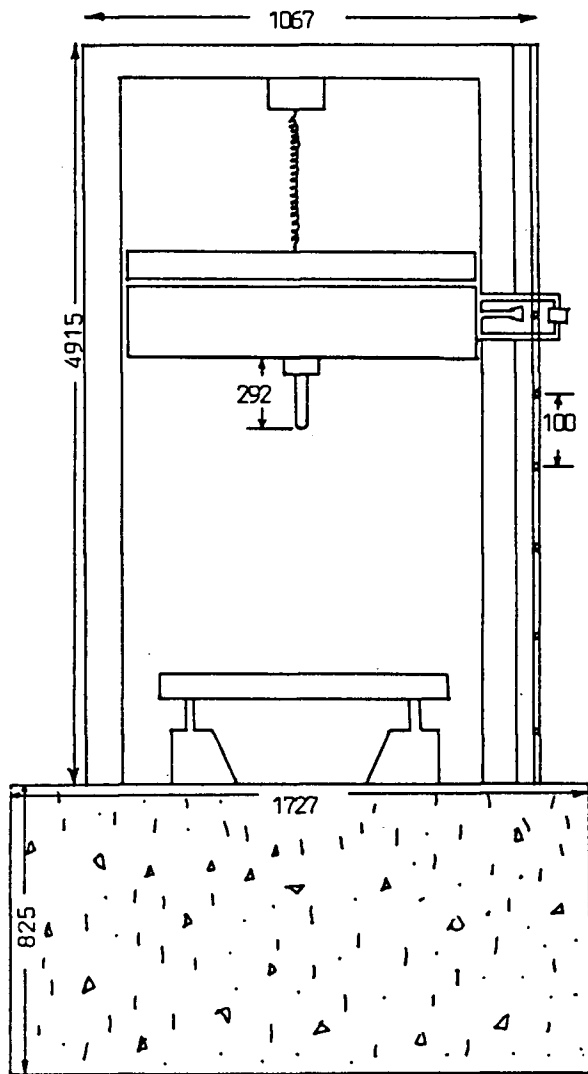
##### *a. General principle of a drop weight impact machine*

A photograph of the instrumented drop weight impact machine is shown in Figure 4.1; a dimensioned sketch is given in Figure 4.2. In these types of machines, a hammer with a substantial mass is raised to a certain height above the specimen. In this position, the hammer has the potential energy  $m_h a_h h$  (mass of the hammer  $\times$  acceleration of the hammer under gravity  $\times$  height to which it is raised) with respect to the top surface of the specimen. If the hammer in this position is allowed to drop on to the specimen, the potential energy of the hammer is converted to kinetic energy as the hammer falls with an acceleration  $a_h$ . (Due to the frictional forces in the machine acting on the hammer, the downward acceleration of the hammer is less than the earth's gravitational acceleration,  $g$ ). Just before the hammer strikes the beam, its velocity is given by

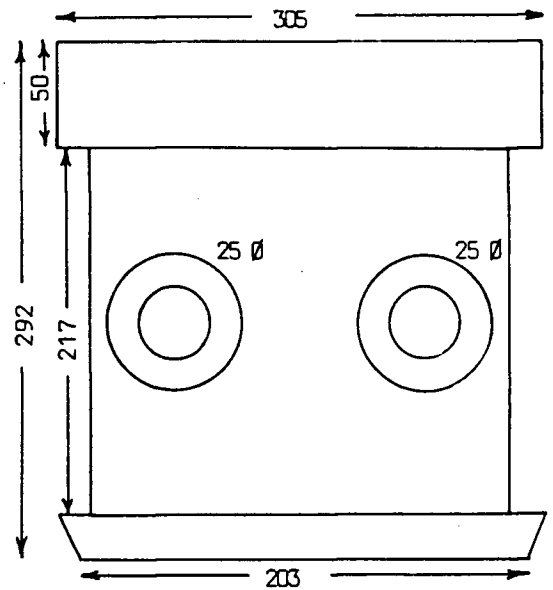
$$v_h = \sqrt{2a_h h} \quad (4.2a)$$



Figure 4.1-The Drop Weight Impact Testing Machine



The IMPACT MACHINE



The TUP

Notes:

- (1) All dimensions in millimetres.
- (2) The drawing is not to scale.

Figure 4.2-The Dimensions of the Machine and the Tup

At this velocity, the hammer has a kinetic energy,

$$\begin{aligned} T_h &= \frac{1}{2}m_h(\sqrt{2a_h h})^2 \\ &= m_h a_h h \end{aligned} \tag{4.2b}$$

When the hammer strikes the beam, a sudden transfer of momentum occurs from the hammer to the beam. As a result, the momentum of the hammer decreases. This, in turn, results in a loss of the hammer kinetic energy, and a corresponding gain in the beam energy. This transfer of energy between the hammer and the beam is very sudden, and results in a sudden build-up of stresses in the beam. In this study, five channels of instrumentation were provided to monitor the response of the beam to impact. Strain gauges were mounted on the striking end of the hammer (called the 'tup') and on one of the support anvils, and three accelerometers were mounted along the length of the beam. The strain gauges in the tup measured the contact load between the hammer and the beam, the strain gauges in the support were designed to monitor the support reaction, and the accelerometers were employed to record the accelerations in the beam undergoing impact. The time base data were acquired by a data acquisition system based upon an IBM PC.

The layout of the testing setup is shown in Figure 4.3. As shown, the hammer is attached to the hoist by means of a

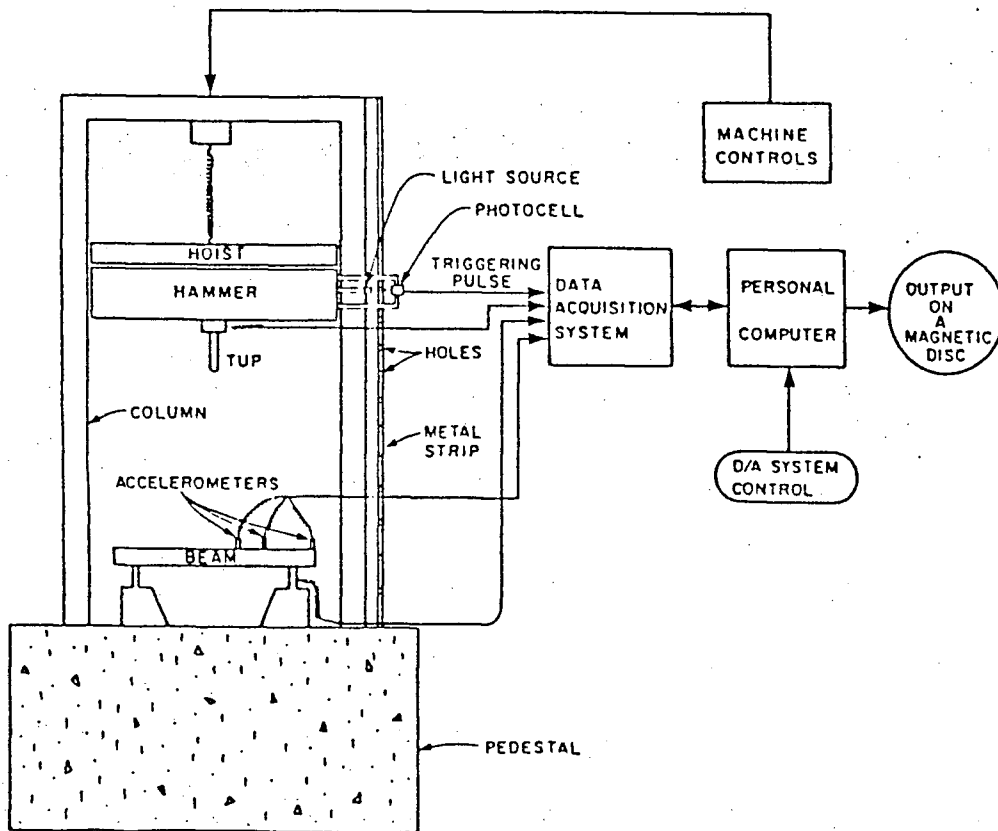


Figure 4.3-The Layout of the Impact Testing Set-up

pin lock. The hoist can be moved up and down by using a chain and motor. Once the hammer is at the desired height above the specimen, the pneumatic brakes provided in the hammer can be applied. With this, the hammer "grabs on" to the columns of the machine. In this position, the hoist can be detached from the hammer. On releasing the pneumatic brakes, the hammer falls under gravity and strikes the beam, thus generating high stress rate loading.

*b. Triggering of the data acquisition system*

The triggering of the data acquisition system, which should occur just before the hammer hits the beam, was accomplished by using a photocell assembly. A strip of metal with holes punched in it ran parallel to the columns of the machine as shown in Figure 4.3. The hammer carried a photocell assembly which slid along the metal strip as the hammer fell upon release. As soon as the photocell assembly reached a hole in the metal strip, the beam of light fell on the photocell through the hole (Figure 4.4), which triggered the data acquisition system.

*c. The tup*

As the tup (Figure 4.5), strikes the beam, the strain gauges in the tup record the contact load. The arrangement of the strain gauges in the tup is shown in Figure 4.6(a), and the circuit diagram is shown in Figure 4.6(b). The

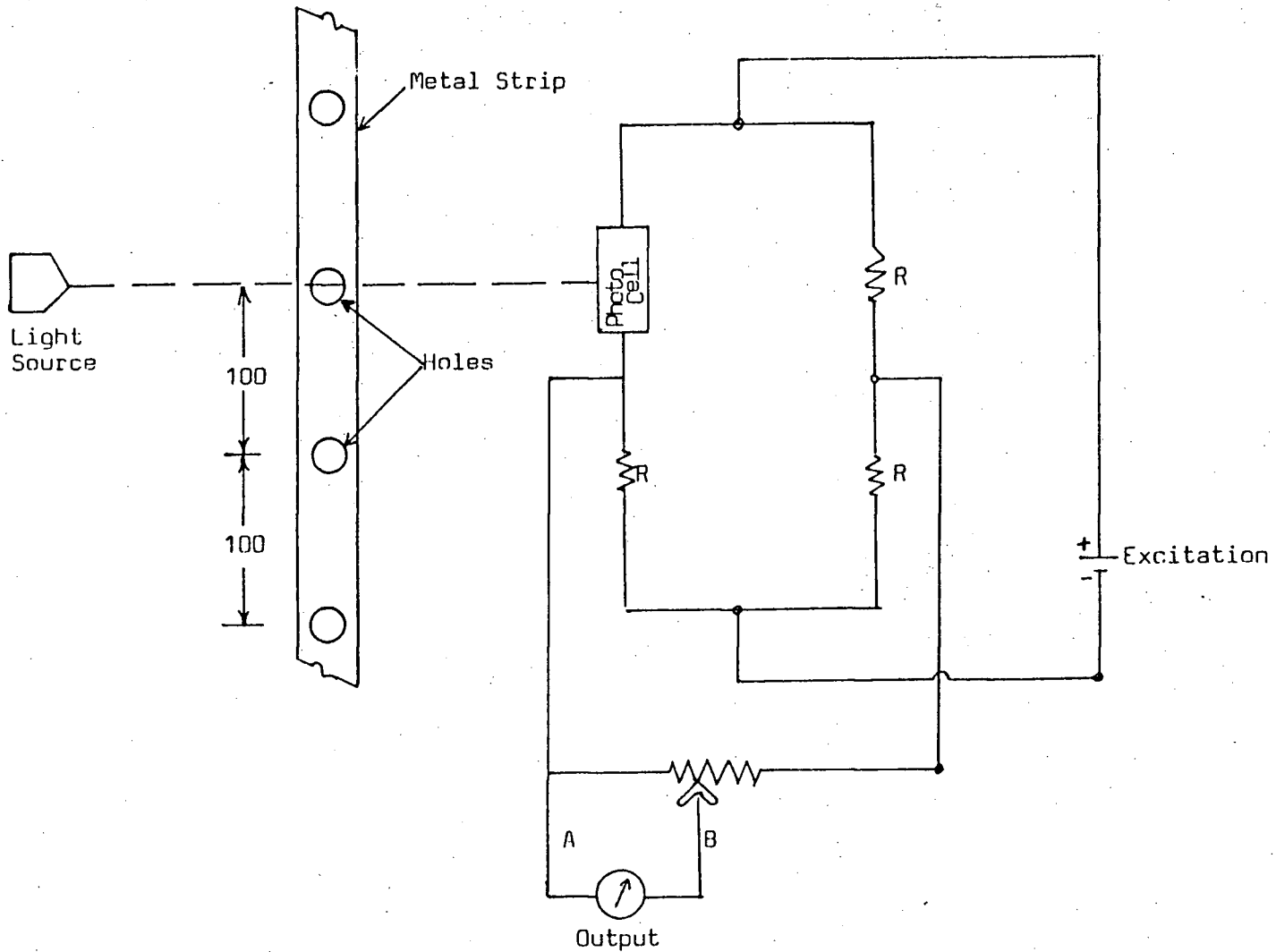


Figure 4.4-Triggering of the Data Acquisition System

Wheatstone bridge, shown in Figure 4.6(b) is balanced in the "no load configuration". The 8 strain gauges are installed in two 25 mm diameter circular holes, in order to obtain an amplification in the signals by making use of the stress concentrations at the boundaries of the holes. The tup was calibrated statically using a hydraulically loaded universal testing machine.

*d. The support anvil*

The support anvil (Figure 4.7) was capable of reading the vertical support reaction as well as the horizontal

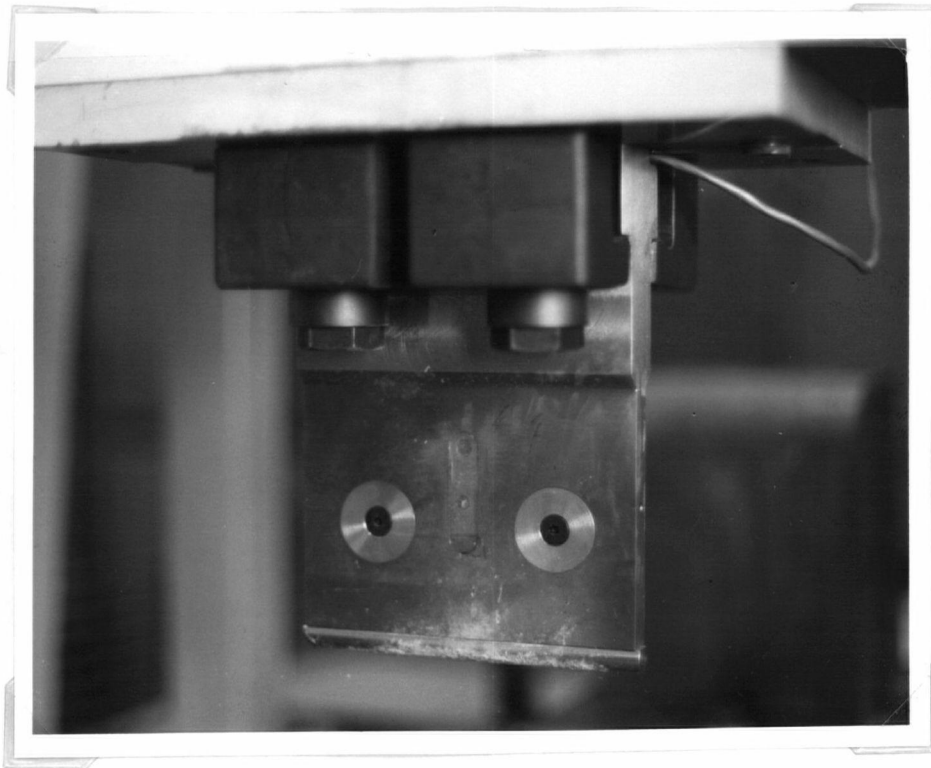


Figure 4.5-The striking end of the Hammer, or "Tup"

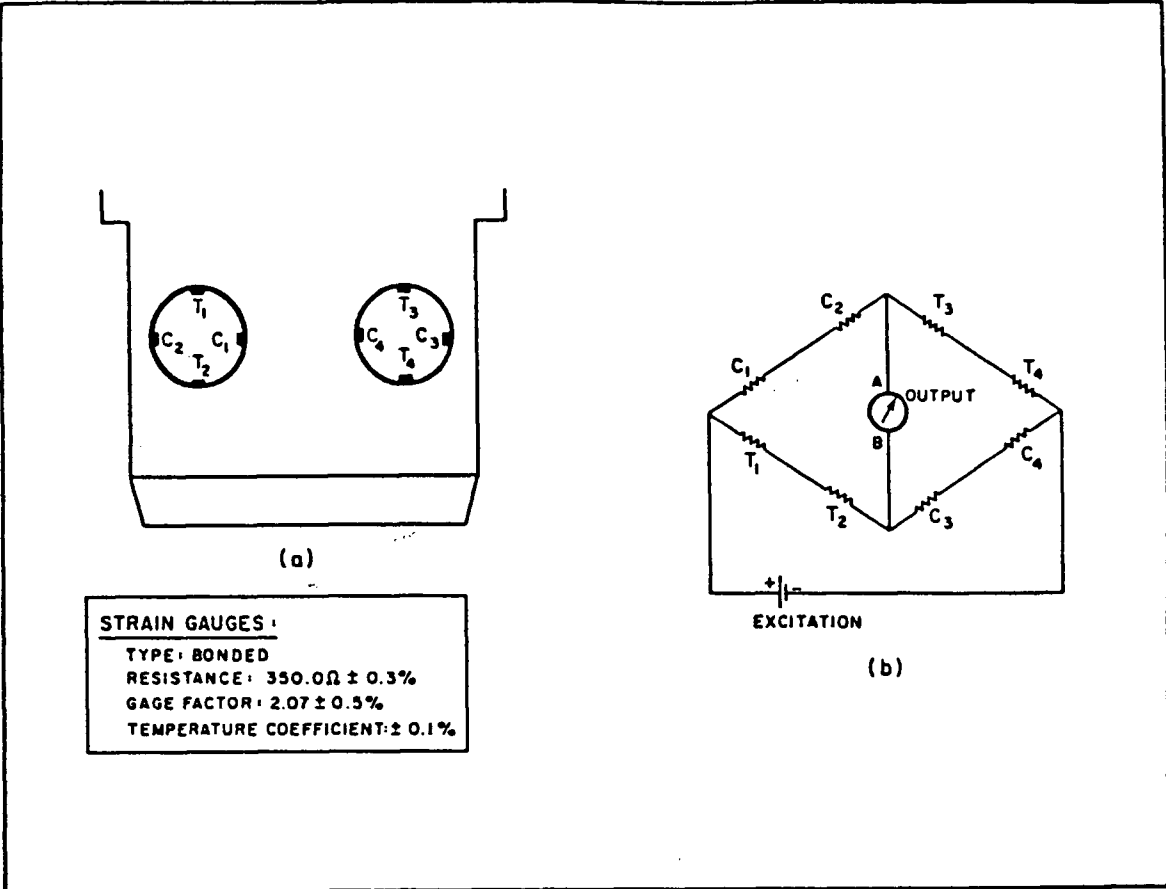


Figure 4.6-The circuit of the Tup

support reaction (Figure 4.8). These two reactions were read separately from the imbalance generated in two different Wheatstone bridges (Figure 4.9). These two reactions could be read by the data acquisition system through two independent channels. The vertical reaction was read from the strain gauges mounted in the circular holes, while the horizontal reaction was read from the strain gauges mounted in between the two holes (Figure 4.9). The strain gauges reading the vertical reaction worked on the same principle as did the ones in the tup. The bridge reading the horizontal reaction, which was balanced in the no load

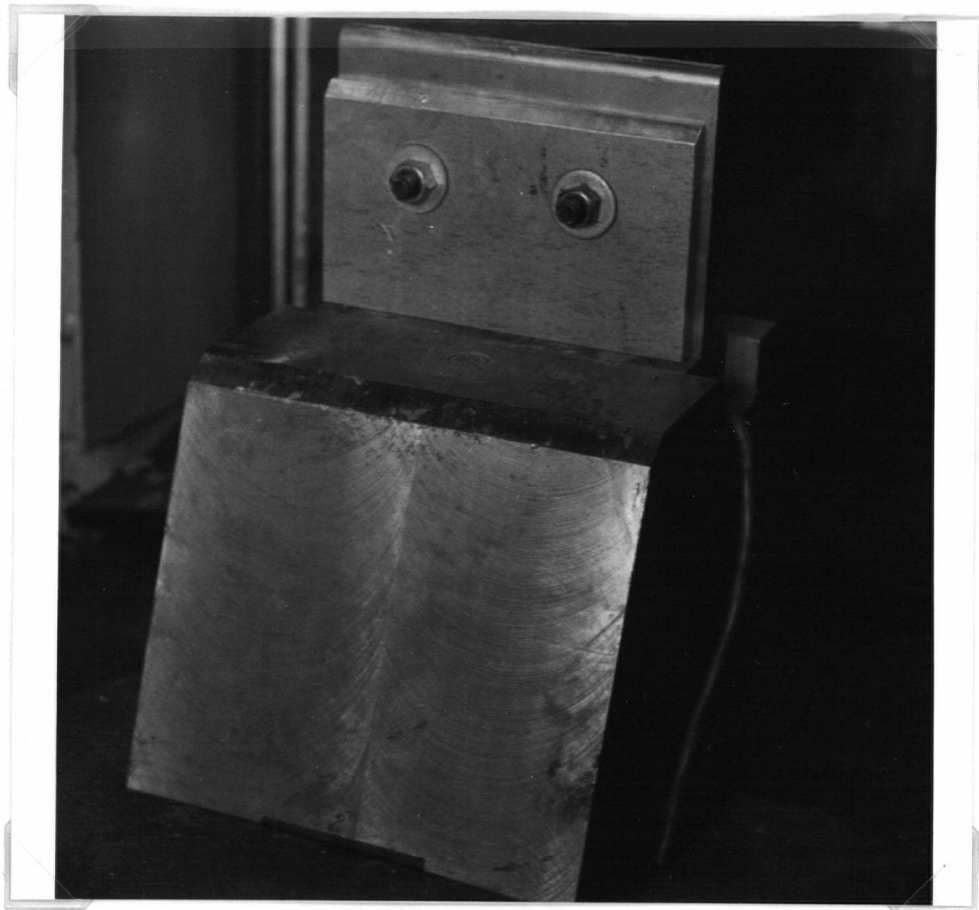


Figure 4.7-The Support Anvil

configuration, was thrown out of balance with a finite horizontal load. In the unbalanced state, the output across A and B in Figure 4.9c was proportional to the magnitude of the horizontal load. It can be seen from Figure 4.9b and 4.9c that these two channels acted independently of each other. In other words, the presence of a finite horizontal load did not affect the balance of the bridge reading the vertical reaction, and vice versa. Calibration of the support anvil was also carried out statically on a hydraulically loaded universal testing machine.

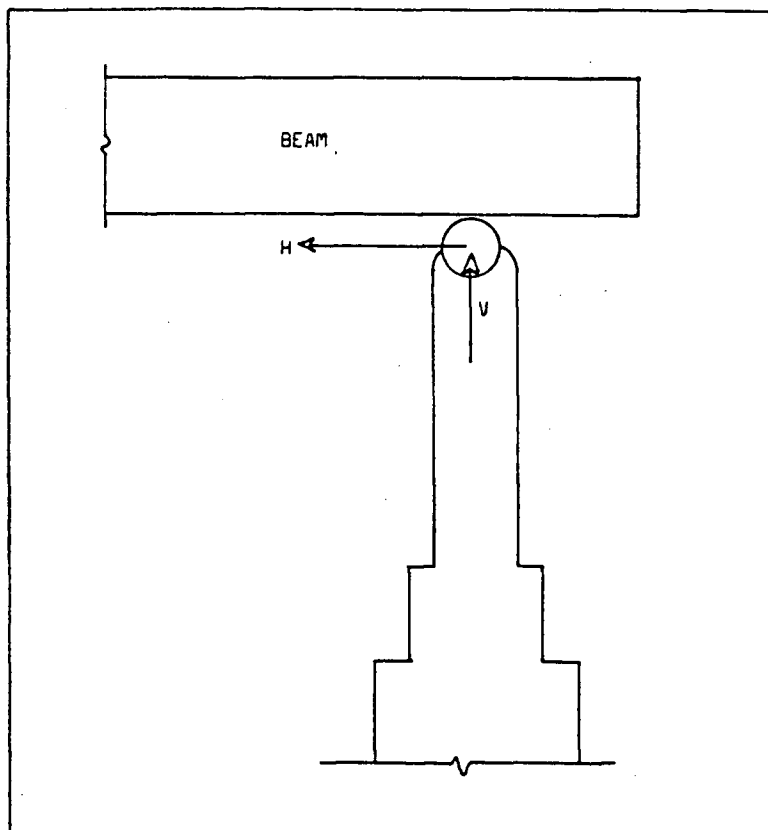


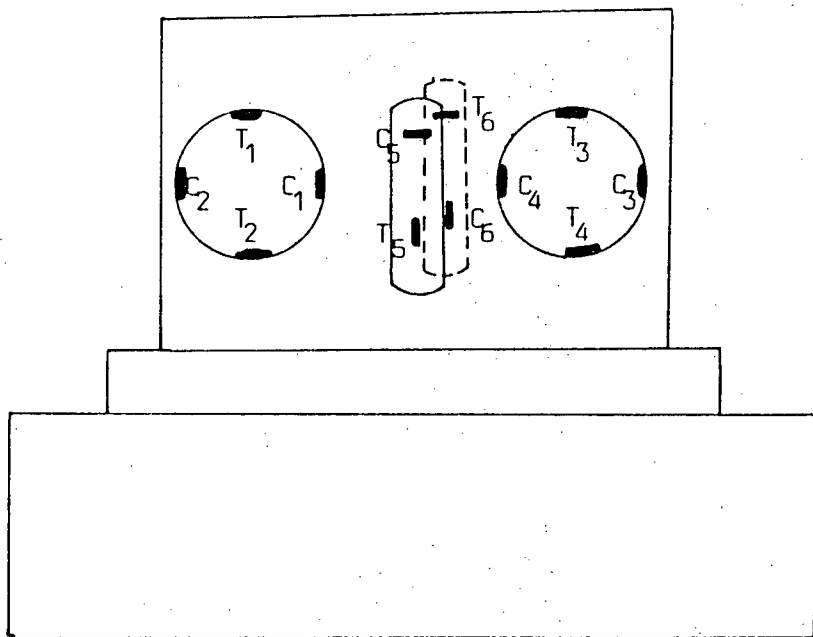
Figure 4.8-The Support Reactions

*e. Accelerometers*

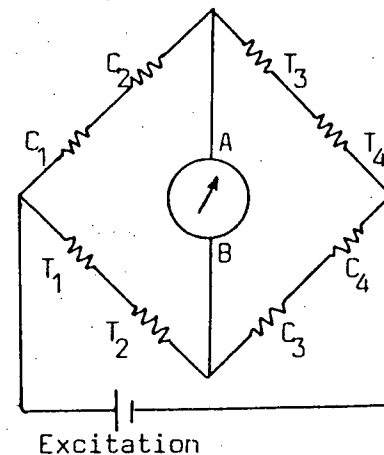
The accelerometers (Figure 4.10) used were piezoelectric sensors with a resonant frequency of about 45kHz.<sup>5</sup> With a resolution of 0.01g, the accelerometers could read to  $\pm 500g$  and had an overload protection of up to 5000g.

---

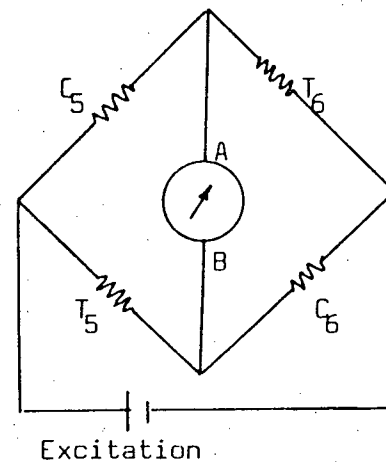
<sup>5</sup>Manufactured by PCB Piezotronics, Inc., Buffalo, New York.



(a)



(b)



(c)

Figure 4.9-The circuit of the Support Anvil



Figure 4.10-The Accelerometers

*f. Acquisition and storage of the data*

Once the data acquisition system is triggered, it begins to transfer the output from the 5 channels into the computer memory, for a preselected length of time. This length of time is chosen appropriately for the expected time of the impact event ( $\approx 15$  ms for plain and fibre reinforced concrete, and  $\approx 150$ ms for conventionally reinforced concrete). The five channels were read simultaneously at 0.2ms intervals. At the end of the event, the data stored in the computer memory are written on to a magnetic disc.

Finally, these data are transferred to an Amdahl computer for further analysis.

#### 4.3.2.2 Calibration

##### *a. Calibration of the tup*

The output from the strain gauges in the tup was in the form of voltage signals. To convert these signals into loads, calibration was needed. Although the tup was to be stressed dynamically in an actual test, the properties of steel under dynamic conditions were assumed to be the same as under static ones, and so a static calibration could be used. The tup was loaded, in steps, up to about 70% of its elastic capacity and the output was read. Figure 4.11 shows the calibration curve. Note from Figure 4.11 that the calibration was linear and the hysteretic loss was nonexistent.

##### *b. Calibration of the support anvil*

Similar to the tup, the support channels were also calibrated statically on a hydraulically loaded universal testing machine. The channel reading the vertical reaction was calibrated by applying a vertical load as in the case of the tup, and a moment was applied to calibrate the horizontal reaction channel (Figure 4.8). Figure 4.11 shows the results from the calibration. As for the tup, the calibration for the support channels was also found to be linear, with no hysteretic loss.

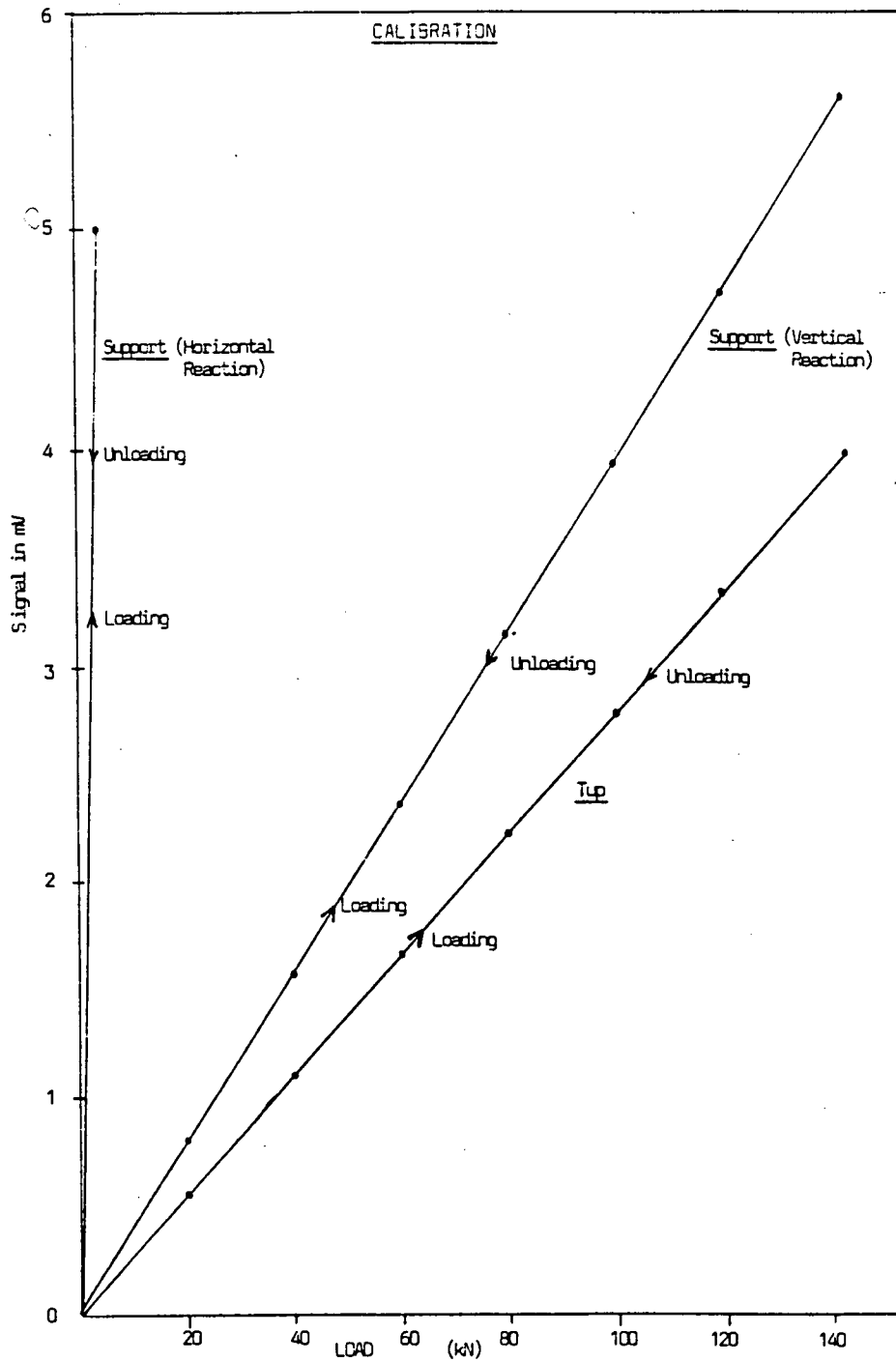


Figure 4.11-The Calibration of the support and the striking tup

*c. Calibration of the hammer acceleration*

As mentioned earlier, the photocell assembly sent out a voltage signal, in the form of a spike, whenever it intercepted a hole in the metal strip. A typical output from the photocell assembly is shown in Figure 4.12; the data from the photocell indicated the time required by the hammer to travel the distances between the successive holes.

If it can be assumed that the downward acceleration ( $a_h$ ) of the hammer is constant, and if we know the time required to travel two adjacent segments of lengths  $s_1$  and

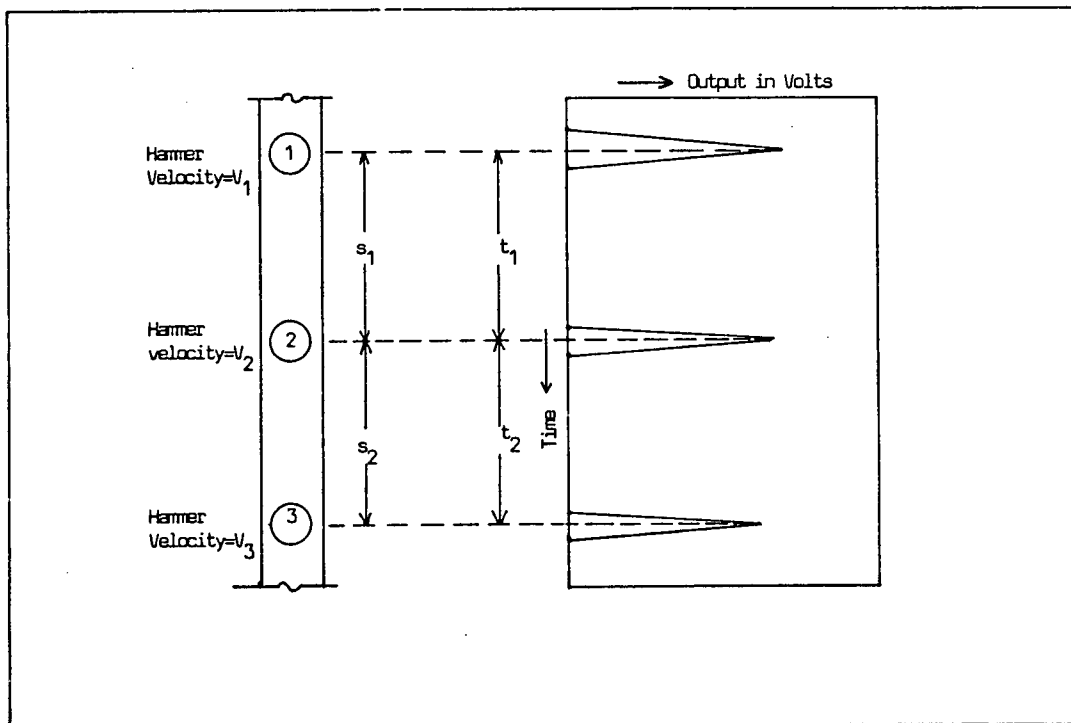


Figure 4.12-The Calibration of the Hammer Acceleration

$s_2$  (Figure 4.12), then from the laws of motion, the acceleration of the hammer " $a_h$ " can be obtained as follows: Between the first and the second hole,

$$s_1 = v_1 \Delta t_1 + 0.5 a_h \Delta t_1^2 \quad (4.3)$$

Between the second and the third hole,

$$s_2 = v_2 \Delta t_2 + 0.5 a_h \Delta t_2^2 \quad (4.4)$$

Also,

$$v_2 = v_1 + a_h \Delta t_1 \quad (4.5)$$

therefore, solving for  $a_h$  we get

$$a_h = \frac{2(s_2 \Delta t_1 - s_1 \Delta t_2)}{\Delta t_1 \Delta t_2 (\Delta t_1 + \Delta t_2)} \quad (4.6)$$

If the holes are equally spaced at  $s$ , as is the case in this study,

$$a_h = \frac{2s(\Delta t_1 - \Delta t_2)}{\Delta t_1 \Delta t_2 (\Delta t_1 + \Delta t_2)} \quad (4.7)$$

Note that all the terms on the right hand side of Eqn. 4.6 or Eqn. 4.7 can be obtained either from the output of the photocell, or from physical measurements. Thus the downward acceleration can be evaluated.

It is worth mentioning here that the acceleration of the hammer was always found to be less than  $g$  ( $9.81 \text{ m/sec}^2$ ). The friction between the columns of the machine and the hammer was thought to be the reason behind this discrepancy. The friction was found to depend upon the cleanliness of the pillars. An acceleration test done right after cleaning the pillars with acetone resulted in a value of hammer acceleration of  $9.60 \text{ m/sec}^2$ . On the other hand, unclean pillars, after repeated use, yielded accelerations as low as  $8.64 \text{ m/sec}^2$ . Therefore, the pillars were cleaned just before every test and a hammer acceleration equal to  $9.60 \text{ m/sec}^2$  was assumed in the analysis.

#### 4.3.2.3 Analysis of the test results

The usual output from the impact tests carried out on the concrete beams consisted of the tup load, the support load, and the accelerations at three locations along the length of the beam. All these data were obtained as a function of time. Figure 4.13 shows the five sets of data obtained from the five instrumented channels from a test done on a plain concrete beam. Since the data were acquired at 200 microsecond intervals, and since an impact event took anywhere from 15ms to 150ms, this resulted in several thousand data points per test. For the efficient handling of this data, a computer program was written. An algorithm of the program is given in Section-4.3.2.3g.

##### *a. The energy lost by the hammer*

If the hammer has fallen through a height "h" before it hits the beam, then the velocity of the hammer just prior to impact is given by Eqn. 4.2a. If this instant corresponds to time  $t=0$  (Fig. 4.13), then,

$$V_h(t=0) = \sqrt{2a_h h} \quad (4.8)$$

After the contact between the hammer and the beam, an impulse, given by the area under the tup load vs. time plot, acts on the hammer. From the laws of Newtonian Mechanics, this impulse must be equal to the change in the momentum of

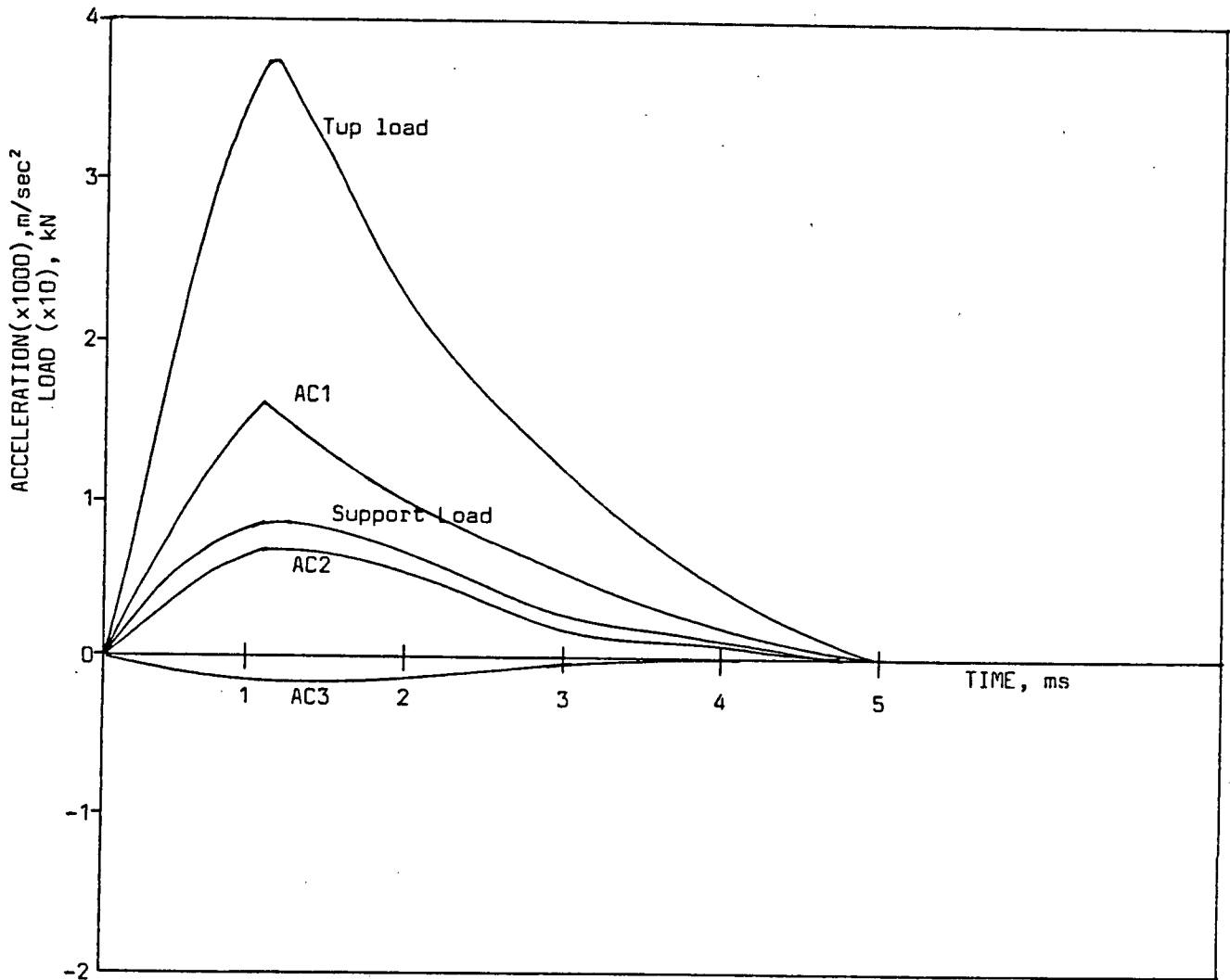


Figure 4.13-Typical output from the five channels of instrumentation

the hammer.

$$\int P_t(t)dt = m_h V_h(0) - m_h V_h(t) \quad (4.9)$$

Using Eqn 4.8 and solving Eqn 4.9 we get,

$$\Delta E(t) = \frac{1}{2}m_h [V_h^2(0) - V_h^2(t)] \quad (4.10)$$

If  $\Delta E(t)$  is the kinetic energy lost by the hammer, then

$$V_h(t) = [\sqrt{2a_h h} - \frac{1}{m_h} \int P_t(t)dt] \quad (4.11)$$

On substituting for  $V_h(0)$  and  $V_h(t)$  in Equation 4.11,

$$\Delta E(t) = \frac{1}{2}m_h [2a_h h - (\sqrt{2a_h h} - \frac{1}{m_h} \int P_t(t)dt)^2] \quad (4.12)$$

Thus, according to Eqn. 4.12, at any time  $t$ , if the area under the tup load vs. time plot is known, the energy lost by the hammer can be calculated. As will be seen later, all of this energy lost by the hammer may not be transferred to the specimen. Some of the energy, at least in the initial

part of the impact, is lost to the testing machine itself (Chapter 8).

*b. The generalized bending load*

The contact load between the specimen and the hammer is not the true bending load on the beam, because of the inertial reaction of the beam. A part of the tup load is used to accelerate the beam from the position of rest. This inertial load, called the d'Alembert force, is discussed in detail in Chapter 5. The inertial load must be subtracted from the observed tup load in order to obtain the actual bending load on the specimen. Various techniques have been used by various investigators to accomplish this (Chapter 5). In this study, the accelerometers data were used in order to apply the inertial correction to the tup load.

In order to arrive at the true bending (or stressing load), it is important to understand the nature of the various loads in question. The tup load is a point load acting at the midspan of the beam, whereas the inertial reaction of the beam is body force distributed throughout the body of the beam. This distributed inertial load should therefore be replaced by an equivalent (or generalized) inertial load,  $P_i(t)$ , which can then be subtracted from the tup load to obtain the generalized (true, or equivalent) bending load  $P_b(t)$ , acting at the centre. As will be shown later, this generalized bending load can then be assumed to act on the beam at the midspan by itself, and will predict

the correct energies, midspan moments and stresses. As shown in Figure 4.14, the three accelerometers are placed at distances  $D_1$ ,  $(D_1+D_2)$ , and  $(0.5l+h)$  from the centre of the beam. If the accelerations between the accelerometers can be obtained by linear interpolation, if the accelerations at midspan can be obtained by linear extrapolation, and if the acceleration distribution can be assumed to be symmetric about the midspan, then the acceleration at every point along the length of the beam is known. If a segment of the beam,  $dx$ , has an acceleration  $\ddot{u}(x,t)$  at its centre, then the inertial force acting on it is given by

$$dI(x,t) = \rho A dx \ddot{u}(x,t) \quad (4.13)$$

where  $\rho$  is the mass density and  $A$  is the area of cross section of the beam.

In this position (Figure 4.14c), let the beam be given a virtual displacement compatible with its constraints. Let the virtual displacement at any point be proportional to the acceleration at that point. If  $\ddot{u}_0(t)$ ,  $\ddot{u}_1(t)$ ,  $\ddot{u}_2(t)$ ,  $\ddot{u}_3(t)$  are the accelerations at the centre, and at the three accelerometer locations, respectively, and if  $\delta u_0$ ,  $\delta u_1$ ,  $\delta u_2$ , and  $\delta u_3$  are the corresponding virtual displacements, then

$$\frac{\delta u_0}{\ddot{u}_0(t)} = \frac{\delta u_1}{\ddot{u}_1(t)} = \frac{\delta u_2}{\ddot{u}_2(t)} = \frac{\delta u_3}{\ddot{u}_3(t)} \quad (4.14)$$

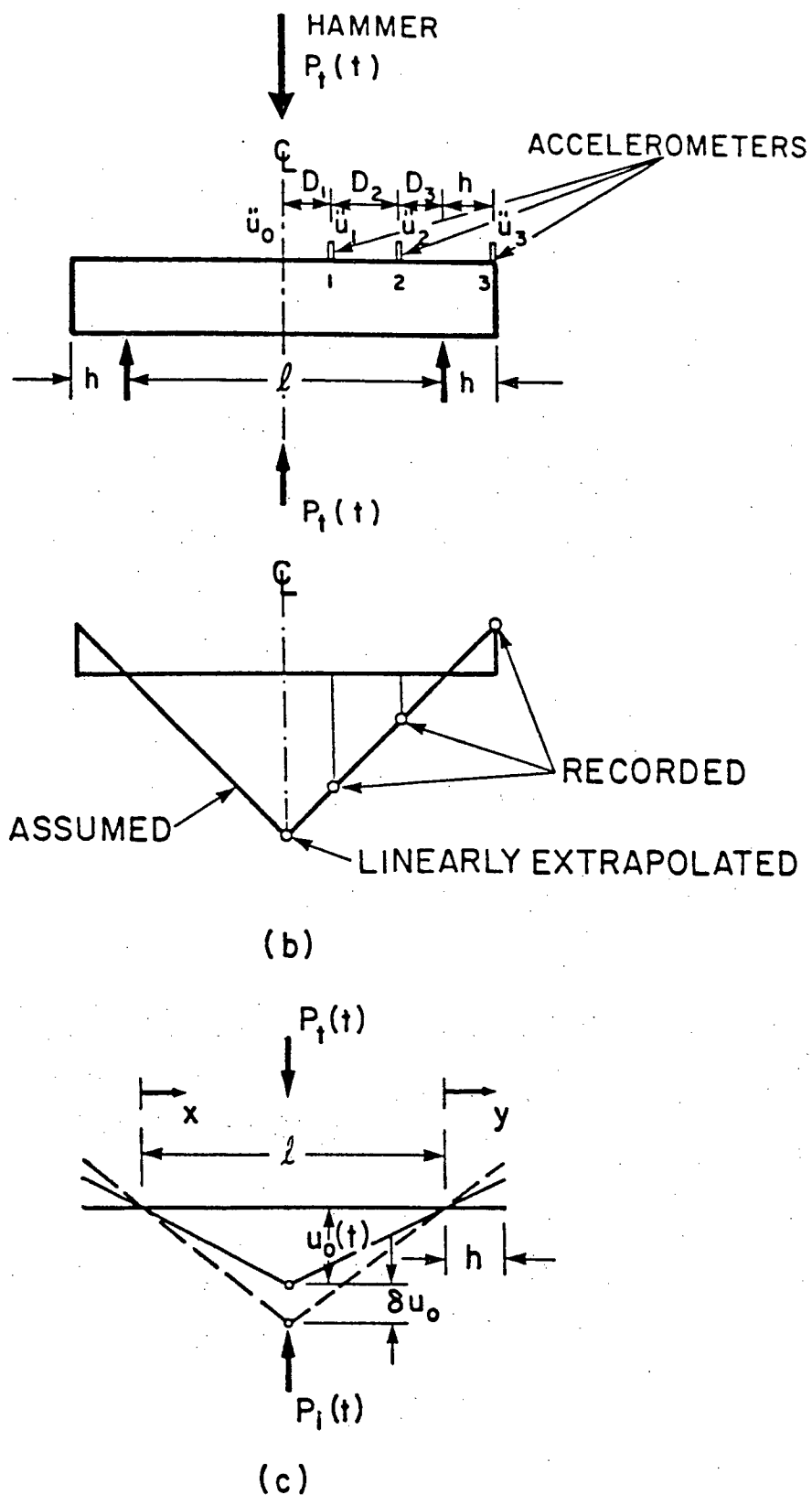


Figure 4.14-(a) Positions of the accelerometers (b) Acceleration distribution and (c) The generalized inertial Load

If the distributed inertial load is to be replaced by a generalized inertial load in the centre, then the virtual work done by the distributed inertial reaction acting over the distributed virtual displacement should be equal to the virtual work done by the central load  $P_i(t)$  acting over the virtual displacement at the centre,

$$P_i(t)\delta u_0 = \int \rho A \ddot{u}(x,t) \delta u(x) dx + 2 \int \rho A \ddot{u}(y,t) \delta u(y) dy \quad (4.15)$$

On expanding,

$$P_i(t)\delta u_0 = 2 \left[ \int \rho A \left[ \ddot{u}_0(t) - \frac{u_0(t) - u_1(t)}{D_1} x \right] \left[ \delta u_0 - \frac{\delta u_0 - \delta u_1}{D_1} x \right] dx \right. \\ + \int \rho A \left[ u_1(t) - \frac{u_1(t) - u_2(t)}{D_2} x \right] \left[ \delta u_1 - \frac{\delta u_1 - \delta u_2}{D_2} x \right] dx \quad (4.16) \\ + \int \rho A \left[ u_2(t) - \frac{u_2(t) - u_3(t)}{D_3} x \right] \left[ \delta u_2 - \frac{\delta u_2 - \delta u_3}{D_3} x \right] dx \\ \left. + \int \rho A (-1) \left[ u_3(t) - \frac{u_3(t) - u_s(t)}{h} y \right] (-1) \left[ \delta u_3 - \frac{\delta u_3 - \delta u_s}{h} y \right] \right]$$

where  $\ddot{u}_s(t)$  and  $\delta u_s$  are the acceleration and the virtual displacement at the support, respectively. If the acceleration and the virtual displacement at the support can be assumed to be zero, and if the beam is prismatic and homogeneous, then Eqn. 4.16 can be simplified to

$$P_i(t)\delta u_0 = 2\rho A \left[ \frac{1}{3} \ddot{u}_1(t)\delta u_0 D_1 + \frac{1}{3} \ddot{u}_0(t)\delta u_0 D_1 + \frac{1}{3} \frac{\ddot{u}_1^2(t)}{\ddot{u}_0(t)} \delta u_0 D_1 \right. \\ + \frac{1}{3} \ddot{u}_2(t)\delta u_1 D_2 + \frac{1}{3} \ddot{u}_1(t)\delta u_1 D_2 + \frac{1}{3} \frac{\ddot{u}_2^2(t)}{\ddot{u}_1(t)} \delta u_1 D_2 \\ \left. + \frac{1}{3} \ddot{u}_2(t)\delta u_2 D_3 + \frac{1}{3} \ddot{u}_3(t)\delta u_3 h \right] \quad (4.17)$$

Expressing  $\delta u_1$ ,  $\delta u_2$ , and  $\delta u_3$  in terms of  $\delta u_0$  using Eqn. 4.14, and on cancelling  $\delta u_0$  on both sides of the equation, we get

$$\begin{aligned}
 P_i(t) = 2\rho A \left[ \frac{1}{3} \frac{D_1}{\bar{u}_0(t)} \left( \ddot{u}_0^2(t) + \bar{u}_1^2(t) + \bar{u}_1(t)\bar{u}_0(t) \right) \right. \\
 + \frac{1}{3} \frac{D_2}{\bar{u}_0(t)} \left( \bar{u}_2^2(t) + \bar{u}_1^2(t) + \bar{u}_1(t)\bar{u}_2(t) \right) \quad 4.18) \\
 \left. + \frac{1}{3} \frac{D_3}{\bar{u}_0(t)} \bar{u}_2^2(t) + \frac{1}{3} \frac{h}{\bar{u}_0(t)} \bar{u}_3^2(t) \right]
 \end{aligned}$$

Thus, knowing the accelerations at the centre and at the accelerometer locations, and the beam properties, the generalized inertial load can be obtained from Eqn. 4.18.

Once the generalized inertial load is obtained, the beam can be modelled as a single degree of freedom system and the generalized bending load can be obtained from the equation of dynamic equilibrium:

$$P_b(t) = P_t(t) - P_i(t) \quad (4.19)$$

#### c. Acceleration distribution

If the acceleration at any point along the length of the beam can be expressed as a function of the acceleration at the centre, then the equation of virtual work can be further simplified. In other words, if the accelerations  $\ddot{u}_1(t)$ ,  $\ddot{u}_2(t)$ , and  $\ddot{u}_3(t)$  can be expressed as a function of  $\ddot{u}_0(t)$ , then Eqn. 4.18 can be written in terms of the load point acceleration ( $\ddot{u}_0(t)$ ) alone.

Several tests conducted on plain, fibre reinforced, and conventionally reinforced beams indicate that such a simplification is possible. The observed acceleration distribution in plain and fibre reinforced concrete is shown

in Figure 4.15 and that for conventionally reinforced concrete in Figure 4.16. As seen from figure 4.15, the acceleration distribution for the plain and fibre reinforced concrete without conventional reinforcement can be approximated as linear. On the other hand, the acceleration distribution for conventionally reinforced concrete can be approximated as sinusoidal. With these approximations the generalized inertial loads can be recalculated as follows:

(i) *Linear case*

For the linear case (Figure 4.17a), the displacements can be written as,

$$\begin{aligned}
 u(x,t) &= \frac{2u_0(t)}{l} x \quad (\text{between the supports}) \\
 u(y,t) &= \frac{-2u_0(t)}{l} y \quad (\text{overhanging the supports})
 \end{aligned} \tag{4.20}$$

Rewriting Equation 4.15 for this case we have.

$$\begin{aligned}
 P_i(t) \delta u_0 &= 2 \int \rho A \left[ \frac{2\ddot{u}_0(t)x}{l} \right] \left[ \frac{2\delta u_0 x}{l} \right] dx \\
 &+ 2 \int \rho A \left[ \frac{-2\ddot{u}_0(t)y}{l} \right] \left[ \frac{-2\delta u_0 y}{l} \right] dy
 \end{aligned} \tag{4.21}$$

once again, if the beam is homogeneous and isotropic, Eqn.4.21 can be simplified to

$$P_i(t) = \rho A \ddot{u}_0(t) \left[ \frac{1}{3} + \frac{8}{3} \frac{h^3}{l^2} \right] \tag{4.22}$$

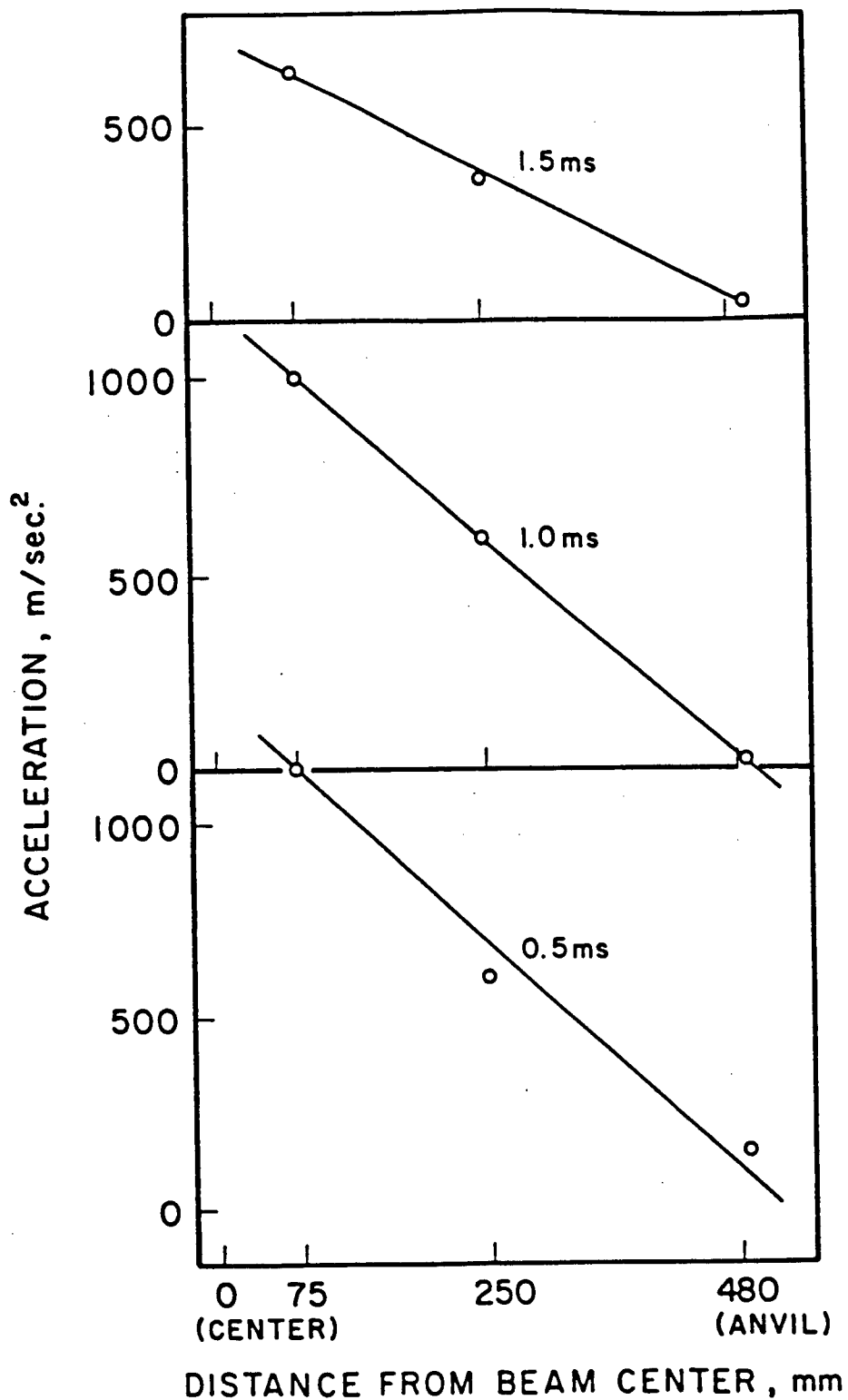


Figure 4.15-Acceleration distribution for plain concrete beams

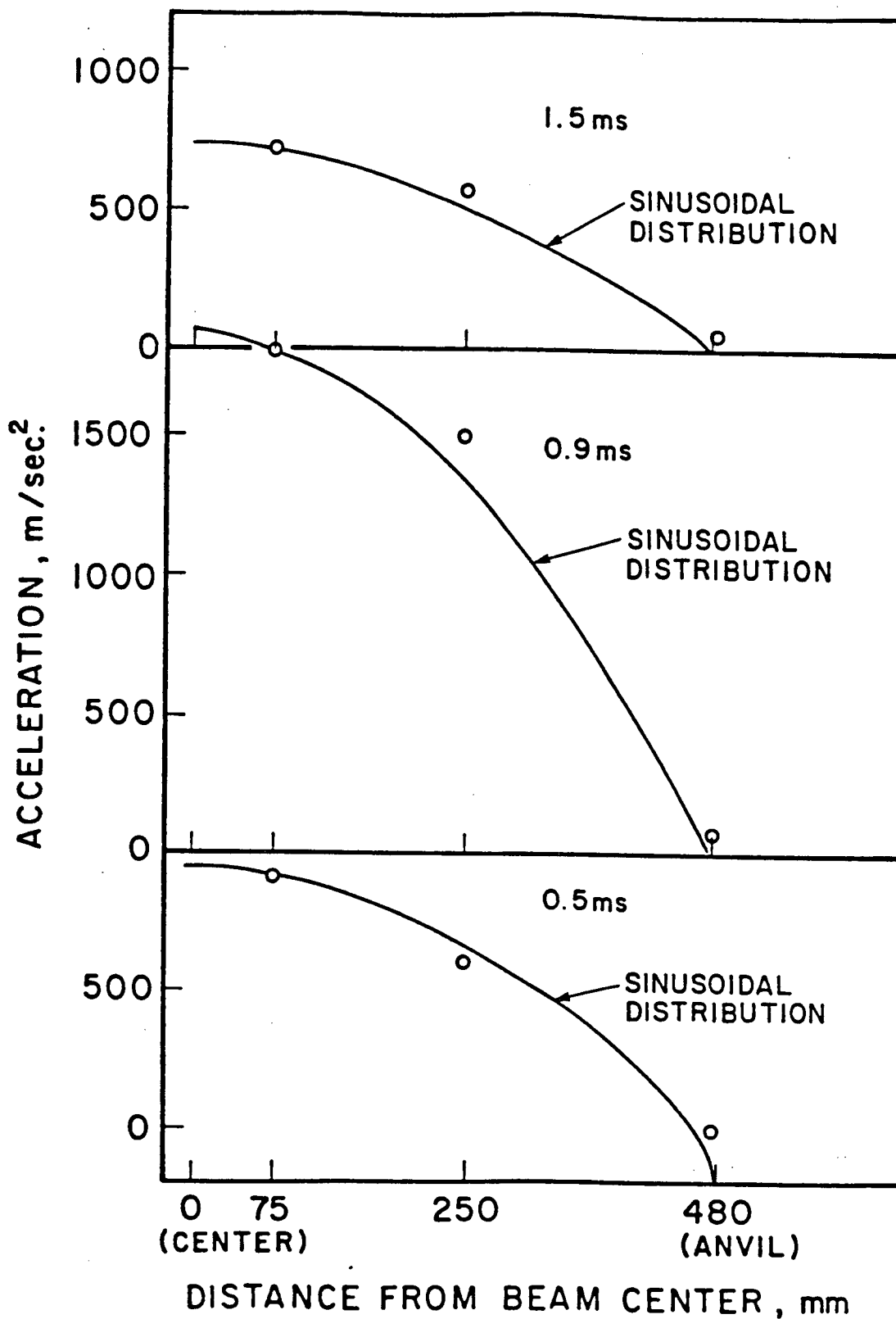


Figure 4.16-Acceleration distribution for conventionally reinforced concrete beams

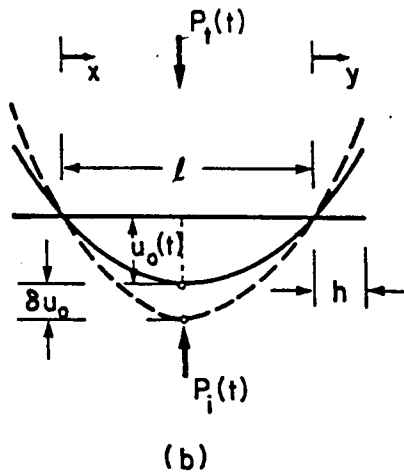
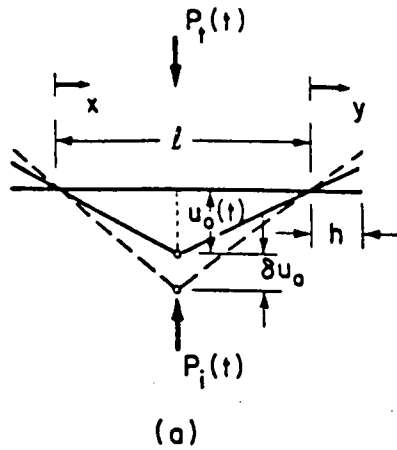


Figure 4.17-(a) Linear acceleration distribution and (b) Sinusoidal acceleration distribution

Note that the above expression can also be obtained from the general expression (Eqn.4.18) by expressing  $\ddot{u}_1(t)$ ,  $\ddot{u}_2(t)$ , and  $\ddot{u}_3(t)$  in terms of  $\ddot{u}_0(t)$ .

*(ii) Sinusoidal case*

In this case, the displacements between the supports are assumed to be sinusoidal, while the displacements on the overhanging portion are assumed to be linear (Figure 4.17b). Accordingly,

$$u(x,t) = u_0(t) \sin \frac{\pi x}{l} \quad (\text{between the supports})$$

$$u(x,t) = -u_0(t) \frac{\pi y}{l} \quad (\text{overhanging the supports}).$$

Rewriting Equation 4.18 for this case,

$$\begin{aligned} P_i(t) \delta u_0 = & \int \rho A \left[ \ddot{u}_0(t) \sin \frac{\pi x}{l} \right] \left[ \delta u_0 \sin \frac{\pi x}{l} \right] dx \\ & + 2 \int \rho A \left[ -\ddot{u}_0(t) \frac{\pi y}{l} \right] \left[ -\delta u_0 \frac{\pi y}{l} \right] dy \end{aligned} \quad (4.24)$$

For a prismatic and homogeneous beam, the above equation can be further simplified to

$$P_i(t) = \rho A \ddot{u}_0(t) \left[ \frac{1}{2} + \frac{2\pi^2 h^3}{3l^2} \right] \quad (4.25)$$

In addition, Eqn. 4.19 can be used in both the linear and in the sinusoidal cases to determine the generalized bending load.

#### *d. Moments and stresses*

For a beam undergoing impact, the moment at the centre can be obtained by taking the moment of all the forces acting on the beam about the center (Figure 4.18a). The same moment at the centre should also be predicted in the equivalent static system with the tup load and the inertial reaction replaced by the generalized bending load acting at the centre. The case of a linear acceleration distribution will be used to demonstrate this. If  $F_{i1}$  is the resultant of the distributed inertial reaction of the beam on the left or

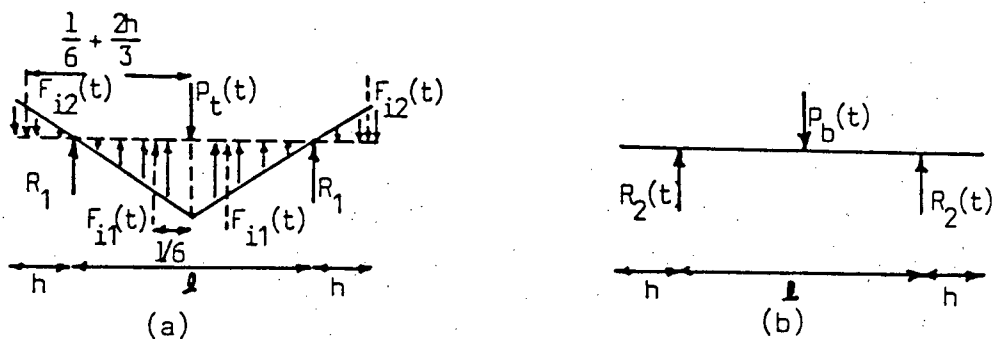


Figure 4.18-(a) Dynamic loading on the beam and (b)  
Equivalent static loading

the right half-span, and if  $F_{i2}$  is the resultant of the distributed inertial reaction of the beam on the overhang (Figure 4.18a), then,

$$F_{i1}(t) = \frac{1}{4} \rho A \ddot{u}_0(t) l \quad (4.26)$$

$$F_{i2}(t) = \frac{1}{1} \rho A \ddot{u}_0(t) h^2 \quad (4.27)$$

From the vertical equilibrium of forces,

$$R_1(t) = \frac{1}{2}P_t(t) - F_{i1}(t) + F_{i2}(t) \quad (4.28)$$

or,

$$\begin{aligned} R_1(t) &= \frac{1}{2}P_t(t) - \frac{1}{4}\rho A \ddot{U}_0(t)l + \frac{1}{1}\rho A \ddot{U}_0(t)h^2 \\ &= \frac{1}{2}P_t(t) - \rho A \ddot{U}_0(t) \left[ \frac{1}{4} - \frac{h^2}{1} \right] \end{aligned} \quad (4.29)$$

If  $M_0(t)$  is the moment at the centre,

$$M_0(t) = R_1(t)\frac{l}{2} + F_{i1}(t)\frac{l}{6} - F_{i2}(t) \left[ \frac{l}{2} + \frac{2h}{3} \right]$$

Substituting for  $R_1(t)$  from Eqn. 4.29,  $F_{i1}(t)$  from Eqn. 4.26, and  $F_{i2}(t)$  from Eqn. 4.27, we get

$$M_0(t) = P_t(t)\frac{l}{4} - \rho A \ddot{U}_0(t) \left[ \frac{l^2}{12} + \frac{2h^3}{3l} \right] \quad (4.30)$$

The generalized bending load  $P_b(t)$  can be obtained from Eqn. 4.19, using the generalized inertial load  $P_i(t)$  obtained from Eqn. 4.22,

$$P_b(t) = P_t(t) - \rho A \ddot{U}_0(t) \left[ \frac{l}{3} + \frac{8h^3}{3l^2} \right] \quad (4.31)$$

If  $M_{e_0}(t)$  is the value of the moment at the centre in the equivalent system, then,

$$M_{e_0}(t) = P_b(t) \frac{1}{4}$$

With  $P_b(t)$  obtained from Eqn. 4.31,

$$M_{e_0}(t) = P_t(t) \frac{1}{4} - \rho A \ddot{u}_0(t) \left[ \frac{l^2}{12} + \frac{2h^3}{3I} \right] \quad (4.32)$$

On comparing Eqn. 4.30 and Eqn. 4.32 it can be seen that the moment predicted by the equivalent system (Eqn. 4.32) is the same as the moment predicted by the dynamic analysis (Eqn. 4.30).

Since the generalized bending load predicts the correct moment at the centre in the equivalent system, it can be used directly for calculating the stresses and the strengths. The stresses in the beam can be obtained from

$$\sigma(c,t) = \left[ P_b(t) \frac{1}{4} \right] \left[ \frac{c}{I} \right] \quad (4.33)$$

where  $c$  is the distance of the fibre from the neutral axis and  $I$  is the moment of inertia. If  $\sigma_{td}$  is the modulus of rupture under the dynamic conditions then,

$$\sigma_{td} = \left[ P_{b,max} \frac{1}{4} \right] \frac{D}{2I} \quad (4.34a)$$

Finally if  $\epsilon_f$  is the extreme fibre strain at the peak bending load  $P_{b,max}$  then,

$$\epsilon_f = \frac{6 u_{o,peak} D}{l^2} \quad (4.34b)$$

Where,  $u_{o,peak}$  is the midspan displacement at the peak load, and  $D$  is the depth of the beam.

#### *e. Velocities and Deflections*

Once the acceleration history at any point along the length of the beam is known, the velocity and displacement histories can be obtained by integrations with respect to time. However, it is the velocity and the displacement history at the load point that are of prime concern to us from the point of view of analysis. The acceleration at the centre  $\ddot{u}_o(t)$ , obtained by the linear extrapolation of the measured accelerations, is used for this purpose. If  $\dot{u}_o(t)$  is the velocity at the centre, and  $u_o(t)$  is the displacement at the centre, then,

$$\dot{u}_o(t) = \int \ddot{u}_o(t) dt \quad (4.35)$$

$$u_o(t) = \int \dot{u}_o(t) dt \quad (4.36)$$

*f. Energy*

As in the static case, the area under the curve of generalized bending load (Eqn. 4.19) vs. midspan displacement (Eqn. 4.36) is a measure of the energy expended in bending the beam. At the end of the impact event, this area represents the fracture energy. If  $E_b(t)$  is the bending energy then,

$$E_b(t) = \int P_b(t) du_0 \quad (4.37)$$

*g. The computer program*

A computer program was written to analyse the data from the impact tests; the flow chart is given in Figure 4.19. The test data stored on the magnetic disc are time based. Thus, the analysis starts at the instant of first contact between the hammer and the beam ( $t=0$ ), and ends at the point of failure ( $t=t_f$ ), when the impact load has fallen back to zero. The output from the program is in the form of the energy loss history of the hammer ( $\Delta E(t)$ ), the energy gain history of the beam ( $E_b(t)$ ), and so on. The results can also be obtained in a graphical form.

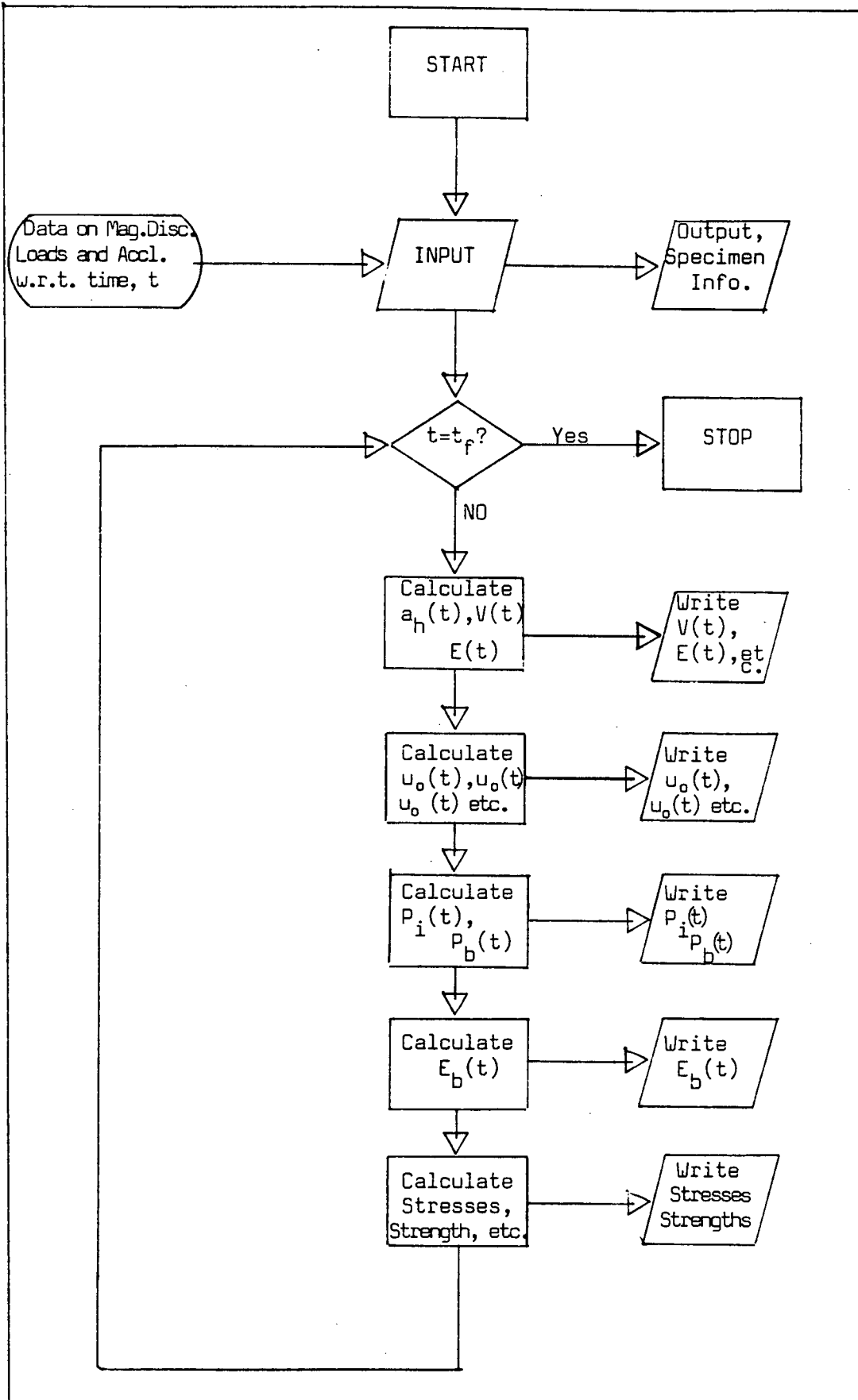


Figure 4.19- The Flow Chart of Analysis.

#### 4.3.2.4 The support reaction

##### a. The vertical reaction

As mentioned earlier, one of the support anvils was also instrumented to read the vertical reaction at the support. This is a completely independent method of checking the validity of Equation 4.29, and also provides a check on the operation of the accelerometers and the strain gauges in the tup. Figure 4.20 shows such a comparison. Figure 4.20 indicated two differences between the reaction  $R_1(t)$

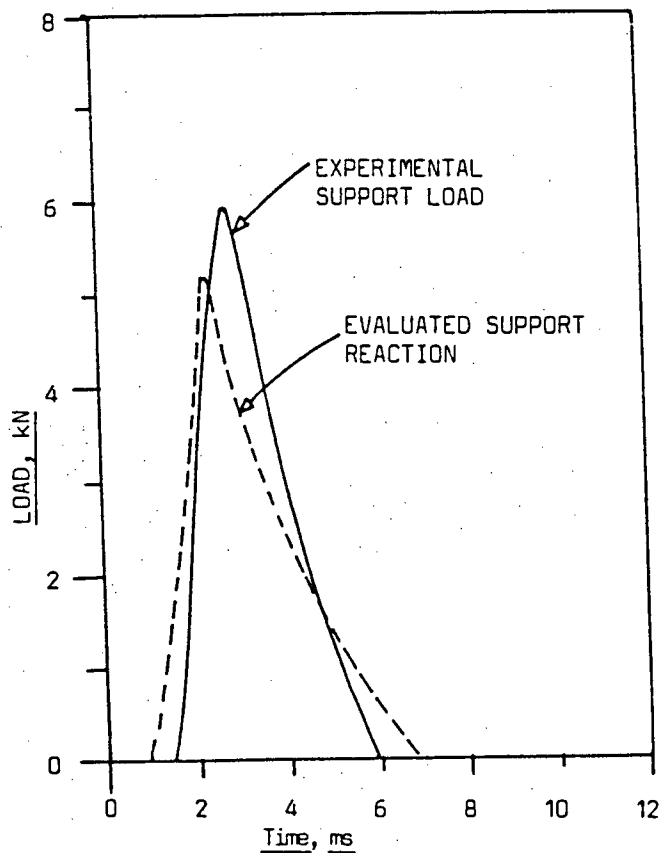


Figure 4.20-Comparison between the evaluated and the observed support reaction

obtained by using Eqn. 4.29, and the measured vertical support reaction. First, the peak value of  $R_1(t)$  is smaller by about 5-12% than the measured value. Secondly, there is a phase shift between the two peaks of about 0.2ms, with the measured peak lagging behind the analytical peak. Although the reasons behind the underestimation of  $R_1(t)$  are not clear, the shift between the two can be attributed to the finite time required for the stress waves to travel from the centre to the support. For concrete ( $E \approx 25 \times 10^9 \text{ N/m}^2$ , and  $\rho \approx 2400 \text{ kg/m}^3$ ), the velocity of the longitudinal stress waves,  $c$ , (given by  $c = \sqrt{E/\rho}$ ) is about 3300 m/sec. At this velocity, a stress wave takes about 0.15ms to travel from the centre to the support (a distance of 480 mm). In addition, the sampling is done at intervals of 0.20ms. The travel time for the stress waves, the discrete sampling interval, and the possible uneven contact of the beam at the supports can, to some extent at least, explain this lag.

The reaction  $R_2(t)$  in the equivalent static system of Figure 4.18b, can be evaluated by summing the forces in the vertical direction.

$$R_2(t) = \frac{1}{2}P_b(t)$$

Using  $P_b(t)$  from Eqn. 4.31 (linear approximation), we get,

$$R_2(t) = \frac{1}{2}P_t(t) - \rho A \ddot{u}_0(t) \left[ \frac{1}{6} + \frac{4h^3}{31^2} \right] \quad (4.38)$$

A comparison of  $R_1(t)$  from Eqn. 4.29 and  $R_2(t)$  from Eqn. 4.38 shows that they are somewhat different. However, for the commonly observed peak top loads and accelerations in this study, the difference between the peaks was less than 6%. Thus, although not strictly valid, the measured support reaction, when doubled and compared to the generalized bending load, can provide another check on the technique for inertial correction used here. Figure 4.21 shows such a comparison. The shift between the two peaks can be explained as above.

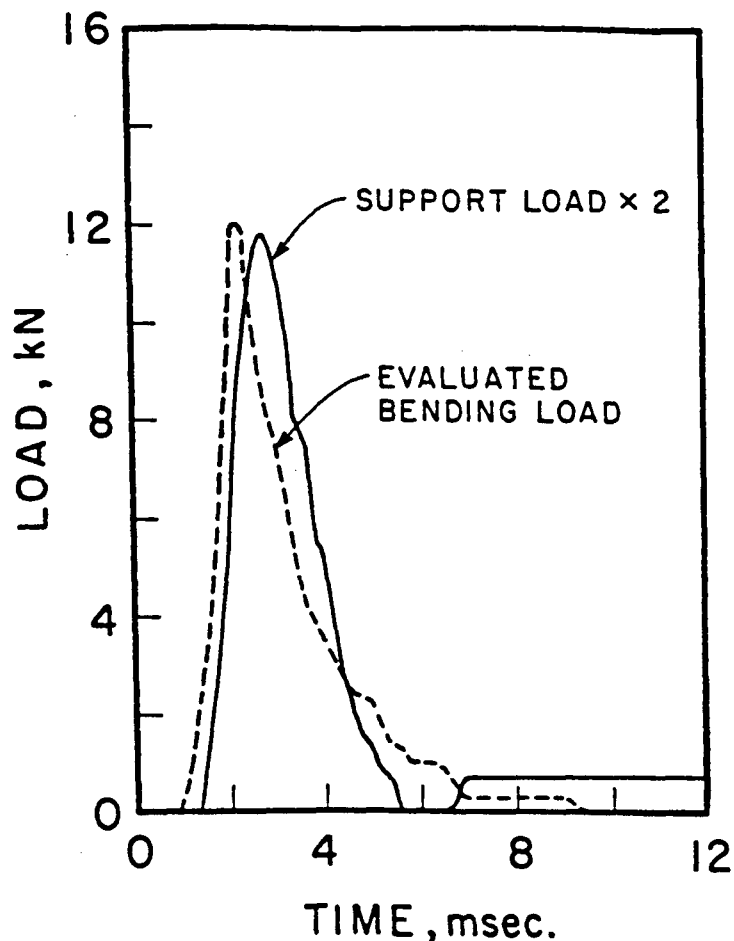


Figure 4.21-A rough check on the validity of the technique used here to account for inertia

*b. The horizontal reaction*

As mentioned earlier, the instrumentation in the support anvil was capable of recording the horizontal reaction as well. In the tests performed in this study, the horizontal reaction was always found to be close to zero. This confirmed the assumption that the beam was simply supported. The horizontal support reaction obtained from an impact test done on a plain concrete beam has been shown in Figure 4.22.

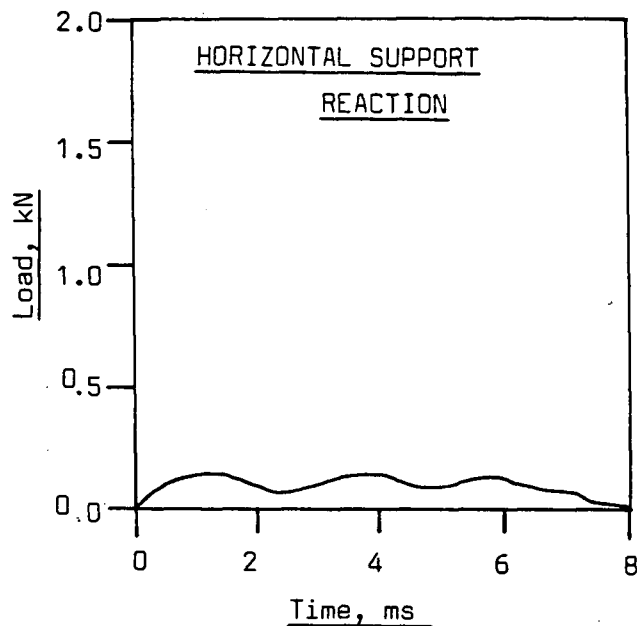


FIGURE 4.22-The Horizontal Support Reaction

## 5. INERTIAL LOADING IN INSTRUMENTED IMPACT TESTS

### 5.1 INTRODUCTION

The testing of concrete at high strain rates requires both a testing system capable of producing high strain rates, and a valid technique to analyse the results. Normally, impact tests on concrete in compression or tension do not pose a serious problem concerning the specimen inertia. However, impact tests on concrete beams loaded in 3-point or 4-point bending give rise to specimen inertia effects which must be considered in the analysis. When the instrumented tup of the hammer strikes the beam, the beam suddenly gains momentum and the unsupported part of the beam accelerates in the direction of the hammer. This gives rise to d'Alembert forces, acting in a direction opposite to the direction in which the beam accelerates. The strain gauges in the tup, sensing the contact load between hammer and the beam, sense this inertial load as well. Thus the tup load consists of the mechanical bending load (the stressing load), and the load due to the inertial reaction of the specimen. The mechanical bending load, which is the obvious goal of testing, can thus be obtained from the tup load only if the "inertial reaction" of the beam is known.

## 5.2 NATURE OF THE INERTIAL LOAD

The nature of the inertial load can best be understood by a single degree of freedom model as outlined in Chapter 7 (Appendix-7.1). The accelerations predicted by the model (Eqn.A7.1-8) have been plotted in Figure 5.1 against time. The accelerations were obtained for a plain concrete beam struck by the hammer falling through 0.5m. The observed peak tup load was taken equal to  $P_0$ , and the frequency of the external load  $\omega$  was determined by the time required by the

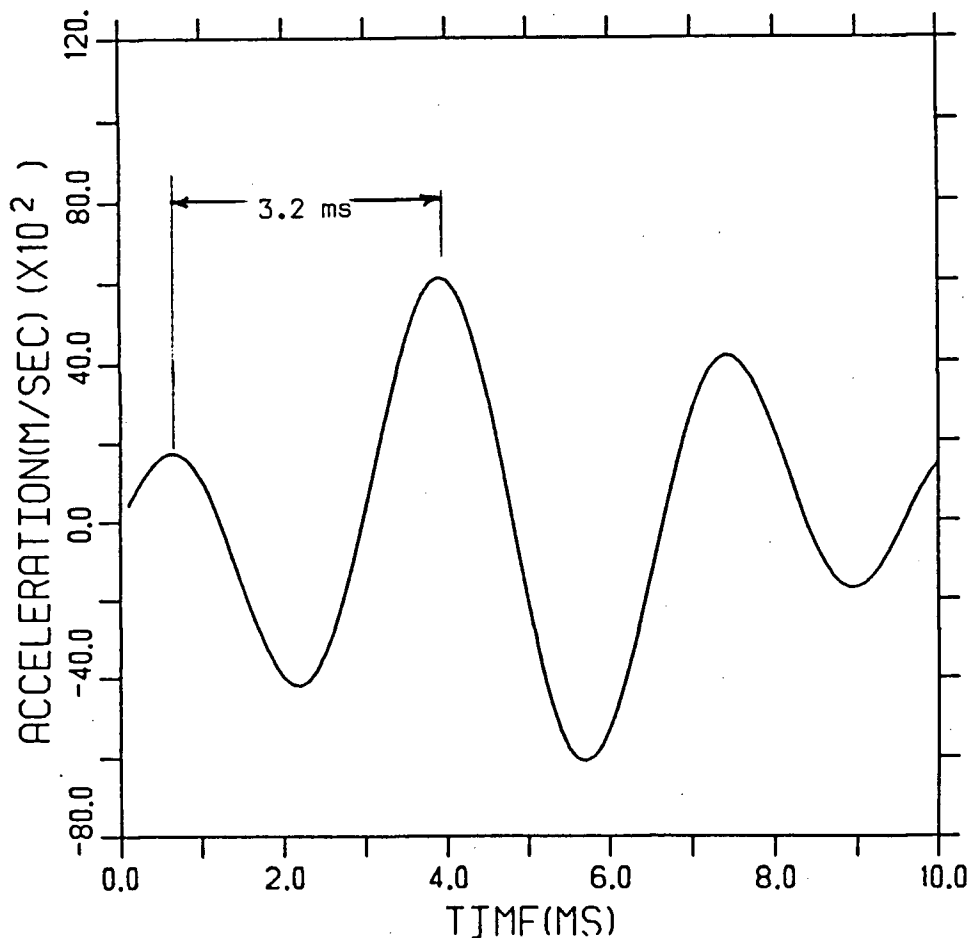


FIGURE 5.1-Period of Inertial Oscillations

tup load to attain the peak in an actual test.

As shown in Figure 5.1, the accelerations seems to vary sinusoidally with a period of about 3.2ms for the plain concrete beams used in this study. Similar plots can be obtained for conventionally reinforced and fibre reinforced concrete as well; the nature of Eqn. A7.1-8 suggests that the acceleration variation with respect to time in these cases will also be sinusoidal, but with a different period than that for the plain concrete. Inertial load, which is the product of the generalized mass and the central acceleration, therefore is proportional to the acceleration, and hence has the same period as does the acceleration.

Server (14) has proposed an empirical expression to predict the period of inertial oscillations in terms of the specimen width B, specimen thickness D, specimen compliance  $C_s$ , and Young's Modulus E:

$$\tau = 3.36(B/D)(EDC_s)^{0.5} \quad (5.1)$$

Server also suggested that reliable measurements could be made only after 3 inertial oscillations, i.e., at any time t given by,

$$t \geq 3\tau \quad (5.2)$$

Thus after three inertial oscillations, the tup load can be

assumed to be represent the true mechanical load on the specimen.

For ductile materials, like metals, the guidelines suggested by Server may be met. However, for brittle materials, like concrete, these guidelines cannot be met in general. The basic difference between ductile and brittle systems is the time required by the specimens to fail. In the case of ductile materials, the specimen usually undergoes more than three inertial oscillations before failing. However, in the case of brittle materials, it may not be possible to avoid failure during the first oscillation (Figure 5.1). Thus, the whole impact event may not last as long as three oscillations; the entire mechanical response of the specimen may take place while the specimen is still being accelerated, and the inertial load can completely overshadow the true mechanical bending load. For brittle specimens, therefore, the approach has to be different than for ductile ones.

Evaluation of the inertial load is possible in two ways: (1) by analytical methods as described in Chapter 7; and (2) by experimentally measuring the accelerations along the length of the beam and then evaluating the generalized inertial load as described in Chapter 4. The analytical models, however, do create some problems in the realm of material testing:

(a) The analysis applies only to elastic systems. This implies that only the beam response up to the peak load can

be determined with the help of these models. This might not be of great concern if concrete were an ideally brittle material, and the loads were to drop suddenly to zero once the peak had been reached. Experimental evidence suggests that this is not true, and the load vs. displacement plot in dynamic conditions seems to have a large post-peak region as well. Unfortunately, the elastic analysis cannot be applied in this region.

(b) The dynamic analysis requires knowledge of the beam stiffness. The estimation of the beam stiffness, in turn, requires knowledge of concrete properties at the relevant stress rates. Since concrete properties at the high stress rates associated with impact are not very well known, the exact estimation of the stiffness of the concrete beam is not possible.

### 5.3 EXPERIMENTAL OBSERVATIONS

Inertial corrections could have been ignored if the "inertial reaction" part of the tup load was a small percentage of the true mechanical bending load. However, experimental evidence suggests that in the initial part of the impact the inertial load can amount to as much as 60% of the observed tup load. Figure 5.2 shows the inertial load vs. time plots for three different hammer drop heights, obtained in the case of plain concrete beams. Figure 5.3 shows the inertial load plotted against time for

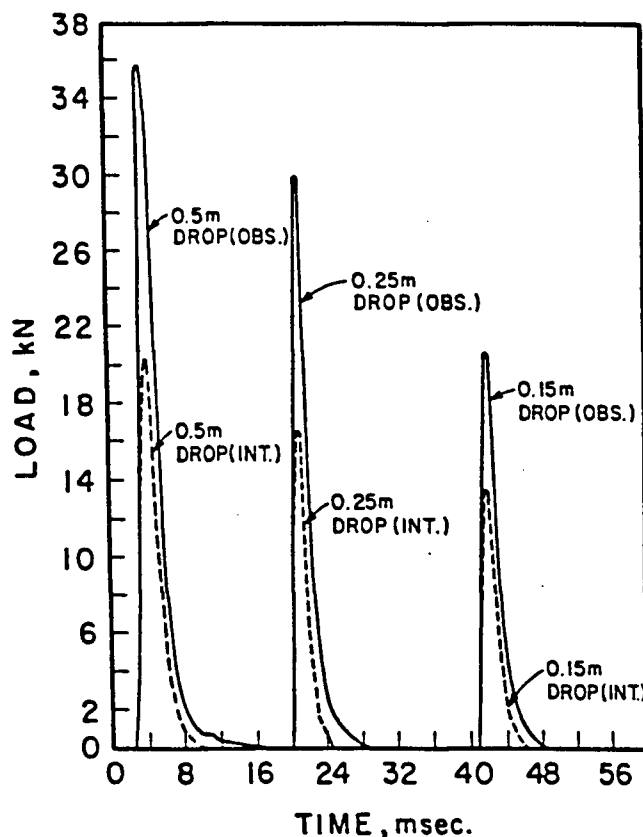


FIGURE 5.2-Observed Tup and Inertial Loads for Plain Concrete

conventionally reinforced concrete for a hammer drop height of 0.5m. For comparison purposes, the results obtained for a plain concrete specimen tested under 0.5m hammer drop (a different specimen than the one shown in Fig. 5.2) are also reproduced in Figure 5.3. The peak tup loads and the peak inertial loads in Figure 5.2 for plain concrete are replotted in Figures 5.4a and 5.4b, respectively, as a function of hammer drop height.

An increase in the drop height of the hammer resulted in an increase in the inertial load. An almost linear variation was observed (Figure 5.4b). This implies that the

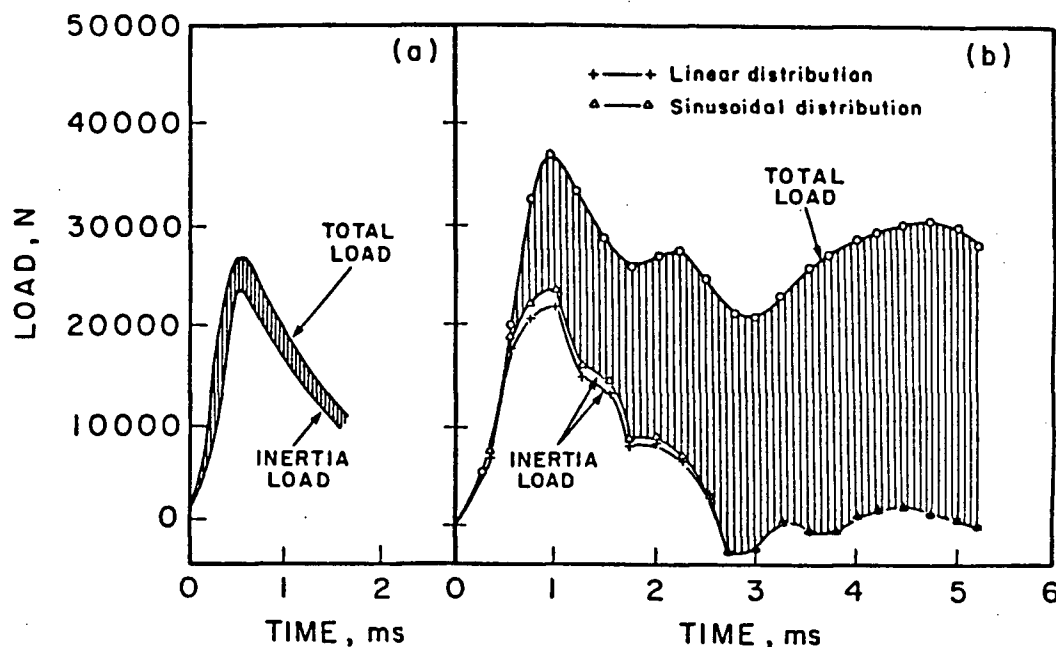


FIGURE 5.3—Observed Top and Inertial Loads for (a) Plain and (b) Conventionally Reinforced Concrete

correction for inertia becomes more and more important as the strain rate at which the testing is done is increased.

Stiffer systems seem to undergo lower accelerations and hence develop lower inertial loads than do specimens that are not as stiff. High strength plain concrete beams, which are stiffer than normal strength plain concrete beams, were found to have lower peak inertial loads than normal strength plain concrete beams tested under identical conditions (Figure 5.4b).

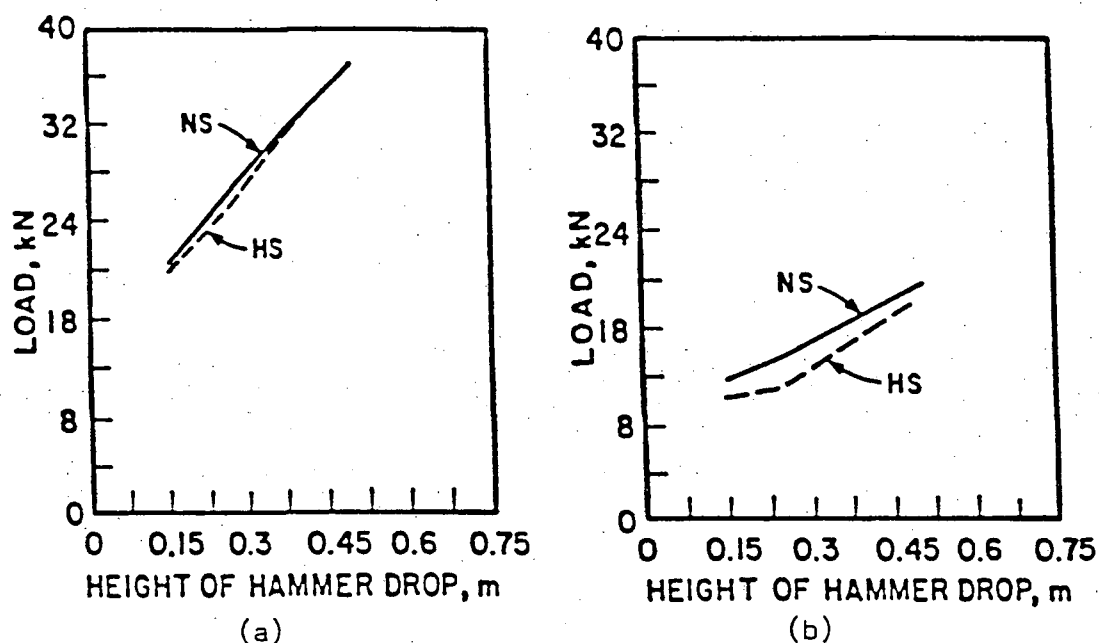


FIGURE 5.4-Effect of Hammer Drop Height on (a) Top and (b) Inertial Loads for both Normal Strength (NS) and High Strength (HS) concrete

#### 5.4 THE USE OF THE RUBBER PAD

One of the suggested experimental methods for eliminating the inertial loading is the use of a rubber pad between the hammer and beam (16). It is argued that the rubber pad delays the occurrence of the peak external load. This gives sufficient time for the beam to reach the tup velocity, and so at the occurrence of the peak external load, the accelerations and hence the inertial load are absent. Thus the measured tup load at the peak can be assumed to be the actual beam bending load.

To examine the validity of this technique, tests were carried out on plain and conventionally reinforced concrete beams with and without a rubber pad in the system. Hammer drop heights ranging from 0.15m to 1.0m were used. The experimentally determined accelerations and the inertial loads for tests done without the rubber pad were compared to those for the tests done with the rubber pad in the system. Similar comparisons were made between the peak external loads, peak bending loads, and the fracture energies. The stiffness of the 40mm thick rubber pad used was 2.83 MN/m.

In general, it was found that although the occurrence of the peak external load was delayed with the rubber pad in the system, the occurrence of the peak beam acceleration was also delayed, and the two occurred at almost the same time. Tables 5.1 and 5.2 and Figs. 5.5 and 5.6 show the results obtained with and without the rubber pad for both plain and conventionally reinforced concrete. The use of the rubber pad resulted in a delay in the occurrence of the peak tup load, a reduction in the peak value of the tup load, and also in a reduction in the peak accelerations attained in a test. A reduction in the peak bending loads was also observed.

It was concluded that with the pad in the system, the accelerations, and hence the inertial loads, were reduced. However, inertial loads were not completely eliminated. Inertial loading, thus, appears to be an inherent characteristic of dynamic testing of this kind, and cannot

**Table 5.1**  
**Effect of Rubber Pad on Plain Concrete Beams Under Impact**  
 Height of Hammer Drop (m)

		0.15 m (6) <sup>1</sup>		0.25m (6) <sup>1</sup>		0.50m (6) <sup>1</sup>	
		Without Pad	With Pad	Without Pad	With Pad	Without Pad	With Pad
Peak Load (N)	Tup	19776	12358	25386	12956	37567	14267
Time to Peak (ms)		1.4	9.0	1.2	8.0	0.8	6.0
Peak Acceleration (m/sec <sup>2</sup> )		1140	766	1340	828	1967	906
Peak Inertial Load (N)		11994	6731	13203	6845	20635	6852
Peak Bending Load (N)		7782	5987	12183	6111	16932	7415
Fracture Energy (Nm)		25.8	40.0	42.0	41.5	90.1	69.6

**Table 5.2**  
**Effect of Rubber Pad on Conventionally Reinforced Beams under Impact**  
 Height of Hammer Drop (m)

		0.5 m (6) <sup>1</sup>		1.0m (6) <sup>1</sup>	
		Without Pad	With Pad	Without Pad	With Pad
Peak Load (N)	Tup	48071	43195	63216	51854
Time to Peak (ms)		1.80	10.6	1.20	7.8
Peak Acceleration (m/sec <sup>2</sup> )		7020	681	1321	1054
Peak Inertial Load (N)		10383	10134	22037	17330
Peak Bending Load (N)		37688	33061	41179	34524
Fracture Energy (Nm) (to 18mm LPD <sup>2</sup> )		603	637	666	610
Fracture Energy (Nm) (to 36mm LPD <sup>2</sup> )		934	882	1340	1190

<sup>1</sup>Number of specimens tested.

<sup>2</sup>Load Point Deflection.

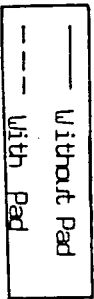
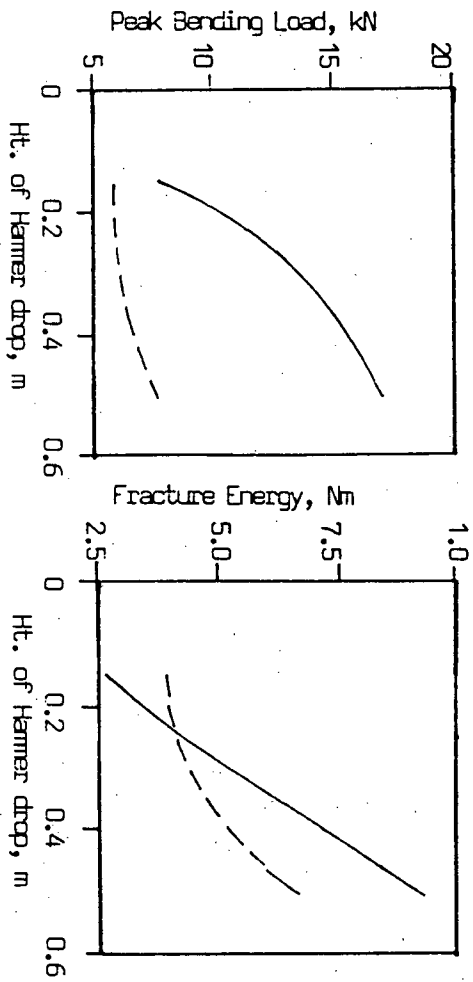
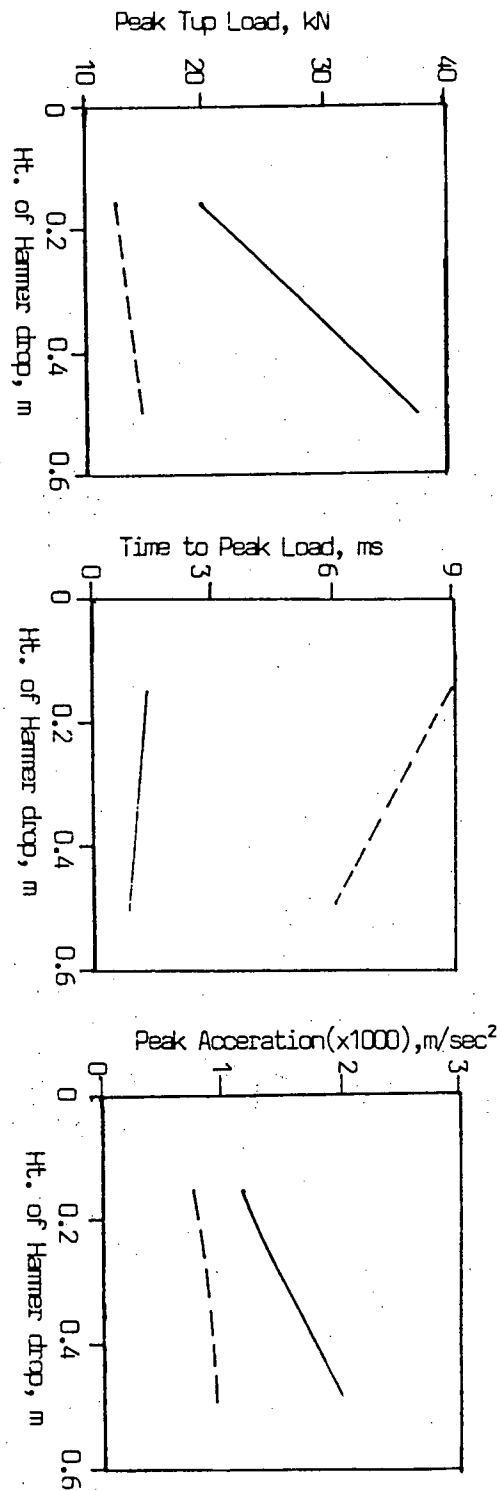


Figure 5.5-Effect of Rubber Pad on Plain Concrete

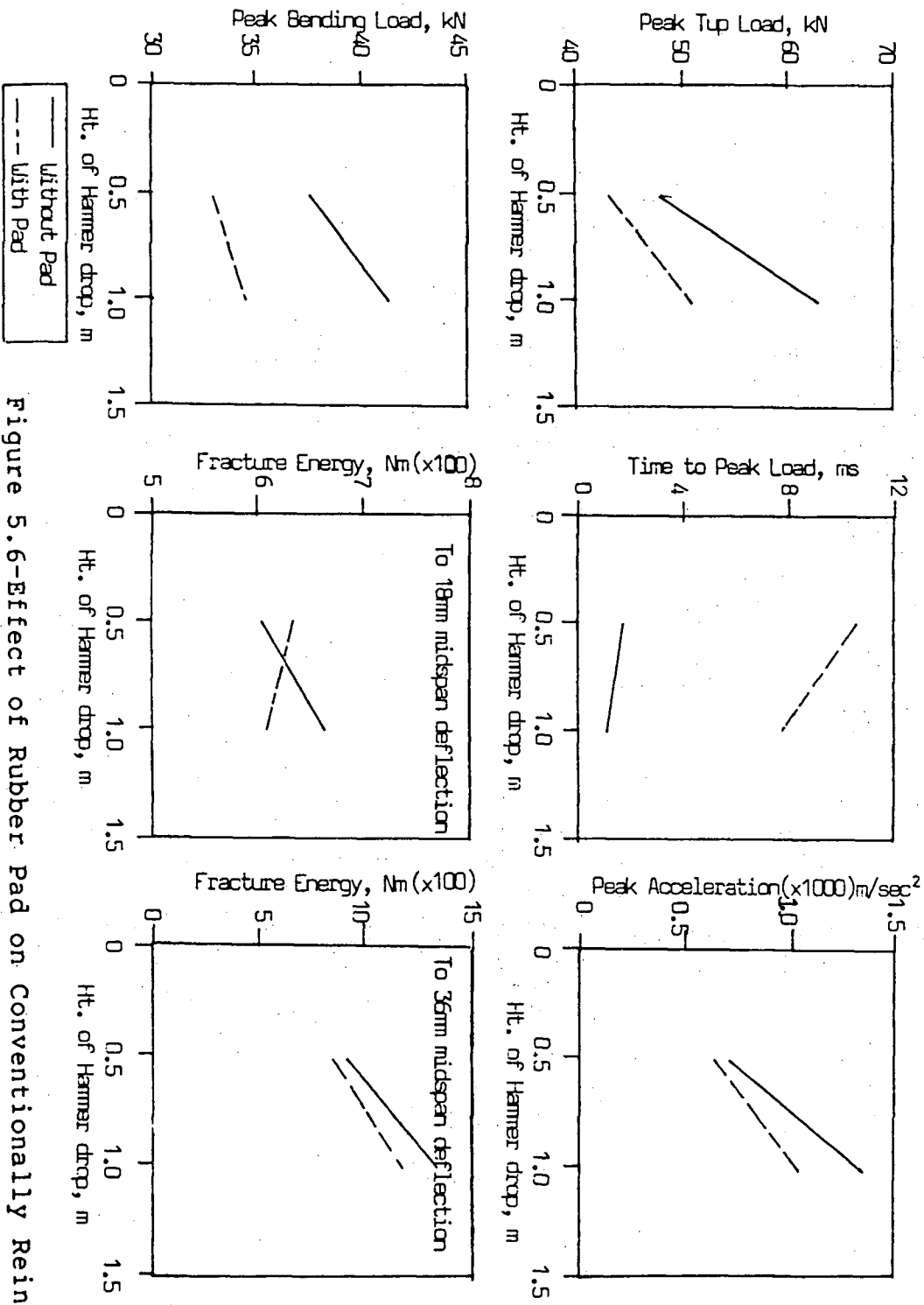


Figure 5.6-Effect of Rubber Pad on Conventionally Reinforced Concrete

easily be eliminated.

The delay in the occurrence of the peak tup load reduces the strain rate achieved in a test. This was thought to be the probable reason behind the reduced peak bending loads observed in the tests done with the rubber pad in the system. Reducing the stiffness of the contact zone decreases the strain rate and hence, to some extent at least, defeats the purpose of high strain rate testing.

In general, the fracture energy values obtained with the rubber pad in the system were found to be lower than the ones obtained without the pad, with certain exceptions. It is not clear if the fracture energies obtained from the tests done with the rubber pad in the system can be assumed to be the true beam fracture energies, because of the energy absorption capacity of the pad itself.

### 5.5 INSTRUMENTING THE SUPPORT ANVILS

Instrumentation of the support anvils has also been suggested as a way of obtaining the true mechanical bending load on the specimen (15) (Chapter 4). However as pointed out in the previous chapter, the support reaction is not strictly equal to one half of the generalized bending load. Also, the finite time required for the stress waves to travel from the beam midspan to the support causes a lag between the two loads. However, the difference between the magnitudes of the two loads is not substantial (Chapter 4). Instrumenting the anvil in this study, provided a rough

check on the inertial correction applied to the tup load, and also provided a check on the behaviour of the strain gauges and the accelerometers.

## 6. PLAIN CONCRETE UNDER IMPACT

### 6.1 INTRODUCTION

Single cycle impact loading on any structural element may occur either as a distributed time varying load due to a wind gust or air blast, or as a concentrated time varying point load as in the case of an object striking a structural member. In both situations, a knowledge of the exact variation of load with time, although desirable from the design point of view, is difficult to acquire. In the absence of a precise knowledge of the load vs. time history of the impact, it is convenient to work with "energy" values. Impact, in most cases, involves an external agency capable of imparting energy to the structural element. The external agency could be the shaking ground underneath a building, or a missile fired at a military installation. The structure, with all of its elements, responds to this externally available energy by deforming. Stresses and strains are developed within the structure, and the structure continues to absorb energy as strain energy. In this situation, there are three possibilities:(1) All of the externally available energy may be absorbed as strain energy without causing any damage to the structure. Once the external load is removed, such a strained structure will dissipate its strain energy by the various dissipation mechanisms, (2) An intermediate case in which the structure is damaged, but collapse is not precipitated, and (3) The externally available energy may be more than the maximum

strain energy the structure or its elements can absorb without fracturing. Fracture will initiate at the locations where the critical stresses are exceeded, and collapse may result.

It is the third possibility that is of serious concern in dynamic loading situations because of the catastrophic nature of failure. The first possibility, in which the structure remains elastic during the whole loading history, although structurally feasible, involves heavily overdesigned sections, economically unacceptable. The problem can be overcome, at least in part, by giving the structure added ductility by which the structure would continue to deform under the load, absorbing the external energy. A catastrophic type of failure could, with this added ductility change to a "yield before fail" type of failure.

Concrete, compared to metals, absorbs very little energy before a catastrophic failure results. This mode of failure, occurring without much warning, can be changed to some extent by incorporating fibres, or steel reinforcing bars, or both into the matrix. The behaviour of the resulting composites under dynamic conditions depends, among other things, upon the way in which the matrix behaves under these conditions. A knowledge of the behaviour of plain concrete under dynamic conditions is therefore essential, particularly because of the strain rate sensitivity of concrete. An account of the the dynamic properties of

hardened cement paste, and plain concrete, will be presented in this chapter. The succeeding chapters will examine the effect of adding fibres, the effect of adding conventional steel reinforcement, and the effect of adding both.

## 6.2 COMPARISON OF THE IMPACT BEHAVIOUR OF PASTE AND CONCRETE BEAMS

The properties of plain concrete depend to quite an extent on the properties of the hardened paste. Hence an understanding of the behaviour of concrete under high stress rates is possible only with an understanding of the behaviour of the paste under similar conditions. Therefore, in this study, three beams made with pure paste (w/c ratio of 0.35) were tested in the impact machine. A hammer drop height of 0.5m was used.

Table 6.1 contains the results of the above tests. The results obtained with normal strength concrete beams tested under identical conditions have also been tabulated for comparison.

Figure 6.1 presents the general nature of the load vs. displacement plots to failure for both paste and normal strength concrete. Figure 6.2 presents the portions of load vs. displacement plots prior to the peak bending loads.

It can be seen from Figures 6.1 and 6.2 that under impact loading, paste appears to be marginally weaker than

**Table 6.1**  
**Comparison between the Dynamic Properties of Paste and Concrete**

		Paste (3) <sup>1</sup>				Concrete (6) <sup>1</sup>			
		Max	Min.	Mean	s	Max.	Min.	Mean	s
<b>Max. Observed</b>	<b>Tup Load (N)</b>	28793	28093	28428	286	31251	27388	29319	1931
<b>Max. Beam</b>	<b>Accel. (m/sec<sup>2</sup>)</b>	1986	1928	1955	24	1858	1718	1788	70
<b>Peak Bending</b>	<b>Load (N)</b>	8470	7462	7819	461	11658	9267	10462	1195
<b>Deflection at</b>	<b>Peak Bending</b>	479	400	429	35.3	469	384	426	42.5
<b>Load</b>	<b>(x10<sup>-6</sup>)(m)</b>								
<b>Beam Energy</b>	<b>at Peak</b>	2.8	2.2	2.5	0.25	4.7	2.6	3.7	1.0
<b>Bending</b>	<b>Load</b>								
<b>(Nm)</b>									
<b>Failure</b>	<b>Strain</b>	3.11	2.60	2.79	0.23	3.05	2.49	2.77	0.28
<b>(x10<sup>-4</sup>)</b>									
<b>Modulus</b>	<b>of</b>	9.8	8.6	9.0	0.53	13.5	10.7	12.0	1.37
<b>Rupture</b>	<b>(MPa)</b>								
<b>Fracture</b>	<b>Energy</b>	39.2	30.8	34.9	3.5	47.9	44.5	46.2	1.7
<b>(Nm)</b>									

<sup>1</sup>Number of specimens tested.

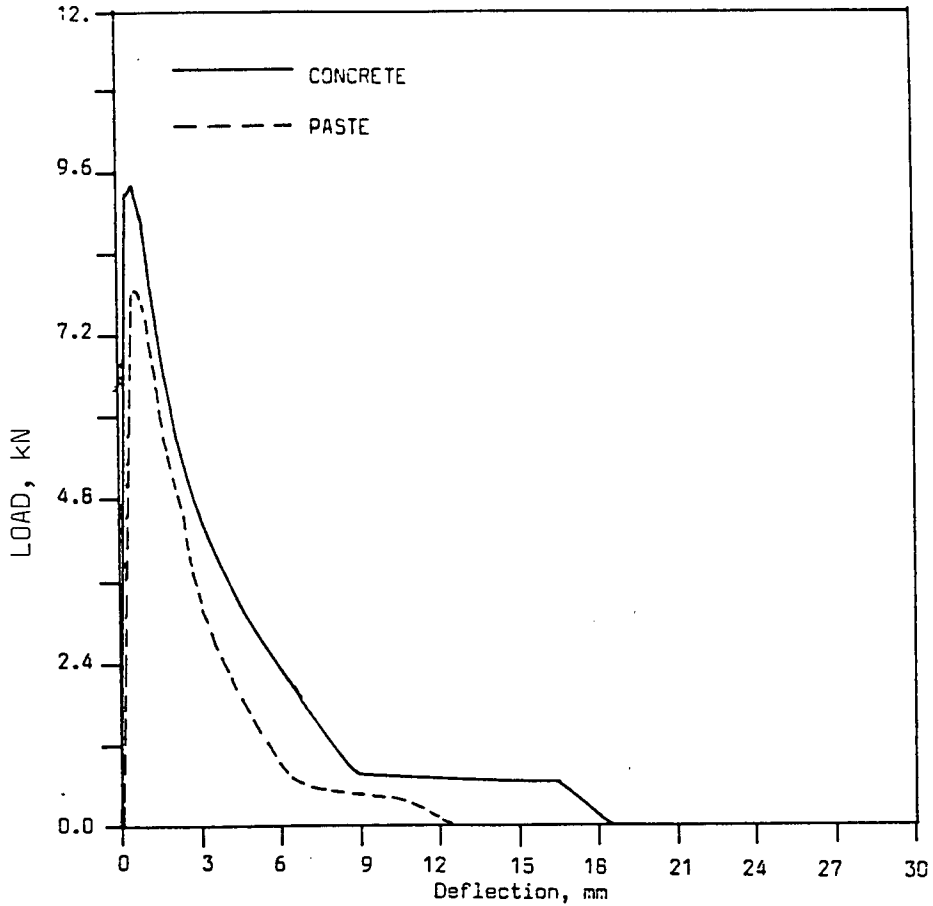


Figure 6.1- Impact Behaviour of Paste and Concrete

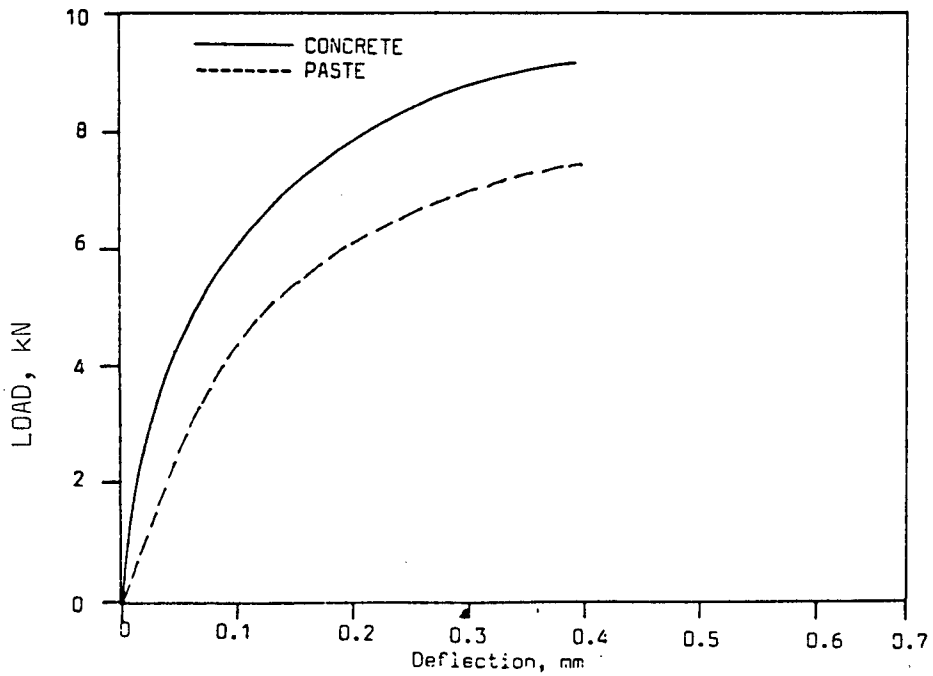


Figure 6.2- Impact behaviour of Paste and Concrete up to the Peak Load.

concrete. The modulus of rupture (MOR), as determined from an elastic analysis (Eqn.4.34a), seems to be about 30% higher for concrete than for the paste. The values of fracture energies in Table 6.1 indicate the more brittle nature of the paste compared to concrete. Interestingly, the failure strains, calculated using the elastic analysis (Eqn. 4.34b), seem to have the same value for paste and concrete. An inspection of the fracture surfaces of the broken halves of the beams indicated that while the surface was very even and smooth for the paste, it was fairly uneven for concrete. The uneven fracture surface suggested that, in concrete, the crack followed a tortuous path around the aggregates,

Concrete can be considered to be a dispersion of inert aggregate particles in a paste matrix. The bond between the paste and the aggregates is in part due to the mechanical interlocking of the aggregates and the paste, and in part due to adhesion. Under static loading, the paste and concrete were found to be very similar in their flexural strengths. The trend was preserved in the dynamic situation as well (Figure 6.2). The occurrence of almost the same value of failure strain in both paste and concrete suggests that it may not be a limiting stress but a limiting tensile strain that determines the strength of concrete at a particular strain rate. The incorporation of aggregates that are stiffer than the paste results in an increase in the stiffness of the resulting concrete over that of the paste. Thus, to achieve the same level of strain both in concrete

and in paste, the effective stress in concrete has to be higher than that in the paste. The higher initial elastic modulus in the case of concrete (Fig 6.2) supports this argument. Thus, at the same failure strain, concrete can support a higher load than the paste.

Complete fracture of the concrete required a higher energy than fracture of the paste. The fracture energy, which is the area under the load vs. displacement plot to failure, depends upon the magnitudes of the loads and displacements. As can be seen from Figure 6.1, for the same displacements, the concrete beam could support marginally higher loads than the paste beam. If the crack is assumed to nucleate at the peak load, the unstable growth of the crack in concrete seems to require a higher driving force, i.e., the crack in the concrete seems to undergo a higher resistance to its growth than that in the paste. The tortuous path taken by the crack around the aggregate particles in concrete, resulting in larger apparent fracture surface area, and the straight path taken by the crack in the paste, resulting in a smooth fracture surface, seem to support this argument.

### 6.3 EFFECT OF STRESS RATE ON PLAIN NORMAL STRENGTH (NS) CONCRETE BEAMS

To study the effect of strain rate on normal strength concrete, plain concrete beams were tested at variable strain rates. Both static and dynamic tests were carried out. The static tests were conducted in a universal testing machine, with its cross-head moving at  $4 \times 10^{-7}$  m/sec. The dynamic tests were conducted in the drop weight impact machine. The dynamic tests were carried out using three different hammer drop heights, of 0.15m, 0.25m, and 0.5m.

Table 6.2a shows the results from the static testing, while table 6.2b contains the results from the drop weight impact tests. It may be seen that the strain rates imposed on the concrete varied from about  $3 \times 10^{-7}$ /sec in the static case to about 0.5/sec in the dynamic case with a 0.5m drop. The behaviour of concrete at these extreme rates of straining is shown in the load vs. deflection plots of Figure 6.3. It can be seen from Figure 6.3 that upon increasing the strain rate from  $3 \times 10^{-7}$ /sec in the static case to about 0.5/sec in the impact range ( $\approx 1.5 \times 10^6$  times increase), the properties of concrete seem to change considerably. Even within the dynamic range, a variation in the drop height of the hammer resulted in a considerable variation in the properties of concrete (Figure 6.3). In general, it may be seen that concrete is a very strain rate sensitive material. The main differences between the static and dynamic properties are the increased strength and the

Table 6.2(a)  
**Static Behaviour of Normal Strength Plain Concrete Beams**

	Static (3) <sup>1</sup>			
	Max	Min.	Mean	s
Peak Bending Load (N)	6766	6000	6344	306
Deflection at Peak Bending Load ( $\times 10^{-6}$ )(m)	388	289	307	20
Beam Energy at Peak Bending Load (Nm)	1.1	0.88	1.0	0.08
Failure Strain ( $\times 10^{-4}$ )	2.7	2.4	2.5	0.17
Modulus of Rupture (MPa)	6.3	5.5	5.9	0.29
Fracture Energy (Nm)	6.5	2.9	5.5	1.5
Mean Strain Rate (/sec)			$3 \times 10^{-7}$	
Mean Stress Rate (MPa/sec)			0.0079	

<sup>1</sup>Number of specimens tested.

Table 6.2(b)  
Dynamic behaviour of Plain Normal Strength Concrete  
Height of Hammer Drop (m)

	0.15m (6) <sup>1</sup>				0.25m (6) <sup>1</sup>				0.50m (7) <sup>1</sup>			
	Max	Min	Mean	s	Max	Min	Mean	s	Max	Min	Mean	s
Max. Top Load (N)	21309	18803	19776	963	29840	21666	25386	3121	37567	35810	36196	677
Max. Inertial Load (N)	12957	10512	11306	632	15401	11987	13203	1314	20291	16868	19264	1278
Peak Bending Load (N)	9440	7782	8470	604	14668	9178	12183	2401	17727	16452	16932	428
Energy at Peak Load (Nm)	3.5	1.5	2.5	0.7	3.7	2.7	3.0	0.4	9.0	2.2	6.4	2.5
Fracture Energy (Nm)	30.9	19.1	25.8	4.3	59.6	26.5	42.0	12.4	100.5	87.8	90.1	6.5
Modulus of Rupture (MPa)	8.7	7.2	7.8	0.5	13.6	8.5	11.3	2.2	16.4	15.2	15.7	0.4
Failure Strain ( $\times 10^{-4}$ )	3.0	2.1	2.7	0.4	3.6	3.0	3.5	0.3	4.0	2.9	3.5	0.4
Mean Stress Rate (MPa/sec)			3920				8057				19587	
Mean Strain rate (/sec)			0.14				0.25				0.44	

<sup>1</sup>Number of specimens tested.

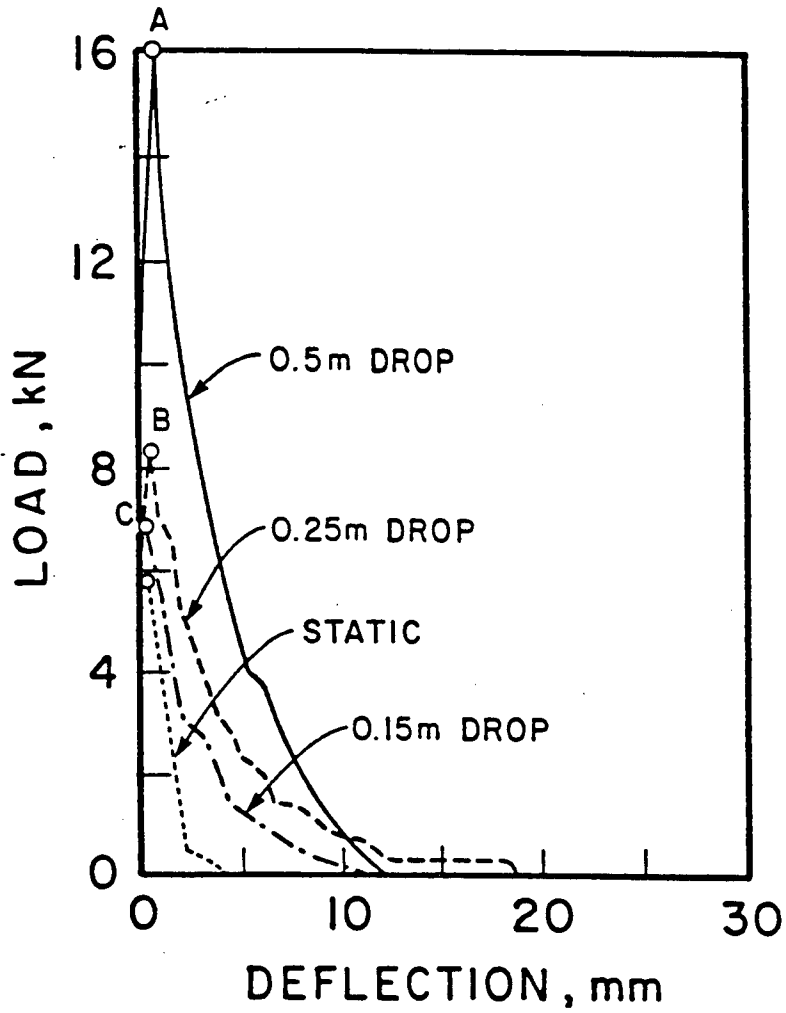


Figure 6.3-Static and Dynamic Load Deflection Plots for Normal Strength Concrete

higher fracture energies in the dynamic case compared to those in the static case.

The differences between the static and the dynamic behaviour of concrete can be explained on the basis of fracture mechanics by a combination of the classical Griffith theory, and the concept of subcritical crack growth (static fatigue). According to the Griffith theory, the tip of a crack or a flaw in a loaded continuum is a point of stress concentration. Even when the nominal stress is far below the theoretical strength of the material, the stress at the leading edge of the crack may well approach the theoretical strength and failure may result. The stresses in the vicinity of a loaded crack are a function of the nominal stress, and the crack geometry. The combined effect of these two parameters can be expressed in terms of just one parameter, called the stress intensity factor  $K_I$ . For a brittle material there exists a critical value of the stress intensity factor ( $K_{IC}$ ), a material constant, at which unstable crack growth begins, leading to a sudden failure. Although, Linear Elastic Fracture Mechanics (LEFM) may not be a suitable tool for analyzing the fracture behaviour of concrete (34), its use in predicting the stress rate sensitivity of concrete is often made. In a loaded member the value of stress intensity factor is given by

$$K_I = Y\sigma\sqrt{a} \quad (6.1)$$

and at failure,

$$K_{IC} = Y\sigma_c \sqrt{a_c} \quad (6.2)$$

where  $Y$  is a constant which depends on the specimen geometry,  $\sigma$  is the nominal stress, and  $a$  is the flaw length; the subscript  $c$  denotes the values at failure. Thus, there exists a critical combination of the applied stress and the crack length that can cause failure.

According to the concept of subcritical crack growth, a crack of subcritical size can grow under a subcritical stress by mechanisms such as stress corrosion; when it reaches the critical size (satisfying Equation 6.2) failure will occur. The rate of subcritical crack growth has been found to follow the following equation,

$$V = AK_I^n \quad (6.3)$$

where  $V$  is the crack velocity,  $K_I$  is the stress intensity factor in the opening mode, and  $A$ ,  $n$  are constants. The growth of a subcritical crack occurs at an increasing rate under a constant nominal stress as the crack extends (Fig. 6.4a).

If the loading is very slow, the subcritical flaws have enough time to grow, to approach the critical value, and to cause failure. On the other hand, very rapid loading allows

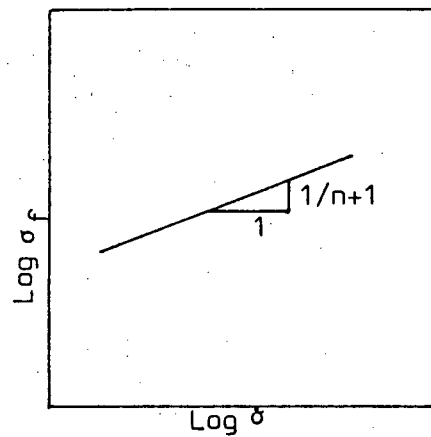
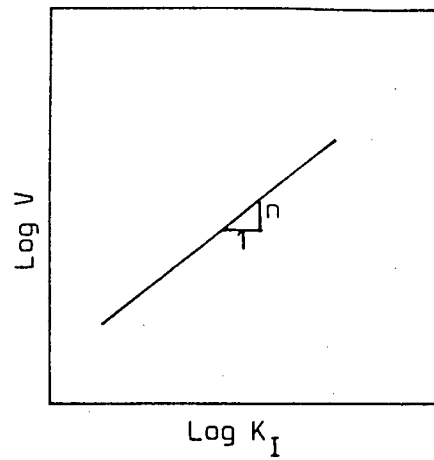


Figure 6.4-The parameter "n", determined from (a) direct observation of the crack velocity and (b) variable stress rate tests little or no time for the subcritical flaws to grow. Therefore, the member can support, momentarily a higher load, giving an apparently increased strength. By how much the strength obtained at one stress rate differs from that obtained at some other stress rate depends the value of n. The value of n can be obtained as follows:

let,

$$\dot{\sigma} = \text{stress rate} = \frac{d\sigma}{dt}$$

$$V = \text{crack velocity} = \frac{da}{dt}$$

$$\frac{d\sigma}{da} = \frac{\dot{\sigma}}{V}$$

Now,

$$V = AK_I^n$$

and,

$$K_I = Y\sigma\sqrt{a}$$

Therefore,

$$\frac{d\sigma}{da} = \frac{\dot{\sigma}}{AY^n \sigma^n a^{n/2}}$$

or,

$$d\sigma = \frac{\dot{\sigma}}{AY^n \sigma^n a^{n/2}} da$$

$$\sigma^n d\sigma = \frac{\dot{\sigma}}{AY^n} \left[ a^{\frac{n}{2}} da \right]$$

On integrating we get,

$$\log \sigma_f = C + \frac{1}{n+1} \log \dot{\sigma}$$

(6.4)

where C is a constant.

Thus plotting  $\log\sigma_f$  vs.  $\log\dot{\sigma}$  would produce a straight line plot as shown in Figure 6.4b, with a slope of  $1/n+1$

When the values experimentally observed in this study for normal strength concrete are plotted, the resulting  $\log\sigma_f$  vs.  $\log\dot{\sigma}$  plot looks like the one shown in Figure 6.5. As can be seen from this plot, the ideal straight line nature of the theoretical plot of Figure 6.4b is not observed experimentally. The observed plot suggests that with an increase in the strain rate, the value of the constant  $n$  decreases. Similar observations have been reported by Suaris and Shah (34). The normally observed values of  $n$ , obtained by varying the strain rate in a strain rate controlled testing machine, are found to lie in the range of 20 to 50. However, in the present study, in the range of strain rates associated with impact, a value of  $n$  as low as 1.50 was observed. Birkimer (53) has reported a value as low as  $n=2.00$  under extremely high strain rates. A reduction in the value of  $n$  with an increase in the strain rate suggests a lower slope for the  $\log V$ - $\log K_I$  plot shown in Figure 6.4a at higher stress rates.

It has been tacitly assumed in the above analysis that the critical stress intensity factor remains the same under different strain rates. However, as will be seen later, the critical stress intensity factor itself increases with the strain rate, further increasing the strain rate sensitivity of concrete at high strain rates.

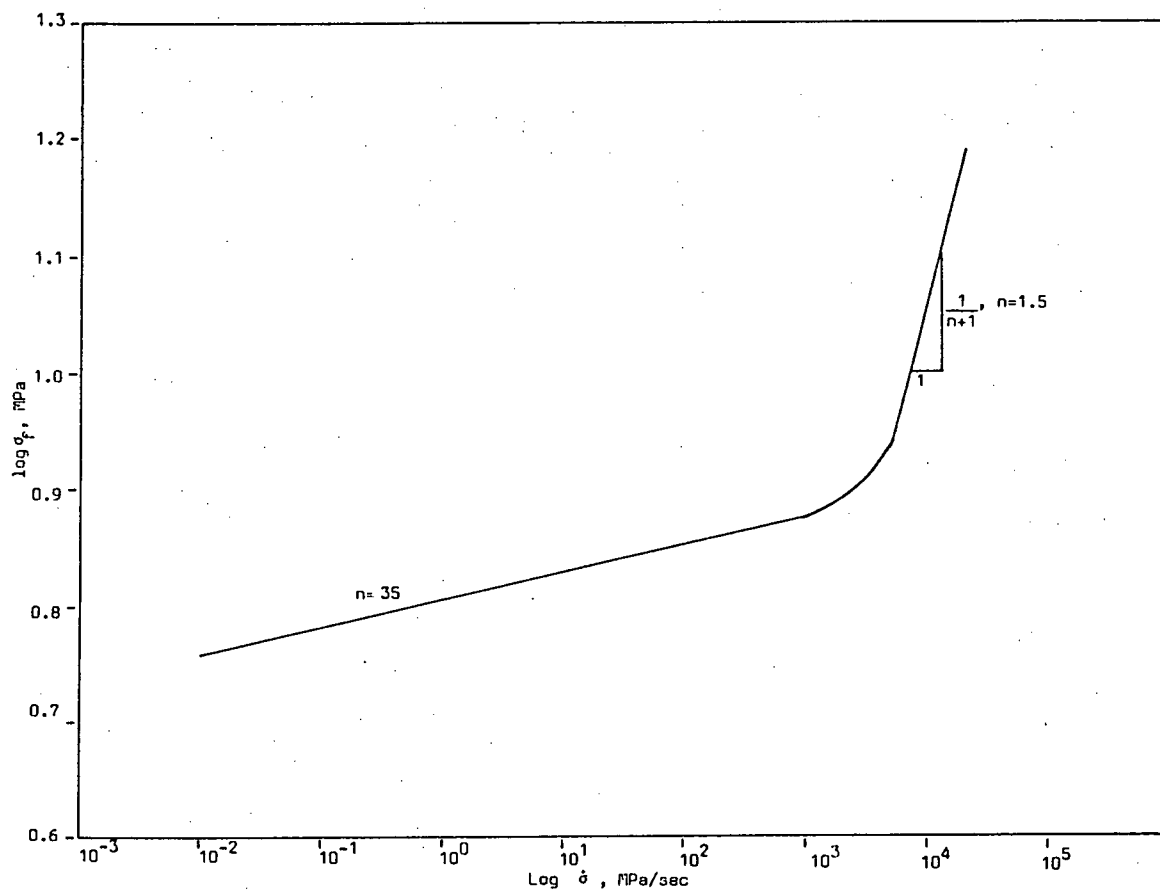


Figure 6.5-Determination of parameter "n" for Normal Strength Concrete

#### 6.4 EFFECT OF STRESS RATE ON PLAIN HIGH STRENGTH (HS) CONCRETE BEAMS

In this study, the high strength concrete mix was produced by adding EMSAC<sup>6</sup> as described in Chapter 4.

Microsilica (or silica fume), is a by-product of the electrometallurgical industry. It plays a double role, first as a filler, and then as a pozzalanic material which reacts with  $\text{Ca}(\text{OH})_2$ , a product of hydration. These ultra fine particles of silica (5 nm to  $0.5\mu\text{m}$ ) are packed in the interstitial spaces between the portland cement clinker grains. The dispersion of the tiny particles in the space around and between the cement grains is shown in Figure 6.6. Efficient mixing of microsilica necessitates the use of a superplasticizer.

-----  
<sup>6</sup> A microsilica produced by Elkem Chemicals, Inc., Pittsburgh, Pennsylvania.

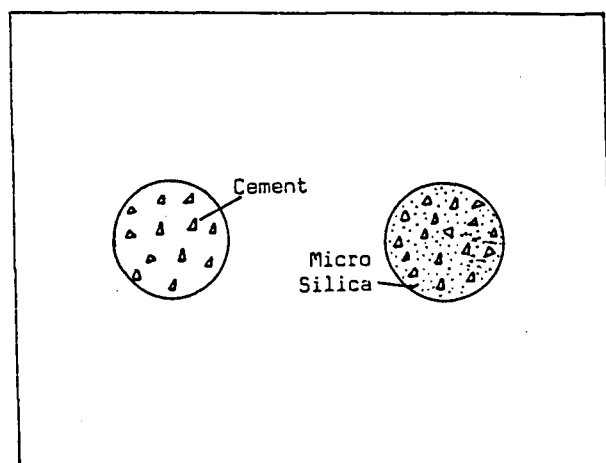


Figure 6.6-Mix without (left) and with (right) Microsilica

The increase in strength due to the addition of microsilica may be attributed in part to the elimination of the larger pores and in part to the more uniform distribution of the hydration products, though the fact that the production technique permits a somewhat lower w/c ratio is probably the most important factor. Intimate dispersion of microsilica improves the performance of the binder and improves its bond with the aggregate particles and the reinforcing bars. The dense microstructure also leads to reduced permeability and increased durability.

To study the effect of strain rate on the properties of high strength concrete (HS), beams were tested in three point bending in an identical manner as the normal strength (NS) beams (Section 6.3). Table 6.3a gives the results of the static tests and Table 6.3b gives the results of the impact testing, carried out at three heights of hammer drop.

It can be noted from Tables 6.3a and 6.3b that, similar to NS concrete, HS concrete is also a very strain rate sensitive material. The main effects of increasing the strain rate are in the increased strength and in the increased fracture energy. Based on the derivation presented in Section 6.3, a plot of  $\log \sigma_f$  vs.  $\log \dot{\sigma}$  for HS concrete is shown in Figure 6.7. This plot suggests that over the range of strain rates used in this study, there does not exist a unique value of the parameter  $n$ . The value of  $n$  seems to

**Table 6.3(a)**  
**Static Properties of Plain High strength Concrete Beams**

	Static (4) <sup>1</sup>			
	Max	Min.	Mean	s
<b>Peak Bending Load (N)</b>	12806	8184	9720	1809
<b>Deflection at Peak Bending Load (x10<sup>-6</sup>)(m)</b>	560	480	500	34
<b>Beam Energy at Peak Bending Load (Nm)</b>	3.6	2.0	2.5	0.7
<b>Failure Strain (x10<sup>-4</sup>)</b>	4.5	3.9	4.1	0.3
<b>Modulus of Rupture (MPa)</b>	11.8	7.6	9.0	1.7
<b>Fracture Energy (Nm)</b>	3.4	2.0	2.8	0.6
<b>Mean Strain Rate (/sec)</b>	-	-	3x10 <sup>-7</sup>	-
<b>mean Stress Rate (MPa/sec)</b>	-	-	0.0075	-

<sup>1</sup>Number of specimens tested.

Table 6.3(b)  
Dynamic behaviour of Plain High Strength Concrete  
Height of Hammer Drop (m)

	0.15m (6) <sup>1</sup>				0.25m (6) <sup>1</sup>				0.50m (7) <sup>1</sup>			
	Max	Min	Mean	s	Max	Min	Mean	s	Max	Min	Mean	s
Max. Top Load (N)	24172	17011	19588	2715	28787	22384	24144	2497	39320	35110	36652	1725
Max. Inertial Load (N)	12456	8606	9682	1604	11777	9480	10773	925	19025	16760	17892	1132
Peak Bending Load (N)	11694	8388	9906	1183	18579	10573	13371	2991	19206	18314	18760	446
Energy at Peak Load (Nm)	2.9	1.8	2.4	0.5	3.0	1.9	2.5	0.4	5.4	3.8	4.6	0.7
Fracture Energy (Nm)	33.5	20.8	25.1	5.0	43.7	31.0	35.0	4.7	100.7	57.4	74.9	18.6
Modulus of Rupture (MPa)	10.8	7.8	9.2	1.1	17.2	9.8	12.4	2.8	17.8	16.9	17.4	0.4
Failure Strain ( $\times 10^{-4}$ )	2.6	1.6	2.0	0.4	3.1	1.6	2.4	0.5	3.9	3.1	3.5	0.4
Mean Stress Rate (MPa/sec)			4584				10316				28905	
Mean Strain rate (/sec)			0.1				0.2				0.6	

<sup>1</sup>Number of specimens tested.

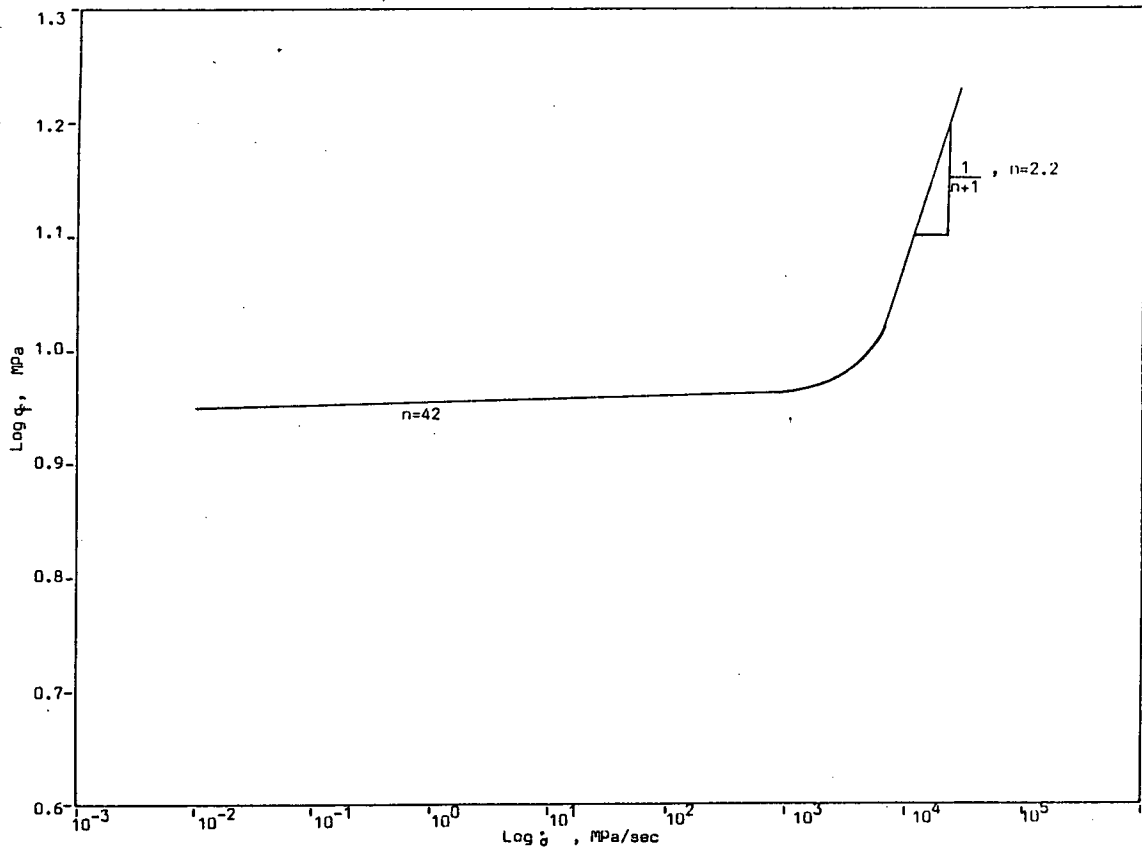


Figure 6.7-Determination of parameter "n" for High Strength Concrete

increase with an increase in the stress rate. Similar observations were reported for NS concrete in Section 6.3. The slope of the high strain rate portion of the plot was found to correspond to a value of  $n=2.2$ .

### 6.5 COMPARISON BETWEEN NORMAL STRENGTH AND HIGH STRENGTH CONCRETE

The addition of microsilica seems to improve the properties of concrete under static loading. However, the superior performance of microsilica concrete over normal concrete in static situations may not necessarily imply its superiority in dynamic situations.

A comparison of the  $\log\sigma_f$  vs.  $\log\dot{\sigma}$  plots (Figures 6.5 and 6.7) shows that high strength concrete behaves in almost the same way as does normal strength concrete. As mentioned earlier, the deviation from the expected linear nature of the  $\log\sigma_f$  vs.  $\log\dot{\sigma}$  plot (Figure 6.4b) is probably because of the change in the fracture toughness ( $K_{IC}$ ) itself with a change in the stress rate.

A comparison of the dynamic performance of HS concrete with NS concrete is presented in Figures 6.8a, b and c. Figure 6.8a shows the peak bending loads obtained for the three drop heights and Figures 6.8b and c show the corresponding variations in the fracture energy and the failure strain, respectively. The higher peak bending loads obtained in the case of HS concrete over NS concrete for a given drop height seem to suggest that a concrete which is

stronger in static conditions is stronger under impact loading as well. However, HS concrete was also found to be more brittle than NS concrete for a given drop height (Figure 6.8b), as indicated by its reduced fracture energy. Finally, the strain at the peak load, referred to here as the failure strain, which is proportional to the displacement at the peak load, was found to be higher for NS concrete than for HS concrete at a given height of hammer drop. It should be noted here that the value of strain at the peak load, obtained by using Eqn. 4.34b, is a measure of the average strain only, and does not indicate either the magnitudes of the strains locally or the variation of strain from one point to another.

Figure 6.9a shows a photograph of the fracture surface obtained from a NS beam tested dynamically. Figure 6.9b shows the corresponding fracture surface obtained with HS concrete. It can be seen that while the fracture surface obtained with normal strength concrete was uneven and without any aggregate failures, the fracture surface for HS concrete was smooth and with many aggregate failures.

Failures in brittle materials occur due to the breaking of the atomic bonds and the propagation of cracks. Since there is resistance to crack growth, energy has to be supplied for continued crack propagation. In the case of an ideally brittle material, the energy consumed during a unit crack extension, called the crack growth resistance  $R$ , consists only of the energy required for the breaking of the

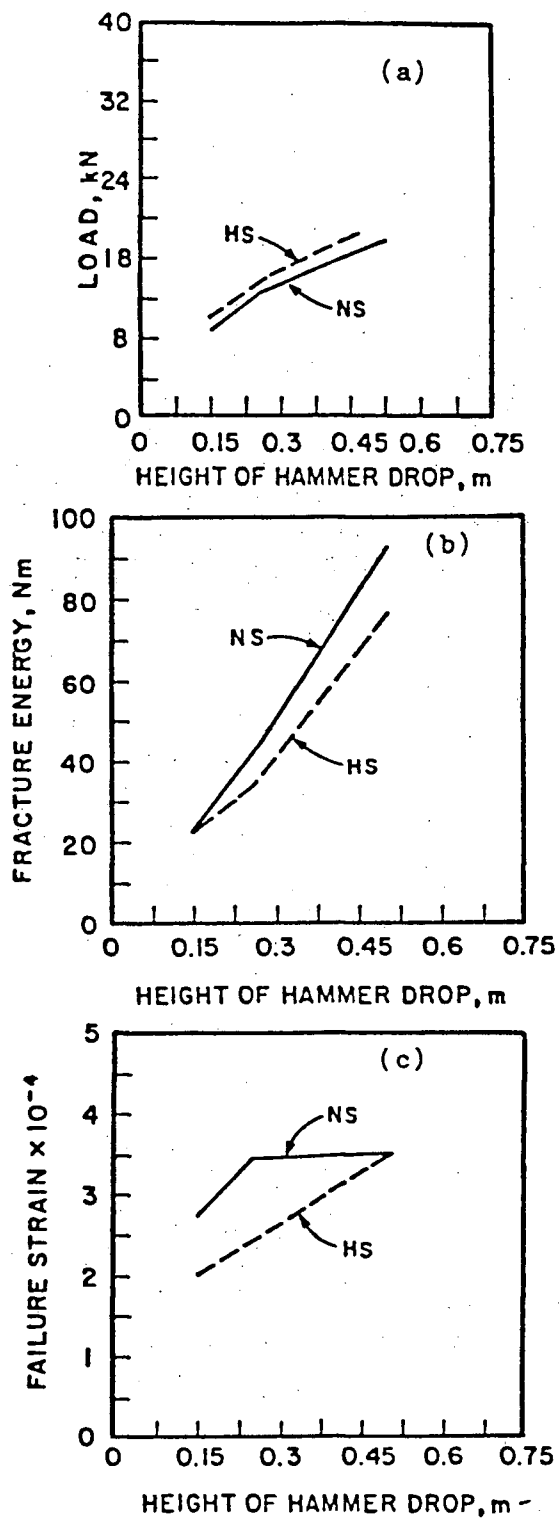
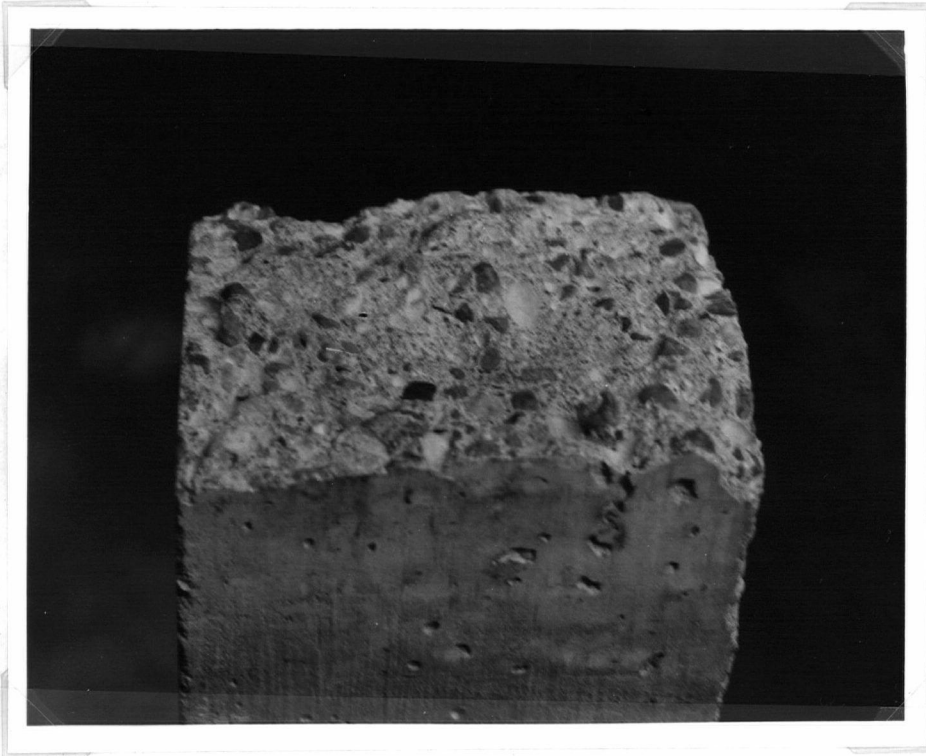


Figure 6.8-Comparison between Normal Strength and High Strength Concrete (a) Peak Bending Load, (b) Fracture Energy, (c) Failure Strain,

Normal Strength



High Strength

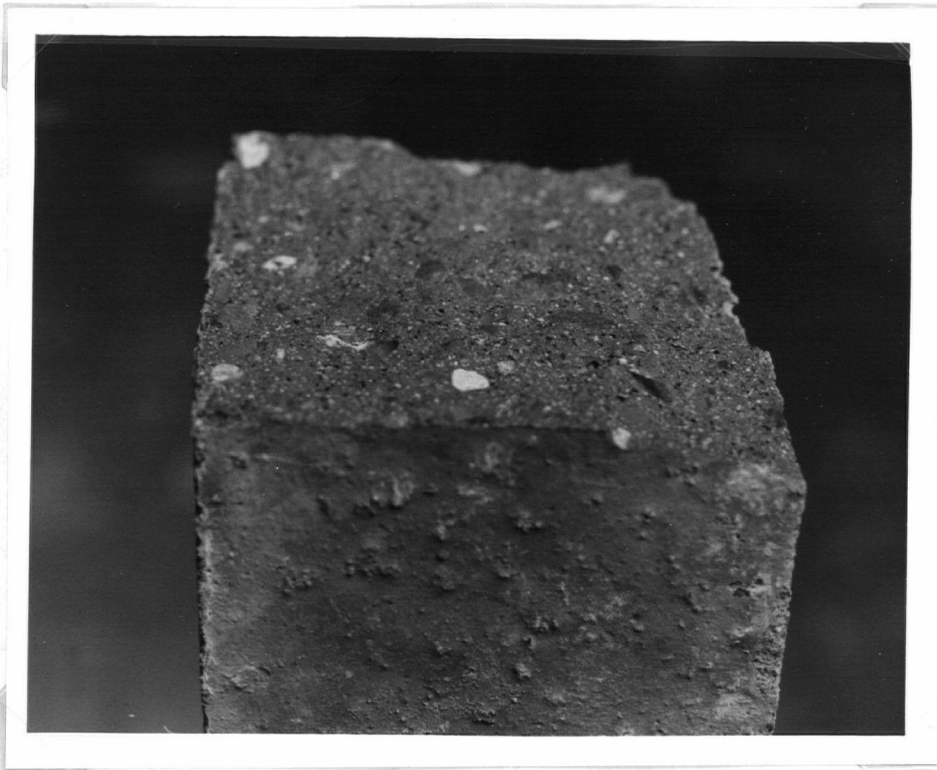


Figure 6.9-Photographs showing the Fracture Surfaces  
obtained for Normal Strength and High Strength Concrete

bonds across the fracture surface, and as such is a constant. Thus, when the strain energy released upon unit crack extension is equal to the crack resistance  $R$ , crack propagation will begin. However, concrete is not an ideally brittle material, and the propagation of cracks seems to be preceded by the formation of a process zone around the crack tip. The formation of this process zone, however, requires energy and thus the crack resistance in concrete ( $R$ ) consists not only of the surface energy component but also of the microcracking component that occurs in a zone of width  $\epsilon$  as shown in Figure 6.10, where  $\epsilon$  is approximately equal to the maximum aggregate size in the case of static loading. As was shown in Figure 6.3 and Table 6.2a, even for a beam loaded statically, the strain energy accumulated up to the peak load ( $\approx 1.00 \text{ Nm}$ ) does not seem to be sufficient to drive the crack a distance equal to the depth of the

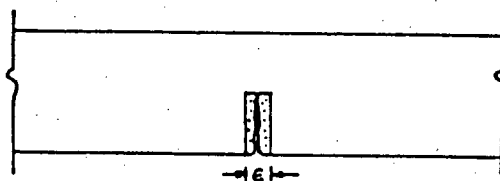


Figure 6.10-The Finite Width Zone of Microcracking That Surrounds a Crack

beam. The finite area under the static load vs. displacement plot in the post-peak load region suggests that the beam continues to absorb energy from the machine to accomplish crack growth. This is true in spite of the fact that the post-peak load energy may have been underestimated, since the machine used for static testing was not very stiff. Thus, ultimately the beam required about 5.5Nm before the complete separation of the broken halves.

In the case of dynamic loading, the same reasoning may be used, the only difference being in the magnitudes of the energies. Referring back to Figure 6.2 and Table 6.2b (0.5m drop), while the energy to the peak bending load was only about 6.4Nm, the total fracture energy was found to be as high as 90Nm. Thus a crack under dynamic loading seems to require more energy to grow than does a crack under static loading. The high energy requirement in the post-peak load region in dynamic loading probably is, in part, a consequence of a wider process zone (53A) or larger  $\epsilon$  (Figure 6.10). However, the exact determination of the width of the cracked zone  $\epsilon$  under dynamic loading is not yet possible. In addition, the fracture mechanisms may also be different under dynamic loading.

It is known that High strength concrete exhibits better paste-aggregate bond than normal strength concrete. It is not surprising therefore that HS concrete appears to undergo less microcracking than normal strength concrete. However, as shown in Figure 6.11 and Table 6.3, dynamic loading on HS

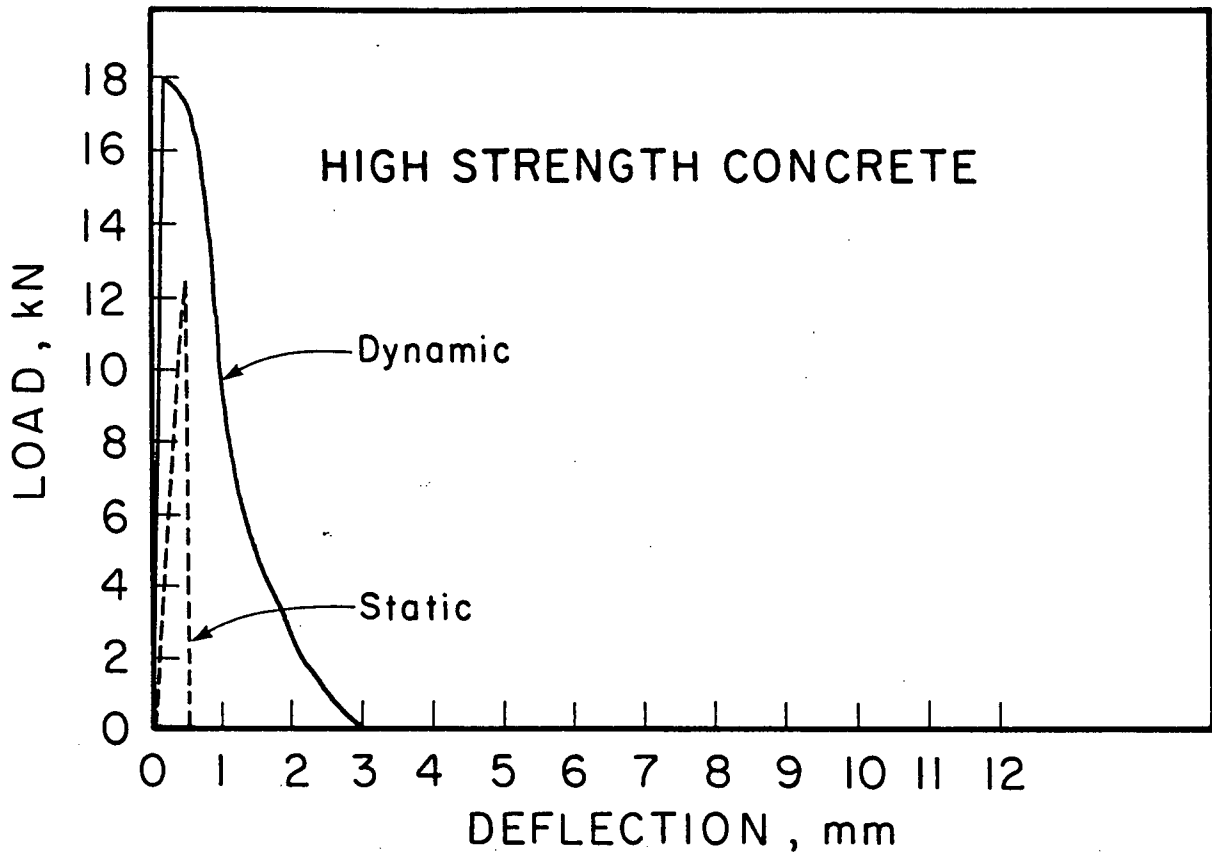


Figure 6.11-Stress Rate Sensitivity of High Strength Concrete

concrete is also associated with the formation of a microcracking zone which results in a finite area under the load vs. displacement plot in the post peak load region. In any case, due to its increased bond quality, HS concrete in this study was always found to be more brittle than NS concrete.

## 6.6 EFFECT OF MOMENT OF INERTIA

To study the effect of the moment of inertia of the beam on its dynamic behavior, beams 100mmx125mm in cross-section were tested on a 960mm span first about their strong axis ( $I=0.0000162m^4$ ), and later about their weak axis ( $I=0.0000104m^4$ ). The results of these tests are given in Table 6.4a for NS concrete and in Table 6.4b for HS concrete.

The average nominal stress rates, which were obtained by dividing the MOR by the time required to reach the peak, for the same drop height of 0.5m, were found to be higher for the beams tested about the strong axis than for the beams tested about their weak axis. Having obtained the results at different stress rates, strictly speaking, they can not be compared. However, since the stress rates are not widely different, a comparison has been attempted here.

When the values of MOR are compared, it can be seen that, for both NS and HS concretes, the MORs obtained for the beams tested about the weak axis are lower than for beams tested about the strong axis. Also, the fracture energies for the weak axis beams are found to be lower than for the strong axis beams.

One possible reason behind this may be the direction in which the beams were cast. All of the beams were cast with the 125mm side vertical. The electric immersion vibrator used for compaction allows the water to bleed to the surface during vibration, reducing the w/c ratio at the bottom of

Table 6.4a  
Effect of Moment of Inertia on the Dynamic Behaviour of Normal Strength Concrete

	$I = 104 \times 10^{-7} \text{ m}^4$ (4) <sup>1</sup>				$I = 162 \times 10^{-7} \text{ m}^4$ (7) <sup>1</sup>			
	Max	Min.	Mean	s	Max.	Min.	Mean	s
Peak Bending Load (N)	12608	8589	10550	1483	17727	16452	16932	428
Modulus of Rupture (MPa)	14.5	9.9	12.2	1.7	16.4	15.2	15.7	0.4
Fracture Energy (Nm)	62.0	49.0	56.0	5.2	100.5	87.8	90.1	6.5
Stress rate (MPa/sec)	-	-	15212	-	-	-	19587	-

Table 6.4b  
Effect of Moment of Inertia on the Dynamic Behaviour of High Strength Concrete

	$I = 104 \times 10^{-7} \text{ m}^4$ (4) <sup>1</sup>				$I = 164 \times 10^{-7} \text{ m}^4$ (7) <sup>1</sup>			
	Max	Min.	Mean	s	Max.	Min.	Mean	s
Peak Bending Load (N)	13660	9799	11250	1464	19206	18314	18760	446
Modulus of Rupture (MPa)	15.7	11.3	13.0	1.7	17.8	17.0	17.4	0.4
Fracture Energy (Nm)	51.0	33.0	40.0	7.2	100.7	57.4	74.9	18.6
Stress rate (MPa/sec)	-	-	21633	-	-	-	28950	-

<sup>1</sup>Number of specimens tested.

the beam while increasing the w/c ratio at the top. Thus, one would expect that the beams tested along their strong axis would show higher MOR values and higher fracture energies.

### 6.7 CRACK DEVELOPMENT IN THE PASTE UNDER IMPACT

Brittle fracture occurs with the rapid propagation of a crack in a loaded continuum. The rate at which the crack propagates in a material seems to depend not only upon the properties of the material, but also upon the rate of loading. However, little work has been carried out so far to measure the velocity at which the crack propagates in cementitious materials. Most of the work on crack propagation has dealt with very low crack velocities, in the range of  $10^{-8}$  m/s to  $10^{-2}$  m/s, obtained in controlled crack growth studies at very low rates of loading.

However, a few studies have been carried out at high loading rates. Bhargava and Rehnstrom (54) loaded concrete prisms by detonating a high explosive in contact with the specimens. Using high speed photography, they found a crack velocity in plain concrete of about 180 m/s. Tests carried out by Alford (55), also using high speed photography, showed crack velocity in hardened cement pastes ranging from 50-160 m/s. He also found the velocities in mortars in the range of 30-80 m/s. Shah and John (56) monitored crack velocities in mortar and concrete beams under impact and reported crack velocities in the range of 100m/s. Takeda et

al (57) used extremely high loading rates, and a special test geometry. They found the crack velocity to be as high as 1000m/s.

As a part of the present study, impact tests were carried out on beams made with paste using a 0.50m hammer drop. To monitor the propagation of the cracks during the impact tests, a high speed motion picture camera was used, running at a speed of 10,000 frames per second. Thus, successive frames represent an elapsed time of 100 microseconds. This time interval was small enough, compared to the duration of the fracture event, to provide a reasonable resolution of the crack development. To determine the rates of crack growth, the film was viewed frame by frame on a small hand viewer; crack length was measured directly on the viewing screen for successive frames, permitting a direct calculation of the crack velocity (at least for the surface traces of the cracks). Since the exact position of the crack tip was hard to judge, the velocities reported are only approximate.

The crack development for the paste is shown in Figure 6.12. These figures are sketches showing the crack pattern at various times after the initial contact between the tup and the specimen. Thus the first frame corresponds to the instant of first hammer and beam contact; a visible crack appears ten frames (1 ms) later, and so on. The energy as computed from the area under the load vs. displacement plot, and the crack velocity have been plotted as a function of

## NEAT CEMENT PASTE

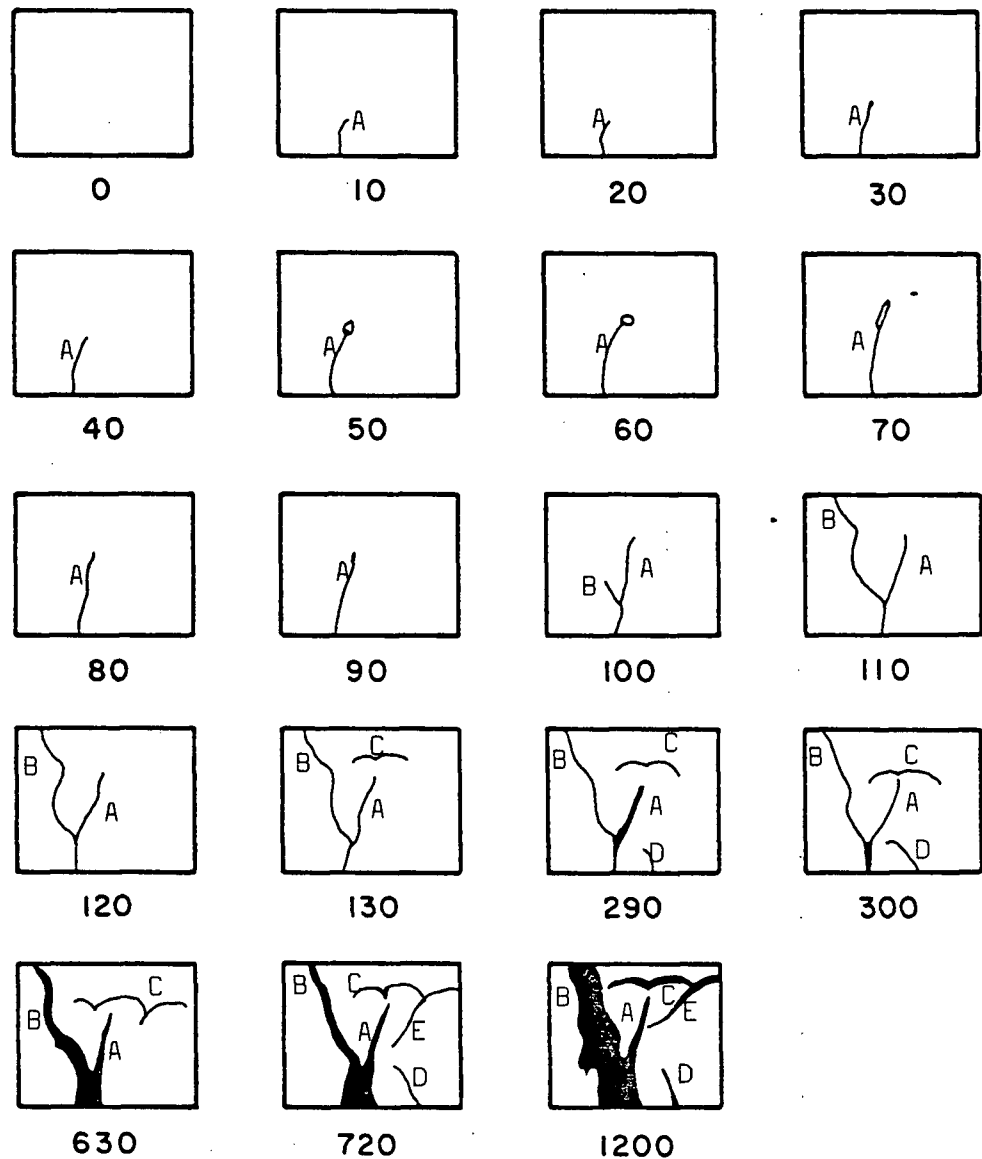


**Figure 6.12** Crack development as a function of time in a hardened cement paste beam subjected to impact loading. The number in each frame represents the time (in units of 0.1 ms) from the first frame shown.

time in Figure 6.13. A visible crack appeared at about the time that the external load reached the peak. The crack was arrested at times and the propagation resumed after every arrest (Figure 6.13b). The velocities plotted in Figure 6.13b are those of the crack marked A up to 9 ms (frame 90). Beyond this time, crack A seemed to have been permanently arrested. After 9 ms and up to failure, the velocities of crack B have been plotted. It is interesting to note that although the load had dropped to zero at about 11 ms (frame 110), the nucleation and propagation of some of the cracks still continued beyond this point. Comparing the 110th frame to the 1200th frame, it can be seen that new cracks C, D, and E have appeared since the load dropped to zero in frame 110. The appearance of a horizontal crack C in frame 130 indicates that the stresses are far from being simple flexural stresses. The growth of crack E in the backward direction (frame 720) also supports the notion of the complex stress pattern within the body of the beam undergoing an impact. The disappearance of crack D between frames 300 and 630 seems to indicate the closing of already existing cracks due to an unloading or a reversal in stresses. The permanent arrest of crack A and the appearance of crack C, indicates a crack arrest phenomenon the basis of which is not yet clear.

The propagation of the crack in the post peak load region can be divided into the following three stages (Figure 6.13).

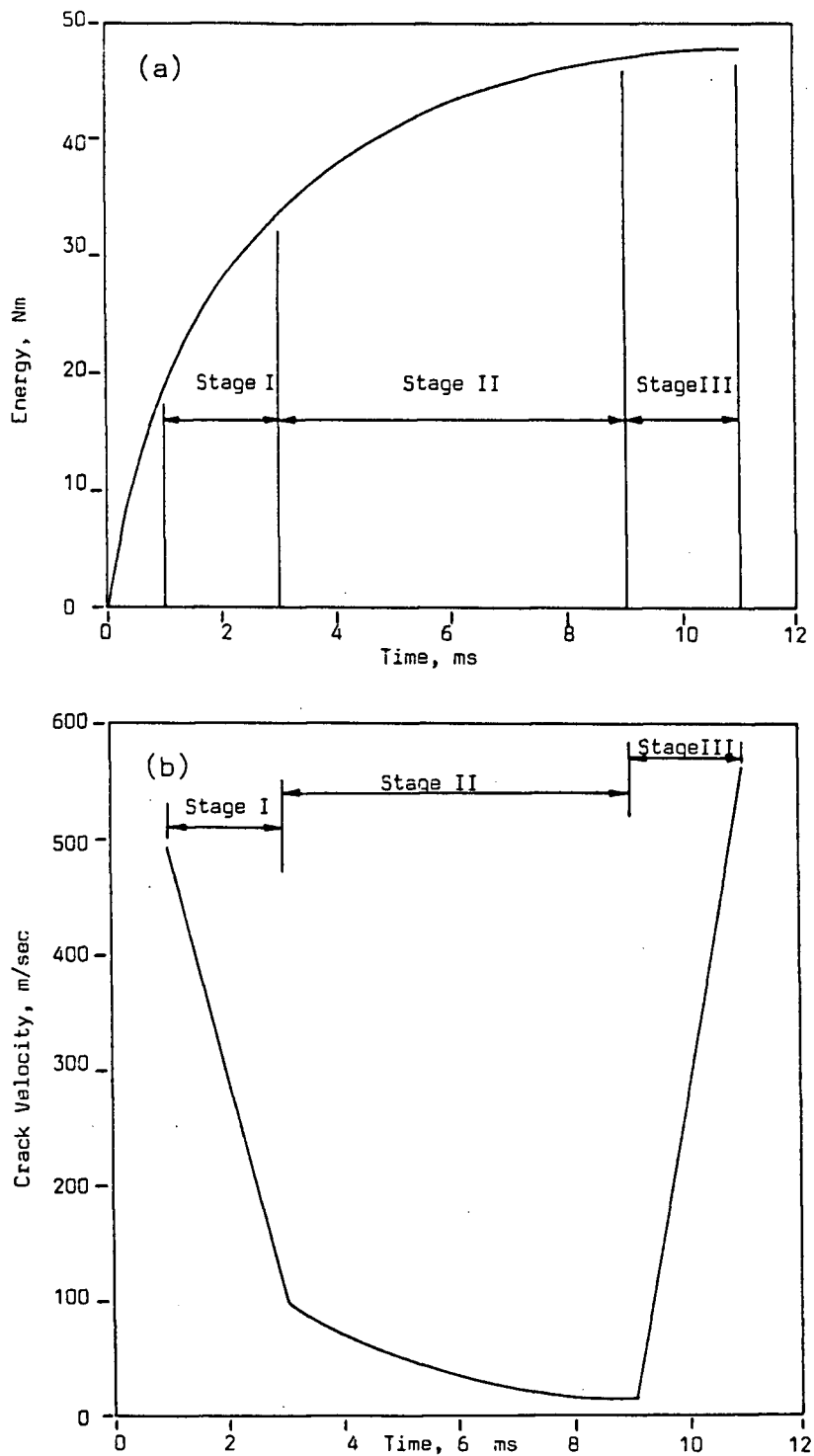


Figure 6.13-(a) Energy absorbed and (b) Crack Velocity as the Crack propagates in Paste

Stage-I: The Nucleation Stage

Stage-II: The Steady State

Stage-III: The Final Stage

As soon as the load reaches the peak, nucleation occurs. The velocity of the crack drops rapidly and linearly to a value from which a slow exponential decay in crack velocity begins and the crack enters the second stage. Stage-II, which continues for the longest period of time, precedes the final stage in which the crack velocity rises again causing a separation.

Stage-I, that accounts for about 50-60% of the total distance travelled by the crack also accounts for about 50-60% of the fracture energy requirement (Figure 6.13a). On the other hand, Stage-III occurring at the end of the impact event accounts for only about 5% of the fracture energy. Stage-III may have its basis in the coalescences of the microcracks already formed in stage-I and II into a macro crack appearing in Stage-III.

The average velocity of a propagating crack in paste was found to be 115 m/sec, and the maximum velocity in the range of 500-600 m/sec. The average velocity of the crack observed here is only about 5% of the "theoretical" crack velocity (given by  $0.38\sqrt{E/\rho}$ ) in brittle materials (58). This suggests that even the hydrated cement paste is not classically brittle.

## 7. MODEL ANALYSIS

### 7.1 INTRODUCTION

The basic aim of experimental work on concrete is to arrive at a set of material properties capable of explaining the experimentally observed facts. The environmental conditions and specimen geometries used in laboratory investigations may or may not prevail in practice. However, the behaviour of concrete under one set of conditions can, to some extent at least, be used to predict its behaviour under other sets of conditions. The inability to generate in the laboratory all possible situations which may be encountered in practice has normally been overcome by the use of mathematical models. However, the development of a successful model necessitates knowledge of the behaviour of the material, and the effect of various parameters on its behaviour. Attempts have generally been made to determine a set of fundamental material properties from a limited number of experimental observations. The material behaviour under load, and the mechanisms responsible for its failure, are two of the parameters needed to design a model.

Sometimes, a model may be required to derive useful information from the experimental observations themselves. Instrumented impact tests on brittle materials can be placed in this category. The load vs. time pulse recorded by the instrumented tup in such impact tests is not the actual bending load on the test beam. A major part of this contact load between the tup and the beam is the inertial load on

the beam. Thus, before any useful information can be derived from such tests, an inertial correction has to be provided to the observed tup load to arrive at the actual bending load. Although some investigators (15,34) have recommended additional instrumentation to measure directly the inertial load or the actual bending load, these techniques are not free from problems: additional instrumentation is expensive; some of these techniques may alter the test conditions; and, some assumptions are still necessary to interpret these additional data. For example, the use of a rubber pad between the tup and the beam, as discussed in Chapter 5, can significantly alter the strain rate. Likewise, the assumption of a linear acceleration distribution may not be true in all the cases.

Appendices 7.1 and 7.2 present the classical solutions to the problem of a beam subjected to an impulse. In Appendix 7.1, the beam has been modelled as a single degree of freedom system (SDOF) and in Appendix 7.2, the multi-degree of freedom (MDOF) solution to the same problem is presented. The external load pulse has been idealized as a sine wave in these treatments. It should be noted that the classical solutions presented here are not capable of handling an arbitrary external load pulse. They also do not take into account microcracking in the concrete and, finally, they are not capable of predicting the beam behaviour after the peak external load is reached. The assumption that the external load pulse can be idealized as

a sine wave may not be grossly in error. However, on the energy side, neglecting the energy absorbed by the beam after the peak load can cause a gross underestimation of the fracture energy. It has been found in the present study that a major part of the fracture energy absorbed by the beam lies in the post-peak load region (Chapter 6), for which the classical solutions of Appendix 7.1 or Appendix 7.2 are inappropriate.

In the pages which follow, two different models are presented. These models apply only to plain concrete (concrete without fibres or reinforcing bars). The basic input to both of these models is the external load pulse acting on the beam, recorded by the strain gauges in the striking end of the hammer.

Model A, which is capable of analyzing the beam only up to the peak external load, is based on the energy balance principle. It is assumed that the energy lost by the hammer up to the peak load is transferred to the beam in the form of kinetic energy and bending energy (strain energy). By assuming a certain beam deflection function, this energy balance concept can be expressed, at every instant of time, as a function of the central deflection of the beam, and its derivatives with respect to time. A finite difference technique has been used to solve the nonlinear differential equation thus obtained in the time domain.

Model B is based upon the dynamic equilibrium of forces. The time step integration technique has been used to

solve the equation of dynamic equilibrium upto the peak load.

It should be noted here that the post-peak load modelling of concrete necessitates a knowledge of the precise manner in which the cracks propagate in that region. In the absence of this knowledge, such a modelling is not possible yet. On the basis of the limited results obtained by the Author (Chapter 6,10 and 11) in the field of crack propagation using high speed photography, very little can be said with any certainty.

## 7.2 MODEL A - EVALUATION OF BEAM RESPONSE TO AN EXTERNAL IMPACT PULSE: ENERGY BALANCE PRINCIPLE

This model is used to evaluate the beam response to an external pulse. It is applicable only to an elastic beam and, therefore, it can be used to analyze the beam response only up to the peak load. At any instant of time up to the peak load, all of the energy lost by the hammer is assumed to have been transmitted to the beam. This hammer energy available to the beam appears in two different forms: bending energy and kinetic energy. All other forms of energy in the beam are ignored. Of these two forms of energy, the bending energy which is used up in stressing the beam is the prime goal of the analysis. In what follows, the separation of the bending energy from the kinetic energy is attempted.

### 7.2.1 Assumptions

1. The beam remains elastic up to the peak load.
2. The beam deflects in, and only in, its first mode.
3. From the instant of first contact, the energy lost by the hammer is absorbed by the beam as kinetic energy and as bending energy.
4. Damping is ignored.
5. The energy lost in the elastic deformations of the various parts of the testing machine is ignored.
6. The beam deflection can be assumed to be sinusoidal in shape, and can be expressed as

$$u(x,t) = u_0(t) \sin(\pi x/l) \quad (7.1)$$

### 7.2.2 Notation

$u(x,t)$ : Deflection of the beam at location  $x$  at time  $t$  (Figure 7.1(a)).

$u_0(t)$ : Deflection at the centre of the beam at time  $t$ .

$\Delta E_0(t)$ : The total energy lost by the hammer up to time  $t$ .

$T(t)$ : Kinetic energy in the beam at time  $t$ .

$U(t)$ : Bending energy in the beam at time  $t$ .

$\rho$ : The mass density of concrete.

$l$ : Distance between the beam supports.

$B$ : The breadth of the beam.

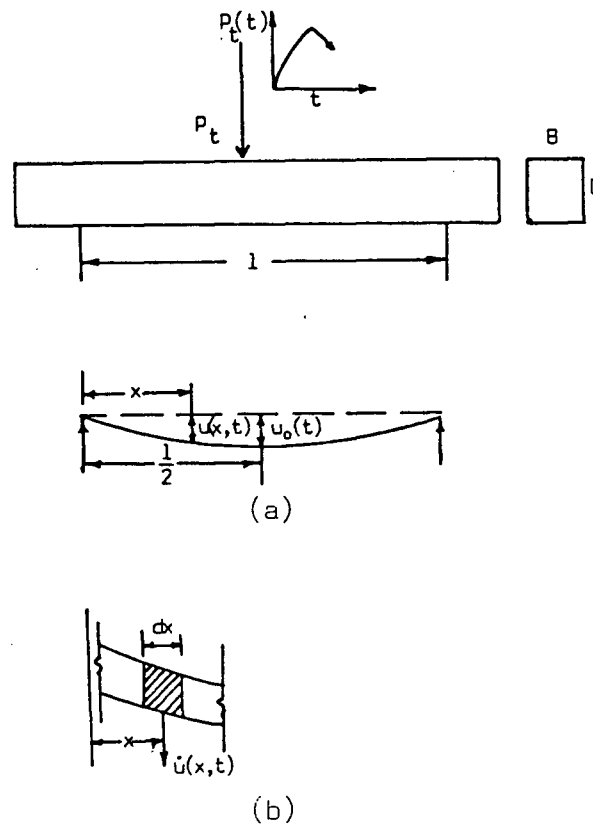


FIGURE 7.1-Assumed Beam Displacements

D: The depth of the beam.

$\Delta E_0(t)$ , the total energy lost by the hammer at time  $t$ , can be obtained by using the impulse vs. momentum relationships. Equation 4.12 is used for this purpose.  $\Delta E_0(t)$ , is assumed to have been fully transferred to the beam (Assumption 3). If the rest of the terms in the energy balance equation (Eqn. 3.2) can be ignored, then,

$$\Delta E_0(t) = T(t) + U(t) \quad (7.2)$$

If the deflection at any point is given by Eqn. (7.1), then the velocity is given by,

$$\dot{u}(x,t) = \dot{u}_0(t) \sin \frac{\pi x}{l} \quad (7.3)$$

The slope at any point will be,

$$u'(x,t) = u_0(t) \left[ \frac{\pi}{l} \right] \cos \left[ \frac{\pi x}{l} \right] \quad (7.4)$$

and the curvature at any point will be,

$$u''(x,t) = -u_0(t) \left[ \frac{\pi}{l} \right]^2 \sin \left[ \frac{\pi x}{l} \right] \quad (7.5)$$

### 7.2.3 Evaluation of the Kinetic Energy(T(t))

As shown in Figure 7.1(b), if  $dT$  is the kinetic energy of the elemental mass then,

$$dT = \frac{1}{2}(\text{mass})(\text{velocity})$$

$$= \frac{1}{2} (\rho B D dx) \dot{u}^2(x, t) \quad (7.6)$$

$$T(t) = \int dT \quad (7.7)$$

$$= \int \frac{1}{2} \rho B D \dot{u}^2(x, t) dx \quad (7.8)$$

Substituting for  $\dot{u}(x, t)$  from Eqn. 7.3 in Eqn. 7.8 and simplifying, we get,

$$T(t) = \frac{\rho B D l}{4} \dot{u}_0^2(t) \quad (7.9)$$

#### 7.2.4 Evaluation of the bending energy(U(t))

If  $dU$  is the strain energy in the elemental mass of Figure 7.1(b) then,

$$dU = \frac{1}{2} EI (u''(x, t))^2 dx \quad (7.10)$$

$$U(t) = \int dU \quad (7.11)$$

$$= \frac{1}{2} \int EI (u''(x, t))^2 dx \quad (7.12)$$

Substituting for  $u''(x, t)$  from Eqn. 7.5 in Eqn. 7.12 and simplifying we get,

$$U(t) = \frac{\pi^4 EI}{4l^3} u_0^2(t) \quad (7.13)$$

#### 7.2.5 The total Energy

Finally, substituting Eqns. (7.9) and (7.13) into Eqn. (7.2), we can obtain the total energy:

$$\Delta E_0(t) = \frac{\rho B D l}{4} \dot{u}_0^2(t) + \frac{\pi^4 EI}{4l^3} u_0^2(t) \quad (7.14)$$

It is more convenient to write this as

$$\Delta E_0(t) = A\dot{u}_0^2(t) + Bu_0^2(t) \quad (7.15)$$

where,

$$A = \frac{\rho B D^4}{4} \quad (7.16)$$

and

$$B = \frac{\pi E I}{4 l^3} \quad (7.17)$$

Equation (7.15) is the nonlinear differential equation in  $u_0(t)$  and  $\dot{u}_0(t)$  which must be solved. The technique of finite differences is used here for this purpose.

#### 7.2.6 Finite difference technique

In this technique, an attempt is made to satisfy the differential equation successively at every point along the time axis. If  $(u_0)_n$ ,  $(u_0)_{n-1}$ , and  $(u_0)_{n+1}$  are the deflections at time  $t$ ,  $(t-\Delta t)$ , and  $(t+\Delta t)$  respectively, (Fig. 7.2), then,

$$\text{slope to left of the } n\text{th point} = \{(u_0)_n - (u_0)_{n-1}\} / \Delta t \quad (7.18)$$

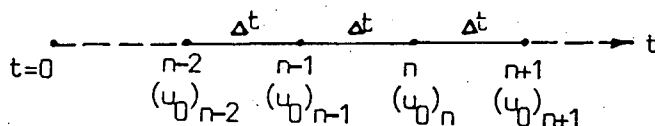


FIGURE 7.2-Finite Difference Technique

$$\text{slope to right of the } n\text{th point} = \{(u_0)_{n+1} - (u_0)_n\} / \Delta t \quad (7.19)$$

Thus, the average slope at the  $n$ th point is

$$(\dot{u}_0)_n = \frac{1}{2} \left[ \frac{(u_0)_{n+1} - (u_0)_{n-1}}{\Delta t} \right] \quad (7.20)$$

Substituting Eqn. 7.20 into Eqn. 7.15 and solving for  $(u_0)_{n+1}$ , we get,

$$(u_0)_{n+1} = \sqrt{\frac{4}{A} [(\Delta E_0)_n - B(u_0)_n^2] \Delta t^2} + (u_0)_{n-1} \quad (7.21)$$

Thus, knowing the deflections at the two previous points along the time axis, and the energy input just prior to the point in question, the deflection at any point can be obtained from Eqn. 7.21. To start the process, the deflections at the first two points  $(u_0)_1$  and  $(u_0)_2$  were both assumed to be zero. Eqn. 7.21 could then be used from the 3rd point onwards.

Once the deflections at the various points along the time axis up to the occurrence of the peak load are known, Eqns. 7.20, 7.9, and 7.13 can be used to compute the velocity, the kinetic energy, and the bending energy of the beam, respectively.

### 7.2.7 Results

This method of separating the total hammer energy into the beam kinetic energy and the beam bending energy was

applied to a plain concrete beam struck in the middle by the hammer falling through a height of 0.5m. The properties of the beam are given in Table 7.1.

TABLE-7.1

Beam properties for the attempted application of Model A

Property	Unit	Value
E	N/m <sup>2</sup>	32.0x10 <sup>9</sup> (assumed)
$\rho$	Kg/m <sup>3</sup>	2400.0 (assumed)
B	m	0.100
D	m	0.125
l	m	0.960

Figure 7.3 shows that the majority of the energy lost by the hammer appears in the beam as kinetic energy, and only about 10% of this externally available energy appears as the bending energy. Figures 7.4(a), 7.4(b), and 7.4(c) present the comparison between the values computed by using the model and those measured experimentally (see Chapter 4 for the Experimental Procedures).

It is clear from Figure 7.4(a) that the model overestimates the bending energy in the beam. Likewise, the deflections (Fig. 7.4(b)), and the velocity (Figure 7.4(c)) have also been over-estimated. There are several reasons responsible for this, but probably the most likely is that Eqn. 7.2 is invalid. As pointed out in Chapter 3, and later

## ENERGY BY MODEL

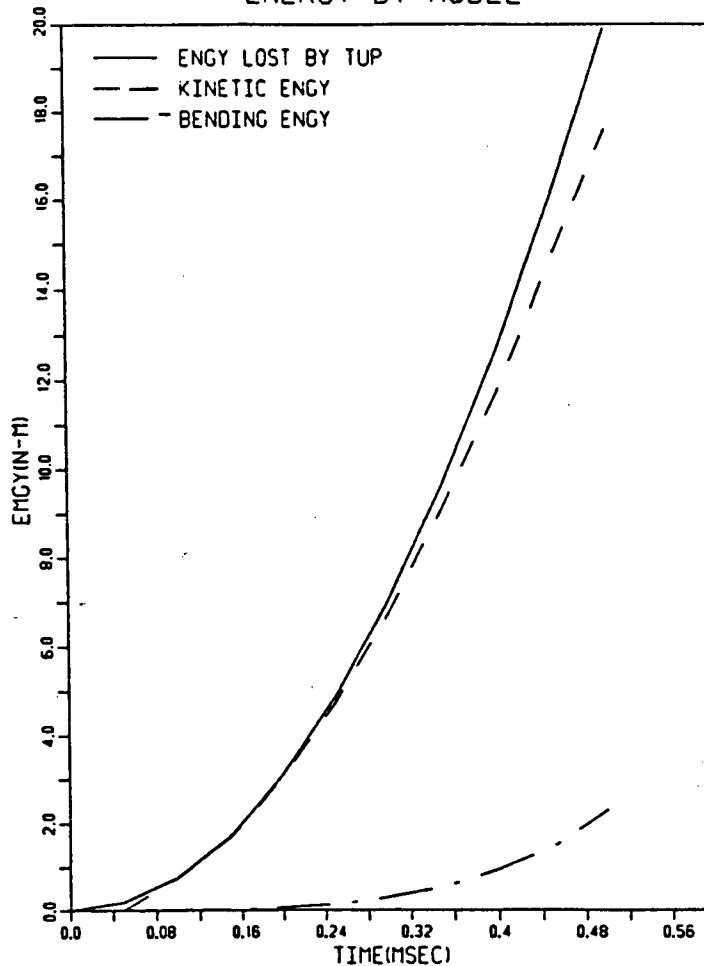


FIGURE 7.3-Energy predictions using Model A

in Chapter 8, Eqn. 7.2 is an over-simplification of the situation. It is likely that, initially, only a small portion of the energy lost by the hammer is consumed by the beam. A large portion of the energy lost by the hammer appears in the form of machine strain energy and machine vibrations. This is particularly true for a machine with a tall slender frame and a heavy hammer. With the hammer almost 8 times as heavy as the beam in our case, the energy loss is particularly significant. Unfortunately, it is not possible, at this stage, to account for these losses and to add more terms to the right hand side of Eqn. 7.2.

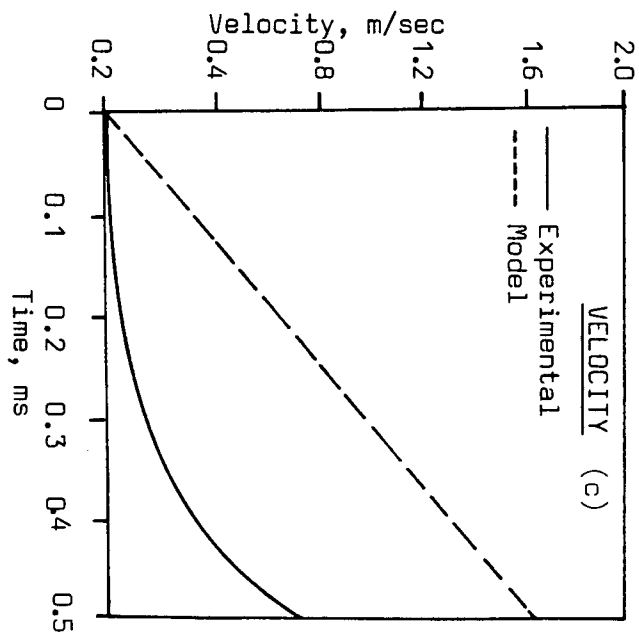
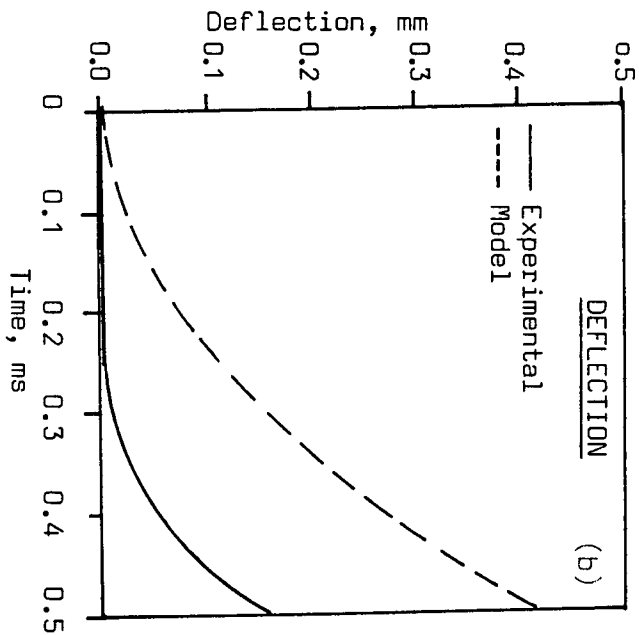
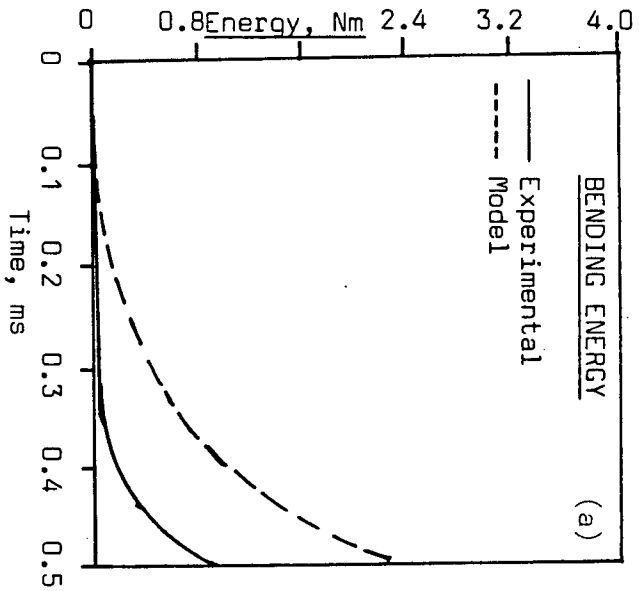


Figure 7.4- Model Predictions vs. the Experimental Findings.  
(MODEL A)

### 7.3 MODEL B- EVALUATION OF BEAM RESPONSE TO AN EXTERNAL IMPACT PULSE: SOLUTION TO THE EQUATION OF DYNAMIC EQUILIBRIUM USING TIME STEPS

When an arbitrary external load pulse acts on a beam, along with the quick build-up of stresses, inertial forces are generated. Thus at any instant of time, after the initial contact, the equation of dynamic equilibrium can be written as

$$P_b(t) = P_t(t) - P_i(t) \quad (7.22)$$

where  $P_t(t)$  denotes the external load,  $P_i(t)$  denotes the inertial load, and  $P_b(t)$  denotes the bending or the stressing load.

If the material of the beam is linearly elastic up to failure, the linear models presented in Appendices 7.1 and 7.2 could be used. However, concrete does not behave linearly up to failure under either compression, tension or flexure, and as such, these models are of limited usefulness. Moreover, use of the model in the case of high stress rate loadings requires a knowledge of the properties of the material at those high stress rates. In the case of concrete, the exact properties at high stress rates are not known. The first natural step, therefore, is an attempt towards the formulation of the constitutive law for concrete under high stress rates from the experimental findings.

### 7.3.1 The constitutive law for concrete

One generally accepted constitutive law for concrete is (59)

$$\sigma = \sigma_f \left[ \frac{2\epsilon}{\epsilon_f} - \left( \frac{\epsilon}{\epsilon_f} \right)^2 \right] \quad (7.23)$$

where

$\sigma$  = The stress.

$\sigma_f$  = The stress at failure.

$\epsilon$  = The strain.

$\epsilon_f$  = The strain at failure.

Both  $\sigma_f$  and  $\epsilon_f$  have been found to be affected by a variation in the stress rate  $\dot{\sigma}$  (Chapter 6). On the basis of the results obtained in Chapter 6, it can be shown that

$$\sigma_f = C_1 \dot{\sigma}^{C_2}, \text{ where } C_2 = 1/(1+n) \quad (7.24)$$

and

$$\epsilon_f = C_3 \dot{\sigma}^{C_4} \quad (7.25)$$

Upon substituting for  $\sigma_f$  and  $\epsilon_f$  from Eqns. 7.24 and 7.25, respectively, in Eqn. 7.23 we get,

$$\sigma = C_1 (\dot{\sigma})^{C_2} \left[ \frac{2\epsilon}{C_3 \dot{\sigma}^{C_4}} - \left( \frac{\epsilon}{C_3 \dot{\sigma}^{C_4}} \right)^2 \right] \quad (7.26)$$

On rearranging the terms we get,

$$\sigma = 2K_1\sigma^{K_2}\epsilon - K_3\sigma^{K_4}\epsilon^2 \quad (7.27)$$

where

$$K_1 = C_1/C_3$$

$$K_2 = C_2 - C_4$$

$$K_3 = C_1/C_3^2$$

$$K_4 = C_2 - 2C_4$$

The results obtained for normal strength concrete (Table 6.2b), and high strength concrete (Table 6.3b) were used to evaluate the above constants. The values obtained are shown in Table 7.2.

Table 7.2

The constants in the constitutive law obtained experimentally

Normal Strength Concrete		High Strength Concrete	
$C_1=0.65$	$K_1=9142$	$C_1=0.30$	$K_1=19480$
$C_2=0.40$	$K_2=0.24$	$C_2=0.31$	$K_2=0.01$
$C_3=7.11 \times 10^{-5}$	$K_3=1.29 \times 10^8$	$C_3=1.54 \times 10^{-5}$	$K_3=1.26 \times 10^9$
$C_4=0.16$	$K_4=0.08$	$C_4=0.30$	$K_4=-0.290$

If  $E(\epsilon)$  is the tangent modulus of elasticity at strain level  $\epsilon$ , we get from Eqn. 7.27,

$$E(\epsilon) = d\sigma/d\epsilon = 2K_1\sigma^{K_2} - 2K_3\sigma^{K_4}\epsilon \quad (7.28)$$

Note that the secant modulus is a function of the strain.

### 7.3.2 Time step analysis and results

A summary of the linear acceleration time step integration technique is given in Appendix-7.3. The stiffness  $K(\epsilon)$  at the beginning of each time step was obtained using Eqn. 7.28 and the expression

$$k(\epsilon) = \frac{4}{2l^2} E(\epsilon)I \quad (7.29)$$

The external load pulses (the tup loads) up to the peak, for three hammer drop heights for both normal strength and high strength concretes formed the input to the program written to do the time step analysis.

The results are shown in the form of the load ( $P_b$ ) vs. deflection plots of Figures 7.5 and 7.6. Figure 7.5 corresponds to normal strength concrete while Figure 7.6 corresponds to high strength concrete. The experimentally obtained results are also shown. The bending energy in the beam at the peak load, which can be obtained by taking the area under the bending load vs. deflection plots (Figures 7.5 and 7.6) has been shown in Figure 7.7 for both normal and high strength concretes. It can be seen that the model proposed here reasonably predicts the behaviour of a beam subjected to impact. The model also predicts the brittleness shown by high strength concrete.

One major drawback with the model, that should be pointed out here, is the inability of the model to predict the response of the beam beyond the peak load. With the

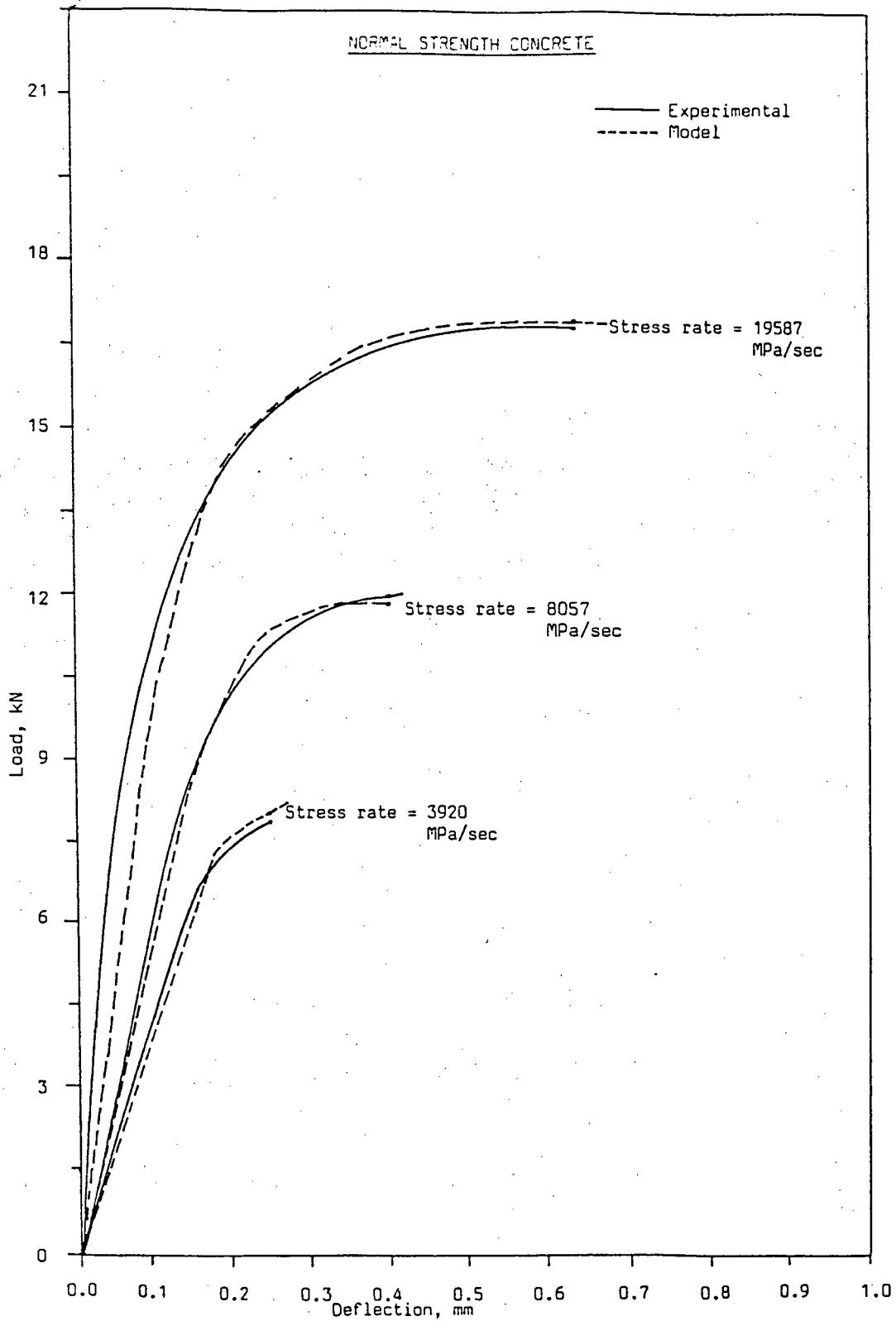


FIGURE 7.5-Model B predictions vs. the Experimental Results (Normal Strength Concrete)

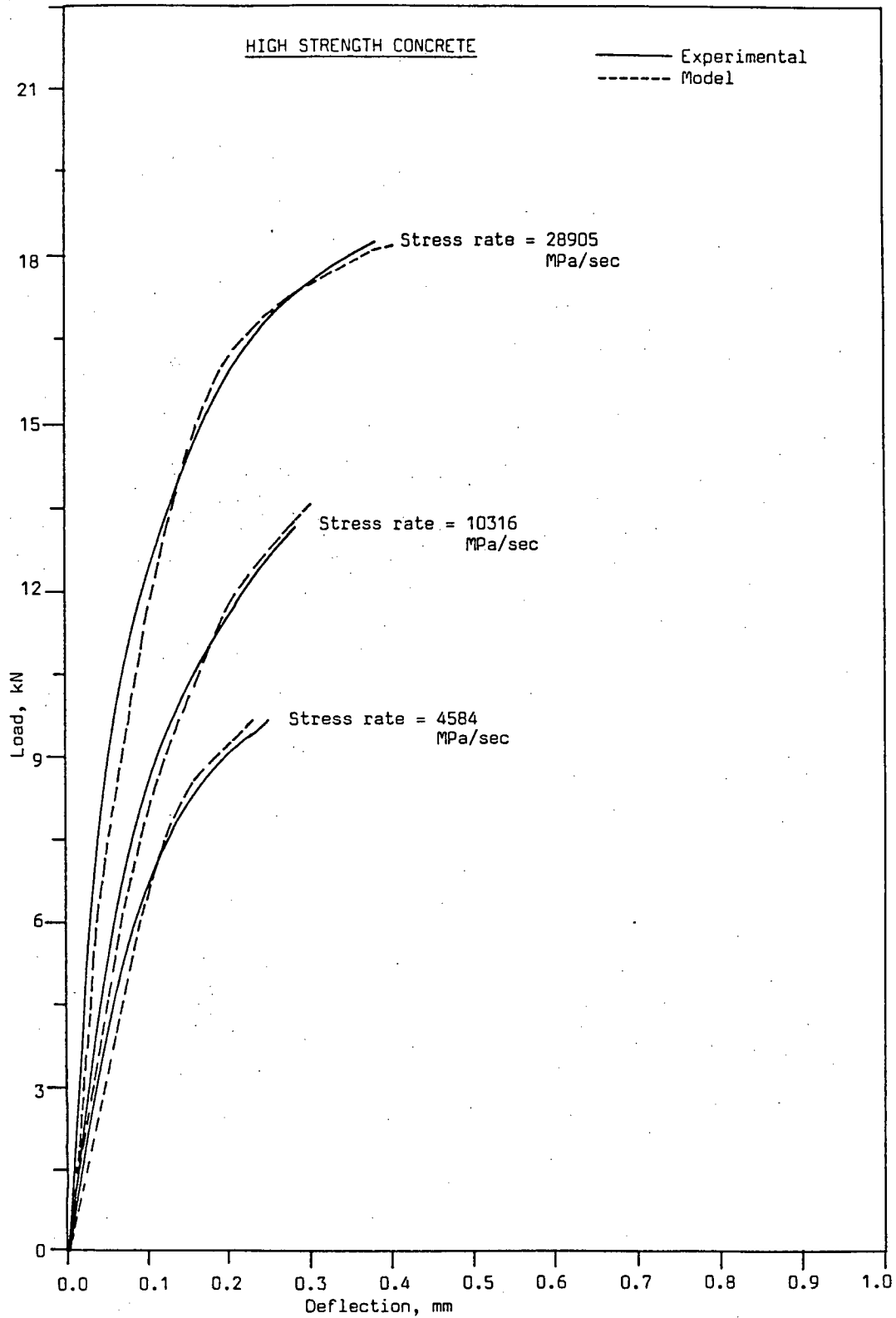


FIGURE 7.6-Model predictions vs. the Experimental Results  
(High Strength Concrete)

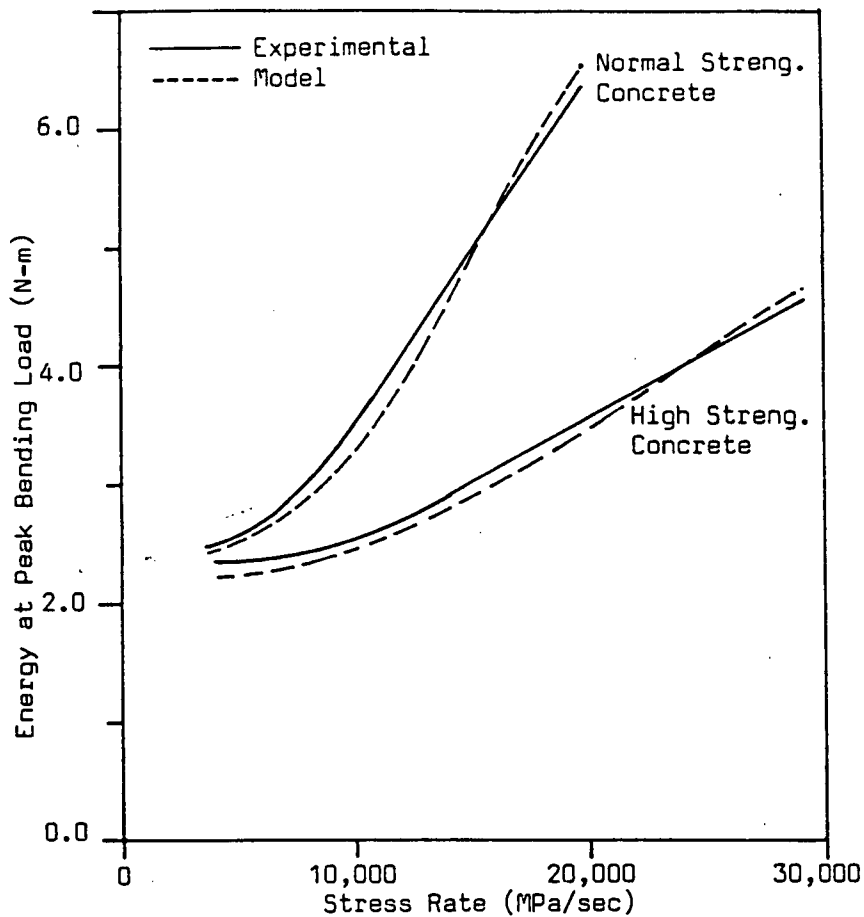


FIGURE 7.7-Bending Energy at the Peak Load

crack starting to grow at the peak load, the response of the beam, among other things, depends upon the velocity of the propagating crack, crack branching if any, and also upon the width of the microcracked zone around the propagating crack. In the absence of a precise knowledge of crack propagation under impact loading, such modelling is not possible at the present time.

APPENDIX-7.1EVALUATION OF BEAM RESPONSE: BEAM MODELLED AS A SINGLE DEGREE OF FREEDOM SYSTEMAssumptions

1. The beam remains elastic up to the peak tup load.
2. The external load pulse (the tup load) can be approximated as a sinusoidal pulse.
3. The beam deflects in, and only in, the first mode.
4. Damping can be ignored.

The Equation of dynamic equilibrium

Let,

$m_b$  be the generalized mass of the beam,

$k$  be the generalized stiffness,

$P_t(t) = P_0 \sin \omega t$  be the external load pulse,

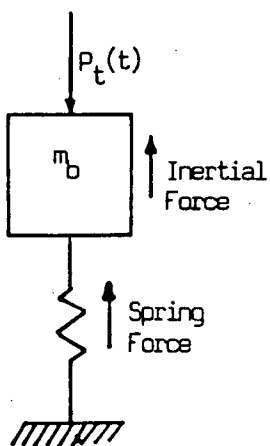


FIGURE A7.1-1-Single Degree of Freedom Model to evaluate the beam response

$\omega_n$  be the natural frequency of the beam,

$u_0(t)$  be the displacement of the mass,

$\dot{u}_0(t)$  be the velocity of the mass,

$\ddot{u}_0(t)$  be the acceleration of the mass,

$\beta = \omega/\omega_n$  be the frequency ratio.

From the vertical equilibrium in Figure A7.1-1 we can write,

$$m_b \ddot{u}_0(t) + k u_0(t) = P_0 \sin \omega t \quad (\text{A7.1-1})$$

The solution to Eqn. A7.1-1 can be written in the form of

$$u_0(t) = A \cos \omega_n t + B \sin \omega_n t + C \sin \omega t \quad (\text{A7.1-2})$$

where,

A and B are constants depending on the initial conditions and

$$C = \frac{P_0}{m_b \omega_n^2 (1 - \beta^2)}$$

From Eqn. 7.1-2 we get,

$$\dot{u}_0(t) = -\omega_n A \sin \omega_n t + \omega_n B \cos \omega_n t + C \omega \cos \omega t \quad (\text{A7.1-3})$$

On substituting the initial conditions, i.e.  $u_0(t=0) = 0$ , and  $\dot{u}_0(t=0) = 0$  into Eqn A7.1-2 and Eqn. A7.1-3 we get,

$$A = 0 \quad (\text{A7.1-4})$$

and,

$$B = \frac{-P_0 \beta}{m_b \omega_n^2 (1 - \beta^2)} \quad (\text{A7.1-5})$$

On substituting for A, B, and C into Eqn. A7.1-2 and Eqn.

A7.1-3 we get,

$$u_0(t) = C(\sin\omega t - \beta\sin\omega_n t) \quad (\text{A7.1-6})$$

and,

$$\dot{u}_0(t) = C(\omega\cos\omega t - \beta\omega_n\cos\omega_n t) \quad (\text{A7.1-7})$$

Finally, from (A7.1-7) we get,

$$\ddot{u}_0(t) = C(\beta\omega_n^2\sin\omega_n t - \omega^2\sin\omega t) \quad (\text{A7.1-8})$$

The generalized mass of the beam Let the displacements in the beam be given by,

$$u(x,t) = u_0(t) \sin\frac{\pi x}{l} \quad (\text{supported span}) \quad (\text{A7.1-9})$$

$$u(y,t) = -u_0(t) \frac{\pi y}{l} \quad (\text{overhangs}) \quad (\text{A7.1-10})$$

If the beam is given a virtual displacement  $\delta u_0$  in the centre, then from the principle of virtual work we can

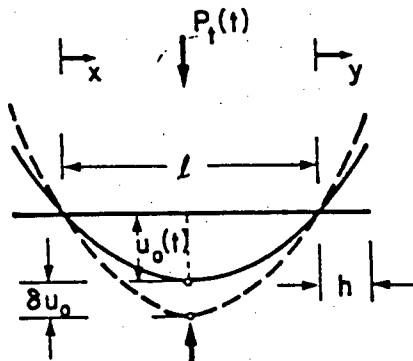


FIGURE A7.1-2-Determination of the generalized mass

write,

$$m_b \ddot{u}_0 \delta u_0 = \int \rho A \left[ \ddot{u}_0(t) \sin \frac{\pi x}{l} \right] \left[ \delta u_0 \sin \frac{\pi x}{l} \right] dx + 2 \int \rho A \left[ -\ddot{u}_0(t) \frac{\pi y}{l} \right] \left[ -\delta u_0 \frac{\pi y}{l} \right] dy$$

Using Eqns. A7.1-9 and A7.1-10, and assuming that the beam is prismatic and homogeneous we can write,

$$m_b = \frac{\rho A l}{2} + \frac{2 \rho A \pi^2 h^3}{3 l^2} \quad (\text{A7.1-11})$$

The generalized stiffness of the beam

If the displacements are given by Eqn A7.1-9 and A7.1-10, then the generalized stiffness is given by,

$$k = \int EI [\phi_1''(x)]^2 dx + \int EI [\phi_2''(y)]^2 dy \quad (\text{A7.1-12})$$

Where  $\phi_1(x) = \sin\left(\frac{\pi x}{l}\right)$ , and  $\phi_2(y) = -\frac{\pi y}{l}$  and,

where primes denote derivatives with respect to x.

Solving Eqn. A7.1-12 for k we get,

$$k = \frac{\pi^4 EI}{2 l^3} \quad (\text{A7.1-13})$$

The natural frequency

The natural frequency of the beam is given by,

$$\omega_n = \sqrt{\frac{k}{m_b}}$$

where  $m_b$  and  $k$  are given by Equations A7.1-11 and A7.1-13, respectively.

APPENDIX 7.2

EVALUATION OF BEAM RESPONSE: BEAM MODELLED AS A MULTI-DEGREE  
OF FREEDOM SYSTEM

Assumptions

1. Damping can be ignored.
2. Beam remains elastic up to the peak external load.
3. The beam is prismatic and homogeneous.
4. The external load can be approximated as a sinusoidal pulse.

Notation

$P_t(t) = P_0 \sin \omega t$  = The external load pulse.

$u(x,t)$  = The vertical displacement.

$\phi_n(x)$  = The nth mode shape.

$Y_n(t)$  = The nth generalized coordinate.

$\omega_n$  = The nth natural frequency.

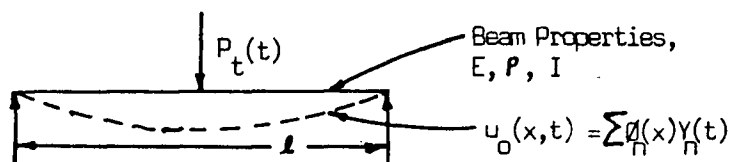


FIGURE A7.2-1-Multi Degree of Freedom Model to evaluate the beam response

$\rho$  = The mass density of beam material.

$l$  = Distance between the beam supports.

$E$  = Modulus of elasticity of the beam material.

$I$  = Moment of Inertia.

$A$  = Area of cross-section.

$m = \rho A$  = Mass per unit length of the beam.

With the damping ignored, the dynamic equation of beam equilibrium can be written as

$$EI \frac{\delta^4 u(x,t)}{\delta x^4} + m \frac{\delta^2 u(x,t)}{\delta t^2} = P_t(t) \quad (\text{A7.2-1})$$

$$= P_0 \sin \omega t$$

If we choose the solution in the form

$$u(x,t) = \sum \phi_n(x) Y_n(t) \quad (\text{A7.2-2})$$

On substituting the derivatives of  $u(x,t)$  with respect to  $x$  (denoted by superscripts), and with respect to time (denoted by dots) in Eqn. A7.2-1 we get

$$EI \sum \phi_n^{(4)}(x) Y_n(t) + m \sum \phi_n(x) \ddot{Y}_n(t) = P_0 \sin \omega t \quad (\text{A7.2-3})$$

Multiplying Eqn. A7.2-3 by  $\phi_m(x)$ , integrating over the

length, and using the following orthogonality conditions

$$\int m \phi_m(x) \phi_n(x) dx = 0$$

$$\int EI \phi_n^{iv}(x) \phi_m(x) dx = 0 \quad (\text{A7.2-4})$$

$$\int EI \phi_n(x) \phi_n^{iv}(x) dx = \omega_n^2 \int m \phi_n^2(x) dx$$

we get,

$$\ddot{Y}_n(t) \left[ \int m \phi_n^2(x) dx \right] + Y_n(t) \left[ \omega_n^2 \int m \phi_n^2(x) dx \right] = \int P_0 \sin \omega t \phi_n(x) dx \quad (\text{A7.2-5})$$

Let

$$\int m \phi_n^2(x) dx = M_n$$

and,

$$\begin{aligned} \int P_0 \sin \omega t \phi_n(x) dx &= \alpha_0 P_0 \sin \omega t \\ \alpha_0 &= 1 \text{ for } n=1, 5, 9 \dots \\ &= -1 \text{ for } n=3, 7, 11 \dots \\ &= 0 \text{ for } n=2, 4, 6 \dots \end{aligned}$$

With the above notation, Eqn.A7.2-5 can be written as

$$M_n \ddot{Y}_n(t) + \omega_n^2 M_n Y_n(t) = \alpha_0 P_0 \sin \omega t \quad (\text{A7.2-6})$$

The solution to Eqn. A7.2-6

The general solution (including the homogeneous and particular parts) to Eqn. A7.2-6, which is a simple differential equation in  $t$ , can be written as

$$Y_n(t) = A \cos \omega_n t + B \sin \omega_n t + \frac{\alpha_o^p o}{M_n \omega_n^2 (1 - \beta_n^2)} \sin \omega t \quad (\text{A7.2-7})$$

where

$A$  and  $B$  are constants determined from the initial conditions,

and,

$\beta_n = \omega / \omega_n =$  The frequency ratio.

With  $Y_n(0) = 0$ , and  $\dot{Y}_n(0) = 0$  as the initial conditions,

$$A = 0$$

$$B = \frac{-\alpha_o^p \beta_n}{M_n \omega_n^2 (1 - \beta_n^2)}$$

With these constants, Eqn. A7.2-7 may be written as

$$Y_n(t) = \frac{\alpha_o^p o}{M_n \omega_n^2 (1 - \beta_n^2)} \sin \omega t - \frac{\alpha_o^p \beta_n}{M_n \omega_n^2 (1 - \beta_n^2)} \sin \omega_n t \quad (\text{A7.2-8})$$

The mode shapes of a simply supported beam are given by

$$\phi_n(x) = \sin \frac{\pi x}{l} \quad (\text{A7.2-9})$$

With mode shapes given by Eqn. A7.2-9, and the generalized coordinates given by Eqn. A7.2-9, Eqn. A7.2-2 can be finally written as

$$u(x,t) = \sum \sin \frac{n \pi x}{l} \left[ \frac{\alpha_n^p \sin \omega_n t}{M_n \omega_n^2 (1 - \beta_n^2)} - \frac{\alpha_n^p \beta_n \sin \omega_n t}{M_n \omega_n^2 (1 - \beta_n^2)} \right] \quad (\text{A7.2-10})$$

APPENDIX-7.3TIME STEP ANALYSIS

A detailed account of the dynamic time step analysis is given in (60). Here only a short description will be presented.

*Notation:*

$P_b(t)$ : The bending load on the beam.

$P_i(t)$ : The inertial load on the beam.

$P_t(t)$ : The applied load on the beam.

$\Delta P_b(t)$ : The change in the bending load during an interval.

$\Delta P_i(t)$ : The change in the inertial load during an interval.

$\Delta P_t(t)$ : The change in the applied load during an interval.

$\Delta t$ : The length of the time interval.

$u_0(t)$ : The acceleration at the beginning of the interval.

$\dot{u}_0(t)$ : The velocity at the beginning of the interval.

$u_0(t)$ : The displacement at the beginning of the interval.

$\Delta u_0(t)$ : The change in the acceleration during an interval.

$\Delta \dot{u}_0(t)$ : The change in the velocity during an interval.

$\Delta u_0(t)$ : The change in the displacement during an interval.

interval.

$m_b$ : The generalized mass of the beam.

$K(t)$ : The tangent stiffness during an interval.

### Assumptions

1. The beam can be modelled as a single degree of freedom system.
2. Damping can be ignored.
3. Acceleration varies linearly during a time interval.
4. The stiffness does not change during an interval.

In this method, the response of the beam is evaluated for a series of short time increments, generally taken of equal lengths. The condition of dynamic equilibrium is established at the beginning and the end of each interval and the motion of the system during the time increment is evaluated approximately on the basis of an assumed response mechanism.

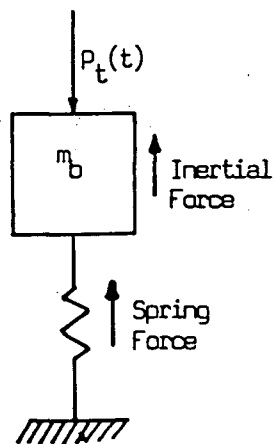


FIGURE A7.3-1-Single Degree of Freedom Model to evaluate the beam response using Time Step Analysis

From the condition of dynamic equilibrium at any time  $t$  we have

$$P_t(t) = P_i(t) + P_b(t) \quad (\text{A7.3-1})$$

After a short interval  $\Delta t$  the condition of dynamic equilibrium would still hold.

$$P_t(t+\Delta t) = P_b(t+\Delta t) + P_i(t+\Delta t) \quad (\text{A7.3-2})$$

Subtracting Eqn.(A7.3-1) from Eqn.(A7.3-2) we get the incremental form of the equation of dynamic equilibrium.

$$\Delta P_t(t) = \Delta P_b(t) + \Delta P_i(t) \quad (\text{A7.3-3})$$

or,

$$\Delta P_t(t) = K(t)\Delta u_o(t) + m_b\Delta \ddot{u}_o(t) \quad (\text{A7.3-4})$$

If the acceleration is assumed to vary linearly during an interval then

$$\Delta \dot{u}_0(t) = \ddot{u}_0(t)\Delta t + 0.5\Delta \ddot{u}_0(t)\Delta t \quad (\text{A7.3-5})$$

$$\Delta u_0(t) = \dot{u}_0(t)\Delta t + 0.5\ddot{u}_0(t)\Delta t^2 + \Delta \ddot{u}_0(t)(\Delta t^2/6) \quad (\text{A7.3-6})$$

Choosing  $\Delta u_0(t)$  as the basic variable in the analysis we get,

$$\Delta \ddot{u}_0(t) = (6/\Delta t^2)\Delta u_0(t) - (6/\Delta t)\dot{u}_0(t) - 3\ddot{u}_0(t) \quad (\text{A7.3-7})$$

$$\Delta \dot{u}_0(t) = (3/\Delta t)\Delta u_0(t) - 3\dot{u}_0(t) - (\Delta t/2)\ddot{u}_0(t) \quad (\text{A7.3-8})$$

Substituting for  $\Delta \ddot{u}_0(t)$  from Eqn. A7.3-7 into Eqn. A7.3-4 and rearranging we get,

$$\{K(t) + (6/\Delta^2)m_b\}\Delta u_0(t) = \Delta P_t(t) + m_b[(6/\Delta t)\dot{u}_0 + 3\ddot{u}_0(t)] \quad (\text{A7.3-9})$$

Equation A7.3-9 is the basic equation for the linear acceleration time step analysis for a system without damping. At any step, knowing the stiffness, the velocity, and the acceleration at the beginning of the interval, Eqn. A7.3-9 can be used to evaluate the incremental displacement  $\Delta u_0(t)$ . Once  $\Delta u_0(t)$  is known, Eqn. A7.3-8 can be used to

find  $\Delta \dot{u}_0(t)$ . These increments  $\Delta u_0(t)$  and  $\Delta \dot{u}_0(t)$  are then added to the displacement and the velocity at the beginning of the interval to obtain the displacement and the velocity at the end of the interval.

The acceleration at the beginning of the interval is obtained from the equation of dynamic equilibrium at the beginning of the interval.

## 8. ENERGY BALANCE IN INSTRUMENTED IMPACT TESTS

### 8.1 INTRODUCTION

Many studies have demonstrated the strain rate sensitivity of concrete. However, our knowledge of concrete behaviour at high stress rates still remains largely empirical. Part of the reason for this has been the inability to compare the results from different investigations, in the absence of any standard testing technique. The results of a particular investigation depend largely on the testing arrangement used in that particular investigation, because of the different energy losses associated with various testing machines, and different methods of analysis. The concept of Energy Balance (17,18), which has its basis in the principle of the conservation of energy, compares the energy lost by the hammer, at any time during the impact, and the energy gained by the specimen. Theoretically, if losses can be ignored, the law of conservation of energy would predict the two energies to be the same. Practically, as will be seen shortly, the losses in the system cannot be ignored, and the energy gained by the specimen is, in general, less than the energy lost by the hammer. In this chapter, the various forms in which the hammer energy in a drop weight type impact machine is dissipated are presented.

The hammer travelling downward, on striking the beam, suffers a loss of momentum. This loss of momentum, according to the impulse-momentum relationship (Chapter 4), is equal

to the impulse acting on the hammer. Using this principle, the loss in the kinetic energy of the hammer ( $\Delta E(t)$ ) can be evaluated (Eqn. 4.12).

$$\Delta E(t) = \frac{1}{2}m_h \left[ 2a_h h - \left( \sqrt{2a_h h} - \frac{1}{m_h} \int P_t(t) dt \right)^2 \right] \quad (4.12)$$

where,

$m_h$  : The mass of the hammer,

$a_h$  : The acceleration of the hammer,

$h$  : The height of hammer drop,

$\int P_t(t) dt$  : The impulse.

This energy lost by the hammer may be transferred to the beam in various forms. The transfer of energy can be studied by subdividing it into two regions (Figure 8.1):

- (1) Energy balance at the peak load (at  $t=t_p$ ).

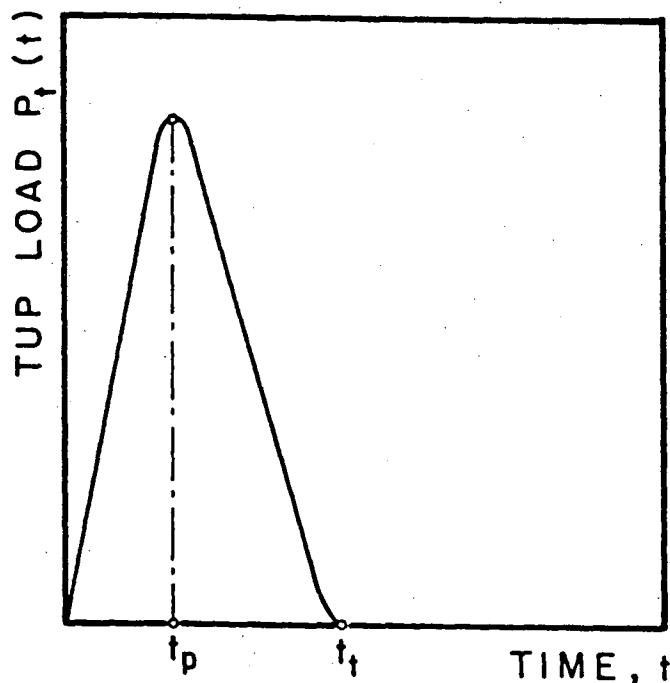


FIGURE 8.1-Typical Tup Load vs. Time plot

(2) Energy balance just after complete failure (at  $t=t_t$ )

The following sections deal with these two regions separately.

### 8.2 ENERGY BALANCE AT THE PEAK LOAD ( $t=t_p$ )

At the peak load the equation of energy balance can be written as

$$\Delta E(t_p) = E_m(t_p) + E_s(t_p) \quad (8.1)$$

where,

$E_m(t_p)$  : the energy lost to the various machine parts at time  $t_p$  in the form of strain energy or machine vibrations,

$E_s(t_p)$  : the energy consumed by the specimen at time  $t_p$

The energy consumed by the beam can be further subdivided into the following two parts,

$$E_s(t_p) = E_{ker}(t_p) + E_b(t_p) \quad (8.1a)$$

where,

$E_{ker}(t_p)$  : the rotational kinetic energy of the specimen,

$E_b(t_p)$  : the bending energy in the specimen.

Therefore,

$$\Delta E(t_p) = E_m(t_p) + E_{ker}(t_p) + E_b(t_p) \quad (8.2)$$

In Equation 8.2, the translational kinetic energy, and the vibrational energy in the specimen have been ignored (18). The bending energy, given by the area under the load vs. centre point displacement plot (Eqn. 4.37), comprises the elastic strain energy  $E_{se}(t_p)$  and the work of fracture  $E_{wof}(t_p)$

$$E_b(t_p) = E_{se}(t_p) + E_{wof}(t_p) \quad (8.3)$$

From a load vs. centre point displacement plot, the elastic strain energy  $E_{se}(t_p)$  can be reasonably approximated by taking the secant modulus at 60% of the peak load (Figure 8.2). The secant modulus was taken at this point, since at this point, in general, the load vs. deflection curve became significantly non-linear.

$$E_{se}(t_p) = 0.5P_b(t_p)u_{oe} \quad (8.4)$$

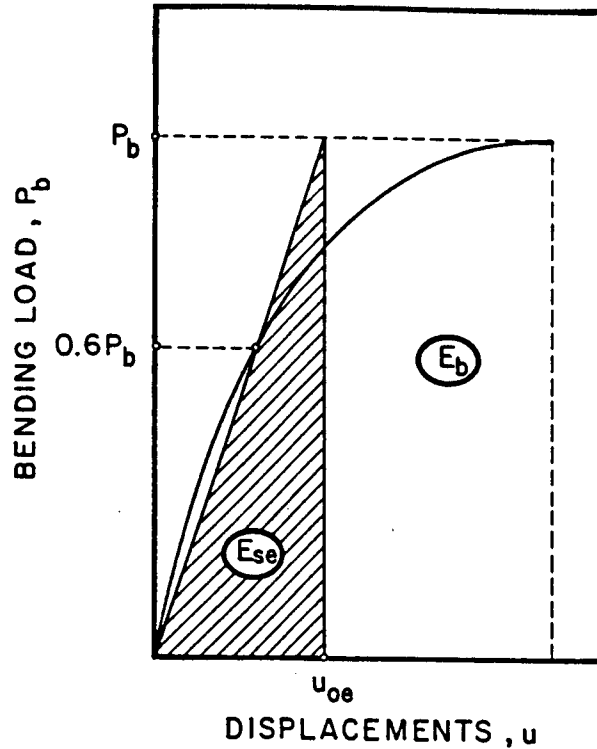


FIGURE 8.2-Components of Bending Energy

where  $u_{oe}$  is the elastic part of the midspan displacement.

The work of fracture  $E_{wof}(t_p)$  can then be obtained by subtracting the strain energy  $E_{se}(t_p)$  from the bending energy  $E_b(t_p)$  (Eqn. 8.3).

Knowing the velocity at the centre, and assuming that the velocity distribution is linear along the length of the beam, the rotational kinetic energy of the specimen can be obtained by integrating over its length.

$$E_{ker}(t) = \frac{8\rho A \dot{u}_0^2(t)}{l^2} \left[ \frac{l^2}{24} + \frac{h^3}{3} \right] \quad (8.5)$$

The energy lost to the machine  $E_m(t_p)$  can be obtained by subtracting the beam energies  $E_b(t_p)$  and  $E_{ker}(t_p)$  from the hammer energy  $\Delta E(t_p)$  (Equation 8.2).

The experimental results are presented in Figures 8.3 and 8.4, and in Tables 8.1 (NS concrete) and 8.2 (HS concrete). The data are presented for three different heights of hammer drop. Since Tables 8.1 and 8.2 show substantial scatter in results, only the mean values were used for drawing Figures 8.3 and 8.4.

Figure 8.3 shows the energy balance for NS and HS concretes at the peak load ( $t=t_p$ ). At the peak load, the energy lost by the hammer ( $\Delta E$ ) is 2 to 4 times the energy gained by the beam ( $E_s$ ). The remainder of the energy is assumed to be absorbed in the machine itself, in the form of vibrations and in stored elastic energy. The energy gained by the beam by virtue of its deformed shape ( $E_b$ ) is found to be much smaller than its kinetic energy ( $E_{ker}$ ). Also, the consistently lower values of energies ( $E_s$ ,  $E_{ker}$ , and  $E_b$ ) for HS concrete compared to NS concrete should be noted.

Figure 8.4 presents the sub-division of the bending energy ( $E_b$ ) at the peak load into the work of fracture ( $E_{wof}$ ) and the elastic strain energy ( $E_{se}$ ). Most of the energy consumed by the beam up to the peak bending load appears as the work of fracture. Both the work of fracture and the strain energy increase with an increase in the hammer drop height; the work of fracture seems to increase at a higher rate than does the strain energy. HS concrete

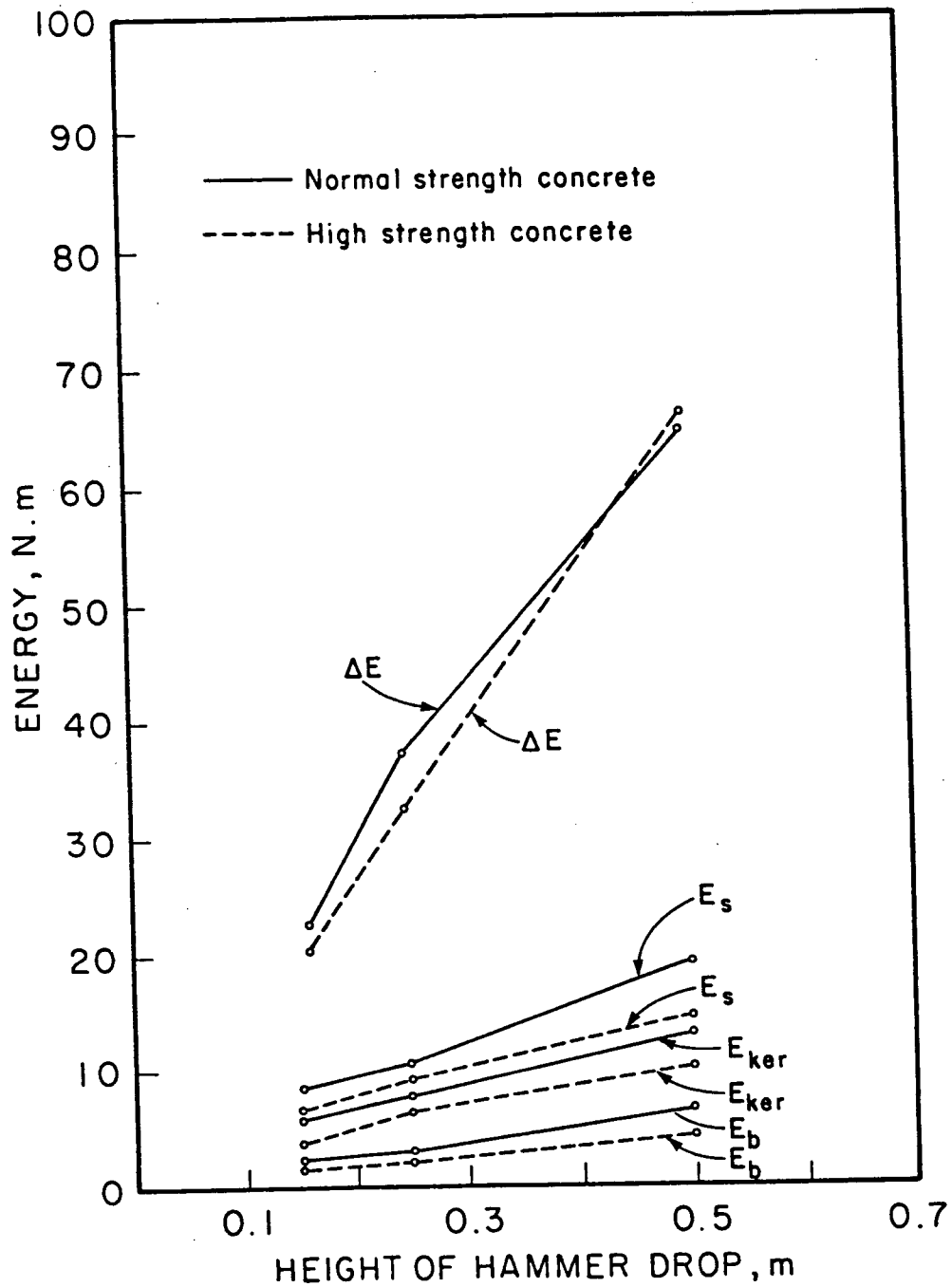


FIGURE 8.3-Energy Balance at the Peak Load

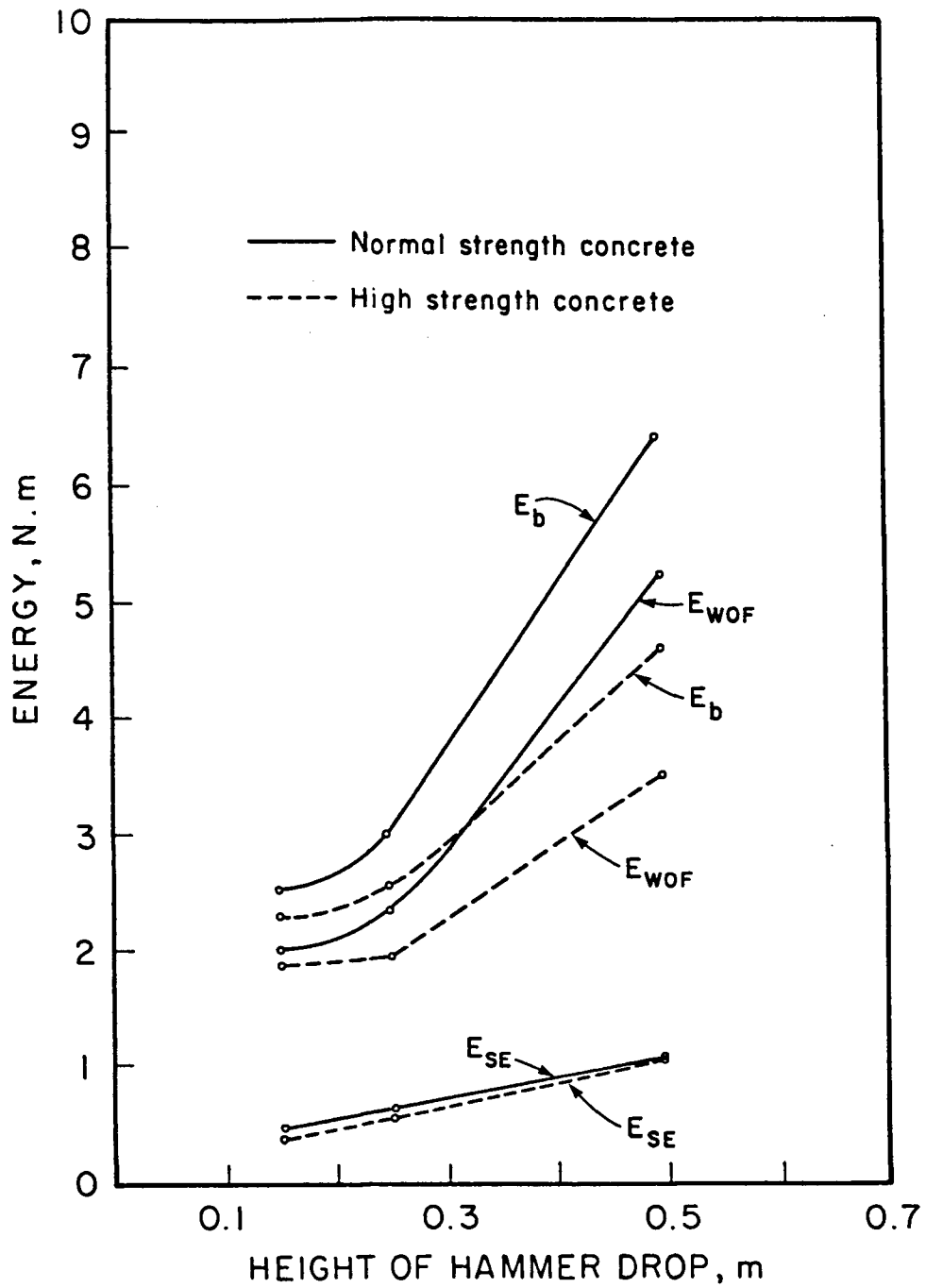


FIGURE 8.4-Components of Bending Energy

Table 8.1-Energy Balance at the Peak Load (Normal Strength Concrete)

ITEM	0.15 m (6)*				0.25 m (6)*				0.50 m (7)*			
	MAX.	MIN.	MEAN	STD. DEVIATION	MAX.	MIN.	MEAN	STD. DEVIATION	MAX.	MIN.	MEAN	STD. DEVIATION
$P_b(t_t)$ (N)	9440	7782	8460	604	14668	9178	12183	2401	17727	16452	16932	428
$\Delta E(t_p)$ (N-m)	25.78	19.75	22.86	2.37	42.06	33.36	37.24	3.21	71.60	60.89	64.64	3.80
$E_{ker}(t_p)$ (N-m)	7.515	4.60	6.20	1.27	10.00	6.12	7.98	1.37	16.96	10.96	13.23	2.00
$E_b(t_p)$ (N-m)	3.50	1.53	2.53	0.708	3.73	2.74	3.005	0.429	9.07	2.21	6.416	2.51
$E_{se}(t_p)$ (N-m)	0.645	0.324	0.499	0.125	0.824	0.523	0.632	0.114	1.357	0.788	1.14	0.192
$E_{wof}(t_p)$ (N-m)	2.855	1.206	2.05	0.588	2.906	2.048	2.38	0.322	7.90	1.422	5.27	2.41
$E_s(t_p)$ (N-m)	10.12	6.13	8.72	1.53	13.47	8.86	10.95	1.64	23.56	14.63	19.60	3.03
$E_m(t_p)$ (N-m)	15.66	12.69	14.12	1.10	31.46	24.45	26.32	2.97	48.39	40.47	45.03	3.49
$\frac{E_m(t_p)}{\Delta E(t_p)} \times 100\%$	69	59	62	4.02	74	64	69	3.77	77	67	70.00	4.18

\* NUMBER OF SPECIMENS TESTED

Table 8.2-Energy Balance at the Peak Load (High Strength Concrete)

ITEM	0.15 m (6)*				0.25 m (5)*				0.50 m (6)*			
	MAX.	MIN.	MEAN	STD. DEVIATION	MAX.	MIN.	MEAN	STD. DEVIATION	MAX.	MIN.	MEAN	STD. DEVIATION
$P_b(t_p)$ (N)	11694	8388	9906	1183	18579	10573	13371	2991	19206	18314	18760	446
$\Delta E(t_p)$ (N-m)	25.21	19.02	20.28	3.54	38.45	33.40	32.20	3.98	76.33	58.82	66.13	7.43
$E_{ker}(t_p)$ (N-m)	6.40	2.68	3.94	1.44	9.61	4.47	6.58	1.67	16.00	4.35	10.13	4.75
$E_b(t_p)$ (N-m)	2.92	1.79	2.37	0.54	2.96	1.86	2.55	0.376	5.41	3.80	4.64	0.659
$E_{se}(t_p)$ (N-m)	0.518	0.339	0.432	0.072	0.639	0.546	0.600	0.052	1.34	1.00	1.14	0.065
$E_{wof}(t_p)$ (N-m)	2.433	1.40	1.930	0.478	2.40	1.287	1.954	0.375	4.23	2.86	3.52	0.560
$E_s(t_p)$ (N-m)	9.32	4.47	6.31	1.83	11.47	7.19	9.14	1.39	19.80	1.08	14.78	4.40
$E_m(t_p)$ (N-m)	25.21	19.02	20.28	3.54	38.45	33.40	32.20	3.98	76.33	58.82	66.13	7.43
$\frac{E_m(t_p)}{\Delta E(t_p)} \times 100\%$	75	63	69	4.47	72	70	72.0	0.80	84	74	78	4.96

\*Number of specimens tested.

and NS concrete, appear to have comparable strain energies, and thus, the vast difference between the beam energies ( $E_b$ ) for NS and HS concretes probably arises because of the higher work of fracture energies ( $E_{wof}$ ) for NS concrete. This observation strengthens the argument presented in Chapter 6 to explain the brittleness of HS concrete.

### 8.3 ENERGY BALANCE JUST AFTER FAILURE (at $t=t_t$ )

At the end of the impact event, the external load  $P_t(t)$  is reduced to zero and the broken halves of the beam swing clear of the striking tup. At this instant, the energy balance can be written as

$$\Delta E(t_t) = E_m(t_t) + E_s(t_t)$$

As before, this can be written as

$$\Delta E(t_t) = E_m(t_t) + E_b(t_t) + E_{ker}(t_t) \quad (8.6)$$

Once again the energy  $E_b(t_t)$  obtained from the area under the load vs. displacement plot measures the work of fracture plus the strain energy in the beam. Since the strain energy can be assumed to be negligible in the broken halves of the beam, all of the energy  $E_b(t_t)$  represents the work of fracture, or the fracture energy.

Equation 8.5 can once again be used at  $t=t_t$  to determine the kinetic energy  $E_{ker}(t_t)$ . Once  $E_{ker}(t_t)$  and  $E_b(t_t)$  are known, Equation 8.6 can be used to determine

$E_m(t_t)$ .

Figure 8.5 and Tables 8.3 and 8.4 present the energy balance at the end of the impact event ( $t=t_t$ ). Here, most of the energy lost by the hammer at  $t=t_t$  ( $\Delta E$ ) is gained by the beam ( $E_s$ ). The energy gained by the beam consists of the kinetic energy of the broken halves ( $E_{ker}$ ) and the bending energy ( $E_b$ ). Probably, the bending energy is the energy required to create two new fracture surfaces. This can also be termed the fracture energy, or the work of fracture. Since, by the end of the impact event, the specimen appears to have little or no strain energy, the bending energy  $E_b$  represents only the fracture energy.

#### 8.4 THE MACHINE LOSSES

If the difference between the energy lost by the hammer ( $\Delta E$ ) and the energy absorbed by the beam ( $E_s$ ) can be assumed to be the energy lost to the machine ( $E_m$ ), then the "machine losses" can be calculated at the peak load ( $t=t_p$ ) and at the end of the event ( $t=t_t$ ). Figure 8.6 presents this machine energy calculated as a percentage of the total energy lost by the hammer ( $E_m/\Delta E \times 100\%$ ). As can be seen from Figure 8.6, at the peak load, 60 to 80 percent of the energy lost by the hammer is stored in the machine. However, by the end of the impact event ( $t=t_t$ ), 90 to 100 percent of the energy lost by the hammer appears as specimen energy. It can also be noted from Figure 8.6 that HS concrete, being a

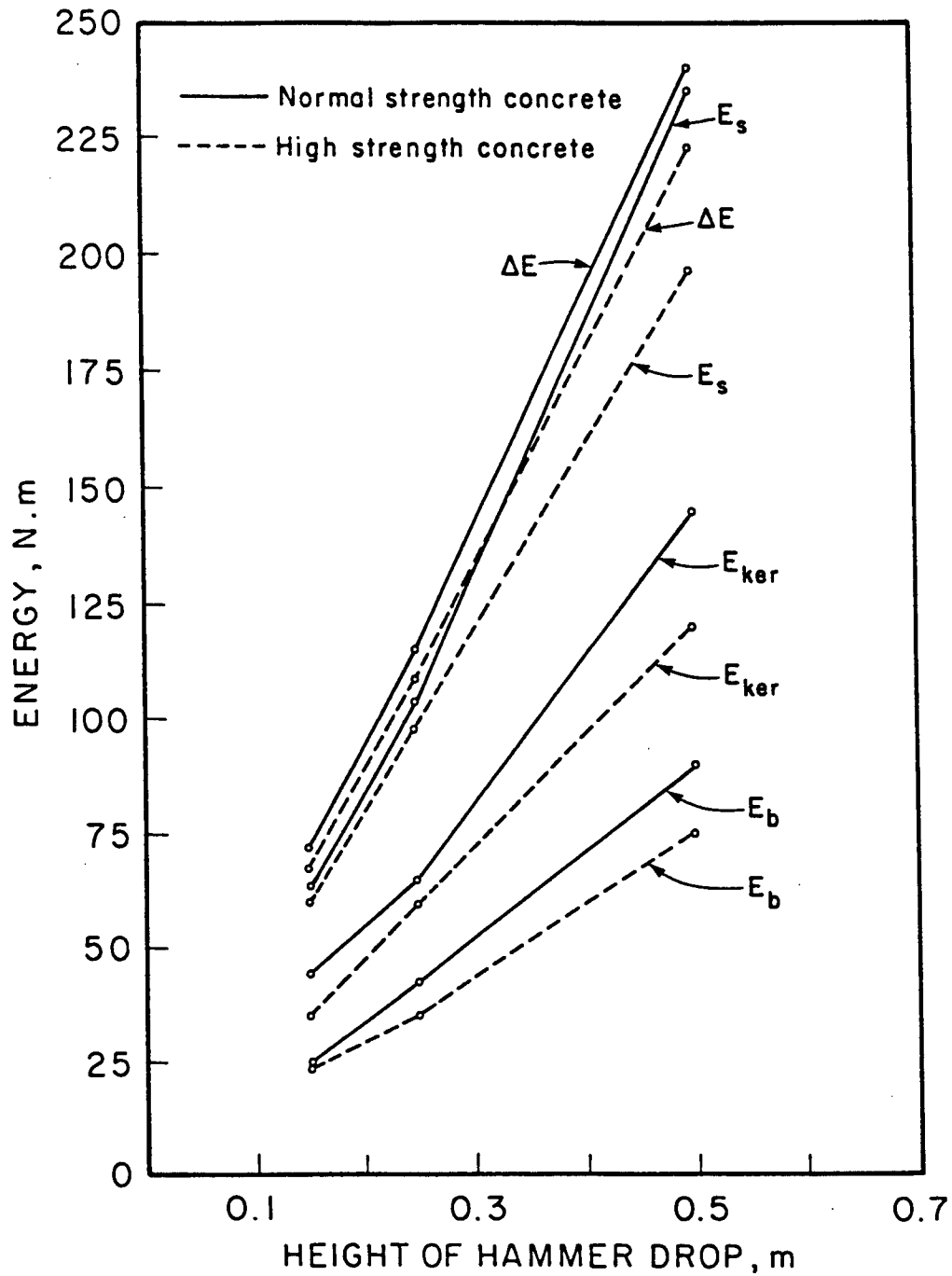


FIGURE 8.5-Energy Balance just after failure

Table 8.3-Energy Balance at the Peak Load (Normal Strength Concrete)

ITEMS	0.15 M (6)*				0.25 M (6)*				0.50 M (7)*			
	MAX.	MIN.	MEAN	STD. DEVIATION	MAX.	MIN.	MEAN	STD. DEVIATION	MAX.	MIN.	MEAN	STD. DEVIATION
$\Delta E(t_t)$ (N-m)	76	64	72	4.7	131	94	116	15.3	249	231	240	5.8
$E_{ker}(t_t)$ (N-m)	45	42	44	1.2	80	47	66	12.0	150	139	145	4.7
$E_b(t_t)$ (N-m)	31	19	25	4.3	60	27	43	12.4	100	87	90	6.4
$E_s(t_t)$ (N-m)	73	63	69	3.90	130	74	109	23.0	248	230	235	7.31
$E_m(t_t)$ (N-m)	3	1	2	1.0	20	1	7	7.7	12	0	5	4.0
$\frac{E_m}{\Delta E} \times 100\%$	4	1.56	2.77	1.0	21	6.76	6.03	8.0	5.02	0	2.08	1.0

\*Number of specimens tested

Table 8.4-Energy Balance at the Peak Load (High Strength Concrete)

ITEM	0.15 m (6)*				0.25 m (5)*				0.50 m (6)*			
	MAX.	MIN.	MEAN	STD. DEVIATION	MAX.	MIN.	MEAN	STD. DEVIATION	MAX.	MIN.	MEAN	STD. DEVIATION
$\Delta E(t_t)$ (N-m)	89	43	68	16.7	133	100	109	12.20	238	214	223	10.5
$E_{ker}(t_t)$ (N-m)	54	13	36	16.8	89	54	64	13.6	127	116	121	5.5
$E_b(t_t)$ (N-m)	33	21	25	5.0	43	31	35	4.6	100	57	75	18.6
$E_s(t_t)$ (Nm)	89	34	61	21.0	133	86	99	18.0	213	193	196	10.0
$E_m(t_t)$ (N-m)	14	0	7	5.9	15	0	10	6.3	30	25	27	2.7
$\frac{E_m}{\Delta E} \times 100\%$	21.12	0	10.3	5.4	10.80	0	9.2	3.7	13.7	10.2	12.1	1.50

\*Number of specimens tested.

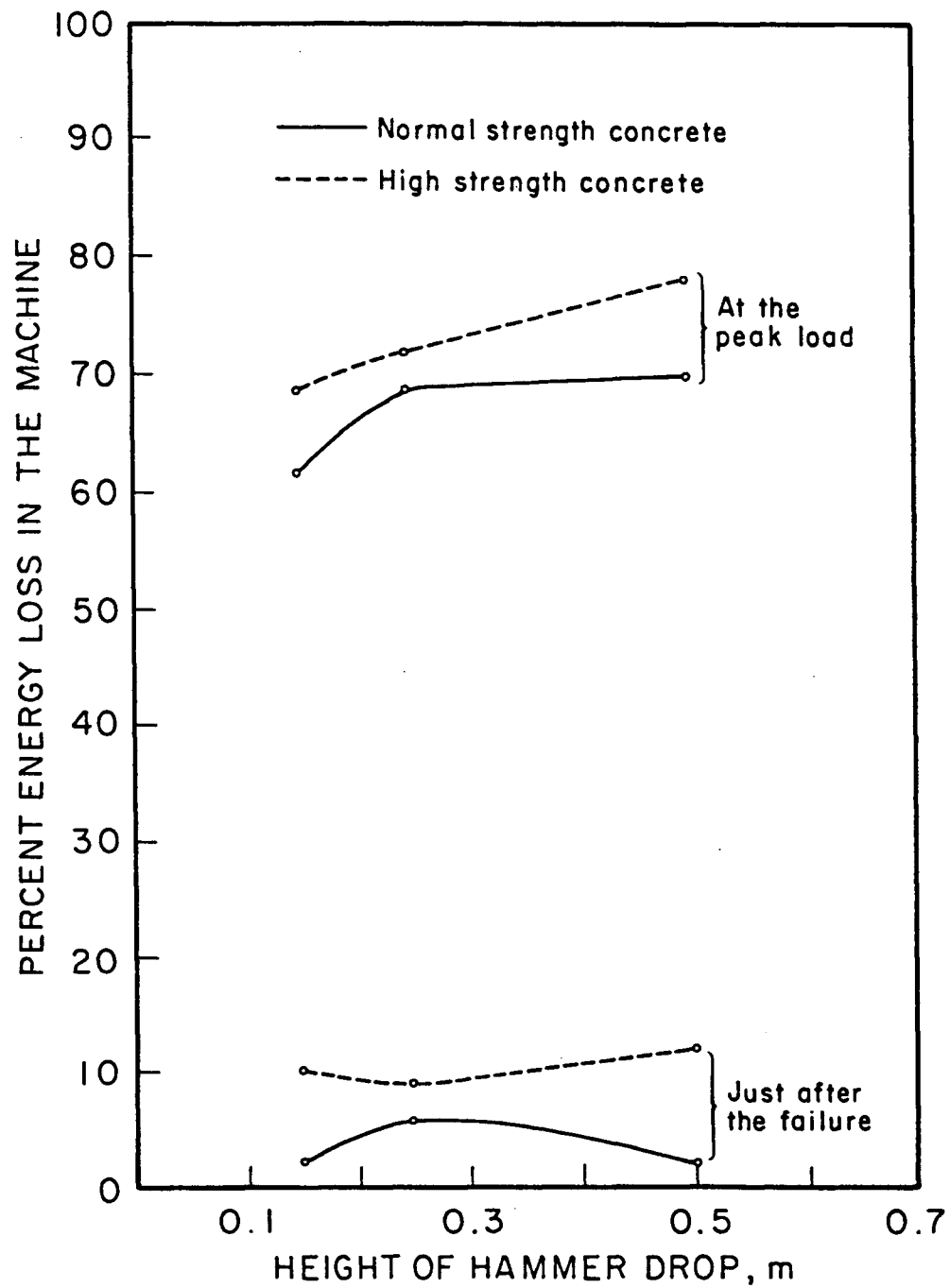


FIGURE 8.6-The Machine Losses

stronger and a stiffer material than NS concrete, showed higher machine losses.

High stress rate testing of cementitious materials requires sophisticated testing equipment. Knowledge of the various modes in which energy can be lost during a test is essential to a proper analysis of the test results. In the absence of this knowledge, the results can be grossly misleading. The energy lost by the hammer cannot be assumed to be the energy consumed by the beam. Even if the machine losses can be assumed to be constant for a given drop height for a given machine, the energy gained by the specimen still has to be corrected for its kinetic energy.

The percentage energy lost to the machine seems to depend on the strength and the stiffness of the material tested. Energy losses in the machine were found to be higher when HS concrete, which is stronger and stiffer than NS concrete, was tested.

If it can be assumed that, after the beam fails, the broken halves of the beam have little or no strain energy, then in the post-peak load region, most or all of the strain energy stored in the beam is used in propagating the crack. Since the stored strain energy at the peak load is much less than the overall fracture energy required, it seems possible that the crack propagates while the beam continues to absorb energy from the hammer and the various other machine parts.

## 9. NOTCHED BEAMS UNDER IMPACT

### 9.1 INTRODUCTION

Numerous microcracks exist in concrete even prior to load application. Under load, the stresses and strains in the vicinity of a crack tip increase, and if the critical conditions are met, crack extension occurs. With an increase in the size of the crack, the stresses and strains increase further causing the crack to extend at an increasing rate till failure occurs. In a linearly elastic material, the stress field in the neighbourhood of a crack tip can be described by a single parameter, the stress intensity factor,  $K$ . Fracture occurs when  $K$  exceeds a critical value  $K_{IC}$ .<sup>7</sup> The critical stress intensity factor,  $K_{IC}$ , thus, is a material property determining the critical condition at which unstable crack propagation occurs.

Many attempts have been made in the past to determine the critical stress intensity factor  $K_{IC}$  for concrete. However, there is no general agreement over its value, or its interpretation.  $K_{IC}$  has been found to depend, among other things, upon the notch width, the notch depth, the specimen geometry, and also upon the rate of loading (61,62). The existence of a process zone in front of an advancing crack tip is now recognized, and nonlinear fracture mechanics has therefore been considered to be a more appropriate tool for concrete. John and Shah (62) have reported that crack extension occurs even prior to the peak

-----  
<sup>7</sup> The subscript I refers to the crack-opening mode of crack propagation.

load, but that this prepeak crack extension decreases with an increase in the rate of loading.

The attempt to determine  $K_{IC}$  has also been extended to fibre reinforced concrete. Harris et al (49) studied the effect of randomly distributed glass fibres, high carbon steel fibres, and mild steel fibres on  $K_{IC}$ , and reported a substantial increase in  $K_{IC}$  due to fibre inclusion. However, Yam and Mindess (63), concluded that the fibres do not restrain crack growth in any significant way once the crack starts propagating.

In the present study, the dependence of  $K_{IC}$  on strain rate for both plain and fibre reinforced concretes was studied by subjecting notched beams to variable rates of loading. The loading rates used varied from those achieved in a static testing machine to those achieved using the impact machine. Two concrete strengths, of 42 MPa and 82 MPa, were examined. The details on the composition of the notched beams, their compressive strengths, and their designations have been presented in Table 4.1.

## 9.2 PLAIN AND FIBRE REINFORCED NOTCHED BEAMS UNDER VARIABLE STRESS RATES.

Notches were cut in beams made with normal strength concrete, high strength concrete, and normal strength polypropylene fibre reinforced concrete beams, using a diamond cutting wheel. The notch depths ranged between 65mm and 70mm; the notch width was about 3mm.

Companion beams were first loaded statically in 3-point bending, with the cross-head moving at  $4.2 \times 10^{-7}$  m/s. The results were obtained in the form of bending load vs. load point deflection plots. Later, several beams in each of the categories were tested using the drop hammer, with the hammer dropping through 0.15m, 0.25m, or 0.50m.

For the computation of the critical stress intensity factor no universally accepted formula exists. In this study, the formula given by Broek (58) has been used.

$$K_{IC}, K_{ID} = \frac{P_b(\max)l}{B D^{3/2}} \left[ 2.9\left(\frac{a}{D}\right)^{1/2} - 4.6\left(\frac{a}{D}\right)^{3/2} + 21.8\left(\frac{a}{D}\right)^{5/2} - 37.6\left(\frac{a}{D}\right)^{7/2} + 38.7\left(\frac{a}{D}\right)^{9/2} \right] \quad 9.1)$$

where,

$(P_b)_{\max}$  = peak bending load.

$l$  = test span of the beam.

$B$  = breadth of the beam.

$D$  = depth of the beam.

$a$  = the notch depth.

$K_{IC}, K_{ID}$  = Static and dynamic critical stress intensity factor, respectively. Note that it was assumed that the same formula could be used in both the static and dynamic cases.

The results for normal strength beams are given in Table 9.1. Table 9.1a shows the impact results, while Table

9.1b shows the results from the static tests. Similarly, Table 9.2 presents the results for high strength concrete, and Table 9.3 pertains to normal strength polypropylene fibre reinforced concrete.

The peak bending loads obtained for the different notched beams have been plotted as a function of the hammer drop height in Figure 9.1. As may be seen, an increase in the hammer drop height, or an increase in the stress rate, resulted in an increase in the peak bending load the beam could support. It may also be noted that high strength

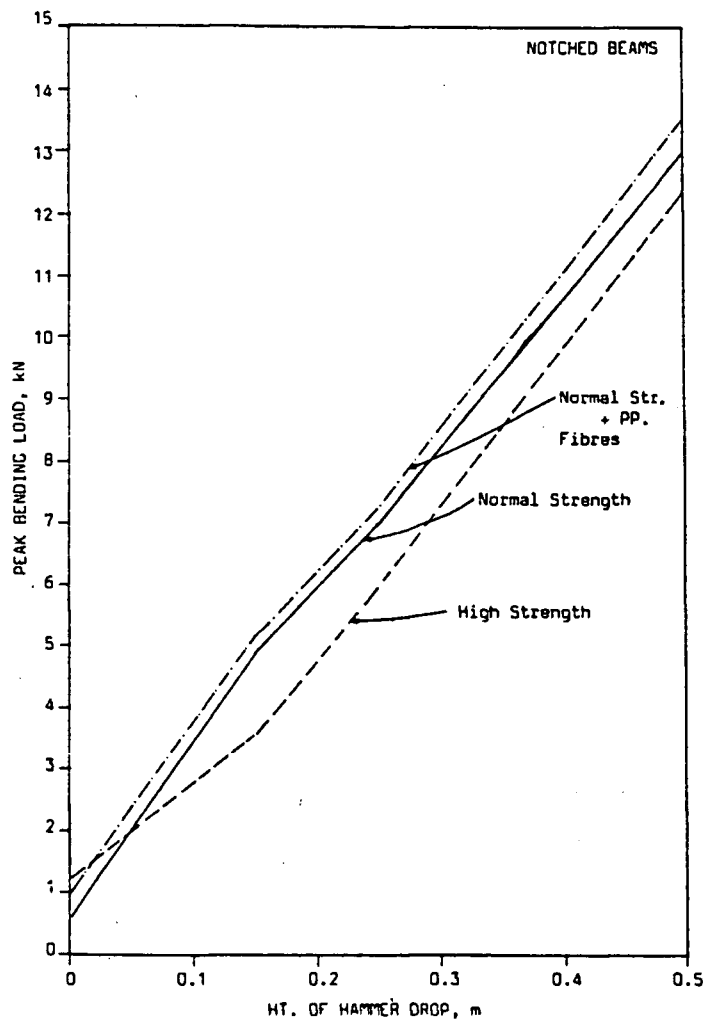


Figure 9.1-Effect of Hammer Drop Height on Peak Bending Load

TABLE -9.1  
Behaviour of normal strength concrete under impact and static loading

	HEIGHT OF HAMMER DROP, m											
	0.15(4)*				0.25(4)*				0.50(4)*			
	Max	Min	Mean	Std.Dev	Max	Min	Mean	Std.Dev	Max	Min	Mean	Std.Dev
Peak Bending Load (N)	7138	3606	4981	1440	8713	4932	7094	1364	16466	9590	13028	3438
Displacement at Peak Bending Load (m) ( $\times 10^{-6}$ )	246	124	192	51	357	211	284	56	597	432	514	82
Energy up to Peak Load (N-m)	1.3	0.4	0.7	0.33	2.1	0.9	1.6	0.46	5.8	4.8	5.3	0.49
Total Fracture Energy (N-m)	23.8	9.8	14.4	5.5	26.8	16.5	22.6	3.7	70.2	41.4	55.8	14.4
$K_{ID}$ ( $MNm^{-3/2}$ )	4.40	2.27	3.14	0.86	5.38	3.00	4.56	0.93	10.17	5.92	8.62	1.92

	STATIC BENDING TESTS <sup>†</sup> (2)*			
	Max	Min	Mean	Std.Dev
Peak Bending Load (N)	647	591	619	28
Displacement at Peak Bending Load (m) ( $\times 10^{-6}$ )	261	203	232	29
Energy at Peak Load (N-m)	0.08	0.07	0.07	0.002
Energy (N-m)	0.37	0.40	0.38	0.02
$K_{IC}$ ( $MNm^{-3/2}$ )	0.46	0.38	0.42	0.04

\* No. of specimens tested  
<sup>†</sup> Static tests carried out at cross-head speed of  $4.17 \times 10^{-7}$  m/s

**TABLE-9.2**  
Behaviour of high strength concrete under impact and static loading

	HEIGHT OF HAMMER DROP, m											
	0.15(4)*				0.25(4)*				0.50(4)*			
	Max	Min	Mean	Std.Dev	Max	Min	Mean	Std.Dev	Max	Min	Mean	Std.Dev
Peak Bending Load (N)	3750	3524	3637	113	6888	5099	5988	632	15166	9612	12462	2400
Displacement at Peak Bending Load (m) ( $\times 10^{-6}$ )	295	217	256	39	443	331	378	443	649	346	480	117
Energy up to Peak Load (N-m)	0.8	0.6	0.7	0.1	2.1	0.9	1.5	0.4	8.6	3.7	5.2	1.9
Total Fracture Energy (N-m)	14.5	6.8	10.6	3.8	23.2	17.5	21.2	2.2	62.5	40.0	54.7	9.1
$K_{IC}$ ( $\text{MNm}^{-3/2}$ )	2.35	2.15	2.25	0.10	4.26	3.47	3.86	0.29	10.27	6.54	8.25	1.60

	STATIC BENDING TESTS <sup>+(2)*</sup>			
	Max	Min	Mean	Std.Dev
Peak Bending Load (N)	1249	1204	1227	22.50
Displacement at Peak Bending Load (m) ( $\times 10^{-6}$ )	370	274	322	48
Energy at Peak Load (N-m)	0.21	0.17	0.19	0.02
Total Fracture Energy (N-m)	0.60	0.40	0.50	0.10
$K_{IC}$ ( $\text{MNm}^{-3/2}$ )	0.80	0.77	0.79	0.01

\* No. of specimens tested  
+ Static tests carried out at cross-head speed of  $4.17 \times 10^{-7}$  m/s

**TABLE- 9.3**  
Behaviour of normal strength concrete reinforced with polypropylene fibres  
under impact and static loading

	HEIGHT OF HAMMER DROP, m											
	0.15(4)*				0.25(4)*				0.50(4)*			
	Max	Min	Mean	Std.Dev	Max	Min	Mean	Std.Dev	Max	Min	Mean	Std.Dev
Peak Bending Load (N)	6196	4370	5283	913	7509	7100	7236	192	13719	13617	13667	51
Displacement at Peak Bending Load (m) ( $\times 10^{-6}$ )	318	230	274	44	375	213	314	72	470	309	389	80
Energy up to Peak Load (N-m)	1.1	0.5	0.8	0.2	2.0	1.4	1.7	0.2	5.7	5.3	5.5	0.19
Total Fracture Energy (N-m)	22.5	9.5	16.0	6.5	26.8	20.2	24.3	2.9	64.7	57.5	61.1	3.5
$K_{ID}$ ( $MNm^{-3/2}$ )	3.82	2.69	3.26	0.57	5.30	4.15	4.76	0.47	9.65	8.36	9.01	0.65

	STATIC BENDING TESTS <sup>†</sup> (2)*			
	Max	Min	Mean	Std.Dev
Peak Bending Load (N)	1115	1049	1082	33
Displacement at Peak Bending Load (m) ( $\times 10^{-6}$ )	210	203	207	3.5
Energy at Peak Load (N-m)	0.13	0.11	0.12	0.01
Total Fracture Energy (N-m)	0.48	0.45	0.47	0.01
$K_{IC}$ ( $MNm^{-3/2}$ )	0.79	0.68	0.73	0.06

\* No. of specimens tested  
<sup>†</sup> Static tests carried out at cross-head speed of  $4.17 \times 10^{-7}$  m/s

concrete, which is, of course, stronger than normal strength concrete in static loading situations, was found to be weaker than normal strength concrete under impact loading (Figure 9.1). Such an observation is in contradiction with the results obtained for the unnotched beams (Chapter 6), in which high strength concrete was found to be consistently stronger than normal strength concrete both for static and impact situations. This suggests the greater notch-sensitivity of high strength concrete compared to normal strength concrete.

The energy absorbed by the beams up to the point of peak bending load as a function of hammer drop height is plotted in Figure 9.2. The fracture energy, calculated to the point at which the load drops back to zero, is also shown in Figure 9.2.

Although the differences amongst the different concrete types (Figure 9.2) are not substantial, high strength concrete was found to absorb less energy than normal strength concrete up to the peak load. The addition of fibres to the normal strength mix was found to increase the energy absorption capacity up to the peak load. If the energy to the peak load may be assumed to represent the energy required to begin unstable crack propagation, then for high strength concrete there was a decrease in this energy, while the addition of fibres resulted in its increase.

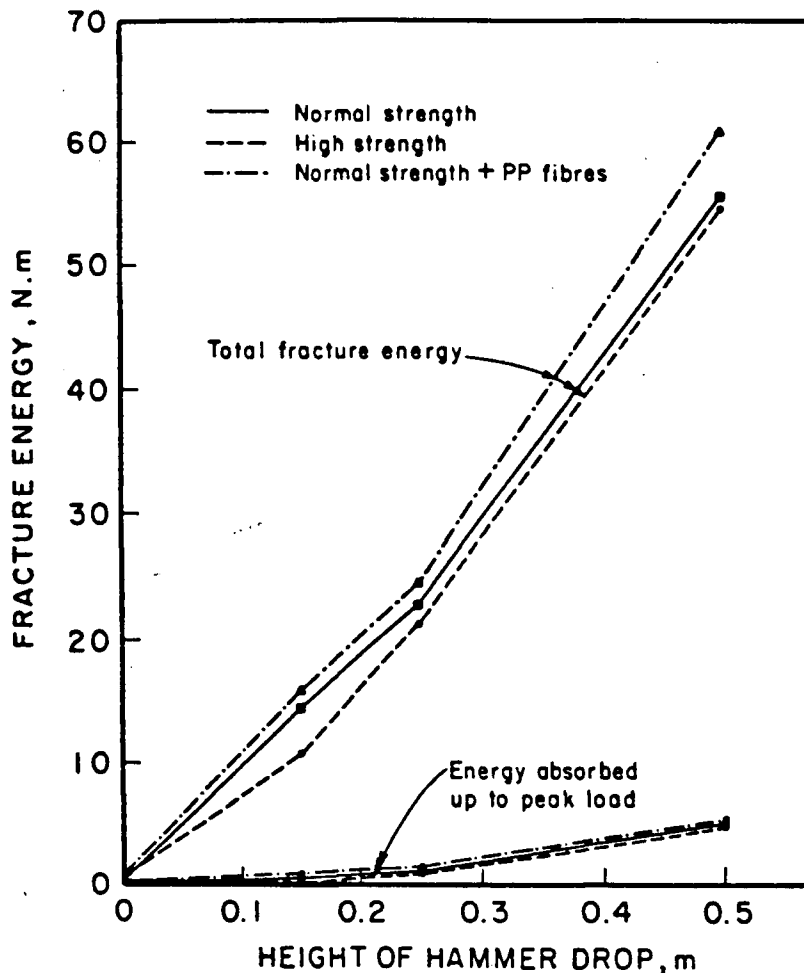


Figure 9.2-Effect of Hammer Drop Height on Energies

The fracture energies required by the notched beams under impact were significantly higher than those required by the beams loaded statically (Figure 9.2). Also, an increase in the drop height of the hammer resulted in a considerable increase in the fracture energy requirement. High strength concrete was found to be more brittle than normal strength concrete, and fibre reinforcement was found to improve the toughness marginally (Figure 9.2). Similar observations have been reported for the unnotched beams in Chapters 6 and 10.

The values of  $K_{IC}$  and  $K_{ID}$  have been plotted for the various types of concretes tested, as a function of hammer drop height in Figure 9.3. High strength concrete (Table 9.2b), which under static loading gave a slightly higher  $K_{IC}$  than either plain (Table 9.1b) or fibre reinforced (Table 9.3b) normal strength concrete, showed particular notch sensitivity under impact and registered lower  $K_{ID}$  values. This may serve as a caution against the presence of notches and flaws in high strength concrete subjected to impact.

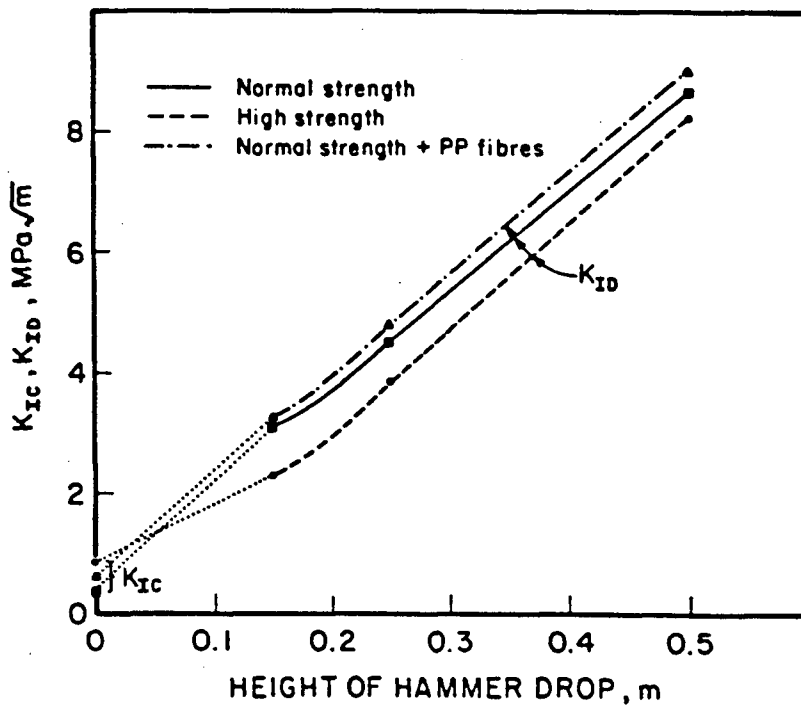


Figure 9.3-Effect of Hammer Drop Height on Fracture Toughness

The use of the polypropylene fibres was found to improve the critical stress intensity factor both in the static and the dynamic cases. Fibres, thus, appear to act as crack arresters, retarding growth of the subcritical flaws. The energy input required to precipitate unstable crack propagation in fibre reinforced specimen was found to be higher than for the plain concrete specimens (Figure 9.2). This may be related, indirectly, to the contribution of the fibres in keeping the matrix coherent, thereby increasing the deformation capacity of the beams.

Increasing the strain rate resulted in an increased critical stress intensity factor for all of the types of concrete tested in this study. However, the values of the critical intensity factor may have been underestimated because of the prepeak crack growth; the crack length "a" used in Equation 9.1 may be too low. As pointed out by John and Shah (62), the prepeak crack growth seems to decrease with an increase in the rate of loading, thus reducing the error at higher loading rates. Indeed, even under static loading, they reported an increase in  $K_{IC}$  of only about 11% when the pre-peak crack extension was considered. Therefore, the fact that pre-peak crack growth was not considered in the present work should not introduce significant errors in the analysis.

## 10. FIBRE REINFORCED CONCRETE UNDER IMPACT

### 10.1 INTRODUCTION

The brittle type of failure observed for cement-based matrices under tensile stress systems or impact loading is an object of concern. The addition of fibres can be used to alleviate this problem, at least in part. The effect of fibres can be seen in the improved tensile strength and flexural strength of the composites, and also in their improved impact resistance or toughness. It is not so much the improved strength, but rather the improved toughness, which is the prime advantage of adding fibres to the matrix. The presence of fibres, by controlling the cracking, imparts to the composite some post-cracking ductility, which leads to the improved toughness.

The fibres form primarily a mechanical bond with the surrounding matrix. As a result, the fibres and the matrix act in a composite manner. When an unreinforced brittle matrix reaches its failure load, the matrix cracks and failure is precipitated without warning. However, in a fibre composite, even when the matrix cracks, the fibres bridging the crack can still transfer some load, and sudden failure is thereby averted. A cracked composite carries load by virtue of the tensile strength of the fibre and the bond that has developed between the fibre and the matrix. Once the composite has cracked, the matrix-fibre system is no longer a continuous medium and therefore conventional theories of mechanics may be inapplicable.

In the case of a composite member undergoing uniaxial tension, the matrix cracks at a certain failure strain in a manner similar to that of an unreinforced member. If the fibres were not present, this would cause separation and sudden failure. However, with fibres present, they take over once the matrix cracks. The fibres, depending upon their geometry and quantity, may support a lower or a higher load than the one at which the matrix cracked. For a given type of fibre, thus, there exists a "critical volume fraction" of fibres which will support just the load the member was supporting at the time of matrix failure. The load will drop if the fibre volume fraction is less than the critical volume. On the other hand additional load can be carried if the critical volume fraction is exceeded.

For a fibre reinforced member under flexure, conventional beam theory is applicable only until the matrix cracks on the tension side; beyond this point, the stress-strain curve on the tension side is very different from the stress-strain curve on the compression side, and as a result, conventional beam theory ceases to apply. When an unreinforced beam cracks, the equilibrium of compressive and tensile forces on its cross-section is disturbed suddenly, the neutral axis moves up, the crack rapidly propagates upward, separation occurs and the load drops to zero. However, in a fibre reinforced beam, as the tensile strains approach the failure value, cracks are formed, but the fibres carry the load on the tension side and equilibrium is

maintained. With the cracks, the strains on the tensile side increase, and the neutral axis moves up. In this regard, a fibre reinforced beam acts similar to an under-reinforced beam with conventional reinforcement. With a reduction in the depth of the neutral axis, the area of the tensile stress block may increase and the load may rise. Since the increase in load is accompanied by a reduction in the neutral axis depth, there exists a limit to strengthening, as failure may then initiate at the compression face. By adding fibres, better use is made of the strength of concrete in compression, since a reduction in the depth of the neutral axis signifies an increase in the mean compressive stress on the compression side of the neutral axis.

The performance of a composite under high stress rates depends upon the performance of both the fibres and the matrix. The performance of the matrix under impact was studied in chapter 6. What remains to be seen is whether the stress rate sensitivity of a fibre reinforced composite is due mainly to the stress rate sensitivity of the matrix or because of fibre-matrix interactions as well.

Both low modulus (polypropylene) and high modulus (steel) fibres were tested. The polypropylene fibres were chopped, fibrillated, 38mm long fibres; the steel fibres were 60mm long, 0.6mm in diameter, with both ends hooked. Volume fractions of 0.5% for polypropylene fibres, and of 1.5% for steel fibres were used. Only 0.5% by volume of

polypropylene fibres were added because higher volumes could not be added to the concrete using conventional mixing techniques.

## 10.2 STEEL FIBRE REINFORCED NORMAL STRENGTH CONCRETE (NSSFRC) UNDER VARIABLE STRESS RATE

Normal strength steel fibre reinforced concrete beams were tested in 3-point bending, both on a static universal testing machine with the cross head moving at  $4.2 \times 10^{-7}$  m/s, and on the drop weight impact machine with a hammer drop height of 0.50m.

Figure 10.1 and Table 10.1 present the results obtained from the static tests, along with the corresponding results obtained from unreinforced normal strength concrete beams. The load vs. deflection plots of Figure 10.1 indicate that the addition of fibres to the matrix was helpful in two ways. First, the observed peak loads were higher for reinforced beams compared to the plain ones; second, the sudden failure or drop in load, after the peak load in the case of plain concrete was replaced by a gradual drop in load in the case of fibre reinforced concrete. The undesirable catastrophic failure in plain concrete could thus be changed to a more desirable pseudo-ductile failure. The load carrying capacity of the fibres in the post-peak load region was reflected in the higher fracture energies required for fibre reinforced beams (Table 10.1).

Table 10.1  
 Static Behaviour of Plain and Steel Fibre Reinforced Normal Strength Concrete

	Plain (3) <sup>1</sup>				Plain + Steel Fibres (3) <sup>1</sup>			
	Max	Min.	Mean	s	Max.	Min.	Mean	s
Peak Bending Load (N)	6766	6000	6344	306	12436	10902	11500	670
Fracture Energy (Nm)	6.5	2.9	5.5	1.5	46.3	42.0	44.8	2.0
First Peak Load (N)	-	-	-	-	9100	7600	8500	648
Cross Head Speed (m/sec)	-	-	$4 \times 10^{-7}$	-	-	-	$4 \times 10^{-7}$	-

<sup>1</sup> Number of specimens tested.

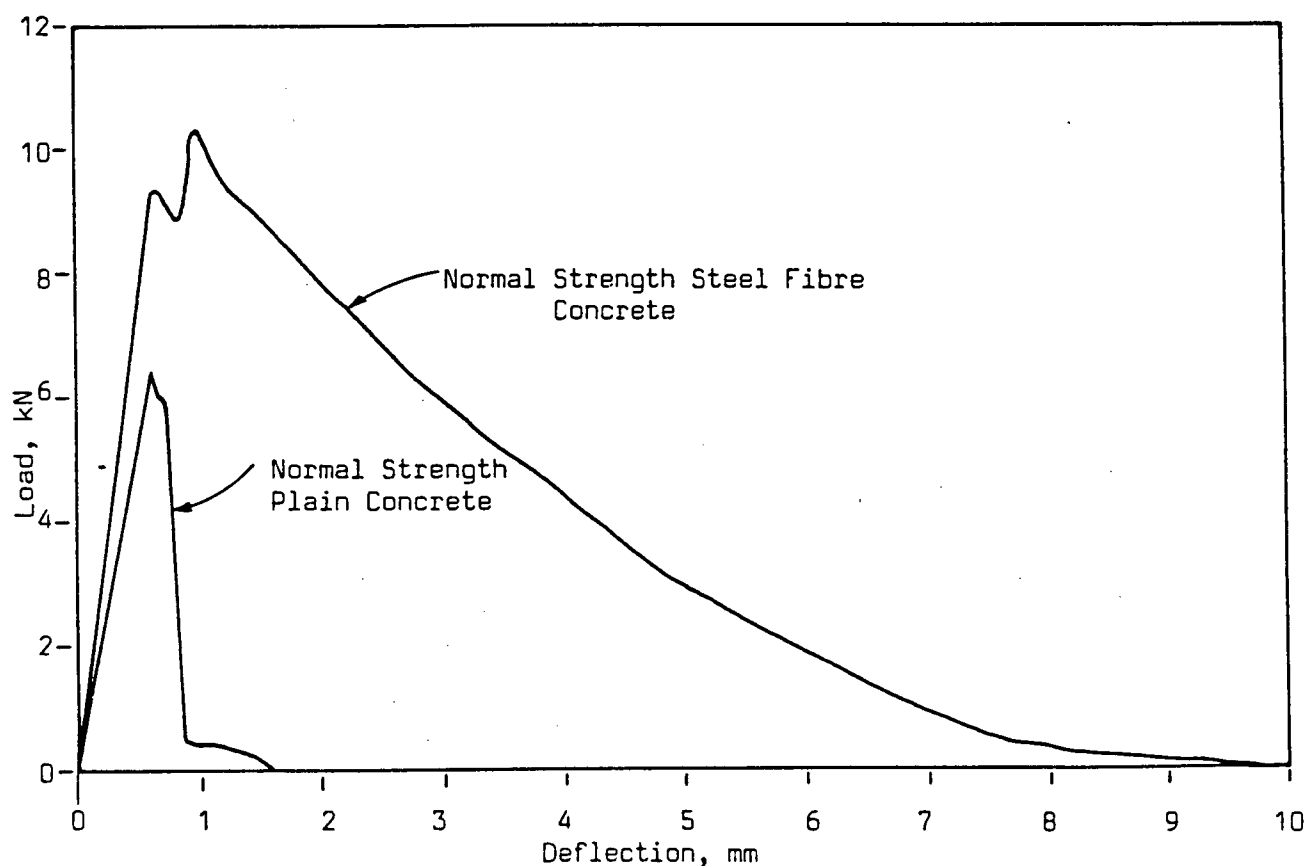


Figure 10.1- Static Behaviour of Plain and Steel Fibre Reinforced Normal Strength Concrete

Table 10.2

Dynamic Behaviour of Plain and Steel Fibre Reinforced Normal Strength Concrete (0.5m drop)

	Plain (6) <sup>1</sup>				Plain + Steel Fibres (6) <sup>1</sup>			
	Max	Min.	Mean	s	Max.	Min.	Mean	s
Max. Observed Top Load (N)	37567	35810	36192	677	43281	37286	39999	2345
Max. observed Inertial Load (N)	20291	16868	19244	1278	17094	13819	15993	1262
Peak Bending Load (N)	17727	16452	16932	428	26800	22786	24006	1629
Fracture Energy (Nm)	100.5	87.8	90.1	6.5	248.0	229.0	237.6	7.5

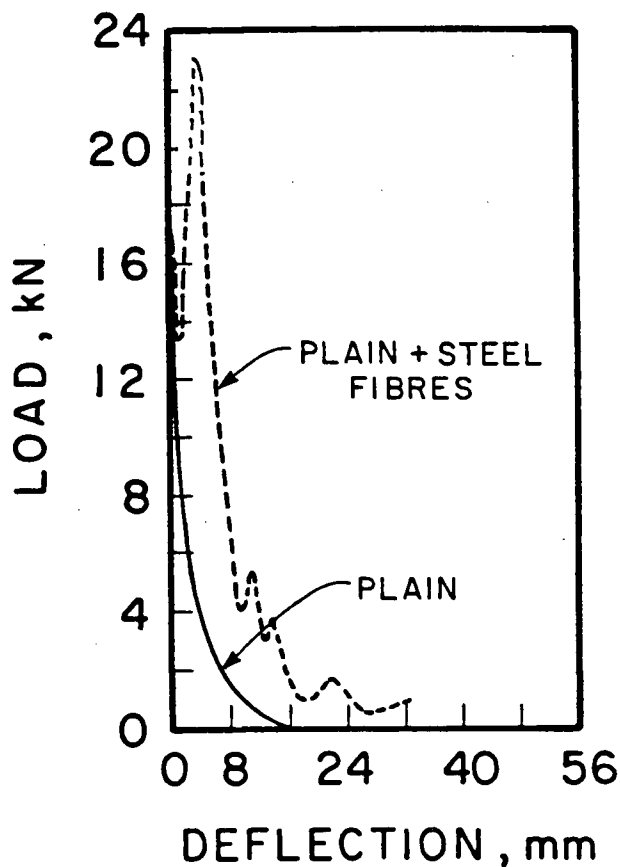
<sup>1</sup> Number of specimens tested.

Figure 10.2- Dynamic Behaviour of Plain and Steel Fibre Reinforced Normal Strength Concrete (0.5m drop)

The results of the dynamic tests are presented in Figure 10.2 and Table 10.2. Similar to the static case, the peak bending loads and the fracture energies for fibre reinforced concrete were found to be higher than those for unreinforced beams, even in the dynamic loading situations. However, an improvement by about eight times in the fracture energy observed in the static case (Table 10.1), was not matched in the dynamic case, where the corresponding improvement was only by about a factor of two (Table 10.2).

Fibre reinforced concrete, whose behaviour depends upon the behaviour of the matrix as well as the fibres, was found to be particularly stress-rate sensitive (Figure 10.3). Since both the matrix (Chapter 6), and the matrix-fibre bond (64) are very strain rate sensitive, it is not surprising that the composite shows a sensitivity to strain rate as well.

To study the effect of moment of inertia on the impact performance of steel fibre reinforced concrete, some beams were tested about their weak axes. Table 10.3 shows the results of this testing. It can be noted that a reduction in the moment of inertia from  $162 \times 10^{-7} \text{m}^4$  to  $104 \times 10^{-7} \text{m}^4$  resulted not only in a reduction in the peak bending load, which is to be expected, but also in a reduction in the fracture energy. The direction in which the beams were cast, and the bleeding due to the use of an electric immersion vibrator (Chapter 6), are the probable causes of this observation.

Figure 10.3-Static and Dynamic Behaviour of Steel Fibre Reinforced Normal Strength Concrete

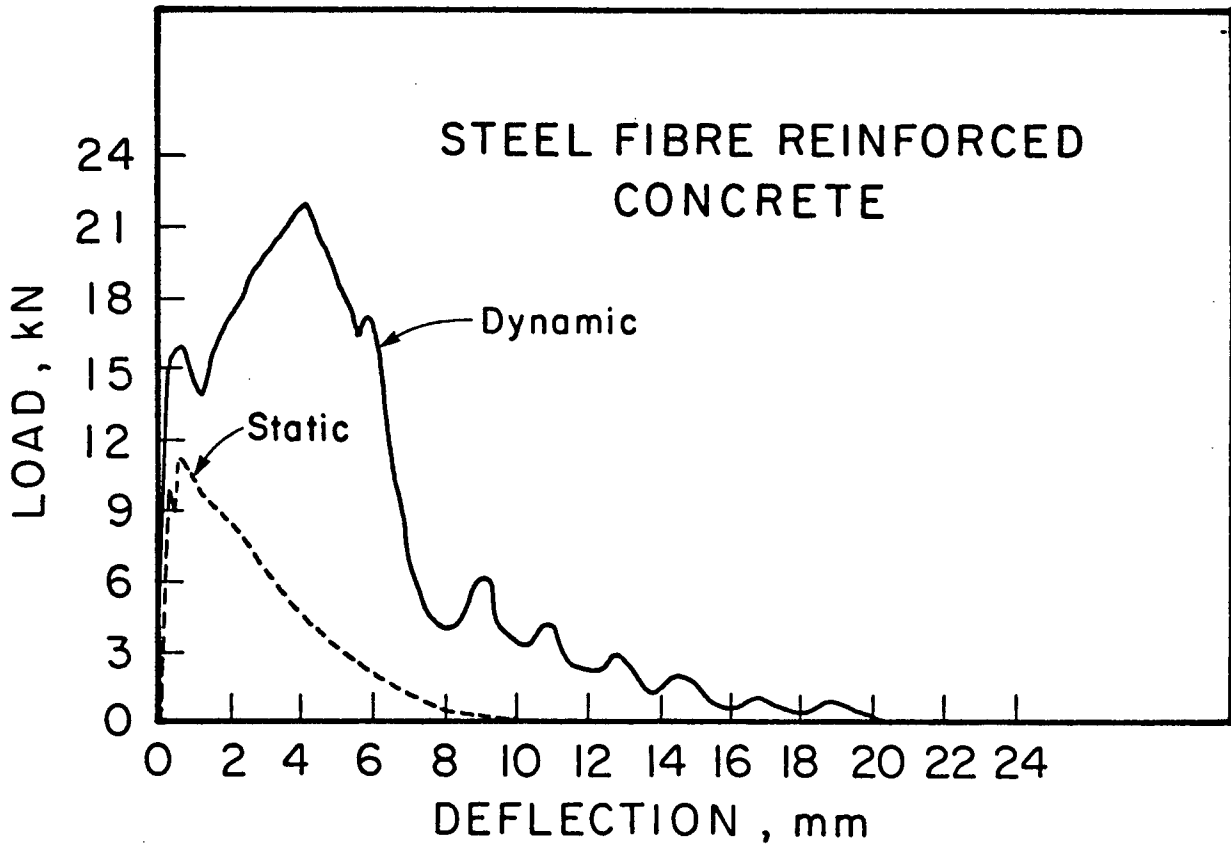


Table 10.3

Effect of Moment of Inertia on Steel Fibre Reinforced Normal Strength Concrete (0.5m drop)

		$I = 162 \times 10^{-7}$ (6) <sup>1</sup>				$I' = 104 \times 10^{-7}$ (6) <sup>1</sup>			
		Max	Min.	Mean	s	Max.	Min.	Mean	s
Max. Observed	Tup Load	43281	37286	39999	2345	33091	32434	32768	268
Max. observed	Inertial Load	17094	13819	15993	1262	16904	14009	15618	1203
Peak Bending Load (N)		26800	22786	24006	1629	19082	15877	17150	1211
Fracture Energy (Nm)		248.0	229.0	237.0	7.5	136.0	93.0	122.0	17.0

<sup>1</sup>Number of specimens tested.

### 10.3 POLYPROPYLENE FIBRE REINFORCED NORMAL STRENGTH CONCRETE (NSPFRC) UNDER VARIABLE STRESS RATE

The effect of fibrillated polypropylene fibres on the performance of normal strength concrete was studied as for the steel fibres. Figure 10.4 and Table 10.4 present the results obtained from the static tests. The results for plain concrete have also been reproduced for comparison. Similar to the steel fibres, the peak bending load and the fracture energy were both found to increase with the addition of polypropylene fibres. However, the increases in these quantities were small, and were not as significant as those for steel fibres (Table 10.1). Similar conclusion can be drawn from the dynamic results (Figure 10.5 and Table 10.5), where once again only marginal increases were observed in the peak bending load and the fracture energy upon adding the fibres.

A comparison of the static performance of NSPFRC with its dynamic performance (Figure 10.6) suggests its strong strain rate sensitivity. However, the strain rate sensitivity demonstrated by the matrix itself (Chapter 6) is probably primarily responsible for the strain rate sensitivity shown by the composite.

As in the case of steel fibers, the effect of moment of inertia on the impact performance of polypropylene reinforced concrete was also studied by testing a few beams

Table 10.4  
 Static Behaviour of Plain and Polypropylene Fibre Reinforced Normal Strength Concrete

	Plain (3) <sup>1</sup>				Plain + PP. Fibres (3) <sup>1</sup>			
	Max	Min.	Mean	s	Max.	Min.	Mean	s
Peak Bending Load (N)	6766	6000	6344	306	7436	7201	7302	99
Fracture Energy (Nm)	6.5	2.9	5.5	1.5	20.2	9.9	14.0	4.5
Cross Head Speed (m/sec)	-	-	$4 \times 10^{-7}$	-	-	--	$4 \times 10^{-7}$	-

<sup>1</sup>Number of specimens tested.

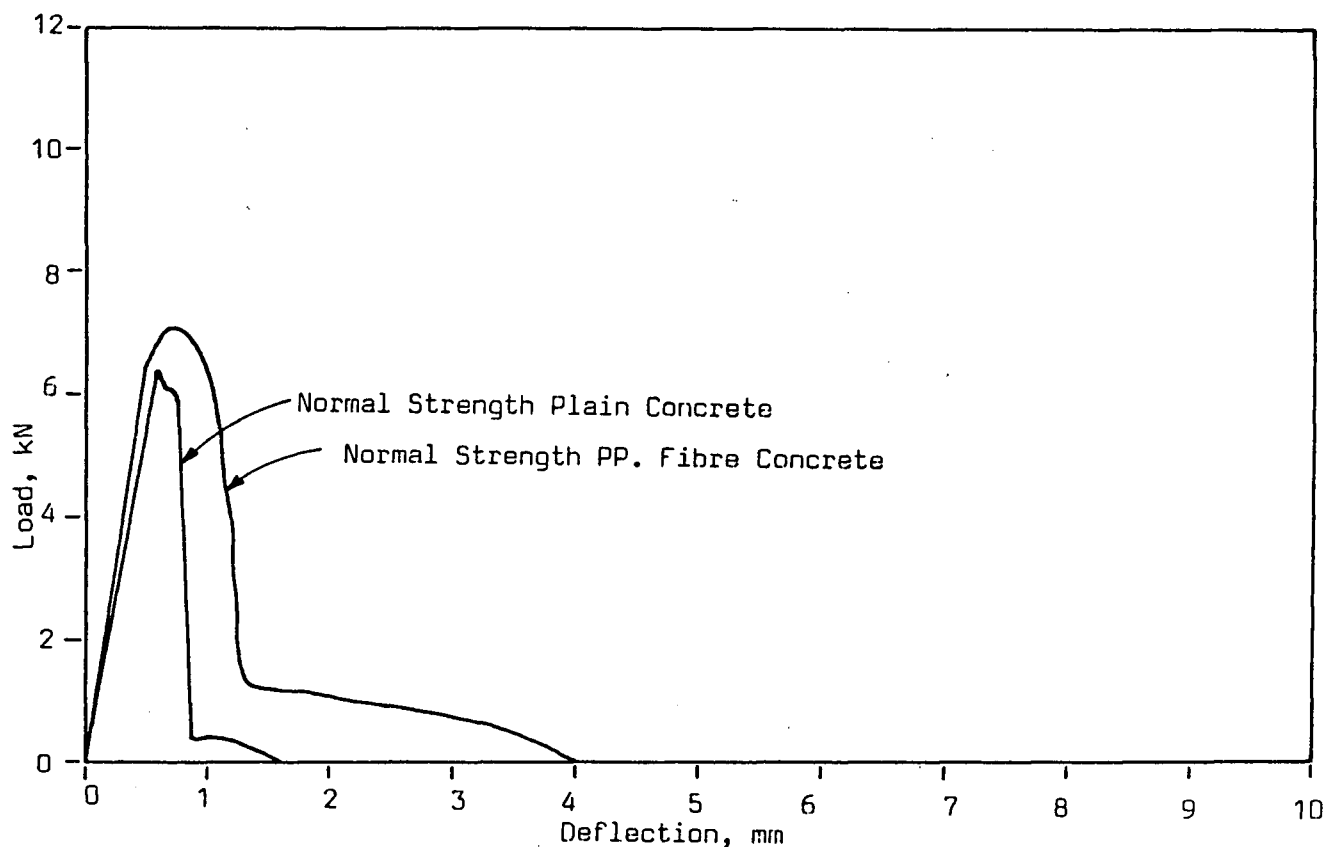


Figure 10.4-Static Behaviour of Plain and Polypropylene Fibre Reinforced Normal Strength Concrete

**Table 10.5**  
**Dynamic Behaviour of Plain and Polypropylene Fibre Reinforced Normal Strength Concrete (0.5m drop)**

	Plain (6) <sup>1</sup>				Plain + PP. Fibres (6) <sup>1</sup>			
	Max	Min.	Mean	s	Max.	Min.	Mean	s
Max. Observed Top Load (N)	37567	35810	36196	677	40431	36008	38318	1584
Max. observed Inertial Load (N)	20291	16868	19264	1278	23000	19804	21018	1267
Peak Bending Load (N)	17727	16452	16932	428	18488	16203	17300	821
Fracture Energy (Nm)	100.5	87.8	90.1	6.5	130.0	112.0	119.4	8.1

<sup>1</sup>Number of specimens tested.

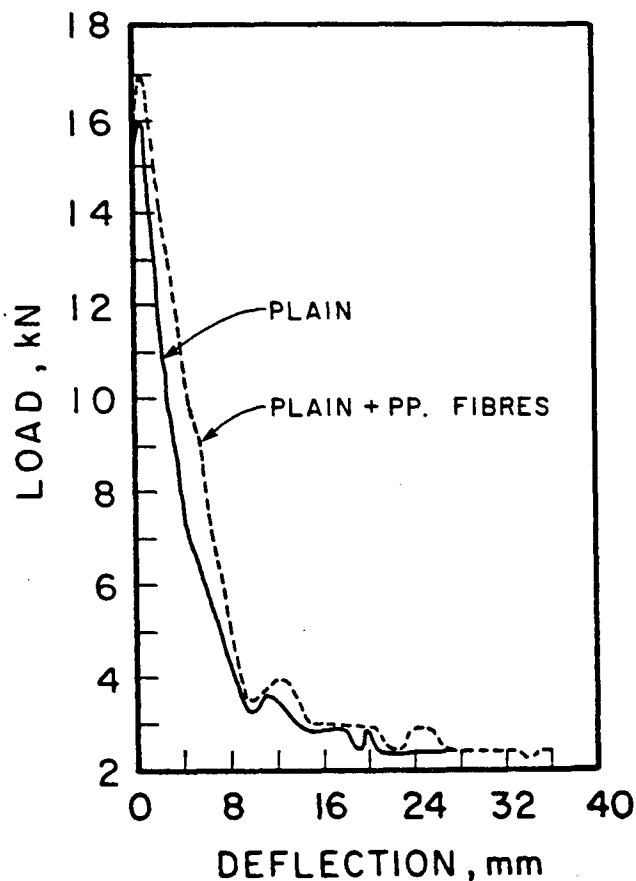


Figure 10.5-Dynamic Behaviour of Plain and Polypropylene Fibre Reinforced Normal Strength Concrete (0.5m drop)

Figure 10.6-Static and Dynamic Behaviour of Polypropylene Fibre Reinforced Normal Strength Concrete

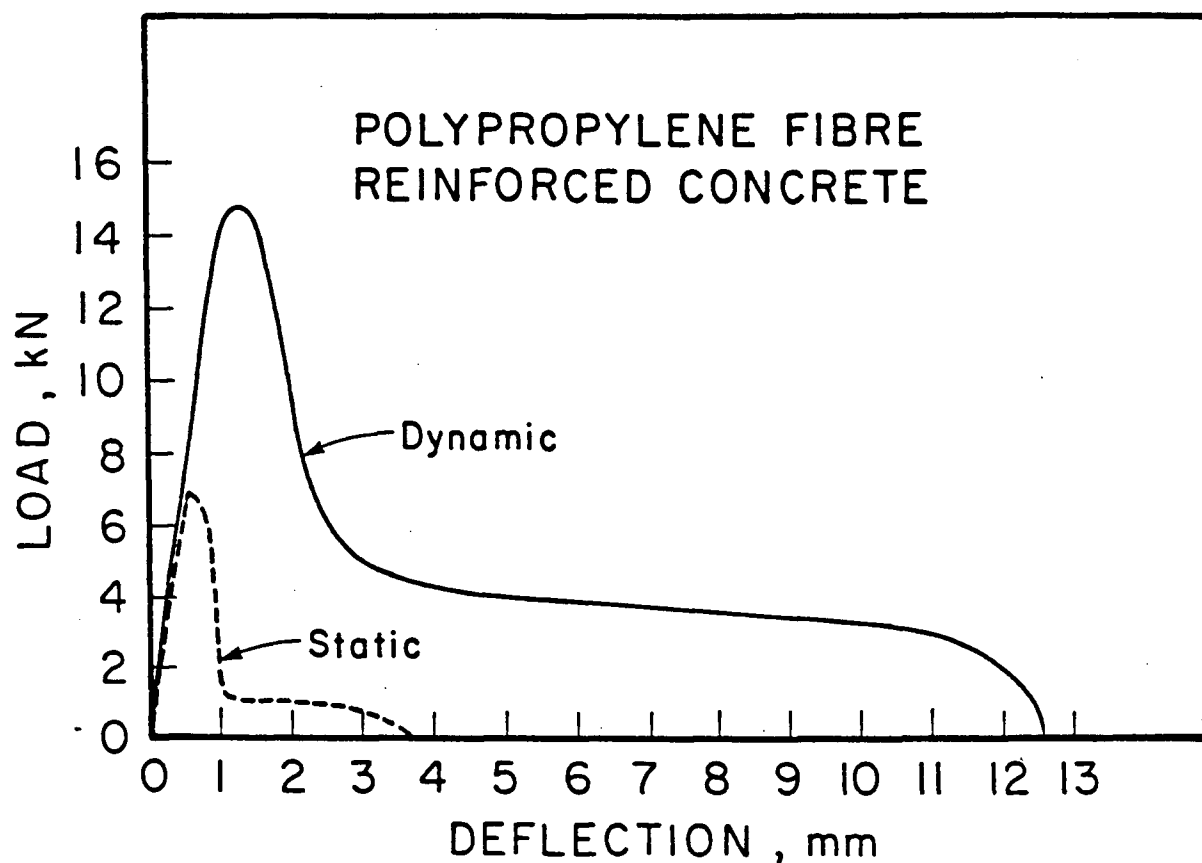


Table 10.6

Effect of Moment of Inertia on Polypropylene Fibre Reinforced Normal Strength Concrete (0.5m drop)

		$I = 162 \times 10^{-7}$ (6) <sup>1</sup>				$I = 104 \times 10^{-7}$ (6) <sup>1</sup>			
		Max	Min.	Mean	s	Max.	Min.	Mean	s
Max. Observed	Tup Load (N)	37567	35810	36196	677	32763	29737	31263	867
Max. observed	Inertial Load (N)	20291	16868	19264	1278	19688	17688	18463	876
Peak Bending Load (N)		17727	16452	16932	428	15075	10049	12800	1850
Fracture Energy (Nm)		100.5	87.8	90.1	6.5	64.0	56.0	60.0	2.9

<sup>1</sup>Number of specimens tested.

about their strong axis ( $I=162 \times 10^{-7}$ ) and also about their weak axis ( $I=104 \times 10^{-7}$ ). Significant reductions in the observed peak bending loads and the fracture energies were observed (Table 10.6) for the tests about the weak axis, probably for the same reasons as for the steel fibre reinforced concrete (Section 10.2).

#### 10.4 COMPARISON OF STEEL FIBRE REINFORCED NORMAL STRENGTH CONCRETE AND POLYPROPYLENE FIBRE REINFORCED NORMAL STRENGTH CONCRETE

Fibres, polypropylene as well as steel, seem to increase the "ductility" of concrete in both the static and the dynamic cases. In addition, the fibres also increased the peak bending loads, or the strengths. However, the extents to which these improvements were achieved were different for the two fibre types. Such a comparison, however, is not completely justified since a fibre volume fraction of only 0.5% was used in the case of polypropylene fibres as compared to a fibre volume fraction of 1.5% used for the steel fibres. Thus the comparison is between the maximum fibre volume fraction of polypropylene that could be included with the conventional mixing techniques and the commonly used fibre volume fraction of steel fibres.

In the static case, while the polypropylene fibers achieved only marginal improvements in the peak bending loads (Table 10.4) the peak loads were almost doubled in the

case of steel fibres (Table 10.1). Steel fibres in the static case were also found to increase the fracture energies by almost a factor of 8, whereas the corresponding increase in the case of polypropylene fibres was only by a factor of 2.

In the dynamic case (Tables 10.2 and 10.5), the same trend was observed. With polypropylene, only marginal increases in the peak bending loads and energies were observed. However, steel fibres increased both the peak bending loads and the energies dramatically. However, an eight-fold increase in the fracture energy in the case of static loading on NSSFRC was reduced to only a three-fold increase in the case of dynamic loading.

The performance of any type of fibre depends upon the strength of the fibre, its geometry, and the quality of its bond with the matrix. These fibre characteristics also determine the mode in which a fibre will fail. In the present study, the polypropylene fibres were always broken, while the steel fibres were in general pulled out. It is probably the pull-out process in the NSSFRC which results in a larger area under the post-peak part of the load vs. deflection plot. The sudden breaking of polypropylene without much inelastic deformation in the fibre itself results in a relatively sudden drop in the load vs. deflection plot in the post-peak load region. Thus it may be concluded that high modulus, short, and high tensile strength fibres with some form of mechanical bonding (like

the hooked ends of the steel fibres) behave better than low modulus, low tensile strength fibres without any mechanical bonding. In other words, the pull-out failure, which results in increased post-elastic deformations compared to failure by breaking, is the desirable mode of failure.

One important distinction between the two types of fibres is the number of peaks observed in the load vs. deflection plots. NSSFRC was found to have multiple peaks in its load vs. deflection plot, as opposed to the single peaks observed in the plain or polypropylene fibre reinforced beams. When a fibre reinforced beam is loaded, at a certain maximum tensile strain, the matrix cracks. After the matrix failure, the fibres bear the load. The stress in any fibre depends upon the general load level and its position relative to the neutral axis. If the stress in the fibre exceeds its tensile strength, the fibre breaks. This was the case with polypropylene fibres. However, if neither the fibre bond strength nor the tensile strength is reached, the load can rise considerably beyond the point of matrix failure. If the fibre has hooked ends, at a certain point crushing of concrete near the hook occurs, the hook straightens under load and the fibre is pulled out. This was apparently the case with NSSFRC.

The first peak in NSSFRC probably corresponds to the matrix failure. The cracking of the matrix disturbs the equilibrium momentarily, and while the stresses are being redistributed, the load drops. Once the fibres take over

completely, the load rises again until the fibre pull-out begins. With the pull-out, the load drops in steps (Figure 10.3). Thus the crushing of the matrix in the vicinity of the hook, the straightening of the hook, and the beginning of the pull-out process as the separation proceeds, give rise to more than one peak in the load vs. displacement plot.

#### 10.5. EFFECT OF VARYING THE STRESS RATE IN THE DYNAMIC RANGE ON THE PERFORMANCE OF STEEL FIBRE REINFORCED NORMAL STRENGTH CONCRETE

To study the effect of varying the stress rate in the dynamic range on the performance of normal strength steel fibre reinforced concrete, beams 150mmx150mm in cross section and 1500mm long were tested on a span of 960mm under four different hammer drop heights. The results are presented in Table 10.7, and also in the form of load vs. displacement plots in Figure 10.7a.

As can be observed from the plots of Figure 10.7a, before the ultimate load peak, a matrix failure peak exists for all of the drop heights. As has been pointed out previously, before the full strength of the steel fibre reinforced beams is attained, the matrix cracking strain is reached, and a sudden cracking of the matrix causes a momentary unloading of the beam before the load can rise again. The first peak load outlined in Table 10.7 thus corresponds to the load at which the matrix cracks; it can

**Table 10.7**  
**Dynamic behaviour of Steel Fibre Reinforced Normal Strength Concrete (150x150x1500 Beams)**

	Height of Hammer Drop (m)															
	0.15m (3) <sup>1</sup>				0.25m (3) <sup>1</sup>				0.50m (3) <sup>1</sup>				0.75m (3) <sup>1</sup>			
	Max	Min.	Mean	s	Max.	Min.	Mean	s	Max.	Min.	Mean	s	Max.	Min.	Mean	s
<b>Peak Bending Load (N)</b>	29855	19043	25384	4607	37096	29731	32275	3410	51003	46092	48547	2455	60638	55150	57268	2409
<b>First Peak Load (N)</b>	20220	18340	19506	774	30698	26992	28534	1575	38912	32178	35130	2811	46082	42786	44930	1517
<b>MOR (First Peak Load) (MPa)</b>	8.6	7.8	8.3	0.3	13.1	11.5	12.2	0.7	16.6	13.8	15.0	1.2	19.7	18.3	19.2	0.7
<b>Mean Stress Rate MPa/sec</b>	-	-	4170	-	-	-	8714	-	-	-	18775	-	-	-	32016	-
<b>Fracture Energy (Nm)</b>	82.3	66.3	73.7	6.6	149.4	94.8	127.6	23.7	212.2	149.2	180.7	31.5	299.6	274.4	286.3	10.0

<sup>1</sup>Number of specimens tested.

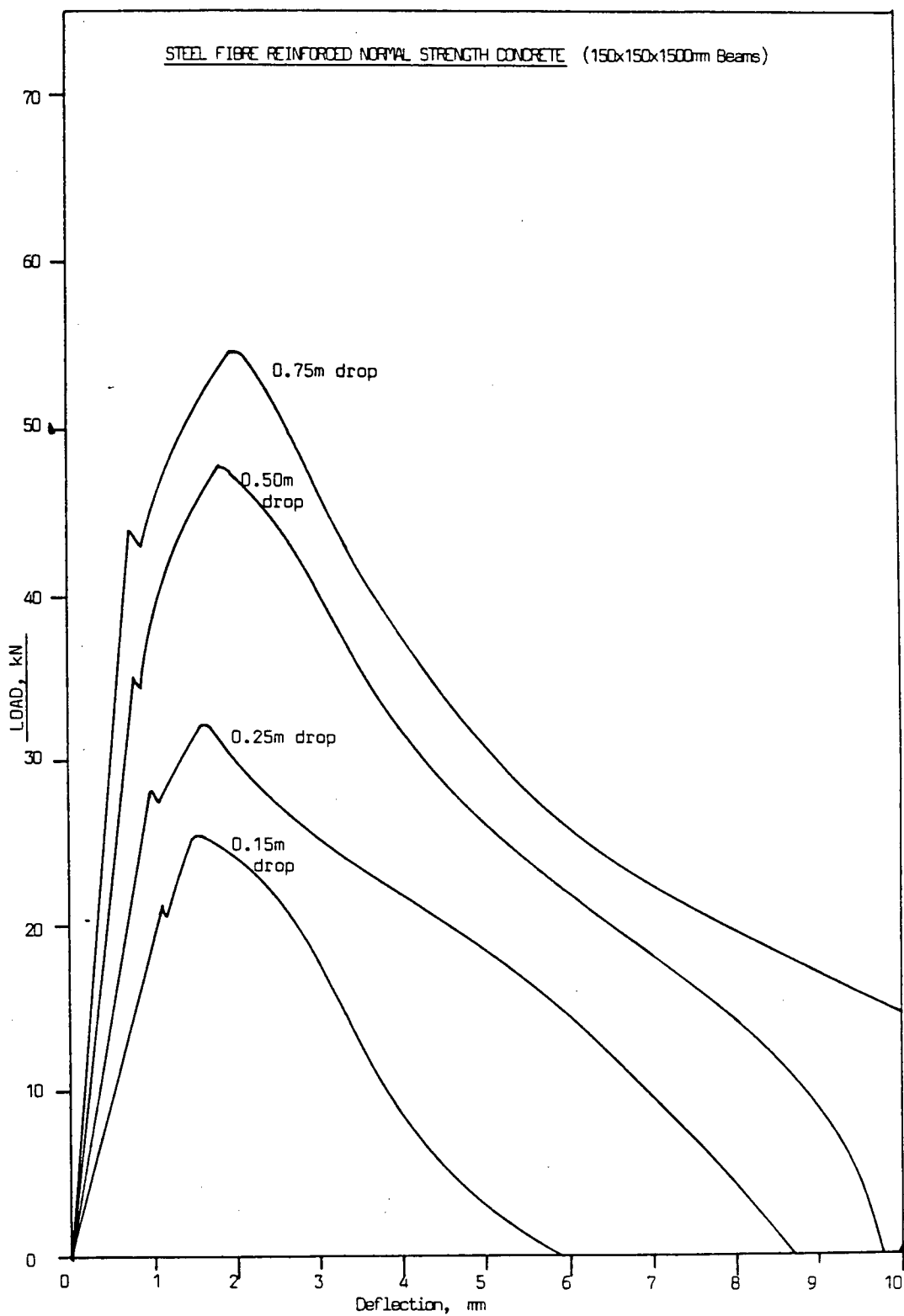


Figure 10.7(a) Load Deflection Plots for SFRC under different Hammer Drop Heights.

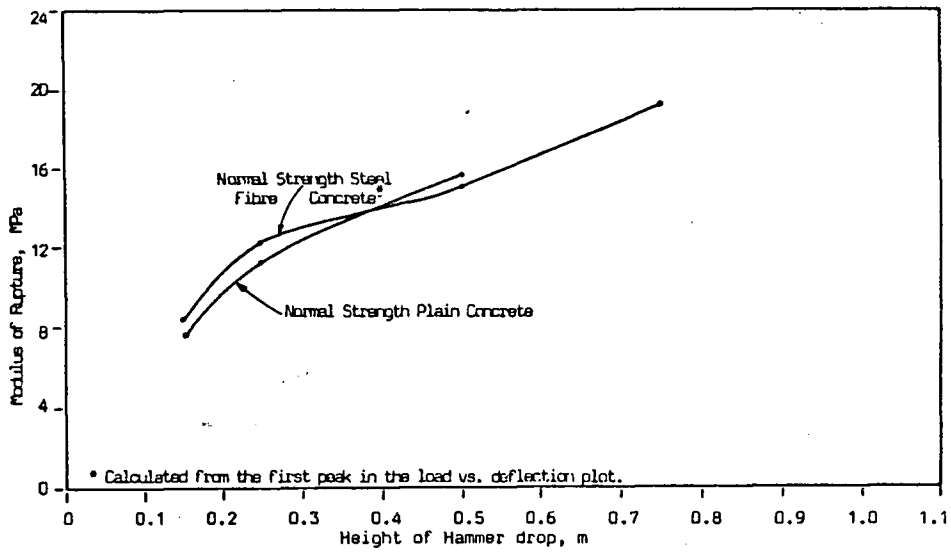


Figure 10.7(b)- Comparison between the matrix behaviour in SFRC and that in Plain Concrete.

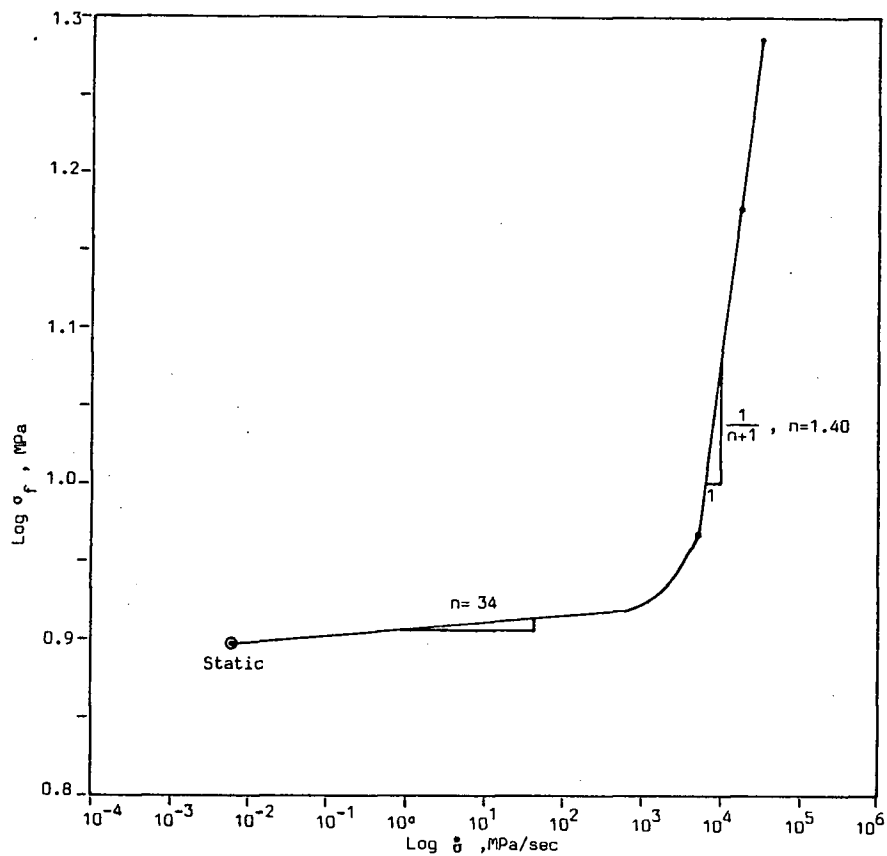


Figure 10.7(c)- Strain Rate Sensitivity of the Matrix in SFRC. Note that the value of "n" in Impact range is the same as Plain Concrete (Fig.6.5)

thus be used to calculate the MOR using elastic analysis. The values of MOR thus obtained are also tabulated in Table 10.7.

A comparison of the MOR values obtained from the unreinforced normal strength concrete beams (Table 6.2b) with those obtained from the first peak of the fibre reinforced normal strength beams indicates that for a given drop height, the moduli of rupture are almost the same. Such a comparison is presented in Figure 10.7b. It is interesting to note that the presence of the fibres was found not to have a significant effect on the performance of the matrix itself.

With the static matrix failure values taken from Table 10.1, and the dynamic values taken from Table 10.7, a plot of  $\log \sigma_f$  vs.  $\log \dot{\sigma}$  for steel fibre reinforced concrete may be drawn. Such a plot is presented in Figure 10.7c. It may be seen from Figure 10.7c that the value of  $n$  decreases under impact loading, compared to its value in the quasi-static loading. Similar findings were reported in Chapter 6 for the plain concrete (Figure 6.5). Similarly, the value of  $n$  was found to have a value of  $n=1.50$  for plain normal strength concrete (Figure 6.5); this is almost the same as the value of  $n = 1.40$  obtained for the NSSFRC (Figure 10.7c). This again suggests that the behaviour of the matrix itself is not modified significantly by the presence of the fibres.

Similar to the behaviour of plain concrete, an increase in hammer drop height (or an increase in the stress rate),

is found to increase the capacity to sustain larger deflections in NSSFRC as well (Figure 10.7a). This resulted in increased fracture energy requirements at higher stress rates (Table 10.7).

#### 10.6 STEEL FIBRE REINFORCED HIGH STRENGTH CONCRETE (HSSFRC) UNDER VARIABLE STRESS RATE

High strength concrete made with condensed silica fume (microsilica) was also reinforced with polypropylene or steel fibres, to study the effect of stress rate on these high strength fibre reinforced concretes.

The static behaviour of steel fibre reinforced high strength concrete (HSSFRC) is compared in Table 10.8 and in Figure 10.8 with that of its unreinforced counterpart. It can be seen that the fibres were very effective in increasing the "ductility" of the composite. The brittle nature of the failure in plain high strength beams, which was evident from the sudden drop in load after reaching the peak load was, to a considerable extent changed to a slow, ductile type of failure by the addition of the fibres.

The dynamic performance of HSSFRC with a hammer drop height of 0.5m has been compared with that of plain high strength beams in Figure 10.9 and Table 10.9. The trends observed in the case of static loading are the same for dynamic loading as well.

A comparison of the static performance of HSSFRC with its dynamic performance has been made in Figure 10.10. As

**Table 10.8**  
**Static Behaviour of Plain and Steel Fibre Reinforced High Strength Concrete**

	Plain (4) <sup>1</sup>				Plain + Steel Fibres (4) <sup>1</sup>			
	Max	Min.	Mean	s	Max.	Min.	Mean	s
Peak Bending Load (N)	12806	8144	9720	1809	18271	16001	17996	1316
Fracture Energy (Nm)	3.4	2.0	2.8	0.5	67.0	56.0	61.4	5.1
Cross Head Speed (m/sec)	-	-	$4 \times 10^{-7}$	-	-	-	$4 \times 10^{-7}$	-

<sup>1</sup>Number of specimens tested.

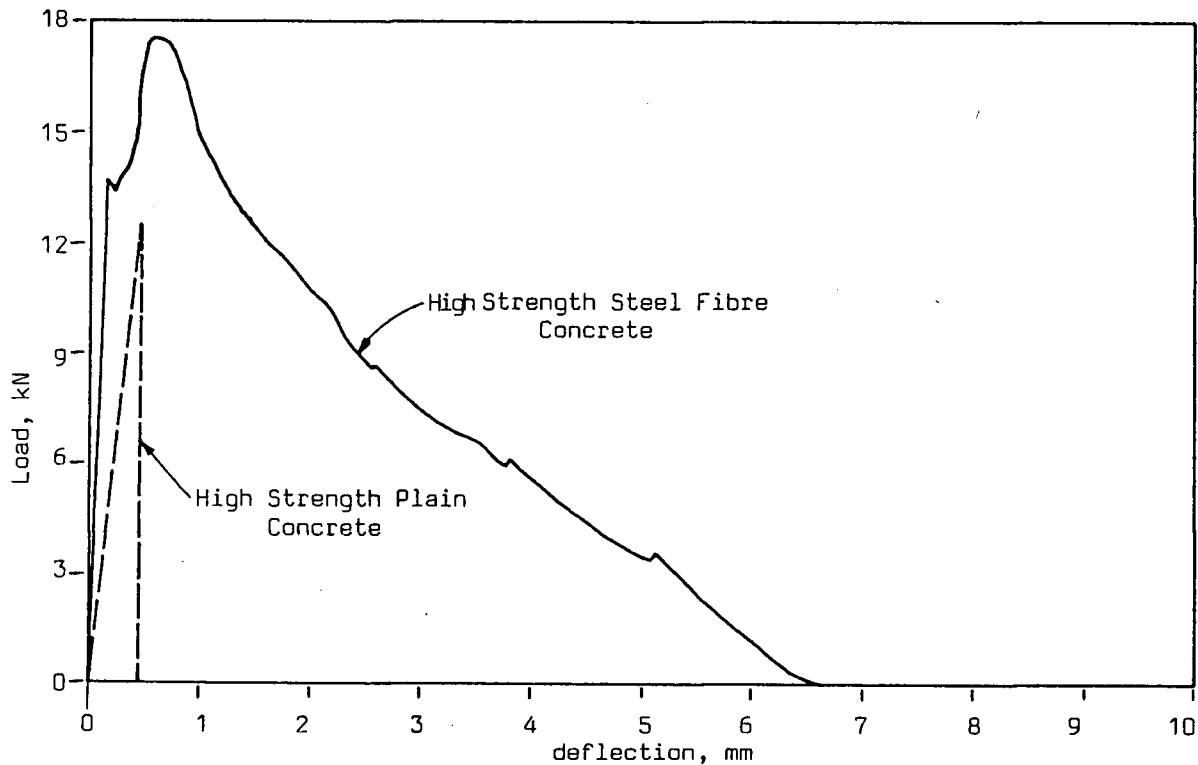


**Figure 10.8-Static Behaviour of Plain and Steel Fibre Reinforced High Strength Concrete**

Table 10.9  
Dynamic Behaviour of Plain and Steel Fibre Reinforced High Strength Concrete (0.5m drop)

	Plain (7) <sup>1</sup>				Plain + Steel Fibres (6) <sup>1</sup>			
	Max	Min.	Mean	s	Max.	Min.	Mean	s
Max. Observed Top Load (N)	39320	35110	36652	1725	47926	44008	46612	1588
Max. observed Inertial Load (N)	19025	16760	17892	1132	20207	17007	19011	1241
Peak Bending Load (N)	19206	18314	18760	446	29632	25049	27601	1646
Fracture Energy (Nm)	100.7	57.4	74.9	18.6	271.0	234.0	252.6	14.58

<sup>1</sup>Number of specimens tested.

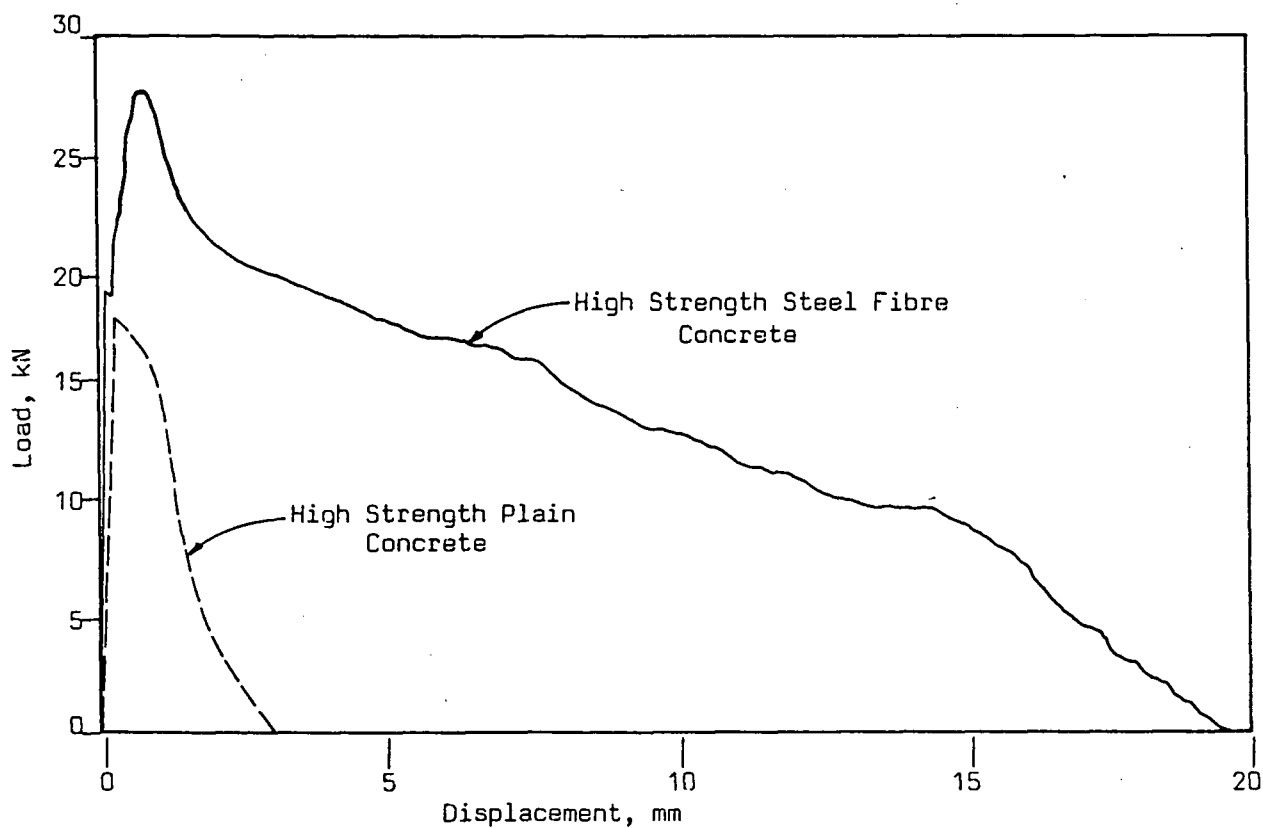


Figure 10.9-Dynamic Behaviour of Plain and Steel Fibre Reinforced High Strength Concrete (0.5m drop)

Figure 10.10- Dynamic and Static behaviour of Steel Fibre reinforced High Strength Concrete.

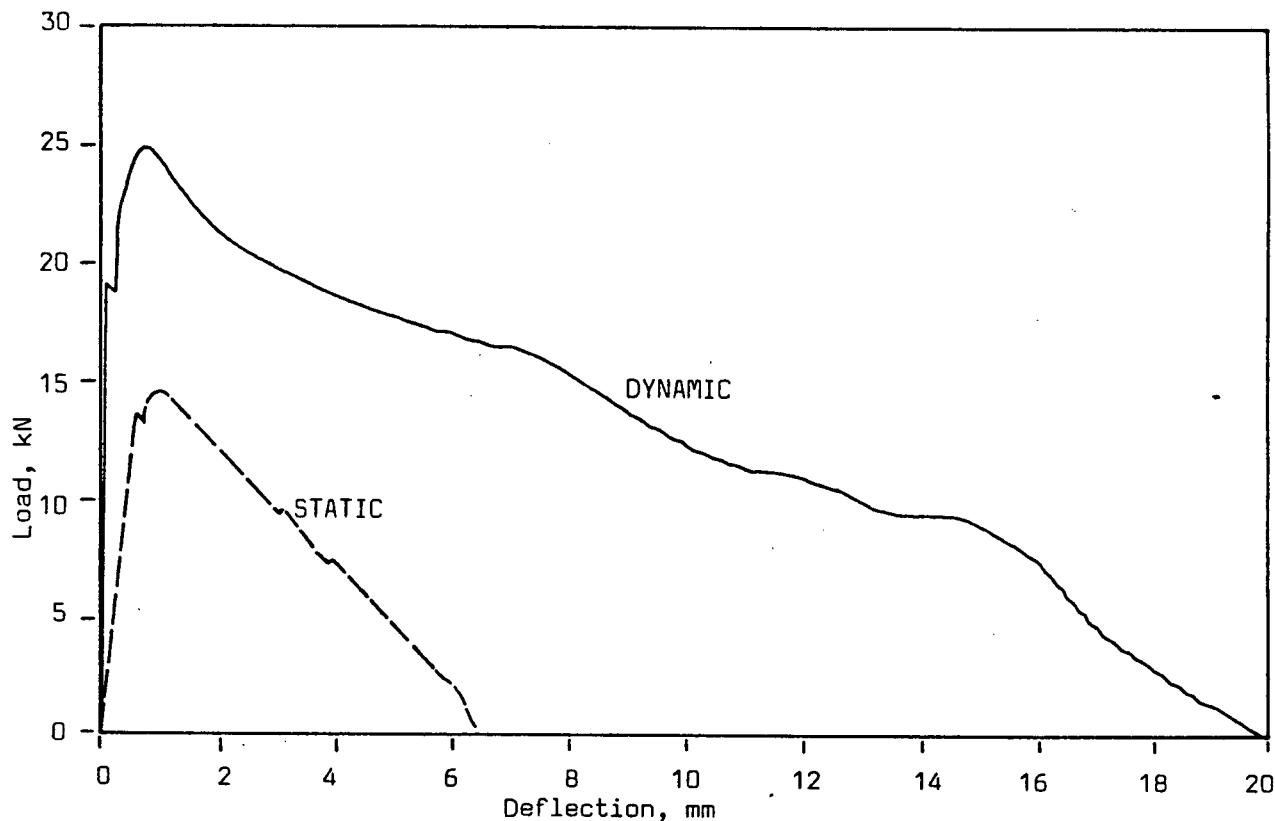


Table 10.10  
Effect of Moment of Inertia on Steel Fibre Reinforced High Strength Concrete (0.5m drop)

		$I = 162 \times 10^{-7}$ (6) <sup>1</sup>				$I = 104 \times 10^{-7}$ (6) <sup>1</sup>			
		Max	Min.	Mean	s	Max.	Min.	Mean	s
Max. Observed	Tup Load (N)	47926	44008	46612	1588	40530	38690	39752	778
Max. observed	Inertial Load (N)	20207	17009	19011	1241	21904	19906	20752	843
Peak Bending Load (N)		29632	25004	27601	1646	20624	16786	19000	1452
Fracture Energy (Nm)		271.0	234.0	252.0	14.6	140.0	126.0	132.0	5.1

<sup>1</sup>Number of specimens tested.

observed in the case of plain concrete, HSSFRC also exhibits a marked strain rate sensitivity; the peak loads and the capacity to sustain deformations increase immensely with an increase in the stress rate.

The effect of moment of inertia on the dynamic performance of HSSFRC was investigated by impacting some beams about their weaker axes. The results have been tabulated in Table 10.10. As in the case of normal strength concrete, a reduction in the moment of inertia of HSSFRC beams also resulted in a reduction in their strengths and fracture energies.

#### 10.7 POLYPROPYLENE FIBRE REINFORCED HIGH STRENGTH CONCRETE (HSPFRC) UNDER VARIABLE STRESS RATE

The addition of 0.5% by volume of fibrillated polypropylene fibres in high strength concrete was found not to modify the properties significantly. Figure 10.11 and Table 10.11 compare the static performance of polypropylene fibre reinforced high strength concrete (HSPFRC) with plain high strength concrete. It can be seen that some advantage was derived by adding the fibres.

Figure 10.12 and Table 10.12 compare the dynamic performance of plain concrete and HSPFRC. No significant improvement could be noticed in the dynamic case. The effect of strain rate on HSPFRC is shown in Figure 10.13, where the static performance of HSPFRC has been plotted along with its dynamic performance. The general strain rate sensitivity as

Table 10.11  
 Static Behaviour of Plain and Polypropylene Fibre Reinforced High Strength Concrete

	Plain (4) <sup>1</sup>				Plain + PP. Fibres (4) <sup>1</sup>			
	Max	Min.	Mean	s	Max.	Min.	Mean	s
Peak Bending Load (N)	12806	8144	9720	1809	14544	12588	13206	787
Fracture Energy (Nm)	3.4	2.0	2.8	0.6	13.0	5.4	8.7	2.9
Cross Head Speed (m/sec)	-	-	$4 \times 10^{-7}$	-	-	-	$4 \times 10^{-7}$	-

<sup>1</sup>Number of specimens tested.

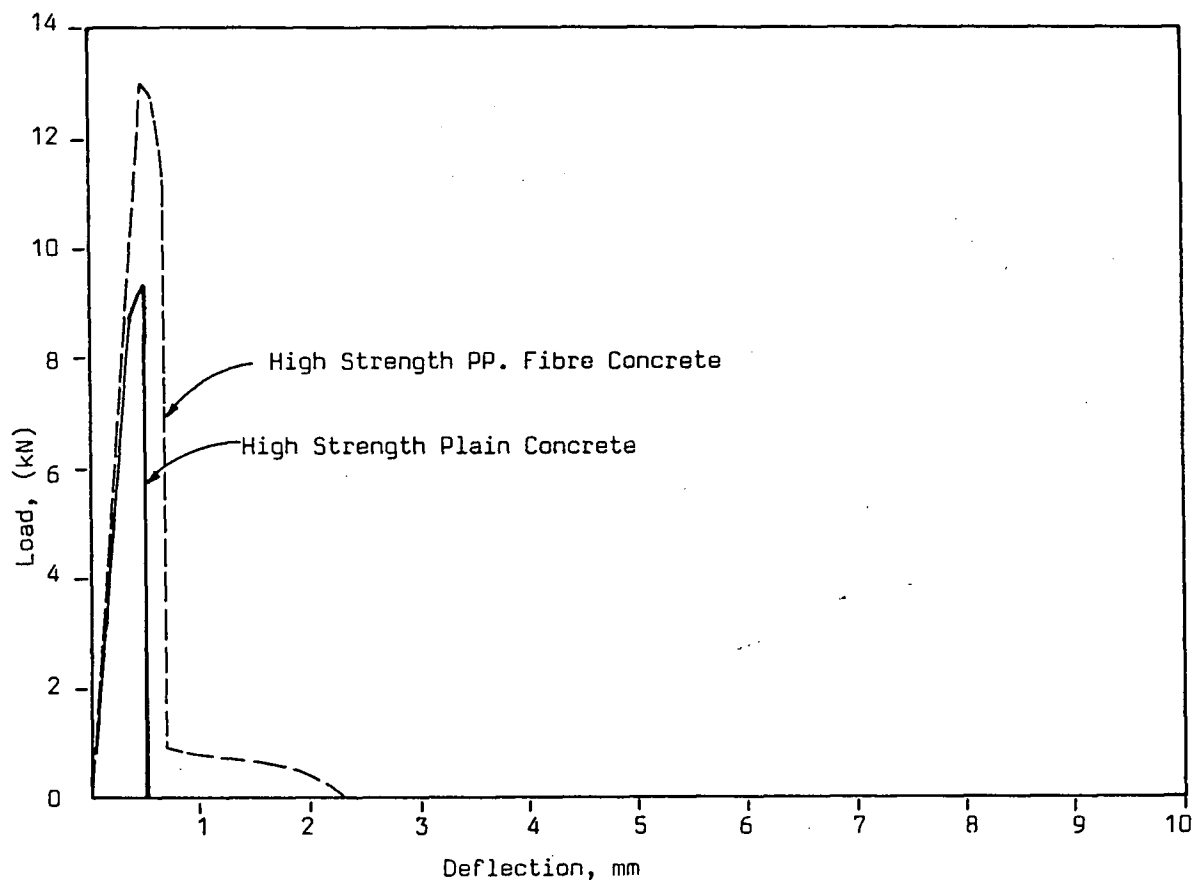


Figure 10.11-Static Behaviour of Plain and Polypropylene Fibre Reinforced High Strength Concrete

Table 10.12

**Dynamic Behaviour of Plain and Polypropylene Fibre Reinforced High Strength Concrete (0.5m drop)**

	Plain (7) <sup>1</sup>				Plain + PP. Fibres (6) <sup>1</sup>			
	Max	Min.	Mean	s	Max.	Min.	Mean	s
Max. Observed Top Load (N)	39320	35110	36652	1725	38377	35796	37207	1109
Max. observed Inertial Load (N)	19025	16760	17892	1132	20904	17692	19063	1189
Peak Bending Load (N)	19206	18314	18760	446	19001	17473	18144	549
Fracture Energy (Nm)	100.7	57.4	74.9	18.6	100.1	80.4	92.2	7.4

<sup>1</sup>Number of specimens tested.

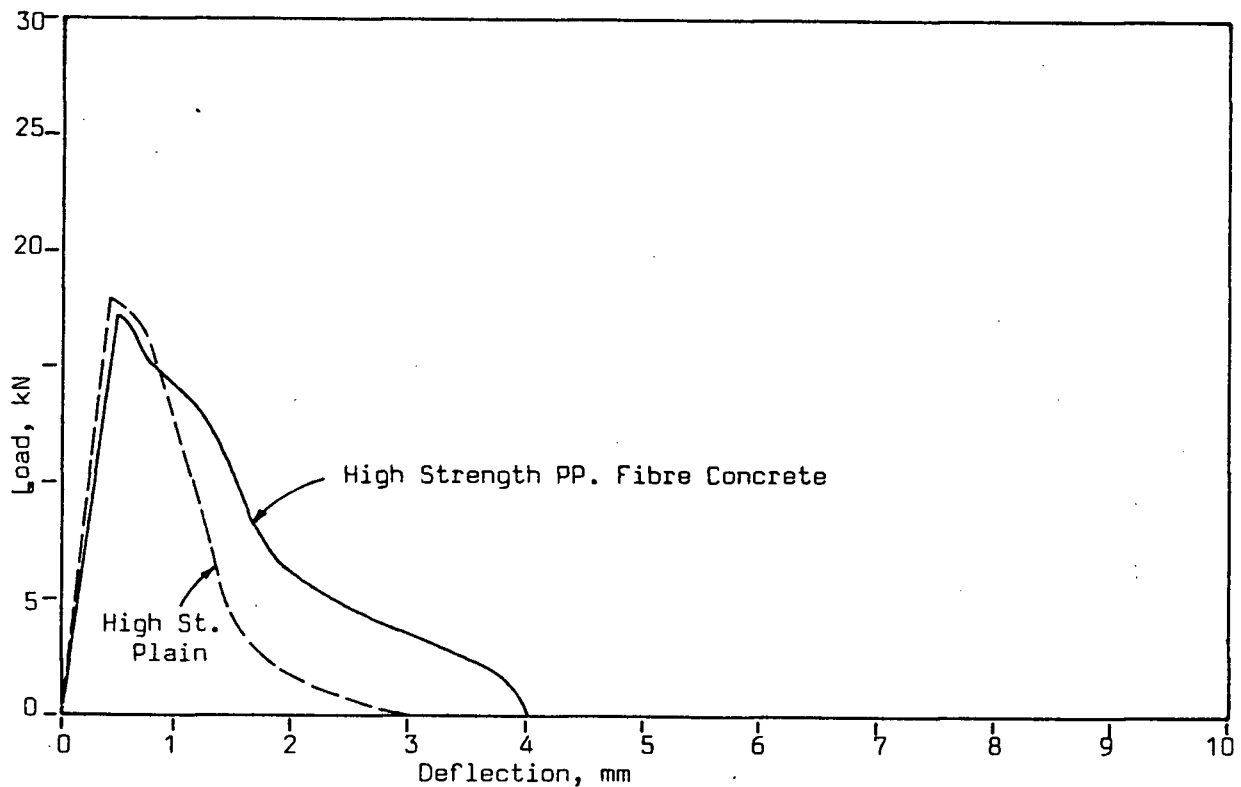


Figure 10.12-Dynamic Behaviour of Plain and Polypropylene Fibre Reinforced High Strength Concrete (0.5m drop)

noticed for unreinforced beams (Chapter 6) was noticed for the HSPFRC beams as well, but the polypropylene fibres were not found to impart to the composite any additional strain rate sensitivity beyond that of the matrix itself.

The effect of changing the moment of inertia of HSPFRC has been tabulated in Table 10.13. Once again, HSPFRC was also found to have reduced strengths and reduced fracture energies when tested about its weaker axis.

Thus, little was achieved by adding polypropylene fibres to a high strength matrix. The only real advantage of this addition was in the general coherence observed in these beams under impact. While extensive spalling occurred in plain unreinforced beams, polypropylene fibre reinforced beams tended to preserve their coherence and the integrity of the composite.

#### 10.8 COMPARISON BETWEEN FIBRE REINFORCED NORMAL STRENGTH AND FIBRE REINFORCED HIGH STRENGTH CONCRETE

Under static conditions, the behaviour of both types of concrete was modified to some extent by adding fibres (Tables 10.1, 10.4, 10.8, and 10.11). Low modulus polypropylene fibres did not result in any major improvement in the mechanical properties of concrete. However, the inclusion of high modulus steel fibres was found to produce significant effects in both types of concrete. The more brittle high strength concrete was found to benefit the most from steel fibre addition. The immense improvement in the

Figure 10.13-Static and Dynamic Behaviour of Polypropylene Fibre Reinforced High Strength Concrete

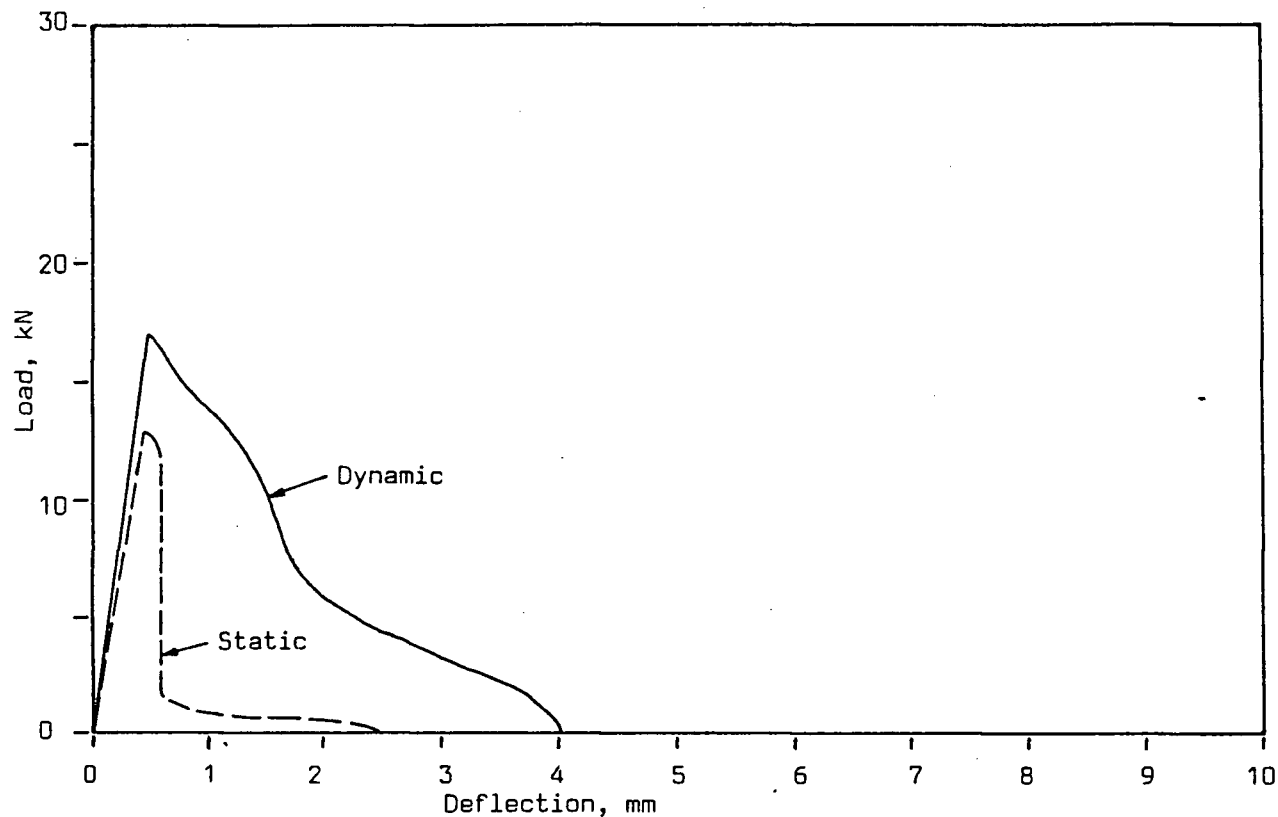


Table 10.13  
Effect of Moment of Inertia on Polypropylene Fibre Reinforced High Strength Concrete (0.5m drop)

	$I = 162 \times 10^{-7}$ (6) <sup>1</sup>				$I = 104 \times 10^{-7}$ (6) <sup>1</sup>			
	Max	Min.	Mean	s	Max.	Min.	Mean	s
Max. Observed Top Load (N)	38377	35796	37207	1109	31290	29262	30080	873
Max. observed Inertial Load (N)	20904	17692	19063	1189	20062	19048	19530	415
Peak Bending Load (N)	19001	17473	18144	549	12242	9200	10550	1103
Fracture Energy (Nm)	100.1	80.4	92.2	7.4	60.0	43.0	51.0	6.1

<sup>1</sup>Number of specimens tested.

ductility and toughness of steel fibre reinforced high strength concrete suggests that the high strength of the matrix, coupled with the improved ductility, makes it a very suitable material under static and dynamic loading conditions. Steel fibres were effective in providing ductility to normal strength concrete as well, although to a lesser degree than to high strength concrete.

Similar conclusions may also be drawn for the dynamic loading case (Tables 10.2, 10.5, 10.9 and 10.12). However, in both the static and dynamic cases, the low modulus polypropylene fibres were found to increase the ductility only marginally as compared to high modulus steel fibres with hooked ends, which produced dramatic effects.

As mentioned earlier, the efficiency of a particular type of fibre in a matrix depends upon how effectively the properties of the matrix have been utilized. High strength concrete, known for its better crushing strength and bond, did not show marked improvement with polypropylene fibres because none of the advantageous matrix properties were utilized. On the other hand, steel fibres with the hooks on their ends utilized the matrix crushing strength in the vicinity of a hook, and made use of the bond strength while being pulled out. This explains, to some extent at least, the better behaviour of steel fibre reinforced high strength concrete over steel fibre reinforced normal strength concrete.

### 10.9 CRACK DEVELOPMENT IN STEEL FIBRE REINFORCED NORMAL STRENGTH CONCRETE UNDER IMPACT

To study the development of cracks in NSSFRC, high speed photography, using a high speed motion picture camera was carried out on a NSSFRC beam undergoing impact, with a hammer drop height of 0.5m. Figure 10.14 shows the results. It should be compared to Figure 6.12, for hydrated cement paste (hcp).

The presence of fibres seems to affect the process of crack development in two ways. First, with fibres, the velocity of the crack is reduced. The average velocity of the crack was found to decrease from 115 m/s in hcp to about 74 m/s in NSSFRC. While only 10ms were required for the crack to traverse the entire beam depth in hcp, almost 16ms were required in NSSFRC. The second noticeable difference is in the extent of damage. The appearance of several cracks running in various directions in hcp seems to have been controlled in the fibre reinforced beam. Fibres thus act as crack arresters and help preserve the coherence and integrity of the composite.

## STEEL FIBRE REINFORCED CONCRETE

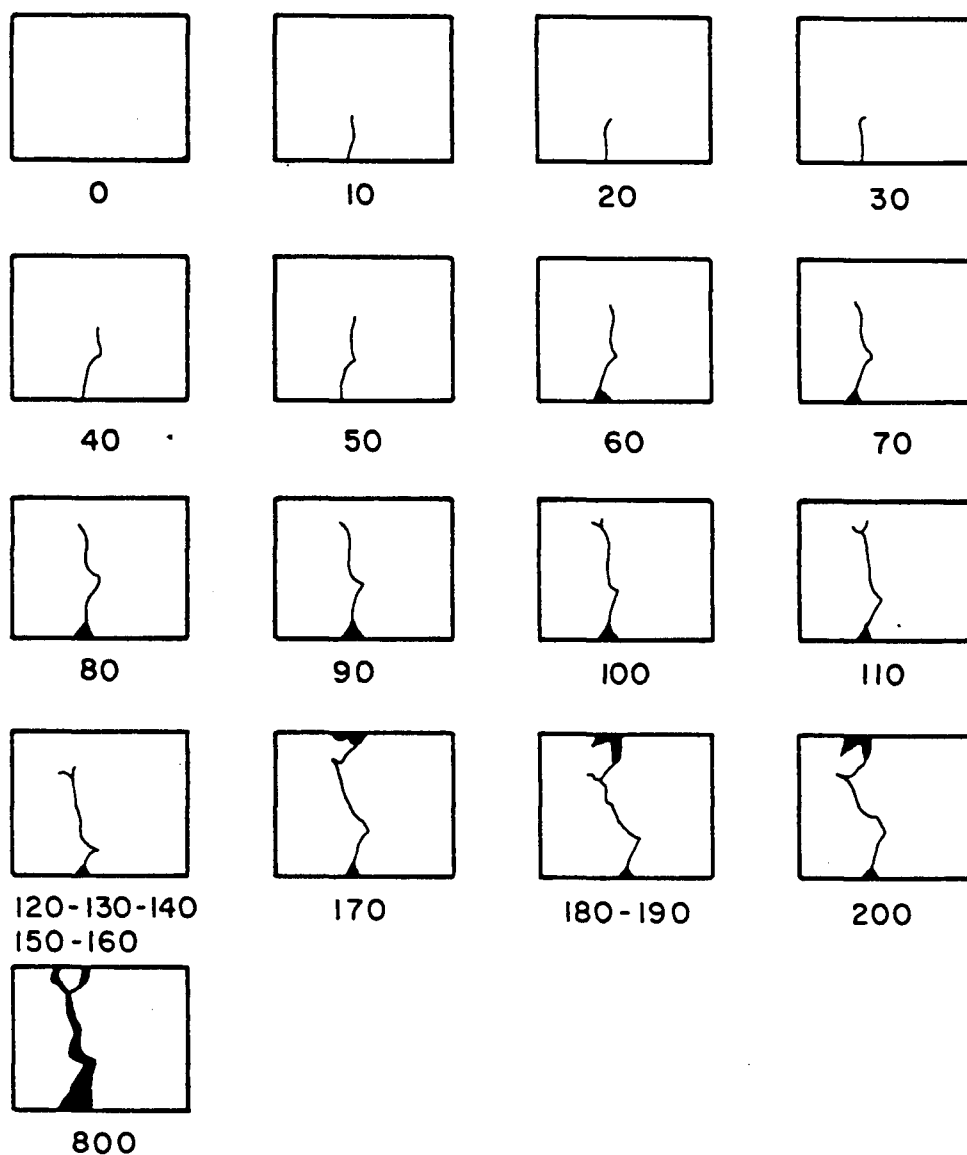


Fig.-10.14 Crack development as a function of time in a steel fibre reinforced concrete beam subjected to impact loading. The number in each frame represents the time (in units of 0.1 ms) from the first frame shown.

## 11. CONVENTIONALLY REINFORCED CONCRETE UNDER IMPACT

### 11.1 INTRODUCTION

The behaviour of plain and fibre reinforced concrete under impact loading has been described in the previous chapters. Although the use of steel fibres has been found to improve the performance of plain concrete dramatically, the fibres can not be used to replace the conventional reinforcing steel bars in concrete. Thus, it is also necessary to assess the properties of conventionally reinforced concrete under impact loading, in order to be able to assess the behaviour of the overall structure.

Dynamic loading imposes a high ductility demand upon a structure and consequently upon its elements. One such element which will be discussed in this chapter is the beam element. The effect of varying the stress rate on plain concrete can shed some light upon the the effect of stress rate on reinforced concrete. However, the conclusions drawn for plain concrete beams undergoing impact (Chapter 6) cannot, in general, be extended to reinforced concrete, where the mode of failure and the mechanism of crack propagation are very different. Conventionally reinforced concrete beams, with a percentage of steel of 1.136%, were tested under static loading conditions in a universal testing machine, and later under impact loading in the drop weight machine, using a variable hammer drop height.

The performance of conventionally reinforced concrete under variable stress rate seemed to be affected by the

concrete strength, by the presence of lateral reinforcement, and by whether deformed or smooth reinforcing bars were used. All of these parameters will be discussed below.

### 11.2 CONVENTIONALLY REINFORCED NORMAL STRENGTH CONCRETE WITH DEFORMED BARS (CRNSC) UNDER VARIABLE STRESS RATE

Conventionally reinforced normal strength concrete (CRNSC) beams were tested in 3-point bending: (1) statically, with the cross-head moving at  $4.2 \times 10^{-7}$  m/s; and (2) in the impact machine, under drop heights of 0.5m, 0.75m, 1.0m, and 1.5m. The concretes, with two different water/cement ratios of 0.4 and 0.33, corresponding to the compressive strengths of 49 and 56MPa, respectively, were cast with two 9.52mm deformed bars (Table 4.1) with a yield strength of 425 MPa, and an ultimate strength of 720 MPa. Table 11.1a represents the static results and Tables 11.1b and 11.1c represent the impact results for w/c ratios of 0.4 and 0.33, respectively.

The effect of varying the stress rate on the load vs. displacement plots is shown in Figure 11.1 for a water/cement ratio of 0.4. Plots for a water/cement ratio of 0.33 look schematically similar. The effects of hammer drop height on the peak bending load and the fracture energy (calculated to the point at which the load drops to 1/3 of its peak value) are shown in Figure 11.2.

An alternative criterion for comparing the fracture energies under different hammer drop heights may be to

**Table 11.1(a)**  
**Static Behaviour of Conventionally Reinforced Normal Strength Concrete**

		<b>w/c = 0.40 (3)*</b>				<b>w/c = 0.33 (3)*</b>			
		<b>Max</b>	<b>Min.</b>	<b>Mean</b>	<b>s</b>	<b>Max.</b>	<b>Min.</b>	<b>Mean</b>	<b>s</b>
<b>Peak Bending Load (N)</b>		25042	18289	22671	3102	24642	22908	23682	1450
<b>Fracture Energy<sup>1</sup> (Nm)</b>		482	379	442	45	522	463	483	28
<b>Fracture Energy<sup>2</sup> (Nm)</b>		403	353	378	21	429	386	404	18
<b>Fracture Energy<sup>3</sup> (Nm)</b>		499	434	468	27	493	473	469	22

\* Number of specimens tested.

Table 11.1(b)  
Dynamic behaviour of Conventionally Reinforced Normal Strength Concrete (w/c = 0.40)

	Ht. of Hammer drop, m															
	...0.50m... (6)*				...0.75m... (6)*				...1.0m... (6)*				...1.50m... (6)*			
	Max	Min.	Mean	s	Max.	Min.	Mean	s	Max.	Min.	Mean	s	Max.	Min.	Mean	s
Peak Bending Load (N)	37553	35776	36664	888	38582	37210	38026	589	40374	37557	39309	1251	45577	36539	39800	3052
Fracture Energy <sup>1</sup> (Nm)	1285	564	880	300	2160	829	1378	567	3059	1723	2421	547	3854	2078	2750	628
Fracture Energy <sup>2</sup> (Nm)	614	544	580	28	625	607	619	8	675	612	644	25	713	634	658	30
Fracture Energy <sup>3</sup> (Nm)	895	719	793	74	1281	873	1132	184	1348	1237	1303	48	1414	1249	1304	58
Fracture Energy <sup>4</sup> (Nm)	-	-	-	-	1876	985	1358	440	1945	1678	1811	133	2078	1800	1912	100
Fracture Energy <sup>5</sup> (Nm)	-	-	-	-	-	-	-	-	2485	2262	2375	113	2626	2249	2430	134
Max. Beam Velocity (m/s)	2.6	2.4	2.5	0.1	3.2	2.9	3.0	0.1	3.8	3.6	3.7	0.1	4.6	2.9	3.9	0.1

\* Number of specimens tested.

**Table 11.1(c)**  
**Dynamic behaviour of Conventionally Reinforced Normal Strength Concrete (w/c = 0.33)**

	Ht. of Hammer drop, m															
	...0.50m... (6)*				...0.75m... (6)*				...1.0m... (6)*				...1.50m... (6)*			
	Max	Min.	Mean	s	Max.	Min.	Mean	s	Max.	Min.	Mean	s	Max.	Min.	Mean	s
<b>Peak Bending Load (N)</b>	41419	37553	39486	1933	43464	39337	41064	1750	46299	40023	43053	2566	46649	40016	43703	2850
<b>Fracture Energy<sup>1</sup> (Nm)</b>	1507	1091	1299	208	1892	1471	1618	193	2600	2496	2562	47	3765	2275	2780	693
<b>Fracture Energy<sup>1</sup> (Nm)</b>	671	606	638	32	682	631	652	22	732	648	688	34	716	665	691	21
<b>Fracture Energy<sup>1</sup> (Nm)</b>	1333	956	1145	189	1396	1149	1246	108	1508	1309	1377	92	1381	1335	1361	19
<b>Fracture Energy<sup>4</sup> (Nm)</b>	-	-	-	-	1712	1272	1432	199	1892	1641	1764	103	1982	1556	1820	188
<b>Fracture Energy<sup>5</sup> (Nm)</b>	-	-	-	-	-	-	-	-	2501	2336	2413	68	2535	1943	2267	243
<b>Max. Beam Velocity (m/s)</b>	2.6	2.5	2.5	0.02	2.8	2.5	2.6	0.1	3.1	2.6	2.9	0.2	4.5	3.4	4.0	0.4

\* Number of specimens tested.

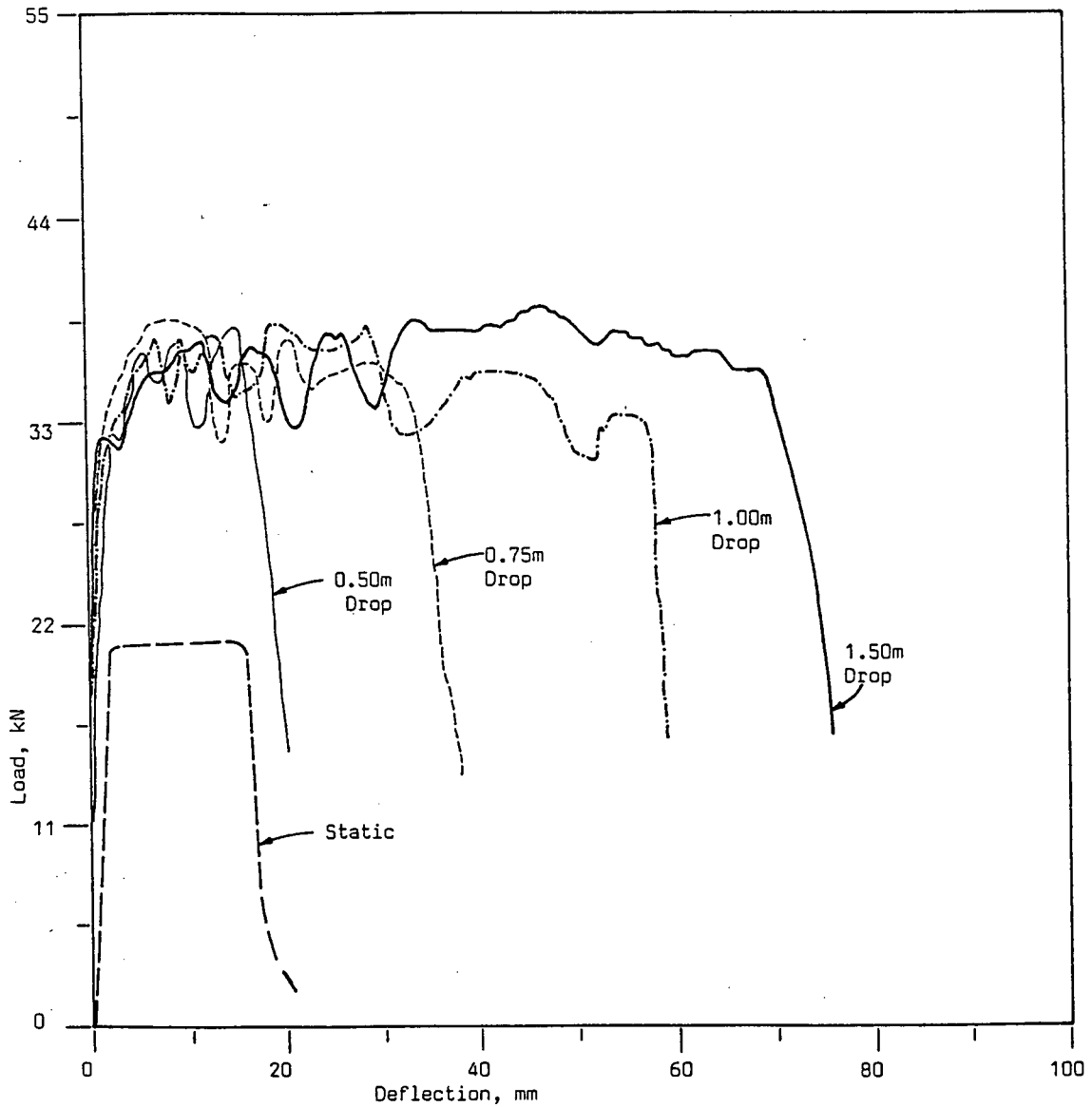


Figure-11.1-Effect of stress rate on the load vs. deflection plots of conventionally reinforced concrete beams

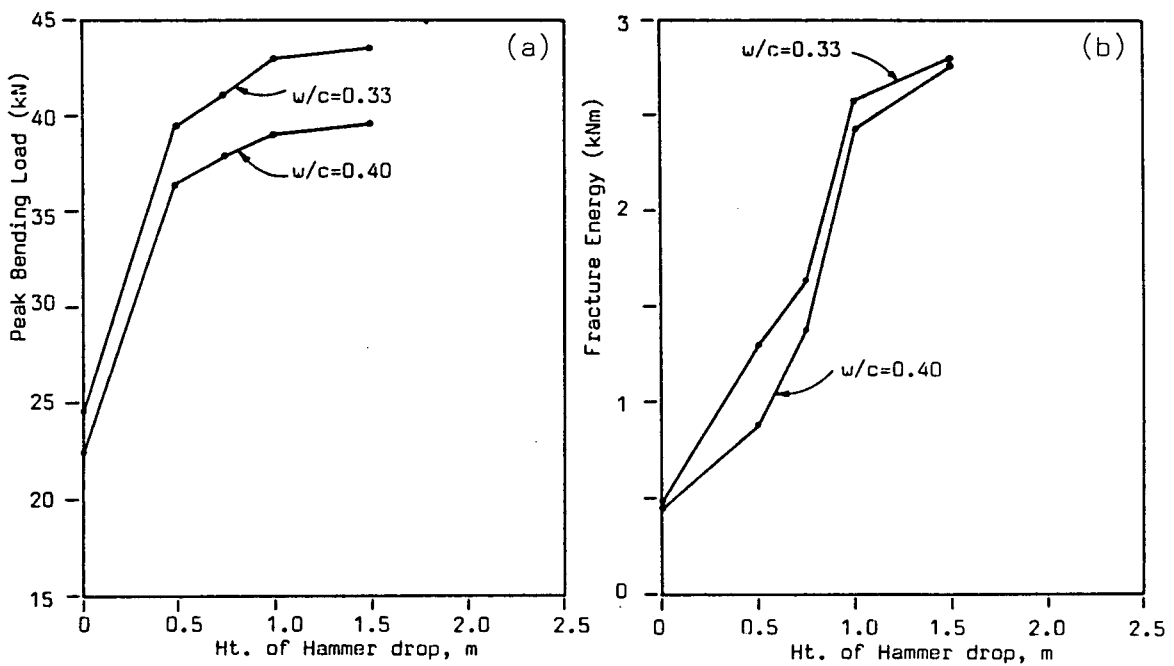


Figure-11.2-Effect of hammer drop height on (a) Peak bending load, and (b) Fracture energy of CRNSC

compute these fracture energies at different midspan deflections. The values of 18mm, 36mm, 54mm, and 72mm were chosen for this purpose. Tables 11.1b and c show these calculated values; they are plotted in Figure 11.3 for a water/cement ratio of 0.4.

Clearly, stress rate has a significant effect on the properties of conventionally reinforced concrete. In general, a large increase in the peak bending load was observed when the stress rate was increased from the static to the dynamic range. However, once in the dynamic range, a change in the hammer drop height did not result in a significant increase in the peak bending load (Figure 11.2a)

In the static case, for a rectangular section, the balanced percentage of steel is given by (59)

$$\rho_b = \frac{0.85f'_c \beta_1}{f_y} \frac{0.003E_s}{0.003E_s + f_y} \quad (11.1)$$

where the notation is defined in Figure 11.4.

With

$$f'_c = 49 \text{ MPa}$$

$$\beta_1 = 0.85$$

$$f_y = 425 \text{ MPa}$$

$$E_s = 200,000 \text{ MPa}$$

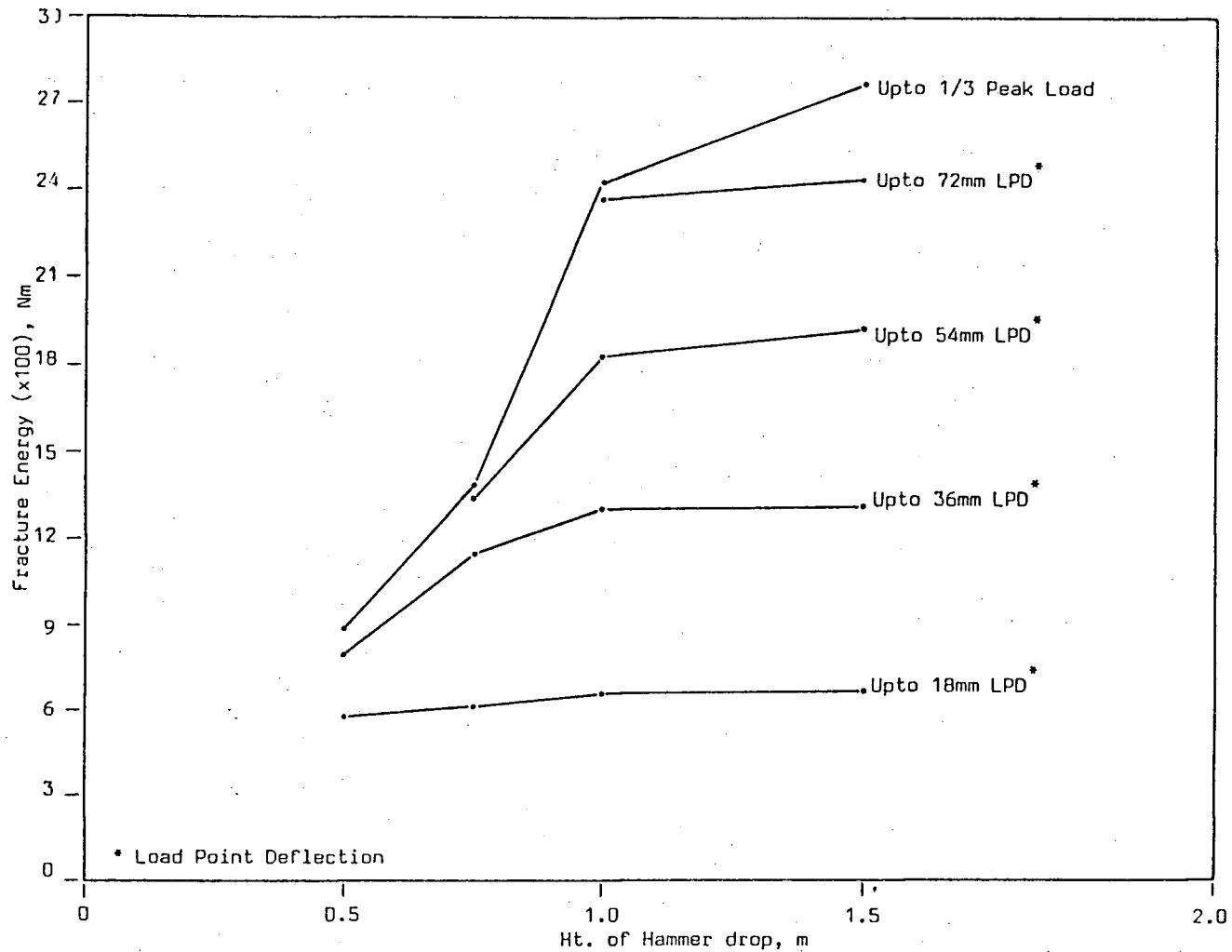


Figure 11.3-Fracture Energy absorbed by Conventionally Reinforced Concrete Beam under different hammer drop heights up to a certain mid-span deflection. Note the higher deformation capacity under higher drop heights, (w/c ratio=0.4).

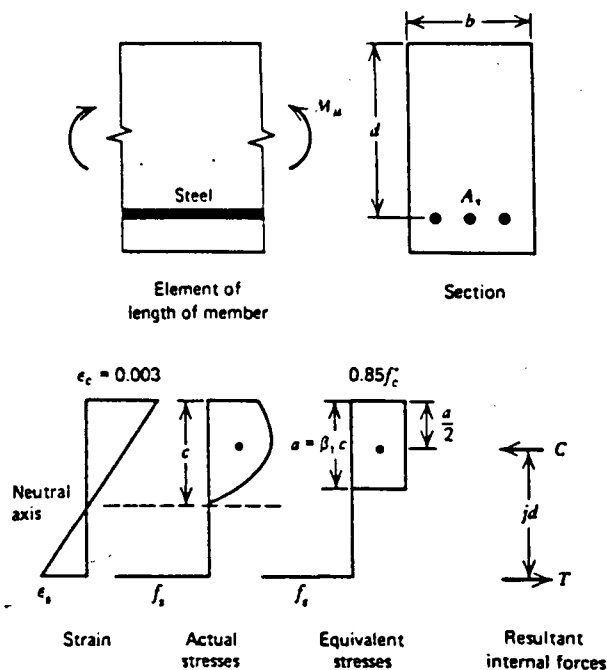


Figure-11.4-Beam Section

we get,

$$\rho_b = 4.87\%$$

Since the percent steel used in this study is only 1.136%, the section is underreinforced. With the steel yielding first, the ultimate moment of resistance under static conditions (ignoring any strain hardening) may be calculated as follows (59):

Referring again to Figure 11.4,

$$\begin{aligned} a &= \frac{A_s f_y}{0.85 f'_c b} \\ &= \frac{140 \times 425}{0.85 \times 49 \times 100} \\ &= 14.28 \text{ mm.} \end{aligned} \tag{11.2}$$

If  $MR(TH)$  is the theoretical ultimate moment of resistance of the section, then,

$$\begin{aligned}
 MR(TH) &= A_s f_y (d - 0.5a) \\
 &= 140 \times 425 (100 - 0.5 \times 14.28) \\
 &= 5.525 \times 10^6 \text{ N-mm}
 \end{aligned}$$

This agrees closely with the observed value of ultimate moment of resistance in the static case (MR(OBS)) (see Table 11.1a).

$$\begin{aligned}
 MR(OBS) &= \frac{(P_b)_{\max}}{4} l \\
 &= \frac{22671 \times 960}{4} \\
 &= 5.541 \times 10^6 \text{ N-mm}
 \end{aligned}
 \tag{11.4}$$

Under impact conditions, although the mechanism of failure may remain the same as under static conditions, the properties of both steel (65) and concrete (Chapter 6), and of the bond between them, seem to change. The compressive strength of concrete (21), and the yield and the ultimate strength of steel (65) increase as the stress rate is increased. Once in the dynamic range, the peak loads were found not to be very different from one drop height to another (Figure 11.1 and 11.2), suggesting that the strengths of both the concrete and steel tend to approach their limiting values at the high stress rates associated with impact. This may also indicate that, once in the dynamic range, the stress rates may not be very different from one drop height to another.

The absolutely limiting value of the moment of resistance in the static case  $MR(\text{lim,static})$  may be obtained by assuming that the steel reaches the ultimate value of stress, and by assuming that the position of the neutral

axis is at the extreme compression fibre. Then,

$$MR(\text{lim, static}) = A_s f_{us} d \quad (11.5)$$

where  $f_{us}$  = the ultimate strength of steel in static conditions = 700 MPa

Therefore,

$$MR(\text{lim, static}) = 140 \times 700 \times 100 = 9.8 \times 10^6 \text{ N-mm}$$

Under dynamic conditions, it has been reported (66) that for an increase in the stress rate of six orders of magnitude, the ultimate tensile strength of steel is approximately doubled. Since, in the present study, the stress rate achieved in the impact tests was approximately six orders of magnitude higher than in the static tests, the absolutely limiting value of the moment of resistance in the dynamic case ( $MR(\text{lim, dyn})$ ) can be estimated to be,

$$MR(\text{lim, dyn}) = A_s f_{ud} d \quad (11.6)$$

where  $f_{ud}$  = the ultimate tensile strength of steel in dynamic conditions = 1400 MPa.

Then,

$$MR(\text{lim, dyn}) = 140 \times 1400 \times 100 = 19.6 \times 10^6 \text{ N-mm}$$

A plot of the absolute limiting moment of resistance, along with the experimentally observed moment of resistance, has been presented in Figure 11.5. The curves of observed moment of resistance fall short of the limiting moment of resistance curve because, in practice, concrete crushing commences before the neutral axis reaches the compression face. However, since the crushing strength and the failure strain for concrete both increase with an increase in the

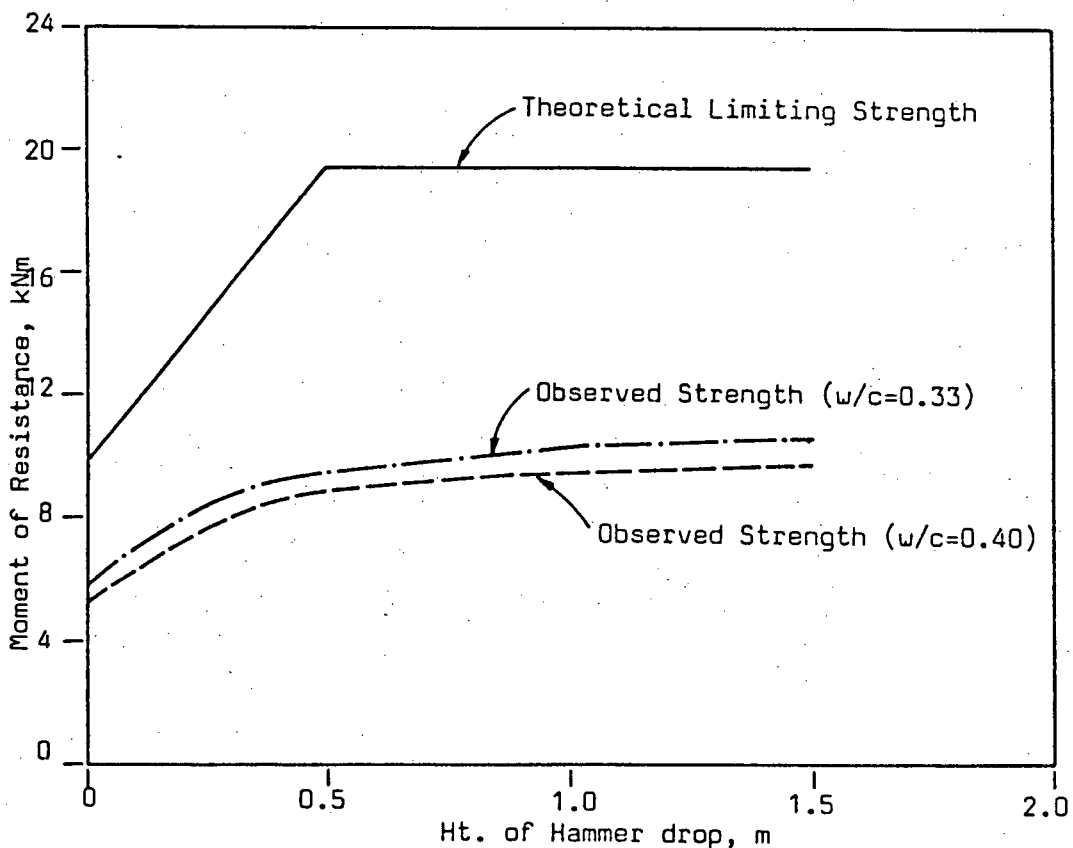


Figure-11.5-Theoretically limiting and the experimentally observed Moment of Resistance

stress rate (21), the neutral axis may move further upwards towards the compression face with an increase in hammer drop height. Moreover, increased failure strains in concrete increase the failure strains in the steel, causing an increase in strain hardening and consequently in the steel stress. The complex nature of stresses and strains in an impacted beams may also give rise to severe localized strains along the length of the steel bars. Indeed, in about 30% of the specimens tested at 1.5m drop, fracturing of the reinforcing bars was noticed. (see Section 11.5 a detailed discussion of the steel fracture).

A reduction in the water/cement ratio caused increased peak bending loads and increased fracture energies (Figure 11.2 and Tables 11.1a and 11.1b). Concrete with a water/cement ratio of 0.33, which had an equivalent cube strength of 56 MPa, as compared to concrete with a w/c ratio of 0.40 with an equivalent cube strength of 49 MPa, also fell far short of the limiting moment of resistance curve.

For a given midspan deflection, the beams subjected to higher stress rates absorbed higher fracture energies. This is a consequence of the higher loads supported by the beams at higher stress rates (Figure 11.3). Beams subjected to higher stress rates could also undergo larger deformations before the loads dropped to one-third of the peak values (Figure 11.1). The higher fracture energies absorbed by the beams subjected to higher stress rates are therefore a

consequence of both higher load capacity and the higher deformation capacity at higher stress rates.

### 11.3 THE USE OF SMOOTH REINFORCING BARS

In conventional concrete practice, only deformed reinforcing bars are used, because they achieve a much better bond with concrete than do smooth bars. However, since the failure mechanism and the behaviour of conventionally reinforced concrete under impact loading was found to be different from the static case, it was decided to examine the behaviour of concrete reinforced with smooth rebars under impact. It should be noted here that in the case of beams reinforced with deformed reinforcing bars under impact, fracture of the rebars was observed in about 30% of the cases (See below). It was therefore considered worthwhile to see if reducing the bond by using smooth rebars solved this problem. The same scheme as used for deformed rebars was adopted. Two w/c ratios, of 0.4 and 0.5, were chosen, corresponding to concrete strengths of 42 and 49 MPa, respectively.

Tables 11.2a and 11.2b,c present the static and the dynamic properties, respectively, of normal strength concrete with smooth reinforcing bars. As in the case of deformed bars, both the peak bending loads and the fracture energies were found to increase with an increase in the hammer drop height (Tables 11.2a,b,c and Figure 11.6). The fracture energies to 1/3 of the peak load and to different

**Table 11.2(a)**  
**Static Behaviour of Normal Strength Concrete Reinforced with Smooth Steel Bars**

		w/c = 0.40 (3)*				w/c = 0.50 (3)*			
		Max	Min.	Mean	s	Max.	Min.	Mean	s
<b>Peak Bending Load (N)</b>		26028	21356	23202	2029	23028	18348	20148	2057
<b>Fracture Energy<sup>1</sup> (Nm)</b>		604	550	586	25	590	430	534	74
<b>Fracture Energy<sup>2</sup> (Nm)</b>		530	377	432	69	456	362	402	40
<b>Fracture Energy<sup>3</sup> (Nm)</b>		672	500	599	73	630	510	560	51

\* Number of specimens tested.

**Table 11.2(b)**  
**Dynamic behaviour of Normal Strength Concrete Reinforced with Smooth Steel Bars (w/c = 0.4)**

	Ht. of Hammer drop, m											
	...0.50m... (6)*				...1.50m... (6)*				...2.36m... (6)*			
	Max	Min.	Mean	s	Max.	Min.	Mean	s	Max.	Min.	Mean	s
Peak Bending Load (N)	37202	35456	36617	820	39727	35494	37314	1778	43441	38636	41038	2402
Fracture Energy' (Nm)	1230	1056	1143	87	2699	1735	2353	438	3748	2959	3353	394
Fracture Energy' (Nm)	606	601	603	2	653	604	624	21	685	674	679	6
Fracture Energy' (Nm)	1213	1171	1127	19	1299	1164	1235	55	1355	1355	1355	0
Fracture Energy' (Nm)	-	-	-		1955	1649	1760	138	1976	1946	1961	15
Fracture Energy' (Nm)	-	-	-		2626	1930	2218	296	2577	2375	2476	101
Max. Beam velocity (m/s)	3.9	2.4	2.9	0.7	4.2	2.8	3.4	0.6	4.5	3.8	4.2	0.4

\* Number of specimens tested.

Table 11.2(c)  
 Dynamic behaviour of Normal Strength Concrete Reinforced with Smooth Steel Bars ( $w/c \cong 0.5$ )

	Ht. of Hammer drop, m															
	...0.50m... (6)*				...0.75m... (6)*				...1.0m... (6)*				...1.50m... (6)*			
	Max	Min.	Mean	s	Max.	Min.	Mean	s	Max.	Min.	Mean	s	Max.	Min.	Mean	s
Peak Bending Load (N)	37553	35090	36321	1231	37530	35784	36483	754	36493	36485	36474	18	36142	35448	35795	347
Fracture Energy <sup>1</sup> (Nm)	1565	1497	1531	34	2703	1349	1929	569	2593	2143	2368	225	3117	2443	2780	337
Fracture Energy <sup>1</sup> (Nm)	592	565	578	13	635	559	595	31	613	605	609	4	631	540	585	45
Fracture Energy <sup>1</sup> (Nm)	1164	1119	1141	22	1233	1160	1194	29	1223	1192	1207	15	1230	1148	1189	41
Fracture Energy <sup>1</sup> (Nm)	-	-	-		1749	1746	1747	2	1832	1762	1797	35	1807	1608	1707	99
Fracture Energy <sup>1</sup> (Nm)	-	-	-		-	-	-		-	-	-		2347	2145	2246	101
Max. Beam Velocity (m/s)	2.7	2.5	2.6	0.1	3.2	2.6	2.9	0.3	3.5	3.2	3.3	0.1	4.4	3.5	4.0	0.4

\* Number of specimens tested.

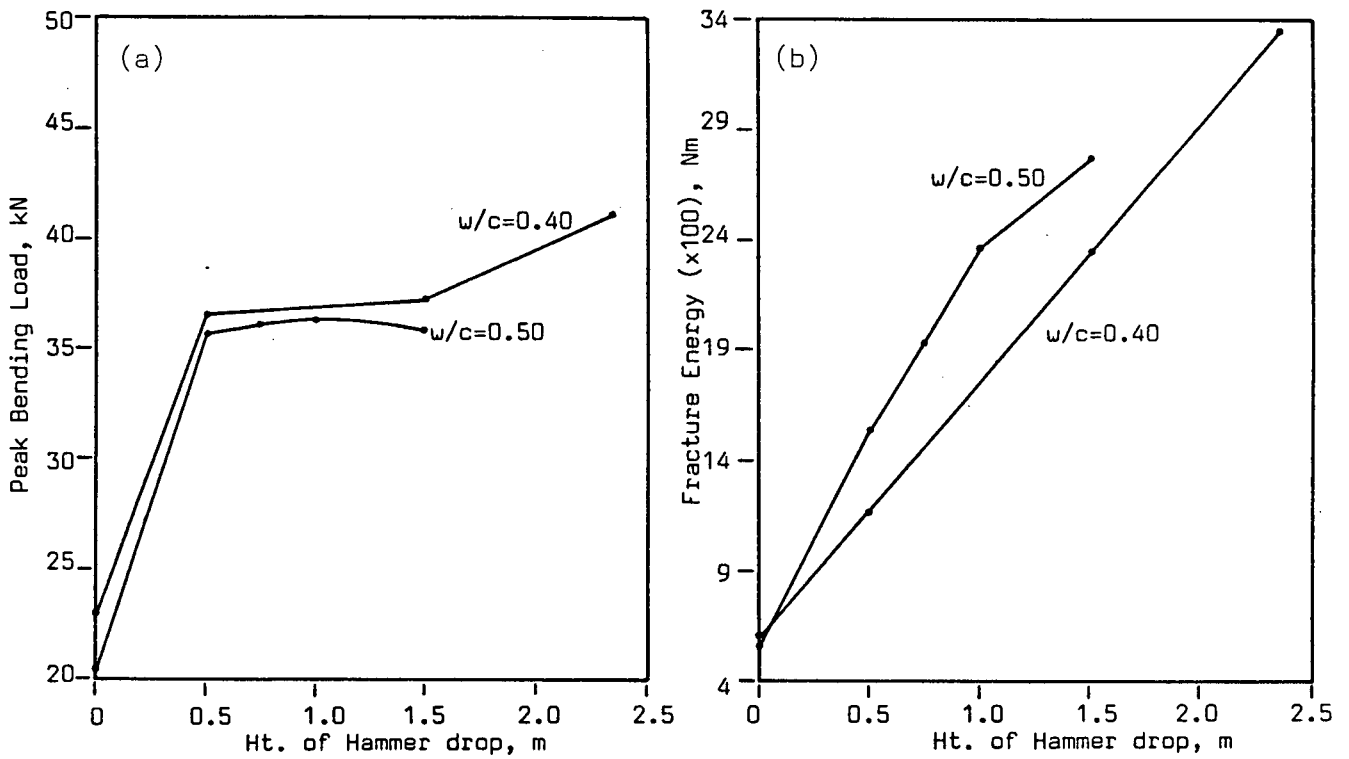


Figure-11.6-Effect of hammer drop height on (a) Peak bending load and (b) Fracture energy for CRNSC-S

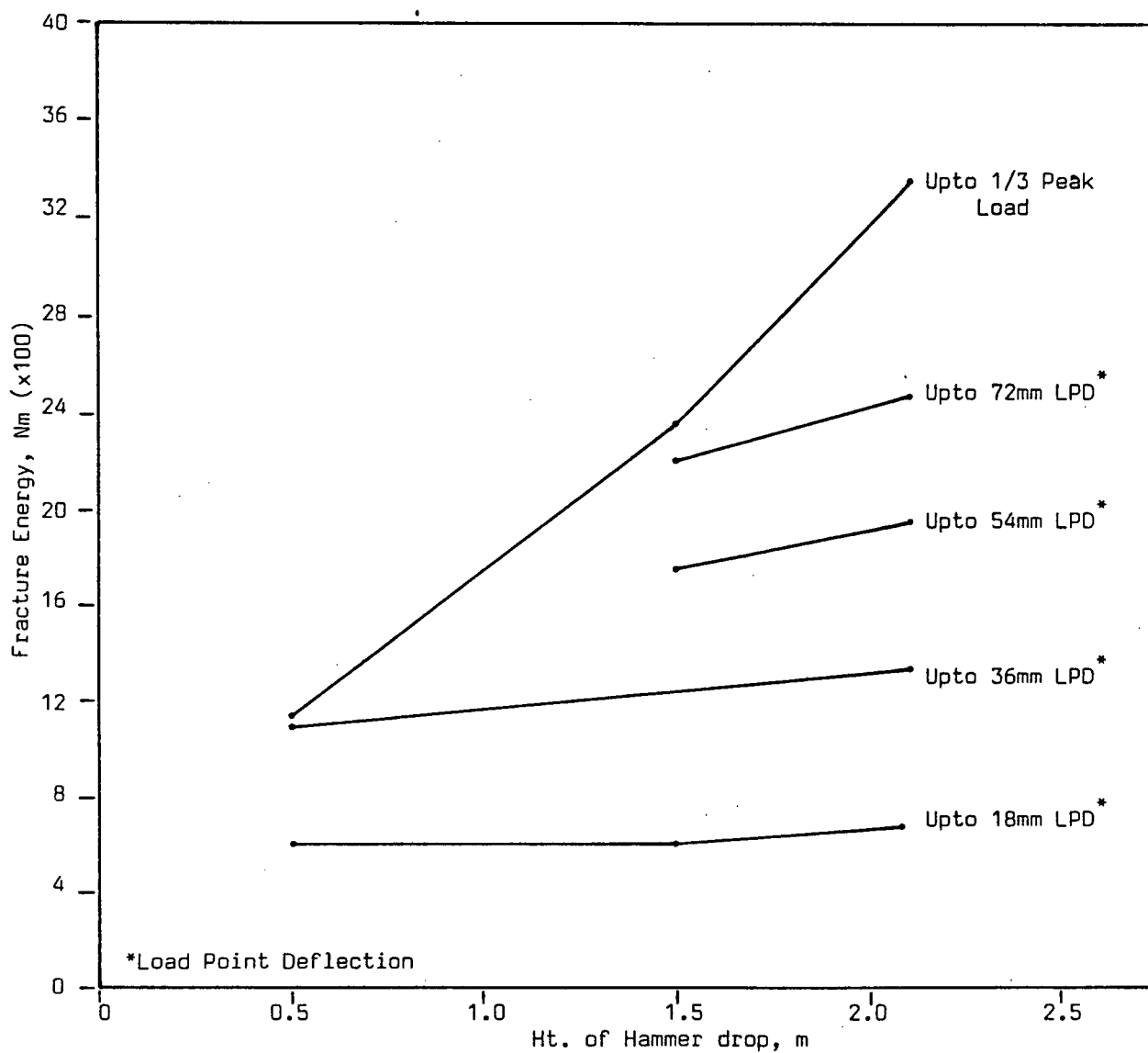


Figure-11.7-Energy at various midspan deflections for reinforced concrete with smooth bars

midspan displacements as a function of hammer drop height are shown in Figure 11.7. Once again, as in the case of deformed bars, the higher drop heights led to larger deformation capacities before the loads dropped to 1/3 of the peak loads. The peak loads in the dynamic range were not very different; the increase in the fracture energy with increasing hammer drop height was primarily a consequence of the larger deformation capacity the beam demonstrated at higher drop heights.

A comparison of the behaviour of concrete with smooth rebars and of concrete with deformed rebars is presented in Figure 11.8, where the peak bending loads and fracture energies have been plotted as a function of hammer drop height. It can be seen from Figure 11.8a that, although their static performances (Tables 11.1a and 11.2a) are almost identical, the use of deformed rebars resulted, in general, in higher peak bending loads in the dynamic cases. This could, in part, be due to the slightly lower measured yield strengths of the smooth rebars as compared to the deformed ones. The poorer bond achieved with smooth rebars compared to deformed rebars may also be responsible for their lower peak bending loads.

With the exception of the 0.5m drop, concrete with deformed rebars was found to be more energy absorbing than concrete with smooth rebars (Figure 11.8b). This may be explained by the poorer bond developed by the smooth rebars. At higher drop heights, it is possible that more debonding

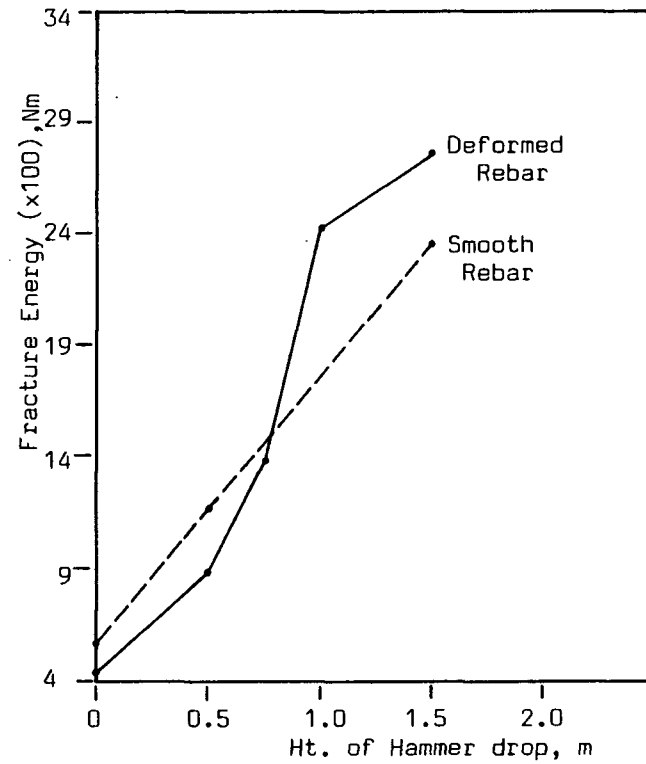
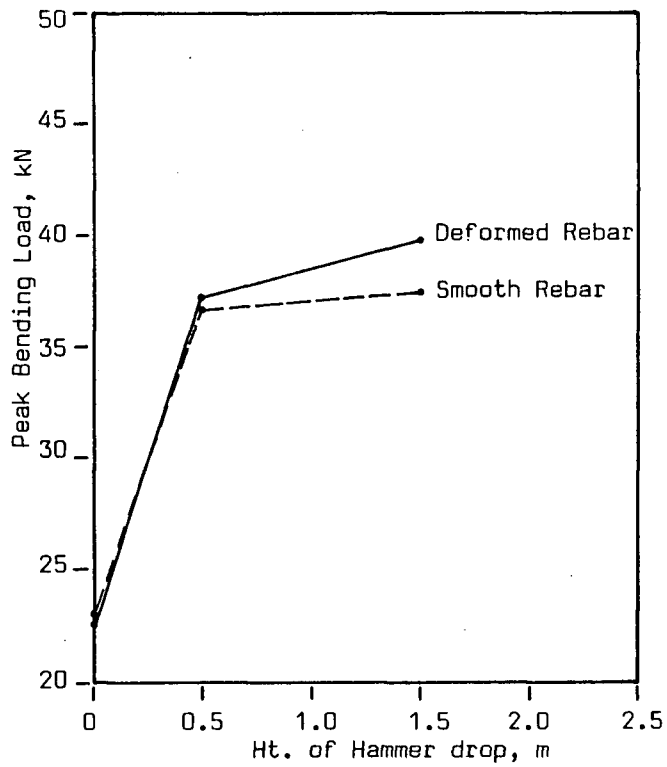


Figure 11.8 Comparison between Conventionally Reinforced Concrete with Deformed Reinforcing bars and that with Smooth Reinforcing bars.

occurred with smooth rebars, resulting in stress relaxation in steel and hence in a diminished use of the steel properties. On the other hand, the deformed bars were likely stressed to a higher level, resulting in strain hardening and higher ultimate steel strains. It is therefore not surprising that the smooth rebars fractured only very occasionally even at a 2.36m drop height, whereas deformed rebars were often seen to rupture at 1.5m drop.

#### 11.4 THE USE OF SHEAR REINFORCEMENT

The effect of shear reinforcement on the dynamic behaviour of conventionally reinforced beams with deformed rebars was also studied. The stirrups used were 5mm in diameter, and spaced 100mm apart (Table 4.1). The results of both static tests and impact tests are presented in Table 11.3. These results can be compared with the results obtained in the case of concrete without the stirrups (Table 11.1a,b, and c). A graphical comparison is made in Figure 11.9.

The use of stirrups, as can be seen from Figure 11.9a, is not very effective in increasing the strength either in the static case or in the dynamic case. However, confinement of the concrete was found to increase the fracture energy requirement, particularly in the dynamic range (Figure 11.9b).

The confinement of concrete has been found to affect not so much the shape of the pre-peak stress-strain plot in

Table 11.3

Static and Dynamic behaviour of Conventionally Reinforced Normal Strength Concrete with Stirrups

	...STATIC... (3)*				...IMPACT...							
	Max	Min.	Mean	s	0.50m drop (6)*				1.0m drop (6)*			
					Max.	Min.	Mean	s	Max.	Min.	Mean	s
Peak Bending Load (N)	23242	21022	22111	907	43042	34586	37770	3754	44692	35092	39788	3921
Fracture Energy <sup>1</sup> (Nm)	562	459	499	46	1892	1521	1665	162	3348	2834	3048	218
Fracture Energy <sup>2</sup> (Nm)	432	294	342	66	641	591	621	22	731	632	689	42
Fracture Energy <sup>3</sup> (Nm)	580	384	453	90	1350	1128	1244	91	1440	1245	1325	83
Fracture Energy <sup>4</sup> (Nm)	-	-	-	-	-	-	-	-	2201	1640	1911	229
Fracture Energy <sup>5</sup> (Nm)	-	-	-	-	-	-	-	-	2842	2262	2531	238

\* Number of specimens tested.

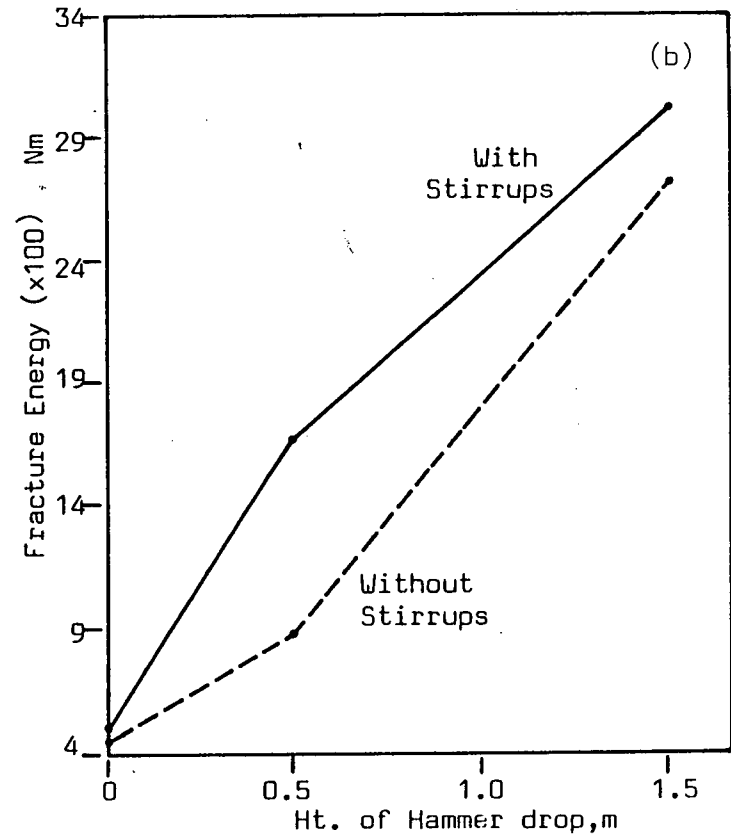
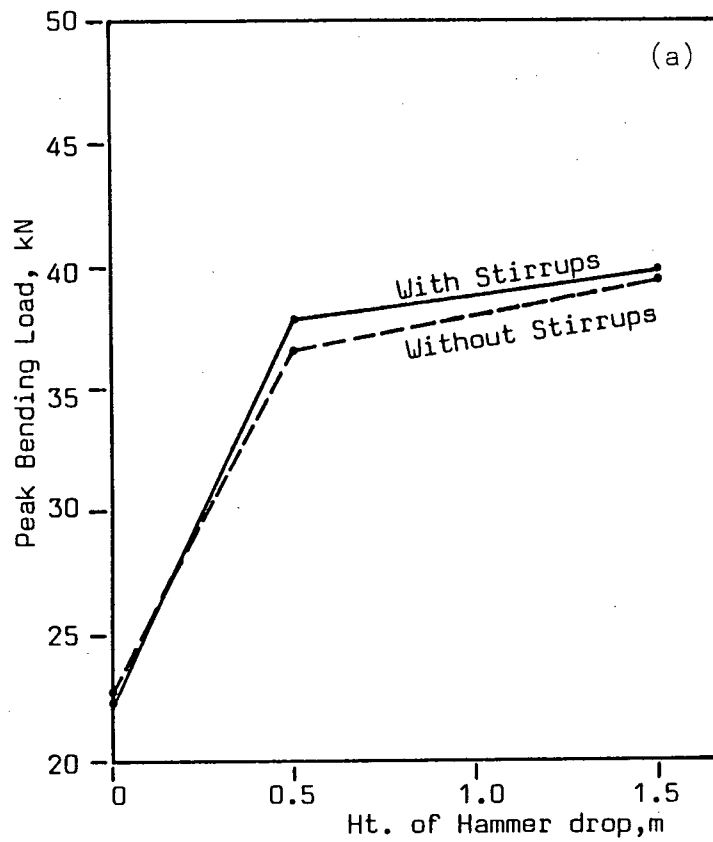


Figure 11.9- Comparison between Conventionally Reinforced Concretes with and without Stirrups.

compression, but the shape of the post-peak stress-strain plot (59). In general, the presence of stirrups increases the ductility; this is manifested by a long, slowly descending post-peak branch of the stress-strain curve (59). This behaviour, observed for static loading, seems to prevail even under dynamic conditions. Under impact loading, the concrete with stirrups was found to be considerably more energy absorbing than the concrete without stirrups.

#### 11.5 CONVENTIONALLY REINFORCED HIGH STRENGTH CONCRETE (CRHSC) UNDER VARIABLE STRESS RATE, AND ITS COMPARISON WITH CONVENTIONALLY REINFORCED NORMAL STRENGTH CONCRETE (CRNSC)

The properties of unreinforced high strength beams were discussed in Chapter 6. It was stated that high strength concrete beams, made with microsilica, were found to be stronger, but more brittle than normal strength plain concrete beams. In this section, the behaviour of high strength concrete beams made with microsilica, with 9.52mm deformed rebars is described.

High strength conventionally reinforced beams were tested both statically and under impact. The results are given in Table 11.4, and are presented graphically in the form of load vs. deflection plots in Figure 11.10. To facilitate a comparison with conventionally reinforced normal strength concrete under identical conditions, Figure 11.1 has been reproduced in Figure 11.11 for the relevant drop heights. To describe the beam response during impact,

**Table 11.4**  
**Static and Dynamic Behaviour of Conventionally Reinforced High Strength Concrete**

	...STATIC... (3) *				...IMPACT...							
	Max	Min.	Mean	s	0.50m drop (6) *				1.0m drop (6) *			
					Max.	Min.	Mean	s	Max.	Min.	Mean	s
Max. Observed Tup Load (N)	-	-	-		53304	39374	47622	5686	63747	61583	62946	824
Max. Observed Inertial Load (N)	-	-	-		9800	3721	7511	2317	12902	8702	10263	1710
Peak Bending Load (N)	28990	20191	24031	3683	44433	35653	40111	3577	54292	50461	52683	1390
Fracture Energy <sup>1</sup> (Nm)	732	611	678	50	534	121	345	153	382	99	175	120
Max. Beam Velocity (m/s)	-	-	-		1.7	0.8	1.3	0.3	1.3	0.5	0.8	0.3

\* Number of specimens tested.

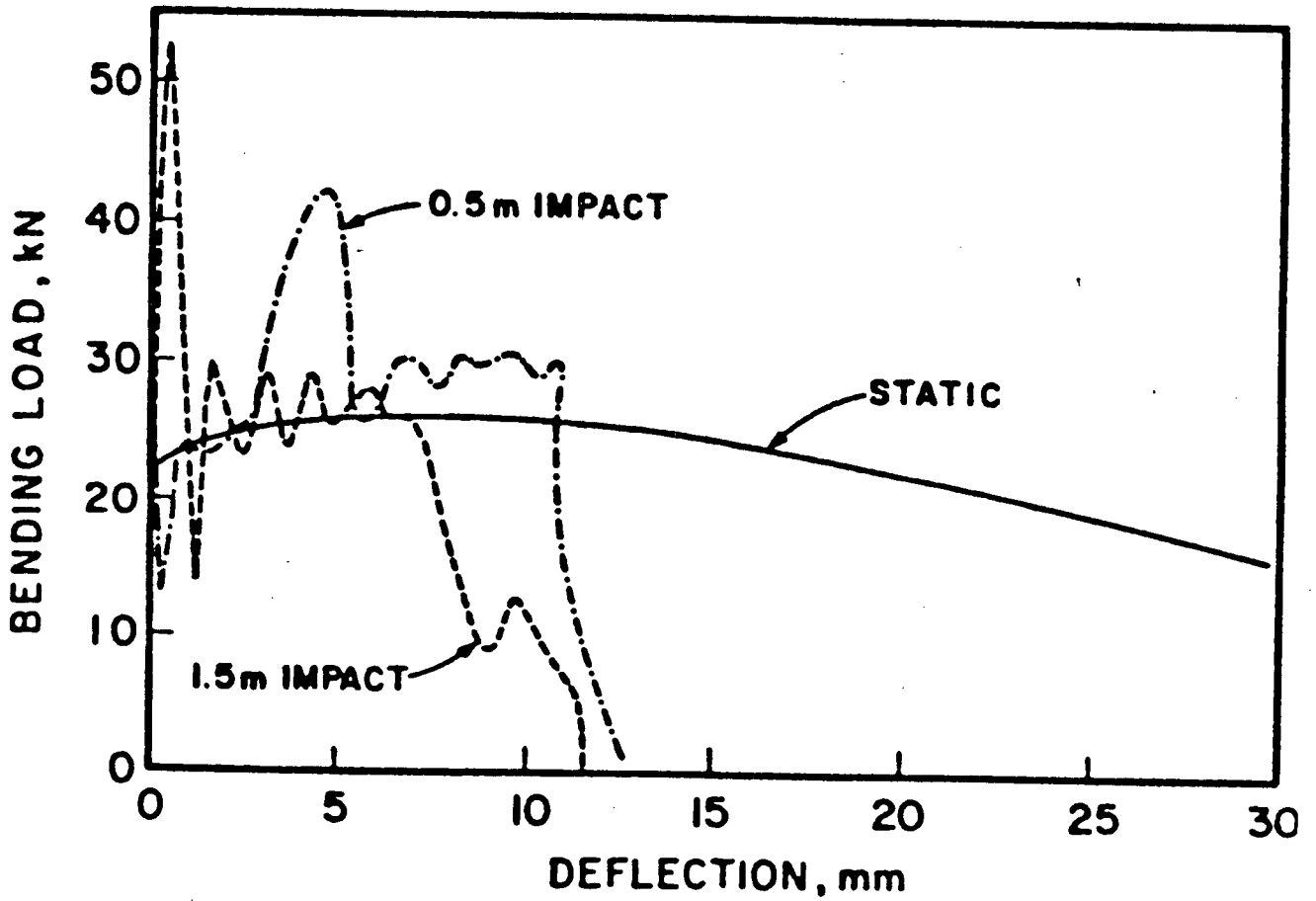


Figure-11.10-Load vs. deflection plots for conventionally reinforced high strength concrete under variable stress rates

the velocity vs. time plots and the tup load vs. time plots for high strength concrete have been plotted in Figure 11.12 (0.5m drop), and in Figure 11.13 (1.5m drop). Once again for comparison, the corresponding plots for normal strength concrete are presented in Figure 11.14 (0.5m drop) and 11.15 (1.5m drop). A final comparison with the normal strength concrete under different drop heights appears in Figure 11.16.

As can be seen from Table 11.4 and Figure 11.10, conventionally reinforced high strength concrete also demonstrates substantial stress rate sensitivity. The peak bending loads were higher for higher stress rate applications. Similar findings were reported for high strength plain concrete beams (Chapter 6), and also for normal strength beams with or without conventional reinforcement (Section 11.2). However, upon considering the fracture energy, a reversal in the trend is observed. The energy required for the impact events in the case of CRHSC was found to be smaller than the energy required statically (Table 11.4), and an increase in the drop height resulted in a reduction in the fracture energy requirement. In other words, high strength concrete with conventional reinforcement behaved in a more brittle fashion as the stress rate or the hammer drop height was increased.

One observation worth making here is the increased rigidity of the high strength beams under increased stress rates. The peak velocities attained by the beam may serve as

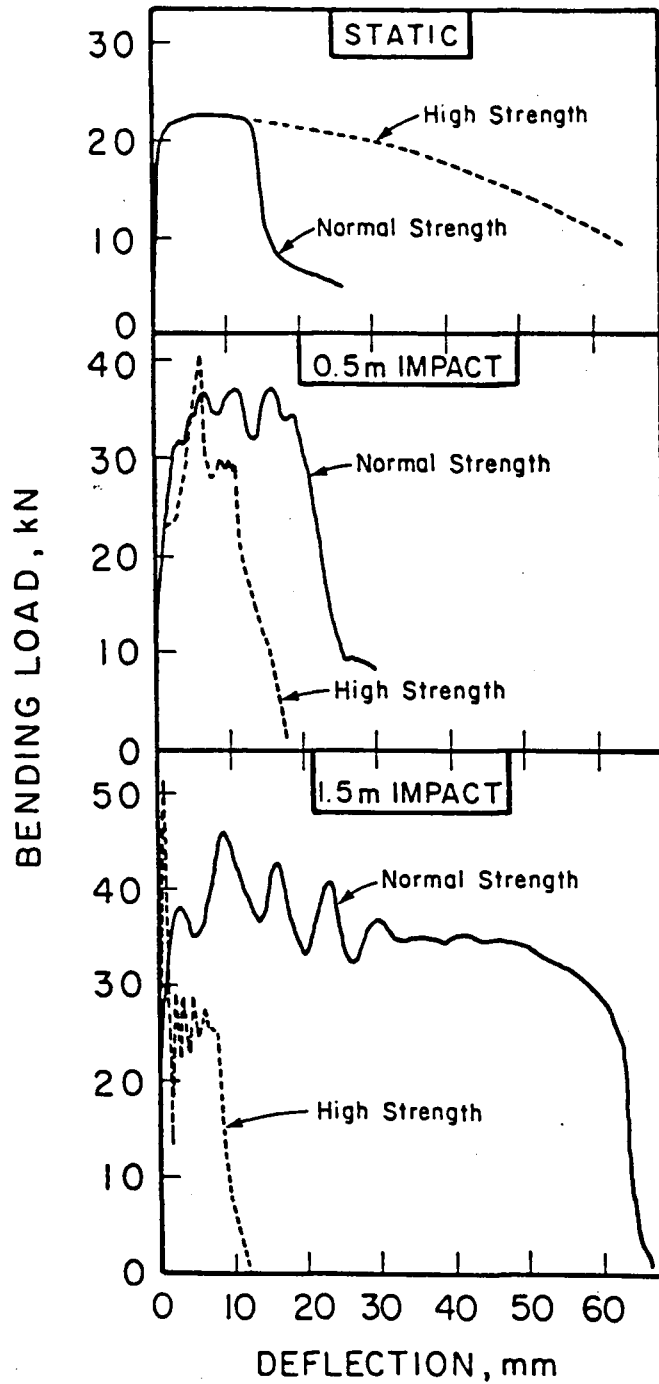


Figure-11.11-Comparison between CRNSC and CRHSC on the basis of load vs. deflection plots

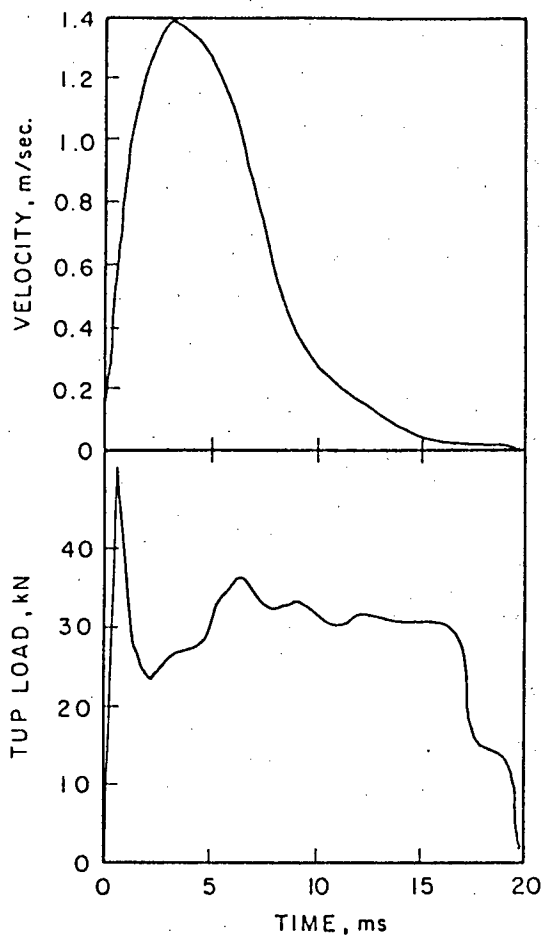


Figure 11.12 Reinforced High Strength Concrete under 0.5m drop.

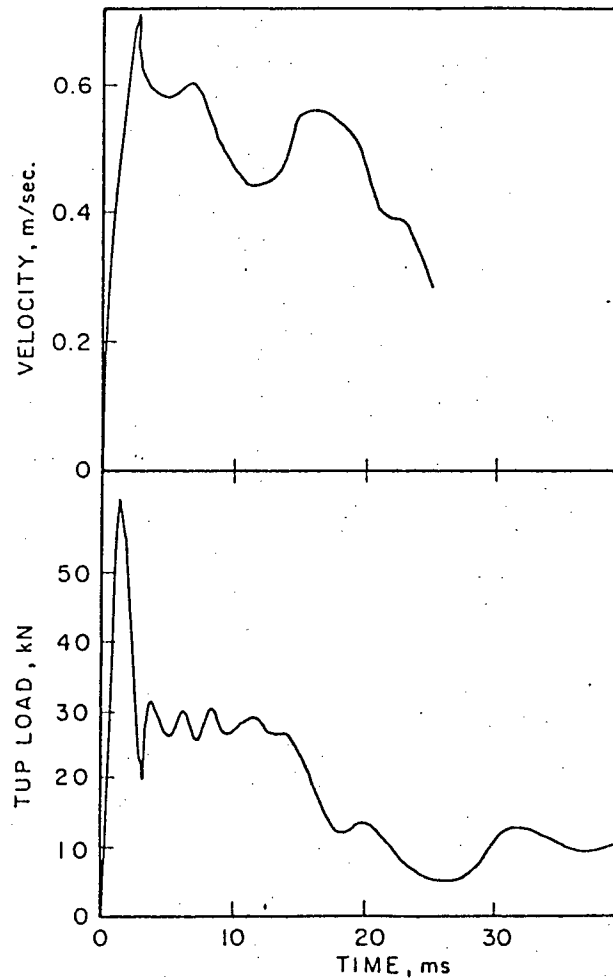


Figure 11.13 Reinforced High Strength Concrete under 1.5m drop. Note the increased rigidity of the beam compared 0.5m drop.

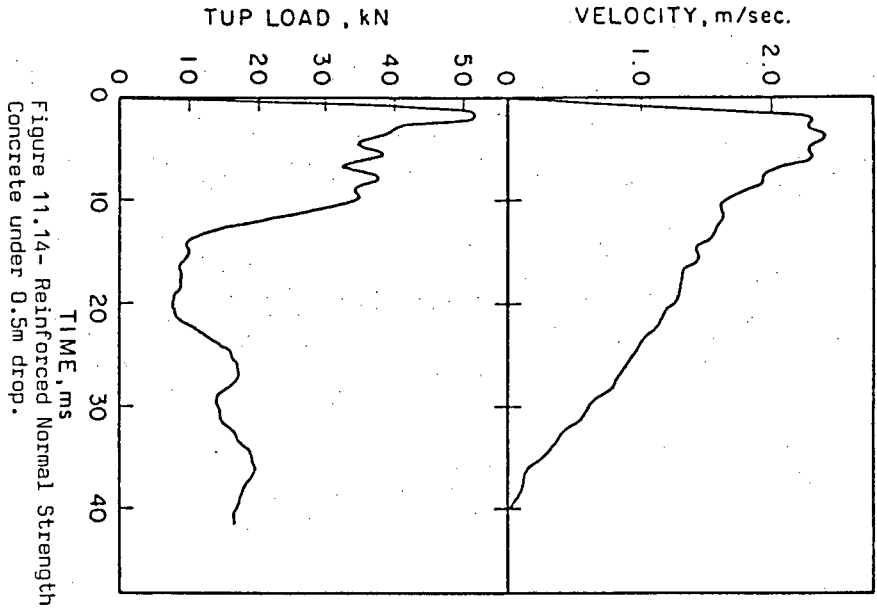


Figure 11.14- Reinforced Normal Strength Concrete under 0.5m drop.

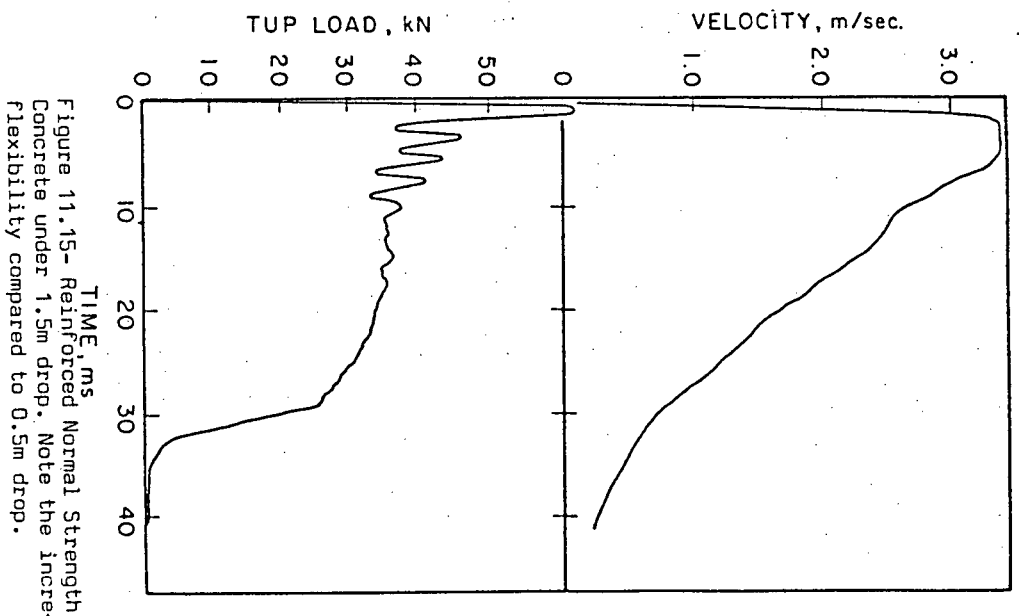


Figure 11.15- Reinforced Normal Strength Concrete under 1.5m drop. Note the increase in flexibility compared to 0.5m drop.

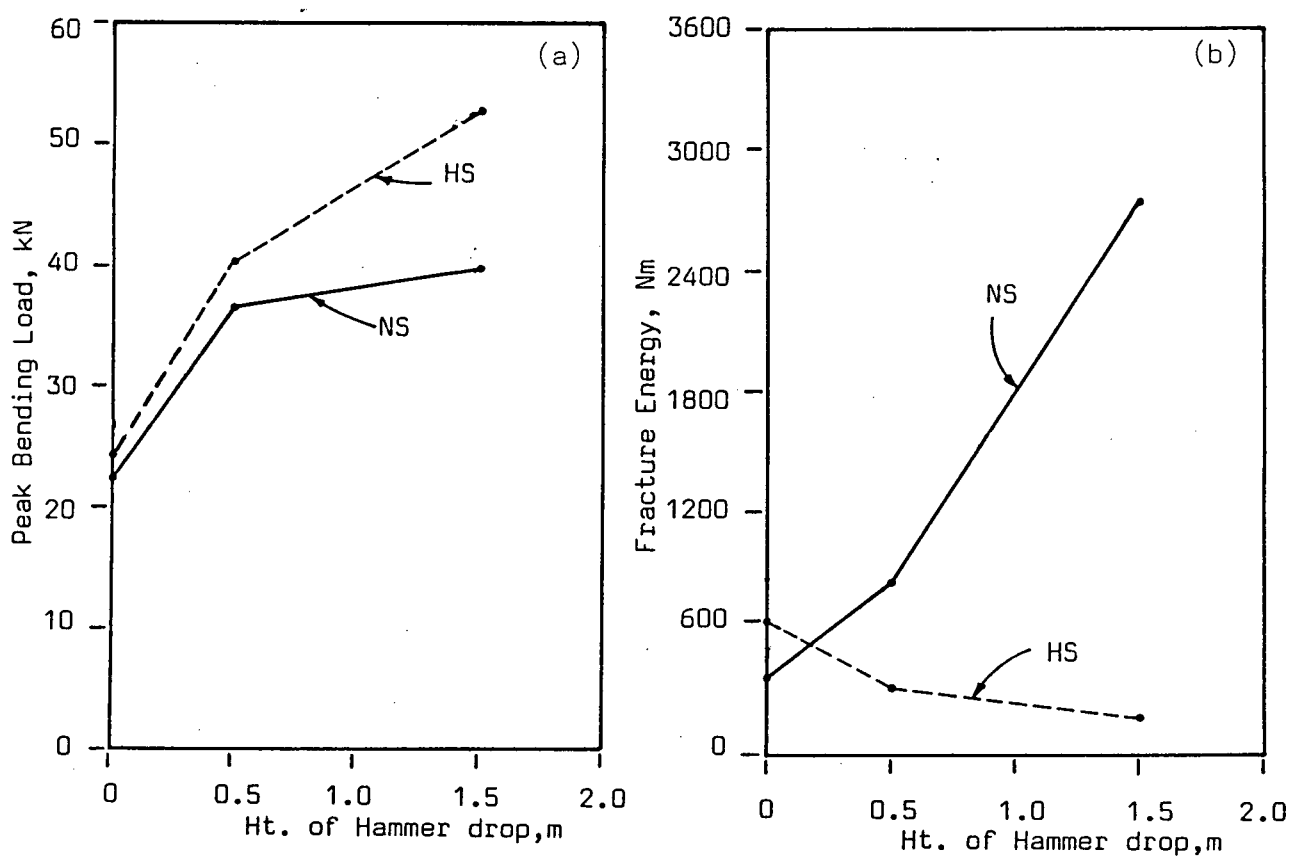
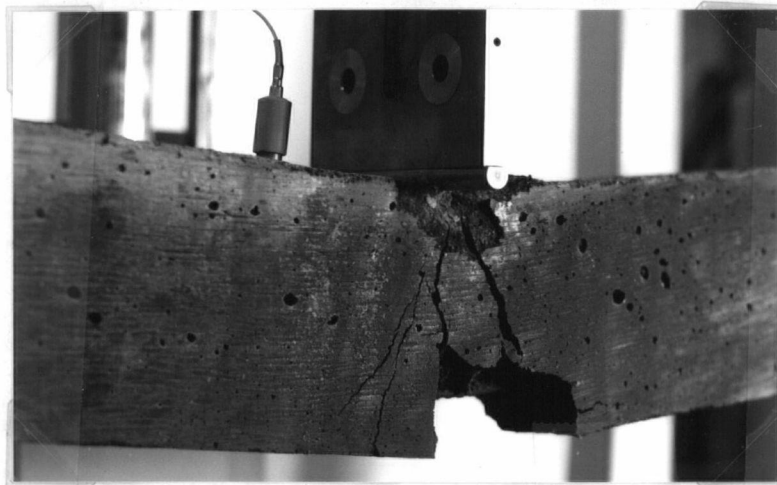


Figure-11.16-Comparison between CRNSC and CRHSC on the basis of (a) Peak bending load and (b) Fracture energy

a measure of this apparent rigidity. For example, a comparison of Fig 11.12 with 11.14, and of Figure 11.13 with Figure 11.15 indicates that while the peak velocities in the case of normal strength concrete increased with the hammer drop height, they decreased for high strength concrete (see also Table 11.4). This apparent rigidity of high strength conventionally reinforced beams resulted in reduced ultimate deflections with increasing hammer drop heights (Figure 11.10). The deformation capacity and the ultimate deflections, which increased with hammer drop height in the case of normal strength concrete, decreased with increasing hammer drop heights for high strength concrete; the reasons for this are not entirely clear. The ductility reduction with hammer drop height in the case of high strength concrete was so pronounced that the fracture energies almost approached the energy required by the unreinforced high strength concrete (Chapter 6).

The embrittlement of high strength concrete with conventional reinforcement may be a consequence of the great improvement in the bond between high strength concrete containing microsilica and steel. The high quality bond apparently resulted in very high local strains in steel, resulting in premature steel failure. Steel failure was observed in many more cases in high strength concrete than in normal strength concrete (Figure 11.17).



Reinforced concrete beam of high strength concrete after 0.5 m impact showing cracking of the concrete.



(a)



(b)

Reinforced concrete beams of high strength concrete after 1.5 m impact showing (a) disintegration of a beam and, (b) disintegration of the beam and fracture of the reinforcing bars.

Figure-11.17

## 11.6 CRACK DEVELOPMENT IN CONVENTIONALLY REINFORCED HIGH STRENGTH CONCRETE (CRHSC) UNDER IMPACT

A study of the crack development in conventionally reinforced high strength concrete was carried out by using a high speed motion picture camera running at 10,000 frames per second. The results were then viewed frame by frame in a small hand viewer, and the surface traces of the propagating cracks were sketched. The results are shown in Figure 11.18.

The average crack velocity (obtained from the time required by the crack to propagate from the bottom to the top of the specimen) was found to be about 83 m/s, which is faster than the velocity observed in steel fibre reinforced concrete (74 m/s) (Section 10.9), but slower than the crack velocity observed in hydrated cement paste (115 m/s) (Section 6.7). This suggests that the presence of the reinforcing bars did not particularly affect crack propagation. The closing of existing surface cracks (Figure 11.18) during the process of impact, suggests that a highly complex stress pattern exists in a beam undergoing impact.

*NOTES: <sup>1</sup>Calculated to the point at which the load dropped back to 1/3rd of its peak value.*

*<sup>2</sup>Calculated to 18mm midspan deflection.*

*<sup>3</sup>Calculated to 36mm midspan deflection.*

*<sup>4</sup>Calculated to 54mm midspan deflection.*

*<sup>5</sup>Calculated to 72mm midspan deflection.*

## CONVENTIONALLY REINFORCED HIGH STRENGTH CONCRETE

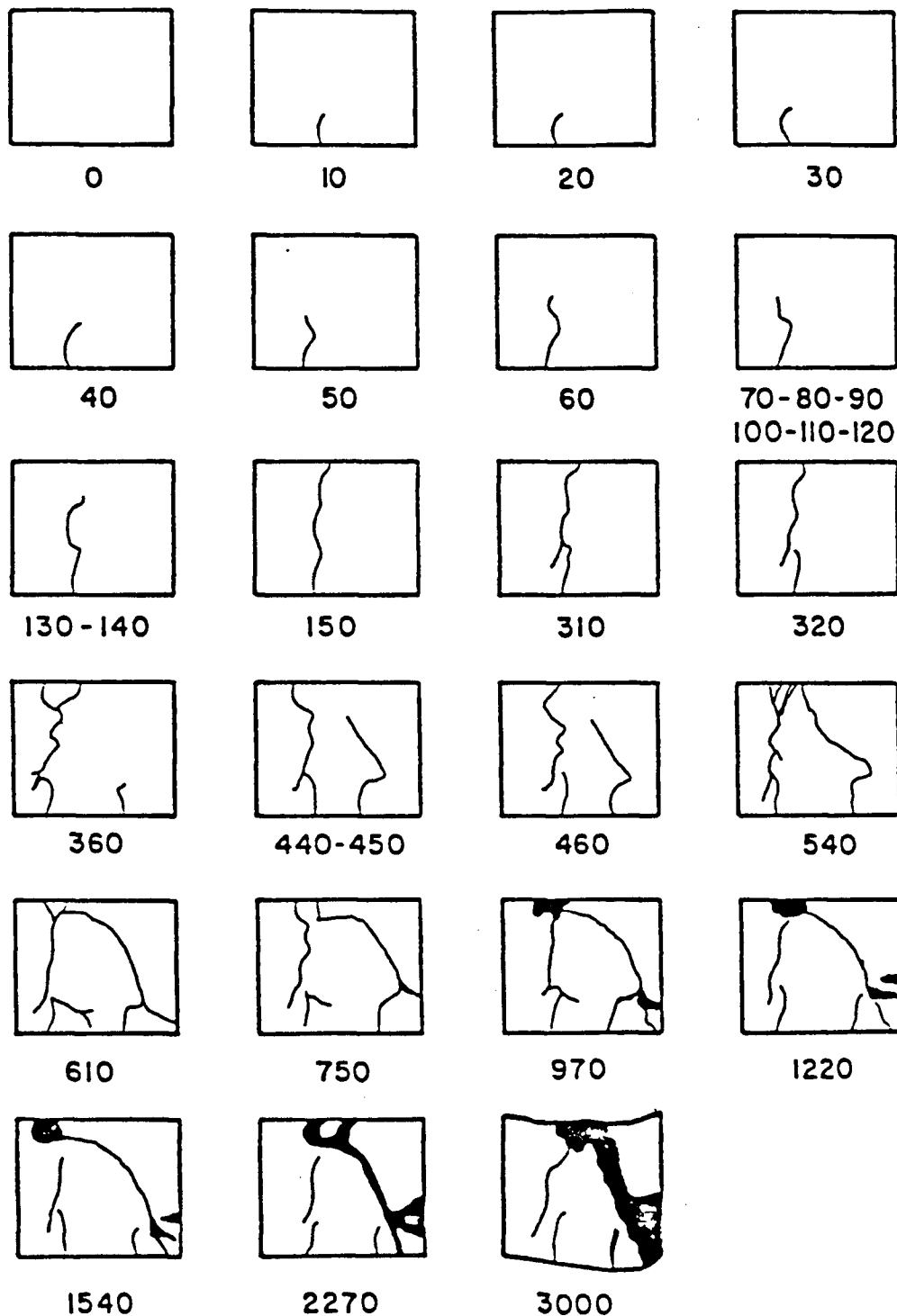


Fig.11.18—Crack development as a function of time for a conventionally reinforced high strength concrete beam subjected to impact loading. The number in each frame represents the time (in units of 0.1 ms) from the first frame shown.

## 12. CONVENTIONALLY REINFORCED CONCRETE CONTAINING FIBRES

### UNDER IMPACT

#### 12.1 INTRODUCTION

It was observed in Chapter 10 that the addition of fibres to a cementitious matrix results in a composite which is far more ductile than the basic matrix. The fibres may, at least in part, offer a solution to the problem of concrete brittleness. However, this statement is only qualitative; quantitatively, little is known about the optimum fibre geometry, optimum fibre volume, and so on, for impact loading.

In Chapter 11, it was shown that the impact resistance of conventionally reinforced high strength concrete made with microsilica was poor. Also, an increased intensity of impact resulted in a reduced impact resistance, warning of the dangers of using such a material under severe impact loading conditions. Conventionally reinforced normal strength concrete beams without microsilica, on the other hand, were reasonably impact resistant, and under an increased impact intensity, the impact resistance did not particularly decrease.

One possible solution to the problem would be to avoid entirely the use of high strength concrete in situations where the possibility of impact loading exists. However, this would place too severe a restriction on the use of a very promising material, which has excellent properties in static loading conditions. Besides, most engineering structures are

designed for static situations only, and impact or shock loadings are not explicitly considered. Therefore, it is worth trying to see whether fibres can help to make conventionally reinforced high strength concrete more energy absorbing. As a comparison, the effect of fibre reinforcement on the impact performance of conventionally reinforced normal strength concrete was also investigated.

## 12.2 CONVENTIONALLY REINFORCED NORMAL STRENGTH CONCRETE WITH POLYPROPYLENE FIBRES (CRNSC-P) UNDER VARIABLE STRESS RATE

Normal strength concrete is known to be more ductile than hydrated cement paste. As has been described earlier, the addition of fibres improved the ductility of normal strength concrete; the inclusion of conventional reinforcing bars was even more effective in increasing the ductility of normal strength concrete beams. To study the effect of both fibres and conventional reinforcement, beams with normal strength concrete, reinforcing bars, and 0.5% by volume of chopped fibrillated polypropylene fibres, were tested in both static and impact loading with hammer drop heights of 0.5m and 1.5m. The results are given in Table 12.1. The fracture energies were calculated to the point at which the load dropped back to 1/3 of its peak value. The behaviour of fibre reinforced beams is compared to that of beams without fibres in the load vs. deflection plots of Figure 12.1. To give an idea of the inertial loading on the beams, the

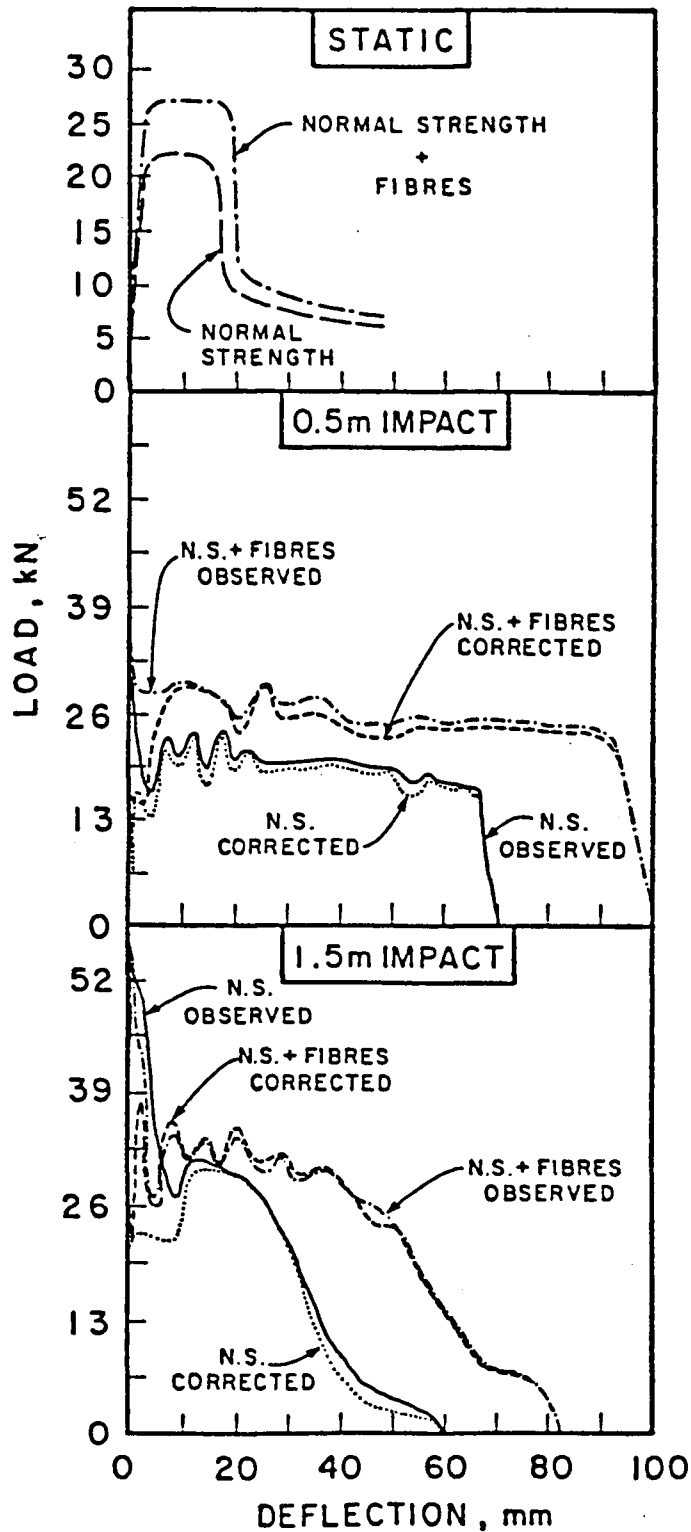


FIGURE 12.1-Effect of adding polypropylene fibres to conventionally reinforced normal strength concrete

**Table 12.1**  
**Static and Dynamic Behaviour of Conventionally Reinforced**  
**Normal Strength Concrete with Polypropylene Fibres**

	....STATIC.....		.....IMPACT.....			
			..0.5m drop..		..1,5m drop..	
	Without Fibres	With Fibres	Without Fibres	With Fibres	Without Fibres	With Fibres
<b>Peak Bending Load (N)</b>	22671 (3102)	24692 (2633)	36664 (888)	38486 (1800)	39800 (3052)	40980 (2224)
<b>Fracture Energy (Nm)</b>	442 (45)	499 (31)	880 (300)	2342 (562)	2750 (628)	3361 (490)
<b>Velocity of the Cross- Head (m/s)</b>	$4.2 \times 10^{-7}$	$4.2 \times 10^{-7}$	3.13	3.13	5.19	5.19

**NOTES:**

1. *Fracture Energies calculated to the point at which the load dropped back to 1/3rd of its peak value.*
2. *The numbers in brackets are the standard deviations.*
3. *Three specimens tested under static, and six specimens tested under impact in each of the categories.*

observed tup load, and the corrected bending load have both been plotted as a function of displacement in Figure 12.1.

As may be seen from Figure 12.1 and from Table 12.1, the effect of adding fibres led to a slight increase in the peak bending load, and to an increase in the fracture energy, particularly in the dynamic cases (Table 12.1). Thus, the primary advantage of adding the fibres was not so much in the increased strength, but in the increased fracture energy. The beams with the fibres had an increased

deformation capacity, and the fibres were effective in maintaining the coherence of the beams with reduced spalling.

### 12.3 CONVENTIONALLY REINFORCED HIGH STRENGTH CONCRETE WITH POLYPROPYLENE FIBRES (CRHSC-P) UNDER VARIABLE STRESS RATE

High strength concrete made with microsilica is more brittle than normal strength concrete without microsilica (Chapters 6 and 11). Since the high concrete strength that can be achieved with the use of microsilica is a very attractive property, any means of overcoming its brittle nature would be welcome. Since fibres in unreinforced high strength concrete were found to be very effective (Chapter 10), their effect on CRHSC was also studied.

Static and impact tests were carried out on CRHSC beams reinforced with 0.5% by volume of polypropylene fibres, and the results are presented in Table 12.2 and Figure 12.2. As in the case of normal strength concrete, improvements in both the peak bending load and the fracture energy were observed due to the addition of fibres. Once again, similar to normal strength concrete, the advantage was not in the increased strength, but in the greatly improved impact resistance.

It was shown in Chapter 11 that an increase in the impact intensity resulted in a considerable embrittlement of CRHSC. However, CRHSC with fibres did not show any signs of increased embrittlement with increased impact intensity. The

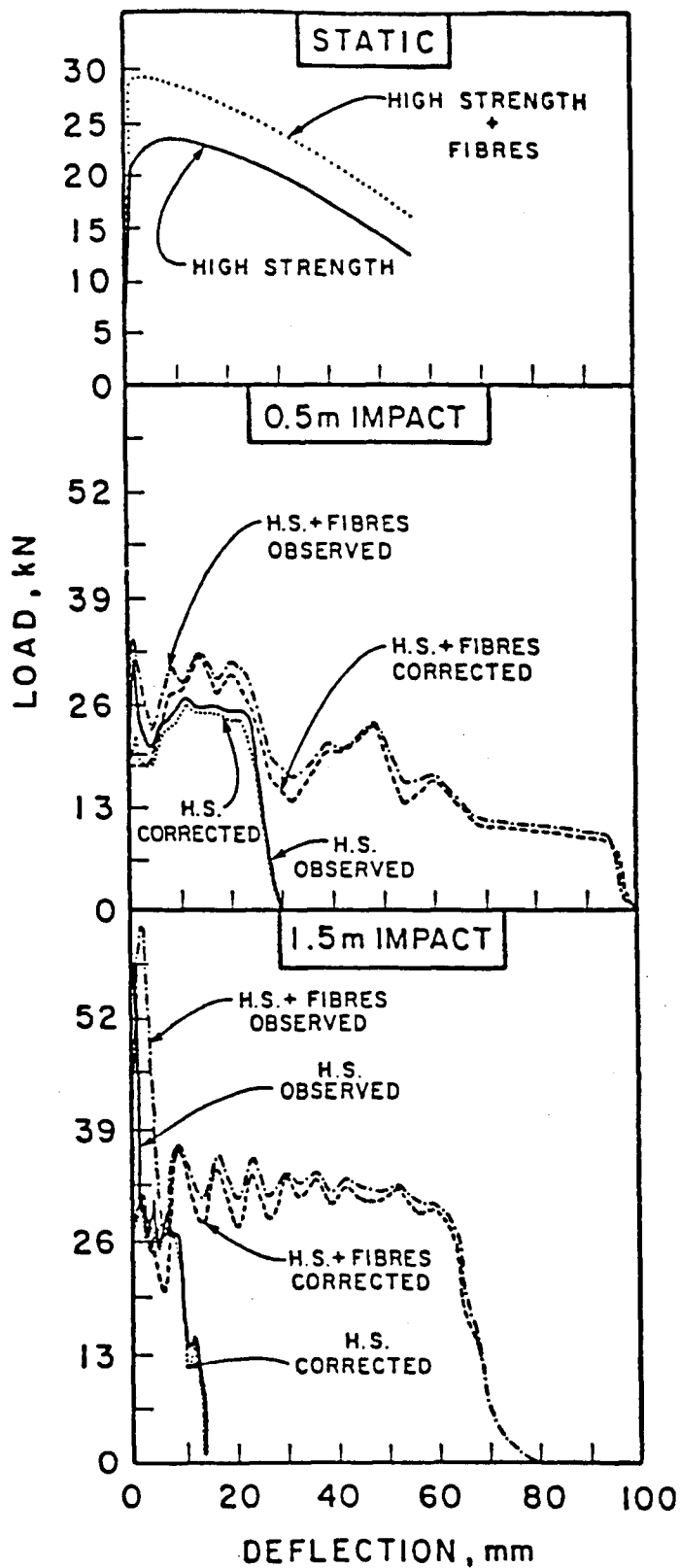


FIGURE 12.2-Effect of adding polypropylene fibres to conventionally reinforced high strength concrete

**Table 12.2**  
**Static and Dynamic Behaviour of Conventionally Reinforced**  
**High Strength Concrete with Polypropylene Fibres**

	....STATIC....		....IMPACT....			
	Without Fibres	With Fibres	...0.5m drop...		...1.5m drop...	
	Without Fibres	With Fibres	Without Fibres	With Fibres	Without Fibres	With Fibres
Peak Bending Load (N)	24031 (3683)	28242 (2493)	40111 (3577)	42642 (2683)	52683 (1390)	52583 (1850)
Fracture Energy (Nm)	678 (50)	889 (72)	345 (153)	1276 (229)	175 (120)	1962 (284)
Velocity of the Cross- Head (m/s)	$4.2 \times 10^{-7}$	$4.2 \times 10^{-7}$	3.13	3.13	5.19	5.19

**NOTES:**

1. *Fracture Energies calculated to the points at which the load dropped back to 1/3rd of its peak value.*
2. *The numbers in brackets are the standard deviations.*
3. *Three specimens tested under static, and six specimens tested under impact in each of the categories.*

beams were found to absorb more energy under higher drop heights (or higher impact intensities).

**12.4 COMPARISON BETWEEN CONVENTIONALLY REINFORCED NORMAL STRENGTH CONCRETE WITH POLYPROPYLENE FIBRES AND HIGH STRENGTH CONCRETE WITH POLYPROPYLENE FIBRES**

As has been shown, both normal strength and high strength concretes with conventional reinforcement were found to benefit from the addition of fibres. The primary advantage of adding the fibres was in the improved

toughness. However, on a percentage basis, a larger gain in toughness was observed for impact loading than for static loading. A comparison between the two types of concretes is presented in Figure 12.3. In Figure 12.3a, peak bending loads have been plotted as a function of hammer drop height. Fracture energy as a function of hammer drop height appears in Figure 12.3b.

For both types of concrete, the addition of fibres resulted in increased strengths, but the increases were only marginal. Fibre reinforced systems were as strain rate sensitive as were the systems without the fibres. The presence of fibres perhaps resulted in a confining effect which marginally increased the crushing strength of concrete in the compression zone, causing the mean stress in the compressive stress block to rise, and thus registering a higher moment of resistance.

Under static as well as dynamic loading, the inclusion of fibres resulted in increased energy absorption capacity. However, the increase in energy absorption was far greater in the case of high strength concrete than for normal strength concrete, particularly at higher drop heights. An increase in the impact intensity caused the fracture energy to increase in normal strength concrete with or without polypropylene fibres. However, the trend seemed to be more complex for the high strength concrete (Figure 12.3b). While an increase in the impact intensity, as observed in Chapter 11, resulted in an embrittlement of CRHSC without

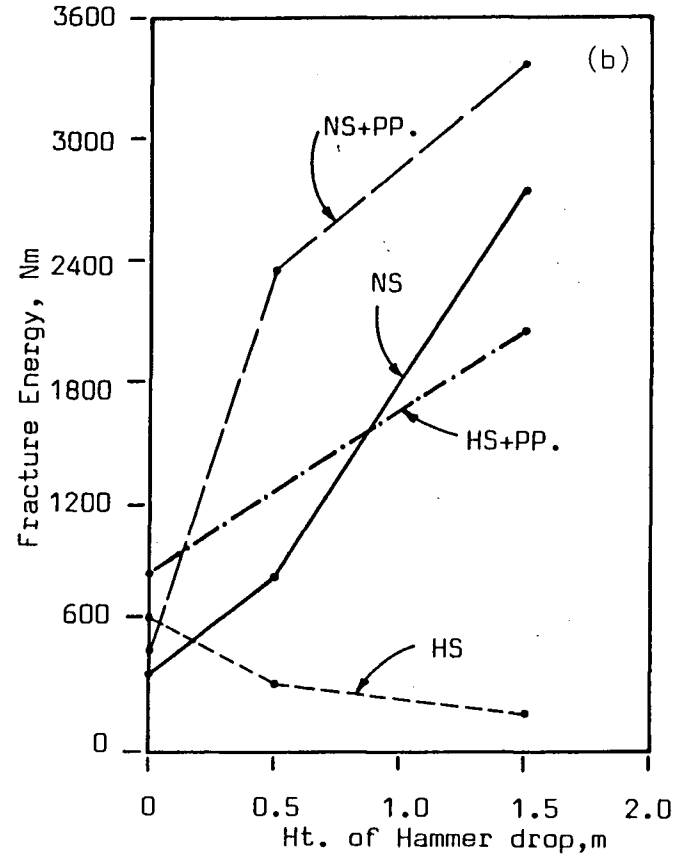
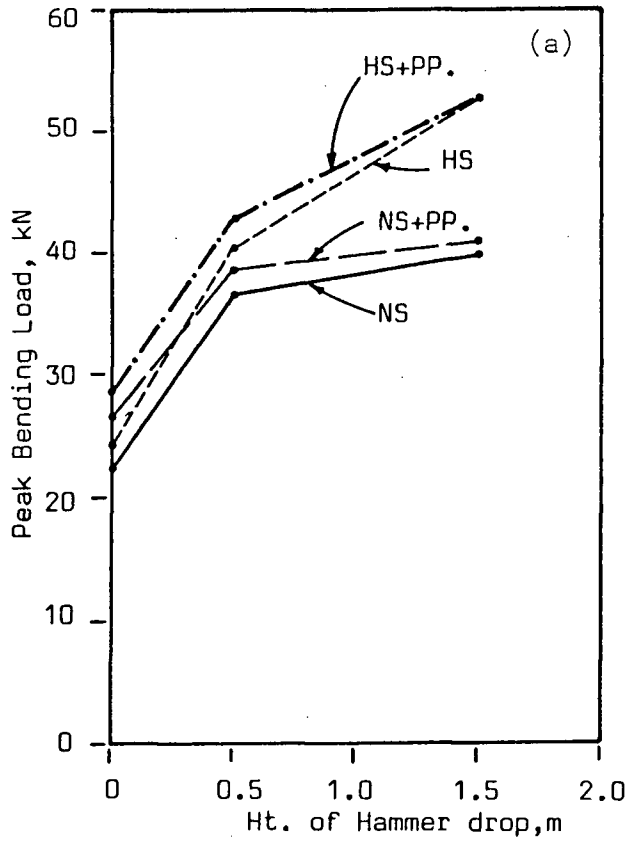


Figure 12.3- Comparison between the effect of Polypropylene Fibres on Conventionally Reinforced Normal Strength Concrete and on Conventionally Reinforced High Strength Concrete.

polypropylene fibres, a similar increase in impact intensity made CRHSC with polypropylene fibres more ductile.

The embrittlement of high strength concrete, thus, was largely remedied by using fibres. While rebar fracture was observed frequently in CRHSC without polypropylene fibres, rebar fracture was uncommon in CRHSC reinforced with polypropylene fibres. Thus, the undesirable and premature rebar failure caused by high localized steel strains in CRHSC without polypropylene fibres did not occur as frequently in CRHSC with polypropylene fibres. The use of fibres appeared to result in a more uniform distribution of strains along the length of the reinforcing bars, avoiding high localized strains, and thus using the reinforcement more effectively. It is not clear, however, how the localized strains are caused and further investigation is needed in this direction.

### 12.5 PREDAMAGED BEAMS

In practice, impact and shock loading generally occur only very occasionally. Usually, a structural element, before it is subjected to an impact loading, has already been loaded statically. Since static loading design does allow for cracks in concrete, the element may be predamaged before it is subjected to the external impact loading pulse. Thus the overall safety of the structure under impact depends upon how these predamaged structural elements cope with the external impact pulse.

**Table 12.3**  
**Dynamic Behaviour of Conventionally Reinforced Pre-Damaged**  
**Concrete beams with Polypropylene Fibres**

	Normal Strength Concrete		High Strength Concrete	
	Without Fibres	With Fibres	Without Fibres	With Fibres
<b>Peak Bending Load (N)</b>	35482 (1894)	36411 (2698)	39806 (4609)	38999 (3809)
<b>Fracture Energy (Nm)</b>	586 (422)	2240 (701)	220 (140)	1223 (330)

**NOTES:**

1. *Fracture Energies were calculated to the point at which the load dropped back to 1/3rd of its peak value.*
2. *Predamage was induced by statically loading the beams to 3mm central deflection.*
3. *The numbers in brackets are the standard deviations.*
4. *Six specimens tested in each of the categories.*

Predamage was induced by static loading of the beam (centre point loading) to a deflection of 3mm, which was approximately double the deflection at which the load first reached the maximum load bearing capacity of the beam. At this point, a tensile crack at the centre of the beam could be seen. This treatment was given to both normal strength and high strength beams with conventional reinforcement, and with or without polypropylene fibres. The beams were then tested in impact using a hammer drop height of 0.5m. The results are given in Table 12.3.

The results for the predamaged beams showed, as expected, much more variability than those observed for the undamaged beams. The general trend was that, for concrete without fibres, predamage had only a very small effect on

the load bearing capacity during impact, but caused a substantial reduction in the energy absorbed by the beams (Table 12.3). The presence of fibres practically eliminated this loss, and the energy absorption capacity of the predamaged beams containing fibres was similar to that of the undamaged beams (Tables 12.1 and 12.2).

The advantage of the presence of polypropylene fibres in the predamaged beams could be clearly appreciated when these beams were observed after the impact loading (Figures 12.4 and 12.5). In normal and high strength reinforced concrete considerable spalling and disintegration could be observed in the predamaged beams that were subjected to impact (Figures 12.4a and 12.5a). However, with fibres, the extent of damage was limited to cracking only, and no spalling and disintegration was seen (Figures 12.4b and 12.5b). This type of damage was very similar to that observed when undamaged beams were subjected to the same impact (Figures 12.4c and 12.5c).

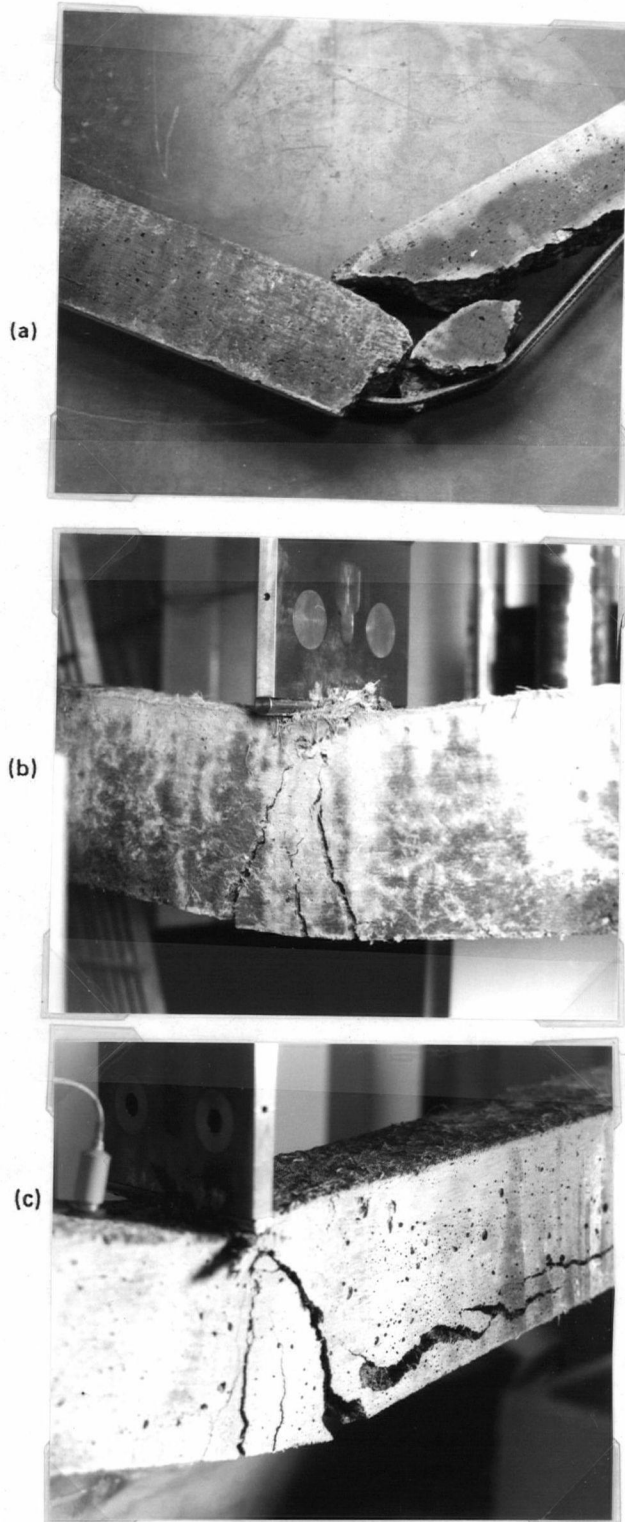


Fig.12.4 Reinforced concrete beams of normal strength concrete after 0.5m impact (a) predamaged beam without polypropylene fibres; (b) predamaged beam with polypropylene fibres; (c) undamaged beam without polypropylene fibres

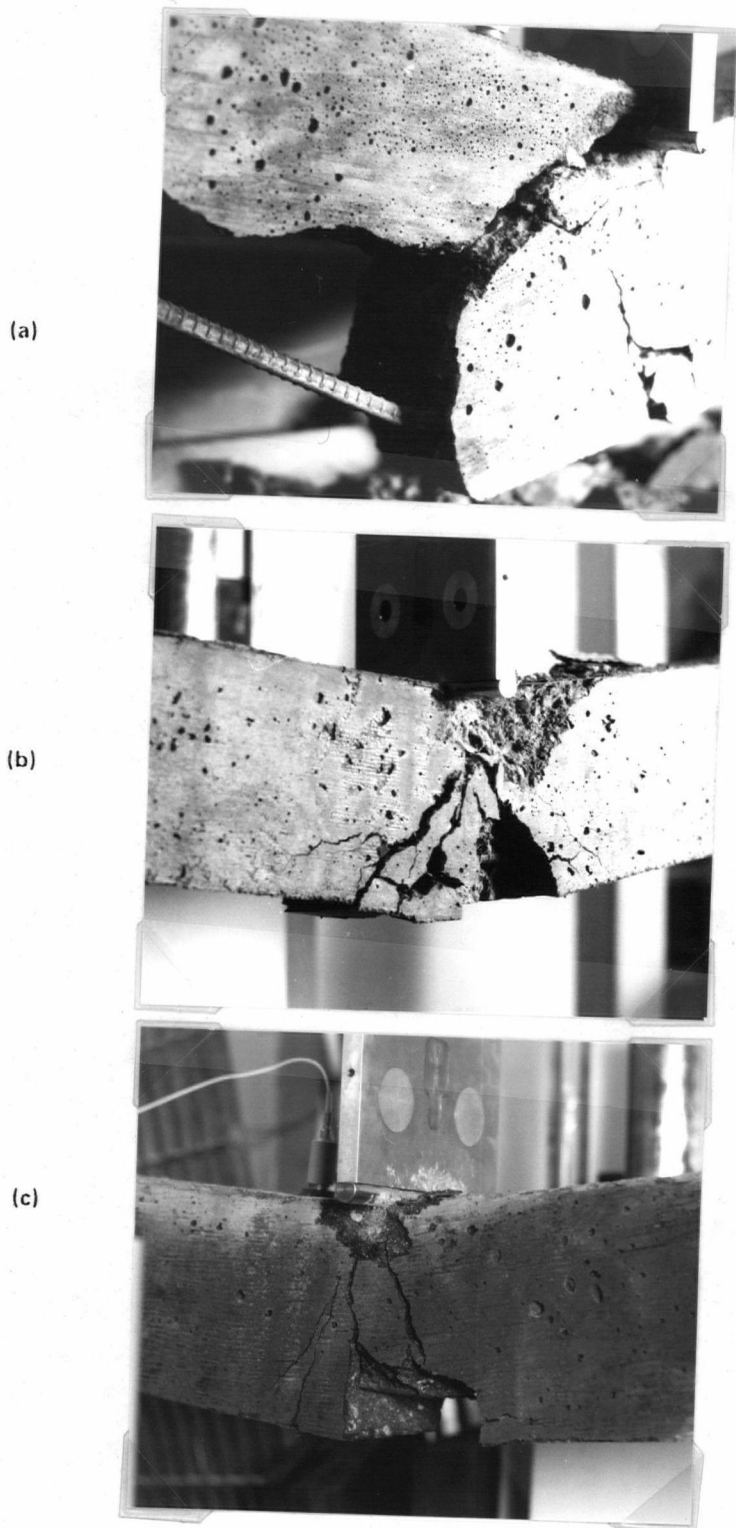


Fig. 12.5—Reinforced concrete beams of high strength concrete after 0.5 m impact (a) predamaged beam without polypropylene fibres; (b) predamaged beam with polypropylene fibres; (c) undamaged beam without polypropylene fibres

## CONCLUSIONS

The brittle nature of concrete poses some serious problems in situations where impact loading may occur; it is manifested by a low failure strain in tension, and a sudden drop in the load after reaching the peak in conventional static tests. However, since concrete is a strain rate sensitive material, its behaviour under high strain rates can not be predicted by conventional static tests. Moreover, the case of impact loading, because of the complex energy transfer and dissipation mechanisms, and because of the complex pattern of stress waves, can not be regarded simply as an extreme case of high stress rate loading. Thus, proper impact tests have to be carried out on concrete and concrete composites in order to evaluate their impact performance. Such impact tests were carried out in this study, and the following conclusions may be drawn.

1. A drop weight impact machine may be successfully used to carry out impact tests on concrete beams. However, the following should be noted.

(a) In the drop weight tests the contact load between the hammer and the beam is not the true bending load because of specimen inertia effects. The actual stressing load on the specimen may be as low as only 15% of the recorded tup load.

(b) The recorded tup load can be corrected for inertia if the acceleration distribution along the length of the beam is known. Three accelerometers were used in this study for this purpose. With a suitable assumption regarding the acceleration distribution between any two accelerometers, the proper inertial correction may be applied. An independent check on the validity of this technique was made by instrumenting one of the support anvils.

(c) A considerable simplification is possible in the mathematical formulation leading to the evaluation of the inertial load if some assumption regarding the acceleration distribution along the entire length of the beam can be made. On the basis of the tests carried out in this study, it was seen that the acceleration distribution was linear in the case of plain and fibre reinforced concrete, and that it was sinusoidal in the case of conventionally reinforced concrete.

(d) Rubber pads have been used by some investigators as a means of eliminating the inertial loading. However, from tests done with a rubber pad in the system, it was concluded that although the rubber pad helped in reducing the beam accelerations and hence the inertial loading, it did not eliminate it entirely. Moreover, the use of rubber pads reduced the strain rate, thereby

defeating the purpose of impact testing. The rubber pad also absorbs the energy during a test which must be considered. Inertial loads, thus, are an integral part of high strain rate testing and can not be eliminated.

(e) According to the law of conservation of energy, the energy lost by the hammer must equal the energy gained by the beam. This law was examined in the case of impacts on plain concrete beams. It was found that up to the peak external load, only a very small fraction of the energy lost by the hammer was consumed by the beam in various forms. The remainder of the energy was considered to be stored in the various strained parts of the machine. However, by the end of the impact event, a reasonable agreement between the the energy lost by the hammer and that gained by the beam was observed. Thus the energy stored in the machine at the peak load was transferred to the beam in the post peak load period.

2. On the basis of the tests on plain concrete beams the following conclusions may be drawn.

(a) Both normal strength as well as high strength concretes (produced by using microsilica) are strain rate sensitive. Under impact loading, the peak bending

loads as well as the fracture energies were found to be significantly higher than those obtained from conventional static tests. In general, under impact, the beams were found to have improved deformation capacities, suggesting increased failure strains. The improved toughness under impact loading was probably due to the increased microcracking in concrete under those conditions.

(b) An evaluation of the fracture mechanics parameter 'n' from the slope of the  $\log \sigma$  vs  $\log \dot{\sigma}$  plot indicated that the value of n decreased as the strain rate was increased. This was true for both normal and high strength concretes. In the impact range, a value of  $n=1.5$  for normal strength, and a value of  $n=2.2$  for high strength concrete was obtained. These low values of "n" indicate the highly stress rate sensitive behaviour of concrete at the extreme rates of loading associated with impact.

(c) High strength concrete made with microsilica was found to be stronger than normal strength concrete without microsilica in both the static and impact conditions. However, high strength concrete was also found to be more brittle than normal strength concrete. The most probable reason behind this may be the improved aggregate-paste bond in high strength concrete

which leads to reduced microcracking or reduced energy dissipation. By separating the energy absorbed up to the peak load into the elastic part and the work of fracture part, it could be seen that high strength concrete had a consistently lower work of fracture. A visual inspection of the fractured surfaces indicated that in normal strength concrete the cracks took a tortuous path around the aggregate particles. On the other hand, in the case of high strength concrete, the cracks went through the aggregate particles rather than around them.

(d) Based on the impact tests carried out on notched beams, it could be concluded that  $K_{IC}$  (fracture toughness or the critical stress intensity factor) is not a material constant and an increase in the stress rate results in an increase in the value of  $K_{IC}$ . Under impact loading, high strength concrete was found to be more notch-sensitive than normal strength concrete.

(e) Analytical predictions of beam response to impact may be based on either *the energy balance principle* or on *the principle of dynamic equilibrium of forces*. In the case of the model based on the energy balance principle suggested in this study, the beam deflections, velocities and so on were overestimated because of the inability of the model to account for

the machine losses. Because of the non-linear nature of the experimentally observed load vs. deflection plot under impact loading, classical single-degree or multi-degree of freedom solutions are inappropriate. To account for this non-linearity, a time step integration technique was devised which was found to give reasonable results. The non-linear nature of concrete behaviour was modelled by choosing a non-linear constitutive law involving stress rate ( $\dot{\sigma}$ ) as an independent variable. By choosing two different sets of constants in the constitutive law, the differences in the behaviours of normal strength and high strength concretes could be modelled. The model was also capable of predicting the more brittle nature of high strength concrete over normal strength concrete.

3. Based on the impact tests on fibre reinforced concrete, the following conclusions may be drawn.

- (a) Incorporation of either high modulus steel fibres or low modulus polypropylene fibres was found to increase the ductility of the composite both under static and dynamic conditions. The hooked end steel fibres, however, were found to be far better than the chopped straight polypropylene fibres. While the improvements in the peak loads and fracture energies

over unreinforced concrete were only moderate in the case of polypropylene fibres, the corresponding improvements in the case of steel fibres were dramatic.

(b) The differences in their modes of failure may, to some extent at least, explain the poorer performance of polypropylene fibre over steel fibres. In static as well as impact conditions, the polypropylene fibres always failed by breaking, whereas steel fibres were mostly pulled out. (An increasing number of steel fibres were found to break as the hammer drop height was increased).

(c) Fibres were effective in both the normal strength and high strength mixes. However, steel fibres performed somewhat better in the high strength mix with microsilica than in the normal strength mix without microsilica. This was thought to be because of the improved fibre-concrete bond in the high strength mixes.

(d) One major difference between the two fibres was in the occurrence of a peak, or a discontinuity, in the load vs. deflection plot prior to the absolute peak load in the case of steel fibre reinforced concrete, while no such discontinuity was observed in the polypropylene fibre reinforced concrete. The

discontinuity was thought to result from the matrix failure, a slight reduction in the load, and a subsequent rise in the load owing to fibres bridging the crack. The idea that the pre-peak discontinuity observed in the case of steel fibre reinforced concrete corresponded to the point of matrix failure was strengthened by the observation that the load at the discontinuity was nearly the same as the absolute peak load observed in the case of plain unreinforced beams.

(e) Impact tests on polypropylene fibre reinforced notched beams indicated that the presence of the fibres marginally increased the fracture toughness ( $K_{IC}$ ) over that of the unreinforced beams. The fibres thus acted as crack arresters.

(f) One major advantage of adding the fibres could be noted in the reduced spalling and disintegration observed in fibre reinforced beams under impact. Fibres, both steel and polypropylene, helped preserve the integrity of the beams.

4. Based on the impact tests done on conventionally reinforced concrete beams, the following conclusions may be drawn.

(a) In the case of conventionally reinforced normal strength concrete with deformed reinforcing bars, an increase in the stress rate from the static to the impact range resulted in a significant increase in the fracture energy. In general, an increase in the stress rate resulted in an increase in the ductility or the deformation capacity of the beams. The peak bending loads obtained under impact loading were higher than those obtained under static loading. However, once in the impact range, an increase in the hammer drop height did not produce a significant increase in the peak bending loads.

(b) On comparing the performance of deformed bars in normal strength concrete with that of smooth bars in normal strength concrete, it may be concluded that in general, the deformed bars behave somewhat better than the smooth ones. The poor bond developed in the case of smooth rebars was thought to be the reason behind this. However, rebar fracture was noticed very occasionally in the case of smooth rebars even under a hammer drop height of 2.3m, while deformed rebars were found to fracture in as many as 30% of the cases under only a 1.5m drop.

(c) The use of shear reinforcement in conventionally reinforced normal strength concrete was found to enhance

the impact resistance. Confining the concrete, thus, seemed to increase its ductility.

(d) An increase in the stress rate in the case of conventionally reinforced high strength concrete beams was found to decrease their deformation capacity, increase their rigidity, and thereby reduce their ductility. An increase in the hammer drop height was found to reduce the ultimate deflections as well as the fracture energy. This is contrary to the behaviour of normal strength concrete where an increase in the hammer drop height increased the fracture energy. Also, reinforcing bars fractured more often in high strength concrete than in normal strength concrete.

5. Based upon the impact tests on conventionally reinforced concrete containing polypropylene fibres, it can be concluded that the fibres increase the ductility in impact. The relative effect of the polypropylene fibres in improving toughness under impact loading was greater in high strength reinforced concrete than in normal strength reinforced concrete. Thus, the addition of the fibres to the high strength concrete seems to be an efficient means of compensating for the more brittle behaviour of this concrete under impact loading.

6. Based upon the high speed photography (at 10,000 frames per second) on beams undergoing impact (0.5m drop), it can be concluded that the crack velocities observed in hydrated cement paste (hcp), fibre reinforced concrete, and in conventionally reinforced concrete were in the range of 75 to 115 m/s, far lower than the theoretical crack velocities in these materials. Also, the presence of reinforcement, either in the form of fibres or continuous bars, tends to reduce the crack velocity compared with that in hydrated cement paste.

To conclude, it may be said that the thesis presents a large amount of experimental data involving practically all kinds of concrete systems used today. The development of a valid testing technique is believed to be a significant contribution since the available data from the other sources is often questionable due to inconsistencies in the experimental results. Through experimentation, and comparative evaluation, it is believed that some practical procedures for improving the impact resistance of concrete have been established. Also, through experimentation, the dangerously brittle behaviour of some concrete systems under impact has been pointed out.

### SCOPE FOR FUTURE WORK

On the basis of the work carried out in this study, future work may be recommended in the following areas.

1. One difficulty often encountered in the realm of impact testing of cementitious materials is the incomparability of the results obtained by different investigators using different testing methods. Different investigators use different specimen geometries, and different ways of generating high stress rate loadings. Different testing machines have different energy losses associated with them, and finally, different techniques are used to analyse the raw data. This all amounts to the test results being very subjective. Therefore, an attempt towards designing a standard test technique is very important, and research in this direction is highly recommended.
2. In this study, only two basic concrete mixes (normal strength and high strength) have been tested. However, the properties and the type of cement, properties of aggregates, mixing technique, additives, and so on, all have a considerable effect on the impact behaviour of concrete. The aggregate-paste interface, which forms the weakest link in concrete, also determines its impact resistance and needs further study.

3. Analytical prediction of concrete behaviour subjected to an external impact pulse needs further attention. Analytical studies are needed particularly in the post-peak load region. Since this region involves a propagating crack, a study of the crack propagation under impact loading must be undertaken prior to such modelling. A study of the process zone in front of a propagating crack and the effect of crack velocity on such a zone are also important. A study of the post-peak load region is important since a substantial portion of the total fracture energy is consumed in this region.
  
4. Because of their high ductility and energy absorption capacity, fibre reinforced composites are becoming very popular. However, our present knowledge of their behaviour under static as well as dynamic conditions is mostly empirical, and further research is needed towards formulating their constitutive laws as a function of the stress rate, so that a more deterministic approach may be adopted while designing with these promising materials. Research is also recommended to determine the optimum fibre geometry, optimum fibre volume, and so on, for maximum efficiency under variable stress rates.

## BIBLIOGRAPHY

1. Mainstone, R.J. and Kavyrchine, M.; *Part-1, Introduction*, Materials and Structures, Vol. 8, No. 44, 1975, pp. 79-80.
2. Struck, W. and Voggenreiter, W.; *Examples of Impact and Impulsive Loading in the Field of Civil Engineering*, Materials and Structures, Vol. 8, No.44, 1975, pp. 81-87.
3. Kavyrchine, M. and Struck, W.; *Practical Application to Testing, Design and Research*, Materials and Structures, Vol.8, No.44, 1975.
4. Sliter, G.E.; *Assessment of Empirical Concrete Impact Formulae*, ASCE (Structural Division), May 1980, pp. 1023-1045.
5. Hibbert, A.P and Hannant, D.J.; *Toughness of Fibre Cement Composites*, 'COMPOSITES' Vol. 13, No. 2, April 1982, pp. 105-111.
6. Suaris, W. and Shah, S.P.; *Strain Rate Effects in Fibre Reinforced Concrete Subjected to Impact and Impulsive Loading*, 'COMPOSITES' Vol. 13, No. 2, April 1982, pp. 153-159.
7. Hibbert, A.P.; *Impact Resistance of Fibre Concrete*, Ph.D. Thesis, University of Surrey, Surrey, England 1979.
8. Cotterell, B.; *Fracture Toughness and the Charpy V Notch Impact Tests*, British Welding Journal, Vol. 9, No. 2, Feb 1962, pp. 83-90.
9. Fearnough, G.D. and Joy, C.J.; *Journal of Iron and Steel Institute*, Vol. 202, Nov. 1964, pp. 912.
10. Radon, J.C. and Turner, C.E.; *Fracture Toughness Testing by Instrumented Impact Tests*, Journal of Engineering Fracture Mechanics, Vol. 1, No. 3, April 1969, pp. 411-428.
11. Turner C.E.; *Measurement of Fracture Toughness by Instrumented Impact Test* Impact Testing of Metals, ASTM STP466 , American Society for Testing and Materials, 1970, pp. 93-114.
12. Venzi, S., Priest, A.H. and May, M.J.; *Influence of Inertial Load in Instrumented Impact Tests*, Impact Testing of Metals, ASTM STP466 American Society for Testing and Materials, 1970, pp. 165-180.
13. Saxton, H.J., Ireland, D.R. and, Server, W.L.; *Analysis and Control of Inertial Effects During Instrumented Impact Testing*, Instrumented Impact Testing, ASTM STP563, American

- Society for Testing and Materials, 1974, pp. 50-73.
14. Server, W.L.; *Impact Three Point Bend Testing for Notched and Precracked Specimens*, Journal of Testing and Evaluation, JTEVA, Vol. 6, No. 1, Jan. 1978, pp. 29-34.
  15. Gopalaratnam, V.S., Shah, S.P. and John, Reji; *A Modified Instrumented Charpy Test for Cement Based Composites*, Experimental Mechanics, Vol. 24, No. 2, 1984, pp.102-111.
  16. Suaris, W. and Shah, S.P.; *Inertial Effects in Instrumented Impact Testing of Cementitious Composites*, ASTM Journal of Cement Concrete and Aggregate, March 1982, pp. 78-83.
  17. Abe, H., Chandan, H.C. and Bradt, R.C.; *Low Blow Charpy Impact of Silicon Carbides*, Bulletin of the American Ceramic Society, Vol. 57, No. 6, 1978, pp.587- 595.
  18. Lueth, R.C.; *An Analysis of Charpy Impact Testing as Applied to Cemented Carbide*, Instrumented Impact Testing, ASTM STP 563, American Society for Testing and Materials, 1974, pp. 166-179.
  19. Iyer, K.R. and Miclot, R.B.; *Instrumented Charpy Testing for Determination of the J-Integral*, Instrumented Impact Testing, ASTM STP 563, American Society for Testing and Materials, 1974, pp. 146-165.
  20. Abrams, D.A.; *Effect of Rate of Application of Load on the Compressive Strength of concrete*, Proceedings, ASTM 17, part 2, 1917, pp. 364-367.
  21. Watstein, D.; *Effect of Straining Rate on the Compressive Strength and Elastic Properties of Concrete*, Journal of the American Concrete Institute, Vol. 49, No. 8, April 1953, pp. 729-756.
  22. Green, H.; *Impact Strength of Concrete*, Proceedings of the Institution of Civil Engineers, Vol. 28, 1964, pp. 383-396.
  23. Macneely, D.J. and Lash, S.D.; *Tensile Strength of Concrete*, Journal of the American Concrete Institute, Vol. 60, No. 6, 1963, pp. 751-760.
  24. Atchly, B.L. and Furr, H.L.; *Strength and Energy Absorption Capacity of Plain Concrete Under Dynamic and Static Loading*, Journal of the American Concrete Institute, Nov. 1967, pp. 745-756.
  25. Goldsmith, W., Kenner, V.H. and Ricketts, T.E.; *Dynamic Loading of Several Concrete Like Mixtures*, Proceedings

- of the American Society of Civil Engineers, Structural Division, July 1968 pp. 1803-1827.
26. Birkimer, D.L. and Lindeman, R.; *Dynamic Tensile Strength of concrete Materials*, Journal of the American Concrete Institute, 68(1971), pp. 47-49.
  27. Hughes, B.P. and Gregory, R.; *Concrete Subjected to High Rates of Loading in Compression*, Magazine of Concrete Research, Vol. 24, No. 78, March 1972, pp. 25-36.
  28. Sparks, P.R. and Menzies, J.B.; *The Effect of Rate of Loading Upon the Static and Fatigue Strength of Plain Concrete in Compression*, Magazine of Concrete Research, Vol. 25, No. 83, June 1973, pp. 73-80.
  29. Hughes, B.P. and Watson, A.J.; *Compressive Strength and Ultimate Strain of Concrete Under Impact Loading*, Magazine of concrete Research, Vol. 30, No. 105, Dec 1978, pp. 189-199.
  30. Mindess, S.; *Rate of loading effects on the fracture of cementitious materials*, in Proceedings of NATO advanced research workshop on Application of Fracture Mechanics to Cementitious Composites, NorthWestern University, Evanston, Illinois, USA, Sept.4-7, 1984, S.P.Shah; Editor.
  31. Mindess, S. and Nadeau, J.S.; *Effect of Loading Rate on the Flexural Strength of Mortar*, Journal of the American Ceramic Society, Vol. 56, No. 44, April 1977, pp 429-430.
  32. Zech, B. and Wittmann, F.H.; *Variability and Mean Value of Strength as a Function of Load*, Journal of the American Concrete Institute, Vol. 77, No. 5, Sept-Oct. 1980, pp. 358-362.
  33. Mihashi, H. and Izumi, Masanori; *A Stochastic Theory for Concrete Fracture*, Cement and Concrete Research, Vol. 7, No. 4, July 1977, pp. 411-421.
  34. Suaris, W. and Shah, S.P.; *Properties of Concrete Subjected to Impact*, ASCE Structural Division, Vol. 109, No. 7, July 1983, pp. 1727-1741.
  35. Zielinsky, A.J. and Reinhardt, H.W.; *Stress Strain Behaviour of Concrete and Mortar at High Rates of Tensile Loading*, Cement and Concrete Research, Vol. 12, No. 3, March 1982, pp. 309-319.
  36. Zielinski, A.J.; *Model for Tensile Fracture of Concrete at High Rates of Loading*, Cement and Concrete Research, 14 (1984), pp. 215-224.

37. Alford, N. McN.; *Dynamic Consideration for Fracture in Mortars*, Journal of Material Science, 56, No. 3, Dec 1982, pp. 279-287.
38. Shah, S.P. and Rangan, B.V.; *Fibre Reinforced Concrete Properties*, Journal of the American Concrete Institute, Vol. 68, No. 2, Feb. 1971, pp. 126-134.
39. Naaman, A.E. and Shah, S.P.; *Pull Out Mechanisms in Steel Fibre Reinforced Concrete*, ASCE (Structural Division), Vol. 102, No.ST-8, August 1976, pp. 1537-1558.
40. Kobayashi, K. and Cho, R.; *Flexural Behaviour of Polyethylene Fibre Reinforced Concrete* International Journal of Cement composites and Light Weight Concrete, Vol.3, No.1, Feb. 1981, pp.19-25.
41. Bhargava, A. and Rehnstrom, A.; *Dynamic Strength of Polymer Modified and Fibre Reinforced Concrete*, Cement and Concrete Research, Vol. 7, 1977, pp. 199-207.
42. Ramakrishnan, V., Brandshaug, I., Coyle, W.V. and Schrader, E.K.; *A Comparative Evaluation of Concrete Reinforced with Straight Steel Fibres with Deformed Ends Glued Together in Bundles*, Proceedings of the American Concrete Institute, Vol. 77, No. 3, May-June 1980, pp. 135-143.
43. Jamrozy, Z. and Swamy, R.N.; *Use of Steel Fibre Reinforcement for Impact Resistance and Machinery Foundation*, International Journal of Cement Composites and Light Weight Concrete, Vol. 1, No. 2, July 1979, pp. 65-76.
44. Radomsky, W.; *Application of the Rotating Impact Machine for Testing Fibre Reinforced Concrete*, International Journal of Cement Composites and Light Weight Concrete, Vol. 3, No. 1, Feb. 1981, pp. 3-12.
45. Hibbert, A.P. and Hannant, D.J.; *Impact Resistance of Fibre Concrete*, Report submitted to the Transport and Road Research Laboratory, 1981.
46. Gokoz, U. and Naaman, A.E.; *Effect of Strain Rate on the Pull Out Behaviour of Fibres in Mortar*, International Journal of Cement Composites and Light Weight Concrete, Vol. 3, No. 3, Aug. 1981, pp. 187-202.
47. Knab, L.I. and Clifton, J.R.; *Cumulative Damage of Reinforced Concrete Subjected to Repeated Impact*, Cement and Concrete Research, Vol. 12, pp. 359-370.
48. Naaman, A.E. and Gopalaratnam, V.S.; *Impact Properties*

*of Steel Fibre Reinforced Concrete in Bending*, International Journal of Cement Composites and Light Weight Concrete, (5) 1983, pp. 225-233.

49. Harris, B., Varlow, J. and Ellis, C.D.; *Fracture Behaviour of Fibre Reinforced Concrete* Cement and Concrete Research 2, (1972) pp. 447- 461.
50. ACI Committee 544; *Measurement of Properties of Fibre reinforced Concrete*, Journal of the American Concrete Institute, Vol.75, No.7, July 1978, pp. 283-289.
51. Daves, R.M., *A critical study of the Hopkinson Pressure bar*, Philosophical Transactions, Royal Society of London, Series A, Vol. 240, pp. 357-457.
52. Davies, E.D.H. and Hunter, S.C.; *The Dynamic Compression Testing of Solids by the Method of Split Hopkinson Pressure Bar*, Journal of Mech. and Physics of Solids, Vol. 11, No. 5, 1963, pp. 155-179.
53. Birkimer, D.L., *A possible Fracture Criterion for the Dynamic Tensile Strength of Rock*, Proceedings of the 12th Symposium on Rock Mechanics, University of Missouri, Nov. 1970, pp. 573-589.  
  
(53a) Reinhardt, H.W.; *Tensile Fracture of Concrete at High Rates of Loading*, in Proceedings of NATO advanced research workshop on *Application of Fracture Mechanics to Cementitious Composites*, NorthWestern University, Evanston, Illinois, U.S.A., Sept. 4-7, 1984, S.P.Shah, Editor.
54. Bhargava, J. and Rehnstrom, A., *Cement and Concrete Research*, 5, 1975, pp. 239-248.
55. Alford, N. McN., *Materials Science and Engineering*, 56, 3, 1982, pp. 279-287.
56. Shah, S.P. and John, R., in Vol. I, Preprints, International Conference on Fracture Mechanics of Concrete, Lausanne, 1985, pp. 373-385.
57. Takeda, J., Tachikawa, H. and Fujimoto, K., in Proceedings, RILEM-CEB-IABSE-IASS Interassociation Symposium, Concrete Structures under Impact and Impulsive Loading,, BAM, West Berlin, 1982, pp. 83-91.
58. Broek, D.; *Elementary Engineering Fracture Mechanics*, Martinus Nijhoff Publishers, The Netherlands, (1982).
59. Park,R. and Paulay, T.; *Advanced Reinforced Concrete Structures*, John Wiley and Sons, 1983.

60. Clough, R.W. and Penzien, J.; *Dynamics of Structures*, McGraw-Hill Book Company, Inc., 1975.
61. Higgins, D.D. and Bailey, J.E.; *Fracture Measurement on Cement Paste*, Journal of Material Science, 11 (1976), pp. 1995-2003.
62. John, R. and Shah, S.P.; *Fracture of Concrete Subjected to Impact Loading*, Cement Concrete and Aggregates, CCAGDP, Vol. 8, No. 1, Summer 1986, pp. 24-32.
63. Yam, A.S.T. and Mindess, S.; *The Effect of Fibre Reinforcement on Crack Propagation in Concrete*, International Journal of Cement Composites and Light Weight Concrete, 4(1982), pp.83-93.
64. Panda, A.K.; *Bond of Deformed Bars in Steel Fibre Reinforced Concrete under Cyclic Loading*, Ph.D. Thesis, Department of Civil Engineering, The University of British Columbia, April, 1984.
65. ACI Committee 439, *Effect of Steel Strength and of Reinforcement Ratio on the Mode of Failure and Strain Energy Capacity of Reinforced Concrete Beams*, ACI Journal, No. 3, Vol. 66, March 1969, pp. 165-173.
66. Lubahn, J.D. and Felgar, R.P.; *Plasticity and Creep of Metals*, John Wiley and Sons, New York, 1961.